KU LEUVEN

ARENBERG DOCTORAL SCHOOL
Faculty of Engineering Science

Robust control of time-delay systems: analysis, computational methods and software

Pieter Appeltans

Supervisor:
Prof. dr. ir. W. Michiels

Dissertation presented in partial fulfillment of the requirements for the degree of Doctor of Engineering Science (PhD): Computer Science

March 2023

Robust control of time-delay systems: analysis, computational methods and software

Pieter APPELTANS

Examination committee:
Em. Prof. dr. ir. B. Puers, chair
Prof. dr. ir. W. Michiels, supervisor
Prof. dr. ir. K. Meerbergen
Prof. dr. ir. P. Patrinos
Prof. dr. ir. D. Breda
(University of Udine)
Dr. ir. S. Gumussoy
(Siemens Technology)
Prof. dr. ir. S. Mondié
(CINVESTAV-IPN)

Dissertation presented in partial fulfillment of the requirements for the degree of Doctor of Engineering Science (PhD): Computer Science

March 2023

© 2023 KU Leuven – Faculty of Engineering Science
Uitgegeven in eigen beheer, Pieter Appeltans, Celestijnenlaan 200A box 2402, B-3001 Leuven (Belgium)

Alle rechten voorbehouden. Niets uit deze uitgave mag worden vermenigvuldigd en/of openbaar gemaakt worden door middel van druk, fotokopie, microfilm, elektronisch of op welke andere wijze ook zonder voorafgaande schriftelijke toestemming van de uitgever.

All rights reserved. No part of the publication may be reproduced in any form by print, photoprint, microfilm, electronic or any other means without written permission from the publisher.

Voorwoord

Detailed studies of the real world impel us, albeit reluctantly, to take account of the fact that the rate of change of physical systems depends not only on their present state, but also on their past history.

R. Bellman and K. Cooke, 1963

Mijn thesistekst is nu eindelijk klaar, een half jaar later dan gepland. Een thesis over *time-delay systems* kan nu eenmaal niet tot stand komen zonder vertraging. Nu deze obligate grap achter de rug is, kunnen we overgaan tot het echte werk.

Het verloop van een doctoraat kan vergeleken worden met een etappe in de Tour de France. Soms heb je tegenwind en lijk je niet vooruit te komen. Gelukkig draait de wind daarna vaak en heb je hem vol in de rug. Het einde van zo een zware rit bereik je echter niet alleen. Daarom zou ik in dit voorwoord graag alle mensen willen bedanken die mij geholpen hebben de eindmeet te bereiken.

Vooreerst wil ik mijn promotor, Wim Michiels, bedanken. Zijn deur stond altijd open zodat ik binnen kon springen met al mijn vragen en problemen. (Als ik Wim een tekst stuurde om na te lezen, kreeg ik altijd snel een antwoord, soms zelfs in het weekend.) Daarnaast, wil ik Wim ook bedanken om mij mee te nemen naar tal van conferenties (zowel virtueel als in Roemenië en Canada) en mij de kans te geven om mijzelf te ontwikkelen.

Ten tweede wil ook de leden van mijn examencommissie, Bob Puers, Karl Meerbergen, Panos Patrinos, Dimitri Breda, Suat Gumussoy, en Sabine Mondié, bedanken voor het lezen van mijn thesis, en de interessante vragen en opmerkingen tijdens de verdediging.

Voorts zou ik graag mijn dankbaarheid uiten aan de buitenlandse onderzoekers waar Wim mij gedurende mijn doctoraat mee in contact heeft gebracht en waarmee ik het genoegen heb gehad samen te werken. In de eerste plaats zou ik Silviu-Iulian Niculescu (CNRS, Centrale Supélec) willen bedanken voor de vlotte samenwerking bij onze paper rond robuuste PID controle van time-delay systemen, beschreven in hoofdstuk 3 van deze thesis. Daarnaast zou ik ook Matthias Voigt (UniDistance Suisse) en Paul Schwerdtner (TU Berlin) willen bedanken, die mij in februari 2020 een week ontvingen in Berlijn. (Juist voordat de pandemie in al zijn hevigheid losbrak en we voor een jaar nauwelijks naar kantoor konden gaan.) Ik zou jullie willen bedanken voor de gesprekken die we in die week hebben gevoerd en die als inspiratie hebben gediend voor de methode beschreven in hoofdstuk 6 van deze thesis rond niet-lineaire Hamiltoniaanse eigenwaardenproblemen. Tot slot zou ik ook Milan Anderle (The Czech Academy

of Sciences), Sergej Čelikovský (The Czech Academy of Sciences) en Tomáš Vyhlídal (CTU Prague), waarmee ik heb samengewerkt rond het controleren van een slinger door de slingerlengte te variëren, willen bedanken.

Tevens is een woord van dank op zijn plaats voor al de toffe collega's waarmee ik de afgelopen vier en een half jaar binnen NUMA heb mogen samenwerken. In de eerste plaats, wil ik Adrian S., Deesh, Francesco, Haik, Kirill, Koen, Libu, Luca, Marco, Yanling, en de twee nieuwkomers Evert en Sanaz (ik heb er alle vertrouwen in dat jullie het geweldig gaan doen en tal van prachtige papers gaan publiceren) willen bedanken voor de wekelijkse lunches in de Alma (lang leve fishsticks ;)) en de discussies bij de koffie over alles en niets. Daarnaast wil ik alle kantoorgenoten die ik door de jaren heen heb gehad: Delbar, Dries, Laurence, Marco, Rob, Sheng, Vincent, Wang Zhijun en (gedurende de ondragelijk warme zomer van 2019) Adrian E., Luca, Francesco, Philippe en Simon D., bedanken voor de goede sfeer die er steeds heerste. (Het mag blijken uit deze lange lijst dat ik door de vele renovatiewerken op het departement regelmatig van lokaal ben moeten veranderen.) Vervolgens wil ook het voltallige TWS-team, Emil, Joris, Karl, Ronald, Thijs, en Wouter, bedanken voor de vlotte samenwerking. Een woord van dank is ook op zijn plaats voor Karl, Nick V. en Pieterjan. Bedankt om op geregelde tijdstippen een koffietrein naar de vijfde verdieping op de rails te zetten. Tot slot wil ik Andreas, Arne, Astrid, Bert, Daan, Elien, Giovanni C., Hannes, Ignace (hierbij ik draag het voorzitterschap van de NUMA wandelclub aan jou over), Kobe, Luis, Maarten, Nick D., Nico, Niel, Nikhil, Pieter V., Sahar, Simon J., Simon T., Stijn, Tom D., Tom K., Toon, Vince, en Weiwen bedanken voor de fijne babbels en toffe activiteiten binnen en buiten het departement.

Tot slot zou ik mijn ouders en familie willen bedanken. Bedankt voor alle steun die jullie mij gaven. Dank je mama om met mij de schapen te gaan voeren als ik het even moeilijk had en de talloze keren dat je mij bent komen halen aan het station. Dank je papa om iedere zondag een route uit te stippelen om te gaan fietsen. Dank je Birgit voor de goede raad die je me steeds gaf.

Veel leesplezier,

Pieter Appeltans,
Dorne, februari 2023.

Abstract

A first step in analyzing the behavior of a dynamical system, such as the swing of a clock pendulum or the spread of an infectious disease, consists of deriving a mathematical model that adequately describes its behavior. Time-delay systems have proven valuable as compact models capable of representing complex phenomena in a wide variety of applications ranging from life sciences over physics and engineering to economics. Nevertheless, the obtained models are typically only an approximation for reality, due to unmodeled behavior, uncertain parameters or external disturbances. The development of novel methods to analyze and quantify the effect of these uncertainties is therefore an important challenge. Besides, also the design of controllers that govern the input of a system in such a way that some desired behavior is achieved, even in the face of uncertainties and external disturbances, is an interesting open problem in literature.

The main objective of this thesis is therefore to develop novel computational methods and software for the analysis and controller-design of linear time-invariant (LTI) time-delay systems with discrete (pointwise) delays, focusing on quantifying the effect of uncertainties and robust controller design, as spelled out in more detail below.

Firstly, the control of an LTI time-delay system with discrete state delays using a proportional-integral-derivative (PID) output feedback law is examined. The focus lies on a fragility problem of the resulting closed-loop system. More specifically, it will be shown that under certain conditions on the derivative feedback gain, closed-loop stability can be destroyed by introducing a parametric perturbation, such as a feedback delay, a finite-difference approximation of the derivative or a high frequency roll-off, even when this perturbation is made arbitrarily small. The notion of *strong* exponential stability, which requires that stability is preserved under (sufficiently small) perturbations, is therefore introduced. Subsequently, it is shown that under a certain algebraic condition on the derivative feedback gain, strong exponential stability can be achieved by applying a low-pass filter with a sufficiently large cut-off frequency to the derivative signal of a stabilizing PID controller. These theoretical results are complemented with a computational design procedure for strongly stabilizing PID controllers.

Secondly, the robust H_∞-norm of a time-delay system with real-valued uncertainties on the system matrices, defined as the worst-case value of the H_∞-norm over all admissible uncertainty values, is examined. Again, special attention is paid to a potential fragility problem. More precisely, the robust H_∞-norm might be a discontinuous function of the delay values, as for a

particular instance of the uncertainties, the H_∞-norm might be sensitive to arbitrarily small perturbations on the delays. Therefore, the robust *strong* H_∞-norm, defined as the worst-case value of the strong H_∞-norm, is considered. In contrast to the robust H_∞-norm, this measure is a continuous function of both the entries of the system matrices and the delays. Thereafter, a characterization of the *robust strong* H_∞*-norm* of an uncertain time-delay system in terms of the robust distance to instability of a corresponding uncertain delay differential algebraic equation (DDAE) is derived. This relation gives rise to a novel procedure for computing the robust strong H_∞-norm, inspired by recent developments in the domain of geometric optimization. The resulting algorithm is subsequently used as a component in a controller design procedure to (locally) minimize the robust (strong) H_∞-norm of an uncertain time-delay system. This approach is illustrated by means of an example arising in the robust control of a certain class of networked systems.

Thirdly, a novel structure-preserving infinite Arnoldi method for computing certain eigenvalues of a class of large-scale delay eigenvalue problems (DEPs) for which the spectrum admits a Hamiltonian-like symmetry, is introduced. These Hamiltonian DEPs typically arise in the context of computing the H_∞-norm of large-scale time-delay systems. The presented method has the advantage that the obtained approximations for simple, purely imaginary eigenvalues are typically simple and purely imaginary themselves, even in the presence of rounding errors, which is an important feature for the considered application.

Finally, a novel software package for the analysis and controller-design of LTI time-delay systems with discrete delays, named `TDS-CONTROL`, is presented. The functionality of this package is illustrated by means of several examples.

Beknopte samenvatting

Om het gedrag van een dynamisch systeem, zoals een satelliet in een baan rond de aarde of de verspreiding van een besmettelijke ziekte, te bestuderen, is er een wiskundig model nodig dat het gedrag van dit systeem voldoende goed beschrijft. In veel gevallen kunnen we hiervoor gebruik maken van gewone differentiaalvergelijkingen, in welke de evolutie van de toestand van het model enkel afhangt van zijn huidige waarde. Echter, voor tal van fenomenen in zowel de fysica, de ingenieurswetenschappen als de economische wetenschappen volstaat zulk een gewone differentiaal vergelijking niet en dient men modellen te beschouwen die de afhankelijkheid van het verleden expliciet in rekening brengen. Differentiaalvergelijkingen met tijdsvertraging laten toe om zulke systemen compact te beschrijven. Hoewel deze modellen typisch een goede benadering zijn voor het gedrag van het systeem, is er in praktijk toch vaak een afwijking tussen model en werkelijkheid omdat bepaalde parameterwaarden in het model niet exact gekend zijn of omdat er externe verstoringen inwerken op het systeem. De ontwikkeling van nieuwe methoden om het effect van deze onzekerheden te analyseren is daarom opportuun. Naast deze analyse, is ook het ontwerp van regelaars die zulke systemen kunnen bijsturen zodat zij het gewenste gedrag vertonen, zelfs wanneer geconfronteerd met onzekerheden en verstoringen, een open probleem dat meer aandacht verdient vanuit zowel een theoretisch als praktisch oogpunt.

Deze thesis presenteert nieuwe methoden en software voor de analyse en controle van lineaire tijdsinvariante (LTI) dynamische systemen met discrete (puntsgewijze) tijdsvertragingen. De focus ligt hierbij op het kwantificeren van het effect van onzekerheden en het ontwerp van robuuste regelaars.

Eerst besturen we het gebruik van PID-regelaars voor de controle van LTI dynamisch systemen met discrete tijdsvertragingen in de toestandsvariabele. We zullen ons hierbij focussen op een *well-posedness* probleem. Zo zal er aangetoond worden dat onder bepaalde voorwaarden op de D-actie (i.e., de term in de regelactie proportioneel met de afgeleide van het foutsignaal), een stabiel systeem gedestabiliseerd kan door een arbitrair kleine verstoring, zoals een terugkoppelingsvertraging of een eindige-differentiebenadering van de afgeleide. Daarom zullen we het concept *sterke exponentiële stabiliteit* introduceren, dewelke vereist dat stabiliteit behouden blijft voor (voldoende kleine) verstoringen. Vervolgens wordt er aangetoond dat indien de D-versterking voldoet aan een bepaalde algebraïsche voorwaarde, sterke exponentiële stabiliteit bereikt kan worden door een laag-doorlaatfilter toe te passen op de D-actie van een stabiliserende PID-regelaar. Naast deze theoretische resultaten, stellen we ook een ontwerpprocedure voor die toelaat

om *sterk stabiliserend* PID-regelaars te ontwikkelen.

Daarna wordt de *robuuste H_∞-norm* van een dynamisch systeem met tijdsvertraging en reële onzekerheden op de systeemmatrices beschouwd. De robuuste H_∞-norm is gedefinieerd als de maximale waarde van de H_∞-norm over alle toegestane waarden van de onzekerheden. Hierbij zullen we extra aandacht besteden aan de gevoeligheid van de robuuste H_∞-norm voor kleine variaties op de tijdsvertragingen. De *robuuste sterke H_∞-norm* wordt vervolgens geïntroduceerd als de maximale waarde van de *sterke H_∞-norm* over alle toegestane realisaties van het onzekere systeem. In tegenstelling tot de robuuste H_∞-norm is deze norm een continue functie van zowel de elementen van de systeemmatrices als de tijdsvertragingen. Daarna beschouwen we een equivalente uitdrukking voor de robuuste sterke H_∞-norm in termen van de *robuuste afstand tot instabiliteit* van een onzekere differentiaal-algebraïsche vergelijking met tijdsvertraging. Gebruikmakend van deze uitdrukking leiden we vervolgens een nieuw algoritme voor het berekenen van de robuuste sterke H_∞-norm af. We passen dit algoritme tot slot toe om een robuuste regelaar te ontwerpen voor de controle van een dynamisch systeem met netwerktopologie.

Ten derde presenteren we een nieuwe structuur-behoudende Arnoldi-methode voor het berekenen van geselecteerde eigenwaarden van een klasse van grootschalige niet-lineaire eigenwaardenproblemen met Hamiltoniaanse symmetrie. Zulke eigenwaardenproblemen duiken op in de berekening van de H_∞-norm van grootschalige dynamische systemen met tijdsvertraging. Deze nieuwe methode heeft als voordeel dat de bekomen benadering voor een enkelvoudige, puur imaginaire eigenwaarde typisch ook puur imaginair is, zelfs wanneer er gewerkt wordt in eindige precisie.

Tot slot wordt het nieuwe softwarepakket `TDS-CONTROL` voorgesteld. Dit pakket laat toe om het gedrag van LTI dynamische systemen met discrete tijdsvertragingen te analyseren en te controleren. De functionaliteit van dit pakket wordt geïllustreerd met behulp van enkele voorbeelden.

List of Abbreviations

BMI	Bilinear Matrix Inequality
CACSD	Computer-Aided Control System Design
DAE	Differential Algebraic Equation
DDE	Delay Differential Equation
DEP	Delay Eigenvalue Problem
DDAE	Delay Differential Algebraic Equation
FDE	Functional Differential Equation
LMI	Linear Matrix Inequality
LTI	Linear Time-Invariant
NDDE	Neutral Delay Differential Equation
NEP	Nonlinear Eigenvalue Problem
ODE	Ordinary Differential Equation
PID	Proportional-Integral-Derivative
RDDE	Retarded Delay Differential Equation

List of Symbols

Sets

$\mathbb{R}$	set of real numbers
$\mathbb{C}$	set of complex numbers
$\mathbb{C}^+$	open right half-plane, $\{\lambda \in \mathbb{C} : \Re(\lambda) > 0\}$
$\mathbb{R}^n$	set of real-valued n-dimensional vectors
$\mathbb{C}^n$	set of complex-valued n-dimensional vectors
$\mathbb{R}^{m\times n}$	set of real-valued $m \times n$-dimensional matrices

Matrix operations and properties

$M^\top$	transpose of a matrix M
M^H	conjugate transpose of a matrix M
M^{-1}	inverse of a matrix M
$\det(M)$	determinant of a matrix M
$\operatorname{rank}(M)$	rank of a matrix M
$\operatorname{diag}(\alpha_1, \ldots, \alpha_n)$	diagonal matrix with $\alpha_1, \ldots, \alpha_n$ on its diagonal
$\sigma_1(M)$	largest singular value of a matrix M
$\sigma_2(M)$	second largest singular value of a matrix M
$\sigma_{\min}(M)$	smallest singular value of a matrix M

Norms

$\|v\|_2$	Euclidean norm of a vector v
$\|v\|_\infty$	infinity norm of a vector v
$\|M\|_2$	spectral norm of a matrix M
$\|M\|_{\text{frob}}$	Frobenius norm of a matrix M
$\|\varphi\|_{\text{s}}$	supremum norm of a function φ
$\|f\|_{L_2}$	L_2-norm
$\|T\|_{H_\infty}$	H_∞-norm
$\|\|\|T\|\|\|_{H_\infty}$	strong H_∞-norm
$\|\|\|T\|\|\|^{\mathcal{D}}_{H_\infty}$	robust strong H_∞-norm

Spaces

X	Banach space of continuous functions $f : [-\tau, 0] \mapsto \mathbb{C}^n$ equipped with the supremum norm $\|\varphi\|_{\text{s}}$
H_∞	Hardy space of analytic functions on $\mathbb{C}^+$
L_2	space of square integrable vector-valued functions
span	linear span

Eigenvalues

Λ	spectrum
ρ	spectral radius
c	spectral abscissa
C	strong spectral abscissa
Λ^{ps}	pseudospectrum
c^{ps}	pseudospectral abscissa
r	distance to instability
$\mathrm{r}_{\mathbb{C},\|\cdot\|_2}(\mathcal{D})$	robust distance to instability
$\mathrm{r}^{\mathrm{nwp}}_{\mathbb{C},\|\cdot\|_2}(\mathcal{D})$	robust distance to non well-posedness
$\mathrm{r}^{\mathrm{chain}}_{\mathbb{C},\|\cdot\|_2}(\mathcal{D})$	robust distance to characteristic root chain crossing
$\mathrm{r}^{\mathrm{fin}}_{\mathbb{C},\|\cdot\|_2}(\mathcal{D})$	robust distance to a finite root crossing

Other

$\jmath$	imaginary unit, i.e., $\jmath = \sqrt{-1}$
$\bar{\alpha}$	complex conjugate of a complex number α
$\|\alpha\|$	modulus of a complex number α
$\arg(\alpha)$	argument of a complex number α
$\Re(\alpha)$	real part of a complex number α
$\Im(\alpha)$	imaginary part of a complex number α
I_n	identity matrix of size $n \times n$
$0_{m\times n}$	zero matrix of size $m \times n$
$\otimes$	Kronecker product
$\cup$	union
$\cap$	intersection
$\setminus$	set difference
$\mathcal{B}(\vec{\tau}, \epsilon)$	open ball of radius $\epsilon > 0$ centered at $\vec{\tau}$
sup	supremum
max	maximum
min	minimum
$\mathrm{clos}(S)$	closure of a set S
$\mathbf{B}(\varphi, \psi)$	bilinear form as defined in (6.14)

Table of Contents

Abstract iii

Beknopte samenvatting v

List of Abbreviations vii

List of Symbols ix

Table of Contents xi

1 Introduction 1
- 1.1 General motivation . . . 1
- 1.2 Research aims . . . 2
- 1.3 Contributions and Outline . . . 5

2 Preliminaries 7
- 2.1 Stability analysis of delay differential equations . . . 7
  - 2.1.1 Introduction . . . 7
  - 2.1.2 Retarded delay differential equations . . . 10
  - 2.1.3 Neutral delay differential equations . . . 14
- 2.2 Modeling errors, robustness analysis and performance . . . 17
  - 2.2.1 Pseudospectra . . . 18
  - 2.2.2 H-infinity norm . . . 23
- 2.3 Controller design . . . 32
  - 2.3.1 Controller architectures . . . 33
  - 2.3.2 Direct optimization framework . . . 34
  - 2.3.3 Nonsmooth, nonconvex optimization . . . 35

3 Strongly Stabilizing PID Controllers 39
- 3.1 Introduction . . . 39
- 3.2 Problem statement . . . 41
- 3.3 Losing stability under small implementation errors . . . 44
  - 3.3.1 Feedback delay . . . 44
  - 3.3.2 Finite-difference approximation of the derivative . . . 45
- 3.4 Strong stability . . . 47
  - 3.4.1 Losing stability under low-pass filtering . . . 47
  - 3.4.2 Strong stability framework . . . 49
  - 3.4.3 Illustration . . . 52
- 3.5 Design of strongly stabilizing PID controllers . . . 54
- 3.6 Extensions . . . 58
  - 3.6.1 Systems with relative degree larger than one . . . 58

3.6.2 Systems with input delay . . . 60
3.6.3 Systems with bounded uncertainties . . . 62
3.7 Conclusion . . . 63

4 The robust strong H_∞-norm of uncertain time-delay systems 65
4.1 Introduction . . . 65
4.2 Preliminaries . . . 67
4.2.1 The strong H_∞-norm . . . 67
4.2.2 Delay differential algebraic equations . . . 71
4.3 The robust strong H_∞-norm . . . 75
4.4 The robust distance to instability of an uncertain DDAE . . . 76
4.5 The robust strong H_∞-norm and the robust distance to instability 80
4.5.1 Preliminary results . . . 80
4.5.2 Robust distances to non well-posedness and a characteristic root chain crossing . . . 82
4.5.3 Robust distance to a finite root crossing . . . 86
4.5.4 Main theoretical result . . . 87
4.6 Illustration theoretical results . . . 88
4.6.1 Robust distance to non well-posedness . . . 88
4.6.2 Robust distance to characteristic root chain crossing . . 90
4.6.3 Robust distance to a finite root crossing . . . 95
4.7 Numerical algorithm for computing the robust strong H_∞-norm 98
4.7.1 High-level description . . . 98
4.7.2 Projected gradient flow method . . . 99
4.7.3 Computing the robust strong asymptotic H_∞-norm . . 99
4.7.4 Computing the pseudospectral abscissa . . . 100
4.8 Conclusion . . . 102

5 A scalable controller design method for networked systems 105
5.1 Introduction . . . 105
5.2 System description and control objective . . . 107
5.3 Upper bound for the H-infinity norm . . . 109
5.4 A scalable H-infinity controller synthesis method . . . 112
5.5 Example . . . 113
5.6 Conclusion . . . 116

6 A structure preserving shift-invert infinite Arnoldi algorithm 117
6.1 Introduction . . . 118
6.2 Preliminary results . . . 121
6.2.1 Properties of the considered DEP . . . 121
6.2.2 A structure preserving shift-invert Arnoldi method . . . 122
6.2.3 Two infinite-dimensional eigenvalue problems . . . 125
6.3 The structure preserving shift-invert infinite Arnoldi method . 128

6.4 Numerical implementation for the shift equal to zero 134
6.5 Numerical implementation for non-zero shift 137
6.6 Numerical illustration 142
6.6.1 Example 1 142
6.6.2 Example 2 145
6.7 Conclusion 145

7 TDS-CONTROL: a software package for time-delay systems 149
7.1 Introduction 149
7.2 Stability analysis 151
7.2.1 Retarded delay differential equations 151
7.2.2 Neutral delay differential equations 152
7.2.3 Delay differential algebraic equations 153
7.3 Stabilisation 154
7.4 The (strong) H-infinity norm and robust control 159
7.5 Robust stability analysis 161
7.6 Conclusion 166

8 Conclusions 167
8.1 Summary 167
8.2 Future work 170

A Controlling the variable length pendulum 173
A.1 Introduction 173
A.2 Problem formulation 175
A.3 Numerical optimization based open-loop control 176
A.4 Analysis of a bang-bang control law 180
A.5 Backstepping procedure 181
A.6 Conclusion 183

B Additional proofs for Chapter 6 185
B.1 Proof of Lemma 6.1 185
B.2 Proof that $\mathbf{B}(\cdot, J\cdot)$ is anti-symmetric 187
B.3 Derivation of the extension step for $\sigma = 0$ 188
B.4 Derivation of the extension step for $\sigma = \jmath\omega$ 188

Bibliography 191

Curriculum Vitae 211

List of publications 213

CHAPTER

1 Introduction

1.1 General motivation

The field of *dynamical systems and control theory* provides a mathematical framework to study the behavior of mechanical, electrical, and hyper-physical systems, such as planetary orbits, (self-driving) cars, the power network, or even the spread of an infectious disease [22, 64]. On the one hand, it is concerned with answering questions about the behavior (both quantitatively and qualitatively) of these systems (= **analysis**), e.g., "*Will the disease disappear or will everyone get infected over time?*". On the other hand, it is concerned with designing controllers that govern the inputs of the system in such a way that it exhibits some desirable behavior (= **controller design**). For example, a cruise control system must apply throttle and brake inputs such that a preset velocity is maintained.

A prerequisite for both analysis and controller design, is an adequate model that describes the system's behavior. However, for almost any application, this model is only an approximation of the real behavior [207, Chapter 8]. Firstly, the model might ignore certain (nonlinear) dynamics to simplify further derivations. Secondly, certain parameters may only be known up to some tolerances (due to the limited accuracy of measuring instruments or variations in the production process). Finally, a system typically does not stand on its own, but lives in an environment. As a consequence, (unmodeled) external influences may act on the system. Let us illustrate these sources of **uncertainty** by means of an example. Imagine that we want to design a self-driving car. Trying to derive a complete model for such a system would be nigh on impossible and working with such a model would be computationally expensive. Inevitably, one has to resort to an approximate model based on a limited number of parameters such as the mass of the car and the torque of the engine. However, these parameters are typically not completely known and may even change over time. Furthermore, there are also external effects such as gusts of wind or bumps in the road surface that may affect our car.

Another consideration that needs to be taken into account when analyzing a system or designing a controller, is that **delays** are inherently present in wide variety of applications. These delays originate for example from heredity in population dynamics, the transport of matter and energy in mechanical and electrical systems, or the time needed to communicate sensor measurements and

compute the control action in feedback systems [139]. More generally, time-delay systems are a class of dynamical systems in which the current evolution of the state does not only depend on its present value but also on its value in the past. To adequately model such systems, ordinary differential equations no longer suffice. Instead, delay differential equations, which explicitly take into account the dependency on the past, are necessary.

Finally, besides uncertainties and delays, another challenge faced by contemporary systems and control theory, is the need for efficient algorithms that can deal with **large-scale** or **networked** systems, such as the power grid [114]. The methods dealing with such systems must maximally exploit the specific structure at hand.

Based on the discussion above, the goal of this thesis is to develop novel analysis and controller synthesis methods

1. that take into account uncertainties on the model;
2. that explicitly consider delays; and
3. that can deal with large-scale and networked systems.

The remainder of this chapter is organized as follows. First, Section 1.2 translates the motivations given above into concrete research aims based on gaps in the current state-of-the-art literature. Subsequently, Section 1.3 summarizes how these challenges are addressed in this thesis.

1.2 Research aims

This thesis considers a wide variety of linear time-invariant time-delay systems with discrete (pointwise) delays. The dynamics of such systems are governed by delay differential equations (DDEs) augmented with input and output channels. Both retarded and neutral DDEs are considered in this thesis. Furthermore, special attention will be paid to a class of delay differential algebraic equations (DDAEs). For these systems, we will focus on analyzing and quantifying the effect of uncertainties and on robust controller design while keeping in mind large-scale and networked systems. More specifically, first we will address a well-posedness problem in which (under certain conditions) a stable closed-loop system consisting of a plant with state delays and a proportional-integral-derivative (PID) controller, can be destabilized by arbitrarily small perturbations. Next, we will consider the H_∞-norm, which is an important performance measure in robust theory as it (among other things) allows to quantify the effect of

uncertainties and disturbances on the behavior of the system. More specifically, we present a novel method to compute the robust H_∞-norm of time-delay systems with uncertainties on the system matrices, which is defined as the worst-case value of the H_∞-norm over all uncertainty values. Special attention will be paid to a fragility problem, namely the robust H_∞-norm might be sensitive to infinitesimal delay perturbations. We will therefore consider the robust strong H_∞-norm which is a continuous function of both the system matrices and the delays. Next, we will propose a controller design method that allows to (locally) minimize the robust (strong) H_∞-norm of the closed-loop system, focusing on an application from networked systems. Subsequently, we propose a structure-preserving infinite Arnoldi method to compute the eigenvalues of a large-scale Hamiltonian delay eigenvalue problem (DEP) close to the imaginary axis. The resulting algorithm can be used as a component in a numerical method for computing the H_∞-norm of large-scale time-delay systems. Finally, we will introduce a novel MATLAB package for the analysis and controller-design of time-delay systems with discrete delays. These research aims are spelled out in more details below.

Firstly, the PID control framework is a popular mechanism for governing the behavior of dynamical systems with and without delays [148, 19, 169]. However, some simple examples show that in certain situations, the resulting closed-loop system might suffer from a fragility problem, in the sense that stability might be lost by introducing arbitrary small perturbations. The **first aim** of this thesis is therefore to characterize this phenomenon in more detail and to subsequently propose a novel control synthesis approach that results in controllers which do not suffer from the aforementioned fragility problem.

Secondly, a novel method for computing the pseudospectral abscissa of a delay differential equation subject to structured, real-valued uncertainties on both the system matrices and the delays was recently presented in [28]. This result was subsequently used in [56] to design robustly stabilizing controllers for uncertain time-delay systems. However, (robust) stabilization is typically only the first step in a control design procedure. A good controller must also guarantee that certain performance criteria, such as good noise suppression or fast tracking with little overshoot, are satisfied. Such criteria can be expressed in terms of the H_∞-norm of appropriately defined transfer functions. However, as the considered model contains uncertainties, these performance criteria must be met for all possible realizations. We are therefore interested in computing the robust H_∞-norm, which is defined as the worst-case H_∞-norm over all admissible uncertainty values. The existing methods [118, 107, 54, 127, 101] for analyzing the robust H_∞-norm of uncertain time-delay systems, grounded in linear-matrix inequalities, are typically conservative, in the sense that they are based on sufficient conditions. Our **second aim** is therefore to develop a

method for explicitly computing the robust H_∞-norm of an uncertain time-delay system. After developing such an algorithm, our **third aim** is to implement a synthesis procedure for fixed-order output feedback controllers that addresses robust H_∞-design problems for uncertain time-delay systems. Developing such a synthesis procedure would extend the current state-of-the-art methods, which are typically conservative and limited to state feedback or dynamic output feedback with controllers whose order is equal to or larger than the order of the plant. Another difference with the existing literature is that this work considers uncertainties that are real-valued, as the model itself is real-valued, and structured, as often only a certain parameter or group of parameters is affected by an uncertainty.

Thirdly, in the past few years, the computation of the H_∞-norm of state-space systems with a large but sparse state matrix has been addressed in [76, 26, 4]. However, these methods only guarantee to return an underestimate for the H_∞-norm. To verify whether the provided value indeed corresponds to the actual H_∞-norm, [165] introduced a certification algorithm. This certification method involves verifying whether a Hamiltonian matrix has strictly imaginary eigenvalues. However, as the number of states is large, computing all eigenvalues of this Hamiltonian matrix is computationally intractable. Schwerdtner, Mengi and Voigt therefore propose to scan the imaginary axis for eigenvalues by repeatedly applying the structure-preserving shift-invert Arnoldi method for Hamiltoninan eigenvalue problems presented in [132, 131]. The main advantage of this structure-preserving Arnoldi method over the traditional Arnoldi methods is that it exploits the special structure of the Hamiltonian matrix. For example, it typically guarantees that simple, purely imaginary eigenvalues are preserved in numerical computations, even in the presence of rounding errors. This makes the structure-preserving Arnoldi method appealing for the application at hand. Our **fourth aim** is therefore to extend this structure-preserving Arnoldi method to Hamiltonian delay eigenvalue problems, which for example arise in the context of computing the H_∞-norm of large-scale time-delay systems.

Finally, there is a growing interest in numerical methods for the analysis and controller synthesis of time-delay systems. This has lead to the development of novel algorithms and implementations [186, 82, 57]. However, a unified framework is lacking. Our **fifth and final** aim is therefore to develop a MATLAB toolbox that provides (non-expert) users with easy-to-use tools for analyzing time-delay systems and designing (structured) fixed-order output feedback controllers. This software package is supplemented with a comprehensive manual that contains a wide range of examples to help new users get started with the provided software.

1.3 Contributions and Outline

This subsection gives an outline of the main contributions presented in this thesis, which seek to address the research aims introduced above.

Chapter 2 gives some preliminary results and introduces the necessary notation.

In **Chapter 3** we address the aforementioned fragility problem encountered when designing PID controllers for dynamical systems with state delays. First, we will demonstrate that under certain conditions on the derivative feedback gain, a stable closed-loop system might be destabilized by an arbitrary small feedback delay, an arbitrary accurate finite-difference approximation of the derivative, or by adding a low-pass filter with an arbitrary large cut-off frequency to the control loop. Subsequently, a 'robustified' notion of stability called *strong exponential stability*, which requires the closed-loop system to remain stable under sufficiently small perturbations, is introduced. We will prove that strong exponential stability can be achieved by adding a low-pass filter with a sufficiently large cut-off frequency to the control loop on the condition that this filter itself does not destabilize the nominal closed-loop system. This results in a computational procedure for designing strongly stabilizing PID controllers.
The results of this chapter were originally presented in [16] and [15].

In **Chapter 4** we present a novel method for computing the robust H_∞-norm of time-delay systems with structured, real-valued uncertainties. However, for the considered system class, this robust H_∞-norm is a fragile measure, as for a particular instance of the uncertainties, the H_∞-norm might be sensitive to arbitrarily small perturbations on the delays. Therefore, we introduce the robust strong H_∞-norm, which is a continuous function of both the elements of the system matrices and the delays. Subsequently, we demonstrate the relation between the robust strong H_∞-norm of an uncertain time-delay system and the robust distance to instability of an uncertain delay differential algebraic equation with both real- and complex-valued uncertainties. This equivalence is subsequently employed in a novel algorithm for computing the robust strong H-infinity norm.
This chapter is based on the results presented in [11] and [12].

In **Chapter 5** we consider a robust H_∞-controller synthesis problem for uncertain time-delay systems. In this way, the presented design algorithm complements the method in [56] for robust stabilization. We will focus on an application arising in the control of networked systems with identical subsystems. More specifically, we will see that under a particular assumption on the adjacency matrix describing the interconnection topology of the network, a H_∞-design problem for the complete network can be reformulated in terms of a robust

H_∞-design problem for a single subsystem. As a consequence, the resulting method can be applied to large networked systems as the computation cost does not depend on the number of subsystems.
This chapter summarizes the results originally presented in [14].

In **Chapter 6** a novel iterative method for computing the eigenvalues of a large-scale Hamiltonian delay eigenvalue problem near the imaginary axis is presented. To this end, a specifically chosen shift-invert transformation, which has the advantage that the corresponding spectrum has a "real skew-Hamiltonian"-like structure, is introduced. Furthermore, it is proven that the Krylov space constructed by applying this operator satisfies an orthogonality property in terms of a specifically chosen bilinear form. We will see that as a consequence the approximations obtained using the presented method for purely imaginary, simple eigenvalues are typically also purely imaginary and simple. As mentioned before, this property is vital for a seamless integration in existing level-set or certification methods for computing the H_∞-norm of time-delay systems. Although the presented method is initially defined on function spaces, it can be implemented using finite dimensional linear algebra operations by approximating the encountered functions using an interpolating Chebyshev polynomial of a sufficiently high degree.
The contents of this chapter were originally presented in [13].

Chapter 7 briefly introduces `TDS-CONTROL`, a novel MATLAB package for the analysis and controller design of time-delay systems. An overview of its capabilities is given by means of several examples, including the code that was used to generate Figures 2.1, 2.2, and 4.1. The code for this package is available for download from `https://gitlab.kuleuven.be/u0011378/tds-control` and the accompanying manual can be found at `https://gitlab.kuleuven.be/u0011378/tds-control/-/blob/main/documentation/main.pdf`.
This chapter is loosely based on the results presented in [17] and the `TDS-CONTROL` manual.

Chapter 8 draws some concluding remarks and gives an outlook to future work.

In **Appendix A** we examine the stabilization of the variable length pendulum. We focus on the numerical solution of two optimal control problems. Subsequently, we briefly summarize the analysis of a bang-bang control law and a backstepping procedure to design a Lyapunov-based controller. Finally, this last control law is experimentally compared with a time-delay based feedback law.
This chapter summarizes the results presented in [5].

CHAPTER

2 Preliminaries

Abstract

This chapter introduces some preliminary results and notation. Section 2.1 considers delay differential equations, focusing on the stability analysis of LTI DDEs with discrete (pointwise) delays. The next section examines how the effect of uncertainties and modeling errors on the behavior of a dynamical system can be quantified. More specifically, it will introduce pseudospectra, the distance to instability, and robust control by means of the H_∞-norm. For simplicity, we will restrict our attention to uncertain ordinary differential equations with brief pointers to extensions for delay differential equations. Finally, Section 2.3 considers controller design by means of a direct optimization approach.

2.1 Stability analysis of delay differential equations

A delay differential equation is a differential equation in which the time-evolution of the state variable not only depends on its current value but also on its past history [21]. As such, DDEs fit within the class of functional differential equations (FDEs). In this section we will briefly examine the behavior of such delay differential equations. Before continuing with the stability analysis of linear-time invariant DDEs, let us formalize the discussion above by introducing the necessary notations and give a brief history of the field. To this end we will start with further subdividing the class of DDEs.

2.1.1 Introduction

Preliminary concepts and notation

Firstly, we consider a class of retarded DDEs, in which the time-evolution of the state variable at time t depends on its current value and its value over a past interval, or mathematically:

$$\dot{x}(t) = f(t, x_t) \text{ for } t \geq t_0 \tag{2.1}$$

with $x(t) \in \mathbb{C}^n$ the state variable at time t and x_t a function segment describing the evolution of the state variable over an interval of length $\tau > 0$, i.e., $x_t(\theta) = x(t+\theta)$ for $\theta \in [-\tau, 0]$. The function segment x_t can be interpreted as the state[1] of the differential equation at time t. In contrast to an ordinary differential equation (ODE), for which the state is a vector, a DDE is thus in some sense infinite dimensional. As corresponding state space we will consider the Banach space of continuous function segments that map the interval $[-\tau, 0]$ to $\mathbb{C}^n$ equipped with the supremum norm. This space will be denoted by X, i.e.,

$$X = \mathrm{C}\left([-\tau, 0], \mathbb{C}^n\right) \text{ and } \|\varphi\|_s := \sup_{\theta \in [-\tau, 0]} \|\varphi(\theta)\|_\infty \text{ for } \varphi \in X.$$

Given an initial segment φ belonging to X, i.e., $x_{t_0} = \varphi$, and by making the necessary assumptions on the right-hand side functional $f : [t_0, \infty) \times X \mapsto \mathbb{C}^n$, it can be shown that the differential equation (2.1) has a unique forward solution [87, Chapter 2].

Secondly, we consider DDEs of neutral type, in which the time-evolution of the state variable also depends on its time-derivative in the past:

$$\frac{\mathrm{d}}{\mathrm{d}t} D(t, x_t) = f(t, x_t) \text{ for } t \geq t_0 \tag{2.2}$$

with $D : [t_0, \infty) \times X \mapsto \mathbb{C}^n$ and x, f, and x_t as defined above. As for the retarded case, by making the necessary assumptions, it can be shown that given an initial function segment, the neutral DDE (2.2) has a unique forward solution [87, Chapter 12].

Finally, there are DDEs of advanced type in which the evolution of the state variable also depends on its future value. As such differential equations are clearly not causal, we will ignore them in the remainder of this thesis.

History, literature overview and applications

Almost one hundred years ago, the topic of FDEs got its first treatment in the work of Sharpe and Lotka on epidemics [167], and in the work of Volterra on viscoelasticity and population dynamics [191, 192]. Since then, the field has gained much attention, witnessed by the vast amount of monographs and books devoted to the topic, including, among others, [145, 109, 21, 60, 87, 126, 108, 89, 73, 67, 139]. For a more complete overview of the history of functional differential equations, we refer the interested reader to [88]. This growing interest in DDEs and FDEs, originates from the fact that differential equations with an explicit dependency on the past arise in many applications in

[1] the minimal information needed to forward simulate the differential equation

biology, physics and engineering. Just to mention a few: lasers [62], modeling of infectious diseases [122], metal cutting processes [95], and even the study of the (asymptotic) distribution of prime numbers [200]. Finally, although neutral DDEs might seem artificial at first sight, they arise in models for lossless transmission lines [35] and vibration suppression systems with delayed acceleration feedback [195].

In the context of control systems, delays typically appear due the time needed to collect measurements and compute a suitable control action. When not properly accounted for, such a feedback delay can be detrimental for the stability and the performance of the controlled system [53, 146]. However, in certain control applications, feedback delays are introduced on purpose. For example, the derivative of a signal can be approximated using finite differences, i.e., $\dot{x}(t) \approx \frac{x(t)-x(t-\tau)}{\tau}$. Furthermore, in some cases introducing or increasing a feedback delay may even induce stability or improve performance [166]. A notable example is the delayed resonator, which uses a delayed feedback signal to turn a physical absorber into a resonator which on its turn allows to suppress the vibrations at a target location in a mass-spring-damper system [149].

Below we will discuss Laplace-domain methods for analyzing the stability of linear time-invariant delay differential equations with discrete (pointwise) delays (sometimes also referred to as differential difference equations). More specifically, we will characterize the exponential stability of their null solution based on the location of their characteristic roots. The presented exposition is based on [21, 89, 175, 73, 139, 37]. A more extensive discussion and the proofs for the presented results can be found in these works and the references therein. In our discussion, we will differentiate between retarded and neutral DDEs, as there are fundamental differences between the two classes.

An alternative for the frequency-based methods discussed below, are time-domain methods, such as generalizations of Lyapunov's second method [124] to functional differential equations [160, 109, 67]. For LTI delay differential equations with discrete delays, these time-domain approaches typically give rise to stability conditions in terms of the feasibility of a linear matrix inequality (LMI), which can be verified efficiently using an interior point method [33]. In contrast to the considered Laplace-domain techniques, Lyapunov analysis is applicable to a broader range of systems, including nonlinear and stochastic differential equations. However, even for LTI delay differential equations the obtained stability conditions are typically only sufficient. A notable exception is [71], which presents a condition that is both necessary and sufficient.

All figures in the remainder of this section were generated using the MATLAB package `TDS-CONTROL`. The code to generate these figures is given in Chapter 7.

2.1.2 Retarded delay differential equations

In this subsection we consider LTI delay differential equations of retarded type with pointwise delays. These DDEs take the following general form:

$$\dot{x}(t) = A_0 x(t) + \sum_{k=1}^{m} A_k x(t-\tau_k) \text{ for } t \geq 0, \tag{2.3}$$

in which the state variable $x(t)$ belongs to $\mathbb{C}^n$ for $t \geq -\tau_m$, the state matrices A_k for $k = 0, \ldots, m$ belong to $\mathbb{R}^{n\times n}$ and the state delays $\tau_1 < \cdots < \tau_m$ are real-valued positive numbers. For ease of notation, we use the vector $\vec{\tau} = \left[\tau_1, \tau_2, \ldots, \tau_m\right]$ in the remainder of this chapter.

Let us first discuss the existence and uniqueness of the solutions for the initial value problem associated with (2.3). It follows from the discussion for general retarded DDEs above that given an initial state φ in X, (2.3) has a unique forward solution, which we will denote by $x(t;\varphi)$ for $t \in [-\tau_m, \infty)$. Another important question when analyzing (2.3) is the existence of equilibrium solutions and the behavior of the DDE near these equilibria, i.e., *"Will a small perturbation on the state eventually grow large or will we return to the equilibrium?"*. It is easy to verify that the null solution $x \equiv 0$ is an equilibrium solution of (2.3). Next we examine the (exponential) stability of this equilibrium. To this end, let us formally introduce the notion of exponential stability.

Definition 2.1. The null solution of (2.3) is **exponentially stable** if and only if there exists constants $\beta > 0$ and $\gamma > 0$ such that

$$\|x(t;\varphi)\|_\infty \leq \beta e^{-\gamma t} \|\varphi\|_s \text{ for any } \varphi \in X.$$

In the reminder of this thesis, we will, with a slight abuse of terminology, say that (2.3) is exponentially stable when its null solution is. Furthermore, notice that for an LTI delay differential equation, exponential stability implies that **all** solutions converge (exponentially fast) to the origin, i.e., local exponential stability of the null solution implies global exponential stability.

Next we will introduce a necessary and sufficient condition for the exponential stability of (2.3). To this end we plug the sample solution $v\, e^{\lambda t}$ with $\lambda \in \mathbb{C}$ and $v \in \mathbb{C}^n \setminus \{0\}$ into (2.3), from which we obtain the characteristic function:

$$\mathbb{C} \ni \lambda \mapsto F_R(\lambda) := \det\left(\lambda I_n - A_0 - \sum_{k=1}^{m} A_k e^{-\lambda\tau_k}\right), \tag{2.4}$$

or, equivalently, the delay eigenvalue problem (DEP):

$$\underbrace{\left(\lambda I_n - A_0 - \sum_{k=1}^{m} A_k e^{-\lambda\tau_k}\right)}_{M(\lambda)} v = 0, \tag{2.5}$$

in which the characteristic matrix $M(\lambda)$ depends nonlinearly on the eigenvalue λ. Notice that where for an ODE the characteristic function is a polynomial of degree n, (2.4) is a quasi-polynomial which generally has infinitely many roots. However, the following proposition shows that any right half-plane can only contain finitely many characteristic roots.

Proposition 2.1. For any $\alpha \in \mathbb{R}$, the retarded DDE (2.3) can only have finitely many characteristic roots in the right half-plane $\{z \in \mathbb{C} : \Re(z) \geq \alpha\}$.

Below we will introduce the relation between the exponential stability of (2.3) and the location of its characteristic roots (or equivalently the eigenvalues of (2.5)). To this end, let us introduce the following two notions.

Definition 2.2. The **spectrum** of (2.3), denoted by Λ, is defined as the set of all its characteristic roots[2], i.e.,

$$\begin{aligned}\Lambda(A_0, \ldots, A_m, \vec{\tau}) &:= \{\lambda \in \mathbb{C} : F_R(\lambda) = 0\} \\ &= \{\lambda \in \mathbb{C} : \exists v \in \mathbb{C}^n \setminus \{0\} \text{ such that (2.5) holds}\}.\end{aligned}$$

Similarly, we can define the spectral abscissa of (2.3).

Definition 2.3. The **spectral abscissa** of (2.3) is defined as the smallest upper bound for the real part of the elements in its spectrum, i.e.,

$$c(A_0, \ldots, A_m, \vec{\tau}) := \sup \{\Re(\lambda) : \lambda \in \Lambda(A_0, \ldots, A_m, \vec{\tau})\}. \tag{2.6}$$

Note that in the following, we will sometimes omit the explicit dependency of the spectrum Λ and the spectral abscissa c on the system matrices and delays for sake of readability.

Remark 2.1. It follows from Proposition 2.1 that the spectrum of a **retarded** DDE can only have a finite number of rightmost characteristic roots. As a consequence, the supremum operator in (2.6) can be replaced by taking the maximum. However, as we will see in the following subsection, this is not the case for neutral DDEs.

We are now ready give a necessary and sufficient condition for the exponential stability of (2.3) based on the location of its characteristic roots.

[2]Using the term "spectrum" to denote the set containing the roots of (2.4) may seem not completely mathematically sound. However, it can be show that the set Λ corresponds to the spectrum of the infinitesimal generator of the solution operator associated with (2.3), which is a linear but infinite-dimensional operator.

Theorem 2.1. The null solution of (2.3) is exponentially stable if and only if its spectral abscissa is strictly negative.

Remark 2.2. For a retarded DDE a negative spectral abscissa corresponds to all characteristic roots lying in the open left half-plane.

Next, we will give an important result which will be necessary in our discussion on controller design and robust stability. The theorem follows from [139, Proposition 1.14], which indicates that the individual characteristic roots of (2.3) move continuously in the complex plane when the entries of the system matrices and the delays values are varied continuously.

Theorem 2.2. The spectral abscissa (as defined in Definition 2.3) depends continuously on the entries of the system matrices $A_0, \ldots, A_m$ and the delay values $\tau_1, \ldots, \tau_m$.

Remark 2.3. Theorem 2.2 implies that for a retarded DDE, a transition from stability to instability corresponds to a finite number of characteristic roots crossing the imaginary axis.

Let us illustrate these results by means of a simple example.

Example 2.1. Consider the following retarded delay differential equation

$$\dot{x}(t) = -2\,x(t) + 2\,x(t-1) + x(t-1.5). \tag{2.7}$$

Figure 2.1 shows the spectrum of (2.7) in the right half-plane $\{z \in \mathbb{C} : \Re(z) \geq -4\}$. (From a stability point of view, we are only interested in the rightmost characteristic roots.) In this case one of the characteristic roots lies in the right half-plane, meaning that (2.7) is not exponentially stable. ◇

In some cases, such as for differential equations with a small number of parameters or a few delays, an analytic characterization of stability in terms of the parameters and the delay values is possible. More precisely, recall from Remark 2.2 that for stability analysis one does not need to know the exact location of the characteristic roots, but rather whether they all lie in the open left half-plane. Therefore, if for a given set of parameters and the delay values the number of right half-plane roots is known, one can construct stability charts by detecting when characteristic roots cross the imaginary axis as the parameters or the delays are varied. The D-decomposition method (the delays are fixed and parameters are varied) and the τ-decomposition method (the parameters are fixed and the delays are varied) are based on this idea. However, for DDEs with more than a few parameters and/or delays such a characterization is often not feasible. In such a case, one needs to rely upon numerical methods to compute

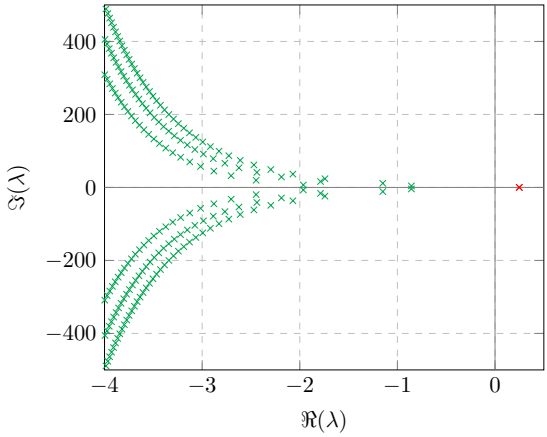

Figure 2.1: The characteristic roots of (2.7) with real part larger than -4.

the characteristic roots of (2.3). Below we will give a brief overview of some well-established approaches for computing characteristic roots of (retarded) DDEs.

Firstly, the Quasi-Polynomial mapping-based Root-finder (QPmR) [196, 197] directly looks for the zeros of (2.4) in a rectangular region of the complex plane. To this end, it evaluates the characteristic function on a grid and uses the MATLAB `contour`-function to estimate the zero-level curves of its real and imaginary part. The characteristic roots of (2.3) are now obtained by finding the intersections of these curves. Because QPmR requires the explicit construction of the characteristic quasi-polynomial, it might run into numerical issues for (large) systems, as the roots of a quasi-polynomial may be (very) sensitive to perturbations on its coefficients.

A second approach is the semi-discretisation method presented in [96, 97]. The main idea of this method is to replace the delays in (2.3) by time-periodic delays with period Δt such that $t - \tau_k(t)$ becomes piece-wise constant. Firstly, this approximation leads to a discretisation of the state x_t, namely its values at multiples of Δt. Secondly, it allows to derive an explicit, linear, finite-dimensional expression for the solution operator $T(\Delta t)$, which maps the state at time 0 to the state at time Δt. By computing the eigenvalues of the matrix $T(\Delta t)$, we obtain (after a suitable transformation) an approximation for the characteristic roots of (2.3). By letting Δt go to zero, the obtained approximations converge to the characteristic roots of (2.3). Other methods based on a finite dimensional approximation of the solution operator underlying (2.3) are used in the MATLAB packages `ddec` [46, 40] and DDE-BIFTOOL [61].

A third category of methods is based on the spectral discretisation of the infinitesimal generator of the solution operator underling the DDE. An example of such a method is the TRACE-DDE software package [36]. In [201] this method is complemented with an approach to automatically determine the number of discretization points necessary to capture all characteristic roots in a desired right half-plane. Furthermore, the authors also propose to improve the approximations obtained from the spectral discretization using Newton's method. A variant of this method is presented in [99], which allows to deal with large and sparse state matrices.

Finally, one can use general methods for computing the roots of analytic functions [55, 110] or for solving nonlinear eigenvalue problems (NEPs) [111, 85, 84, 98].

2.1.3 Neutral delay differential equations

In this subsection, we will see that the stability analysis of neutral delay differential equations, is more involved than for retarded systems. Here we will consider LTI neutral DDEs with discrete delays, which take the following general form:

$$\dot{x}(t) = A_0\, x(t) + \sum_{k=1}^{m} A_k\, x(t-\tau_k) - \sum_{k=1}^{m} H_k\, \dot{x}(t-\tau_k) \tag{2.8}$$

with the state variable $x(t) \in \mathbb{C}^n$ for $t \geq -\tau_m$, the matrices $A_k \in \mathbb{R}^{n\times n}$ for $k = 0, \ldots, m$, the matrices $H_k \in \mathbb{R}^{n\times n}$ for $k = 1, \ldots, m$ and the delays $\tau_1, \ldots, \tau_m$ real-valued positive numbers.

As mentioned before, it can be shown that (2.8) has a unique solution (under certain assumptions on the initial state ϕ). Next we will see how the exponential stability of (the null solution of) (2.8) can be analyzed in terms of the zeros of its characteristic function,

$$\mathbb{C} \ni \lambda \mapsto F_N(\lambda) := \det\Big(\lambda\big(I_n + \sum_{k=1}^{m} H_k e^{-\lambda\tau_k}\big) - A_0 - \sum_{k=1}^{m} A_k e^{-\lambda\tau_k}\Big), \tag{2.9}$$

or, equivalently in terms of the solutions of the nonlinear eigenvalue problem

$$\Big(\lambda\big(I_n + \sum_{k=1}^{m} H_k e^{-\lambda\tau_k}\big) - A_0 - \sum_{k=1}^{m} A_k e^{-\lambda\tau_k}\Big)v = 0 \tag{2.10}$$

with $v \in \mathbb{C}^n \setminus \{0\}$. The definition for the spectrum and the spectral abscissa of (2.8) carry over from the retarded case. The same holds true for the relation

between the exponential stability of (2.8) and its spectral abscissa, i.e., the neutral DDE (2.8) is exponentially stable if and only if its spectral abscissa is strictly negative. However there are two main differences with respect to the retarded case. Firstly, Proposition 2.1 no longer holds, and as a consequence a right half-plane may contain infinitely many characteristic roots (as we will see in the example below). Therefore, both Remarks 2.1 and 2.2 are no longer valid. This means for example that there exist neutral DDEs for which all characteristic roots lie in the open left half-plane, but whose null solution is not exponentially stable [189]. Secondly, also Theorem 2.2 does no longer hold. As we will see in the example below, the spectral abscissa of a neutral DDE might be a discontinuous function of the delay values. As a consequence, the exponential stability of a neutral DDE might be sensitive to infinitesimal delay perturbations [90].

Example 2.2. Consider the following neutral DDE

$$\dot{x}(t) = \frac{1}{4}x(t) - \frac{1}{3}x(t-\tau_1) + \frac{3}{4}\dot{x}(t-\tau_1) - \frac{1}{2}\dot{x}(t-\tau_2) \tag{2.11}$$

with τ_1 and τ_2 positive delay values. Figure 2.2 shows the characteristic roots of (2.11) in the region $[-0.9, 0.2] \times \jmath[-900, 900]$ for several delay values. Firstly, it is clear that Proposition 2.1 no longer holds as the spectrum for $\vec{\tau} = (1, 2)$ contains a vertical sequence (chain) of characteristic roots for which the real part remains confined to the interval $[-0.9, 0.2]$ but for which the absolute value of the imaginary part grows to infinity. Secondly, let us examine the effect of (arbitrarily) small delay perturbations. We notice that for $\tau_1 = 1$ and $\tau_2 = 2$ the differential equation is exponentially stable, as all characteristic roots lie in the open left half-plane and are bounded away from the imaginary axis (i.e., the spectral abscissa is strictly negative). However, by making a small perturbation to the second delay, e.g., $\tau_2 = 2.01$, the spectral abscissa becomes positive and as a consequence (2.11) is no longer exponentially stable. Even when the delay perturbation is further decreased, e.g., $\tau_2 = 2.005$, the NDDE (2.11) remains unstable. It can furthermore be shown that there exist delay values arbitrarily close to $\tau_1 = 1$ and $\tau_2 = 2$ for which (2.11) is unstable. ◇

Remark 2.4. The discontinuity of the spectral abscissa of (2.8) with respect to the delay values is not in contradiction with the continuous variation of the individual characteristic roots under continuous changes on both the entries of the system matrices and the delay values. It can be observed in Figure 2.2 that along the vertical chain the sensitivity (i.e., the derivative) of the characteristic roots with respect to delay changes grows larger as the frequency (i.e., the absolute value of the imaginary part) increases. In fact, this derivative grows unbounded along the chain. As a consequence, when the bound on the size of the delay perturbation goes to zero, the imaginary part of the destabilizing roots must go to infinity (as indicated by the arrows in Figure 2.2c).

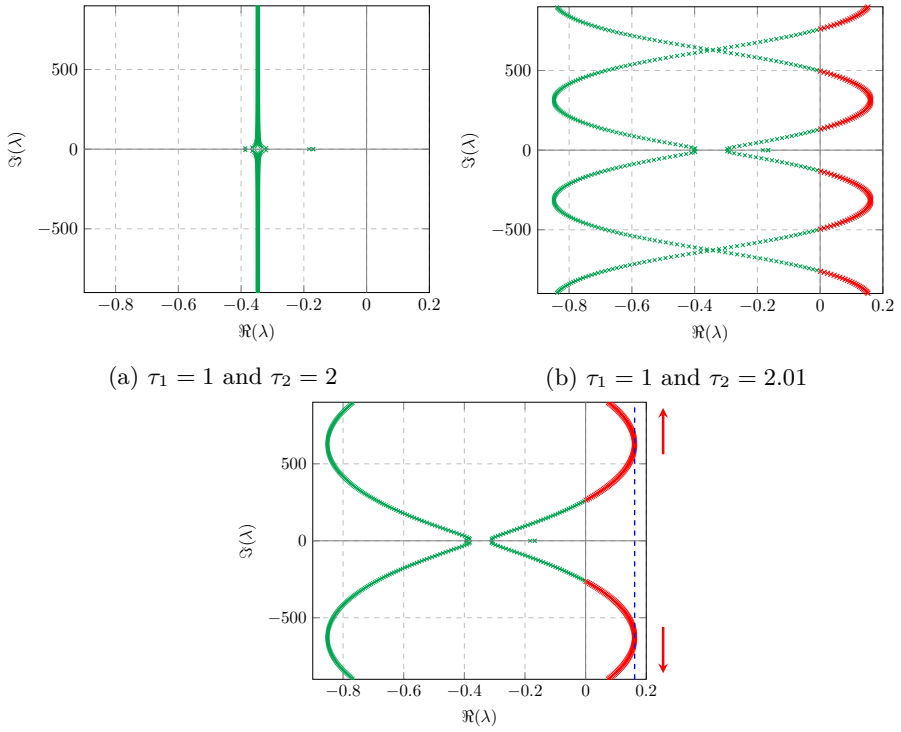

(a) $\tau_1 = 1$ and $\tau_2 = 2$

(b) $\tau_1 = 1$ and $\tau_2 = 2.01$

(c) $\tau_1 = 1$ and $\tau_2 = 2.005$

Figure 2.2: The characteristic roots of (2.11) for several delay values in the region $[-0.9, 0.2] \times \jmath[-900, 900]$.

It is clear from this example that the definition for exponential stability given in Definition 2.2 is a **fragile** notion for neutral DDEs, in the sense that it does not account for (arbitrarily) small delay perturbations (which may destroy stability). Let us therefore introduce the notion of *strong* exponential stability.

Definition 2.4. The null solution of (2.8) is *strongly* exponentially stable if it remains exponentially stable when subjected to (sufficiently) small variations on the delays.

In a similar vain, let us introduce the strong spectral abscissa as the smallest upper bound for the spectral abscissa that is insensitive to small delay changes.

Definition 2.5. The *strong* spectral abscissa of (2.8), denoted by C, is defined as

$$C(\vec{\tau}) := \lim_{\epsilon \searrow 0+} \sup\{c(\vec{\tau}_\epsilon) : \vec{\tau}_\epsilon \in \mathcal{B}(\vec{\tau}, \epsilon) \cap \mathbb{R}_+^m\},$$

in which we dropped the dependency of the (strong) spectral abscissa on the system matrices for notational convenience and $\mathcal{B}(\vec{\tau}, \epsilon)$ is an open ball of radius $\epsilon > 0$ centered at $\vec{\tau}$.

In contrast to the nominal spectral abscissa, the strong spectral abscissa is continuous with respect to both the entries of the system matrices and the delays. Furthermore, we have the following relation between the strong spectral abscissa and the strong exponential stability of (2.8).

Theorem 2.3. The null solution of the neutral DDE (2.8) is strongly exponentially stable if and only if its strong spectral abscissa is strictly negative.

Example 2.3. Let us return to Example 2.2. It can be shown that the strong spectral abscissa of (2.11) for $\vec{\tau} = (1, 2)$ is equal to $-\ln\left(\frac{-3+\sqrt{41}}{4}\right) \approx 0.1616$. Thus, although (2.11) is exponentially stable for $\vec{\tau} = (1, 2)$, it is not strongly exponentially stable, as there exist (arbitrarily) small perturbations on the delays for which the spectral abscissa jumps to approximately 0.1616 (indicated by a blue dashed line in Figure 2.2c). ◇

Remark 2.5. The aforementioned fragility problem can be related to a similar observation for the exponential stability of the following delay difference equation underlying (2.8)

$$x(t) + \sum_{k=1}^{m} H_k \, x(t - \tau_k) = 0.$$

We will come back to this relation in Section 4.2.2, which examines the strong exponential stability of a class of delay differential algebraic equations and which presents a mathematical characterization for the strong spectral abscissa that is amenable for numerical computations.

2.2 Modeling errors, robustness analysis and performance

In the previous section we examined the exponential stability of an LTI delay differential equation, (implicitly) assuming that the given model perfectly matches the underlying (physical) system or process. However, as mentioned in the introduction, in practice there is typically a mismatch between model and reality due to unmodeled (nonlinear) behavior, parameter uncertainties, and external disturbances. The study of **pseudospectra** and the field of **robust control theory** deal with quantifying the effect of these uncertainties. Below we will discuss both methodologies in more detail. Firstly, we will consider

pseudospectra, which have their origin in the study of (non-normal) matrices and operators. Secondly, we will examine the H_∞-control framework, which has its origin in the control engineering community of the eighties. The discussion of the former is mainly based on [93, Chapters 4 and 5], while the discussion of the latter is mainly based on [206] (and the accompanying textbook [207]). For simplicity, we restrict our attention to delay-free systems with brief pointers to extensions for systems with delay.

2.2.1 Pseudospectra

Consider the following (family of) ordinary differential equation(s)

$$\dot{x}(t) = (A + B\Delta C)\, x(t) \tag{2.12}$$

with the state variable $x(t) \in \mathbb{R}^n$ and the state matrix $A \in \mathbb{R}^{n\times n}$. The matrix Δ belongs to $\mathbb{K}^{p\times q}$ models a (time-invariant) uncertainty, in which, depending on the application at hand, $\mathbb{K}$ can either be the set of real or complex numbers. The matrices $B \in \mathbb{R}^{n\times p}$ and $C \in \mathbb{R}^{q\times n}$ are shape matrices that allow to target certain entries of the state matrix A. Consider for example a (frictionless) mass-spring system which is modeled by the following first-order ordinary differential equation

$$\dot{x}(t) = \begin{bmatrix} 0 & 1 \\ \frac{-k}{m} & 0 \end{bmatrix} x(t) \tag{2.13}$$

with k the spring constant and m the mass. In this example, only the entry on position (2,1) of the state matrix depends on the parameters k and m, while the other entries of A follow from the particular transformation used to write the system's dynamics as a first-order differential equation. It is therefore reasonable to assume that only the bottom-left entry of A is uncertain. This can be achieved by choosing

$$B = \begin{bmatrix} 0 \\ 1 \end{bmatrix} \text{ and } C = \begin{bmatrix} 1 & 0 \end{bmatrix}.$$

Remark 2.6. The differential equation (2.12) can be interpreted as the feedback interconnection of the open-loop (state-space) system

$$\left\{ \begin{array}{rcl} \dot{x}(t) & = & A\,x(t) + B\,w(t), \\ z(t) & = & C\,x(t) \end{array} \right. \tag{2.14}$$

with the static output feedback law $w(t) = \Delta\, z(t)$.

The study of pseudospectra (sometimes also referred to as spectral value sets) allows to examines the effect of norm-bounded perturbations on the characteristic

roots of (2.12) (or equivalently, the eigenvalues of A) as stated more rigorously in the following definition.

Definition 2.6. Given an uncertain differential equation of the form (2.12), a normed vector space $\mathbb{K}^{p\times q}$ equipped with a norm $\|\cdot\|$, and a bound ϵ, the ϵ-pseudospectrum of (2.12) is then defined as

$$\Lambda^{\mathrm{ps}}_{\mathbb{K},\|\cdot\|}(\epsilon; A, B, C) := \bigcup_{\substack{\Delta\in\mathbb{K}^{p\times q}\\ \|\Delta\|\leq\epsilon}} \Lambda(A + B\Delta C).$$

In other words, the ϵ-pseudospectrum corresponds to the set in the complex plane to which a characteristic root of (2.12) can be moved by a perturbation $\Delta \in \mathbb{K}^{p\times q}$ with $\|\Delta\| \leq \epsilon$.

Note that both induced norms, such as the spectral norm, as well as, "entry-wise" norms, such as the Frobenius norm can be considered. Next we introduce the pseudospectral abscissa.

Definition 2.7. Given an uncertain differential equation of the form (2.12), a normed vector space $\mathbb{K}^{p\times q}$ equipped with a norm $\|\cdot\|$, and a bound ϵ, the ϵ-pseudospectral abscissa is defined as the smallest upper bound for the real part of the elements in the ϵ-pseudospectrum, i.e.,

$$c^{\mathrm{ps}}_{\mathbb{K},\|\cdot\|}(\epsilon; A, B, C) := \sup\left\{\Re(\lambda) : \lambda \in \Lambda^{\mathrm{ps}}_{\mathbb{K},\|\cdot\|}(\epsilon; A, B, C)\right\}.$$

The ϵ-pseudospectral abscissa thus quantifies the worst-case exponential decay (or growth) rate of (2.12) over all $\Delta \in \mathbb{K}^{p\times q}$ with $\|\Delta\| \leq \epsilon$, i.e.,

$$c^{\mathrm{ps}}_{\mathbb{K},\|\cdot\|}(\epsilon; A, B, C) := \sup_{\substack{\Delta\in\mathbb{K}^{p\times q}\\ \|\Delta\|\leq\epsilon}} \{\Re(\lambda) : \lambda \in \Lambda(A + B\Delta C)\}. \tag{2.15}$$

If a bound on the size of the uncertainty Δ is known, then the ϵ-pseudospectral abscissa allows to characterize the exponential stability of the uncertain system (2.12). More specifically, system (2.12) is exponentially stable for all $\Delta \in \mathbb{K}^{p\times q}$ with $\|\Delta\| \leq \epsilon$ if and only if the corresponding ϵ-pseudospectral abscissa is strictly negative. Next, we consider a related problem: *"What is the largest ϵ such that* (2.12) *is exponentially stable for all $\Delta \in \mathbb{K}^{p\times q}$ with $\|\Delta\| \leq \epsilon$?"*. The notion of the distance to instability (sometimes also referred to as the stability radius) provides an answer to this question.

Definition 2.8. The distance to instability is defined as the smallest ϵ for which the ϵ-pseudospectral abscissa becomes non-negative:

$$\mathrm{r}_{\mathbb{K},\|\cdot\|}(A, B, C) = \inf\{\epsilon \in [0, \infty) : c^{\mathrm{ps}}_{\mathbb{K},\|\cdot\|}(\epsilon; A, B, C) \geq 0\},$$

or, in other words, the distance to instability is the norm of the smallest perturbation that destabilizes the uncertain differential equation.

Remark 2.7. As the characteristic roots of (2.12) move continuously with respect to the entries of Δ, the distance to instability corresponds to the norm of the smallest perturbation that moves a characteristic root to the imaginary axis (assuming stability for $\Delta = 0_{p\times q}$).

In the discussion above, we restricted our attention to the situation in which the uncertain ODE depended affinely on the time-invariant, full-block perturbation Δ. One could however consider more general uncertainty classes. Firstly, a certain (sparsity) pattern can be imposed on the perturbation, e.g., the matrix Δ must be (block)-diagonal (which, in combination with the appropriate shape matrices, allows to model multiple perturbations). Secondly, one can consider time-varying perturbations. Thirdly, the dependency of the uncertain state matrix on the perturbation can be changed. Recall from Remark 2.6 that (2.12) corresponds to the feedback interconnection of the state-space system (2.14) and the static (linear) feedback law $w = \Delta\, z$. However, when introducing a direct feed-through term in (2.14), the system matrix of the uncertain ODE corresponding to the feedback interconnection with $w = \Delta\, z$ becomes

$$A + B(I - \Delta D)^{-1}\Delta C \text{ for } \det(I - \Delta D) \neq 0 \tag{2.16}$$

with $D \in \mathbb{R}^{q\times p}$ the direct feed-through matrix. Similarly, we can replace the linear feedback law by a nonlinear one. For more details, we refer the interested reader to [93]. Finally, let us make a brief remark on DDEs. When considering uncertain delay differential equations there are even more ways in which the perturbations may affect the system. For example, there might be different perturbations acting on the different state matrices or the same perturbation may affect multiple state matrices. Furthermore, there can also be uncertainty on the delay values.

Example 2.4. Consider again (2.13). Let us now assume that the parameters k and m are respectively affected by bounded (real-valued) uncertainties Δ_k and Δ_m with $|\Delta_k| \leq \epsilon_k$ and $|\Delta_m| \leq \epsilon_m$. To model this situation the state matrix of the uncertain differential equation takes the form (2.16) with

$$\Delta = \begin{bmatrix}\Delta_{11} & \Delta_{12}\end{bmatrix},\ B = \begin{bmatrix}0\\ 1/m^2\end{bmatrix},\ C = \begin{bmatrix}-m\epsilon_k & 0\\ k\epsilon_m & 0\end{bmatrix}, \text{ and } D = \begin{bmatrix}0\\ -\epsilon_m/m\end{bmatrix}$$

with $\Delta \in \mathbb{R}^{1\times 2}$ and as corresponding norm we choose the induced 1-norm (which in this case corresponds to $\max\{|\Delta_{11}|, |\Delta_{12}|\}$). The system is now exponentially stable for all $|\Delta_k| \leq \epsilon_k$ and $|\Delta_m| \leq \epsilon_m$ if and only if the corresponding ϵ-pseudospectral abscissa is strictly negative for $\epsilon = 1$. ◇

Applications

It is clear from the discussion above that the pseudospectral abscissa and the distance to instability provide a framework to examine the exponential stability of uncertain dynamic systems. The importance of the distance to instability as a measure for robust stability was first considered in [185, 92]. Related distance problems are examined in [59] (distance to uncontrollability) and [48] (distance to the nearest singular pencil). The study of multiple perturbations (i.e., Δ is blockdiagonal) is closely related to the notion of the structured singular value and μ-analysis [58, 153, 104].

However, as mentioned before, the first interest in examining pseudospectra originated from the study of non-normal matrices and operators [187]. For the case $B = C = I_n$, $\Delta \in \mathbb{C}^{n\times n}$ and $\|\cdot\| = \|\cdot\|_2$, the book [181] gives an extensive overview of the history of pseudospectra and discusses a wide range of applications. Just to mention a few: examining the transient behavior of dynamical systems, studying the convergence of certain matrix iterations, and detecting the onset of turbulence in fluid mechanics.

Finally, in the field of numerical linear algebra, Wilkinson already recognized in the sixties that a small perturbations on the coefficients of a polynomial can have a large effect on the location of its roots, see for example [199] which introduces the (in?)famous Wilkinson polynomial.

Computing psuedospectra, the psuesospectral abscissa and the distance to instability

Below we will introduce several methods for computing the pseudospectrum, the pseudospectral abscissa and the distance to instability of (2.12). We will see that depending on the chosen field and norm, different methods are available.

We will start our discussion with $\mathbb{K} = \mathbb{C}$ and $\|\cdot\| = \|\cdot\|_2$ (the spectral norm). In this case, the ϵ-pseudospectrum corresponds to the $1/\epsilon$-superlevel set of

$$s \mapsto \|T(s)\|_2 = \sigma_1\left(T(s)\right) \tag{2.17}$$

with $\sigma_1(\cdot)$ the largest singular value of its matrix argument and $T(s) = C\left(sI_n - A\right)^{-1}B$, i.e., the transfer function from w to z of (2.14). The ϵ-pseudospectrum can thus be obtained by means of a contour plot of (2.17). For $B = C = I_n$, the distance to instability can be computed using the level-set algorithm presented in [47], while the ϵ-pseudospectral abscissa can be computed using the criss-cross algorithm presented in [43]. However, when n is large, both these methods are computationally expensive as they involve repeatedly

solving an (Hamiltonian) eigenvalue problem of dimensions $2n \times 2n$. Therefore several specialized alternatives were developed to compute the pseudospectral abscissa of large and sparse matrices A. The methods in [77, 79] try to solve the optimization problem in (2.15) by looking for a path (continuous or discrete, respectively) in the space of admissible perturbations along which the real part of the rightmost characteristic root(s) of (2.12) (monotonically) increases. To reduce the search space, the authors exploit the fact that each point in the ϵ-pseudospectrum can be reached using a rank one perturbation with norm no larger than ϵ. In each iteration only the rightmost characteristic root of a particular instance of (2.12) must be computed, which can be found efficiently using an iterative eigenvalue method [161]. In [112] a subspace method is proposed to improve the convergence rate of these methods. Although, these methods only guarantee convergence to a locally rightmost point of the pseudospectrum, the pseudospectral abscissa is found for most example problems. For arbitrary B and C, the distance to instability corresponds to reciprocal of the H_∞-norm of the transfer function from w to z of (2.14) and can thus be computed using the methods presented in the following section. A generalization of the criss-cross algorithm to case is presented in [25]. Finally, extensions of the above methods to delay differential equations have been presented in [81] (bisection algorithm for the pseudospectral abscissa), [136] (local method for computing the pseudospectral abscissa by means of a fixed point iteration) and [188] (computing the distance to instability).

Let us continue with $\mathbb{K} = \mathbb{C}$, but consider other norms. For $\|\cdot\| = \|\cdot\|_{\text{frob}}$ the pseudospectrum coincides with the pseudospectrum for $\|\cdot\| = \|\cdot\|_2$ (a consequence of [93, Remark 5.2.20 (iv)]). When $\|\cdot\|$ is an other induced matrix norm, the ϵ-pseudospectrum can again be interpreted in terms of the $1/\epsilon$-superlevel set of $s \mapsto \|T(s)\|_\star$ with $\|\cdot\|_\star$ an appropriate complementary norm [93, Theorem 5.2.16]. However, the global methods for computing the distance to instability and the pseudospectral abscissa presented in the spectral norm case, cannot be generalized because the connection with the eigenvalues of an Hamiltonian matrix is lost.

Next we consider $\mathbb{K} = \mathbb{R}$ and $\|\cdot\| = \|\cdot\|_2$. As shown in [158], the ϵ-pseudospectrum can now be characterized in terms of the $1/\epsilon$-superlevel set of the function

$$s \mapsto \inf_{\gamma \in (0,1]} \sigma_2 \left(\begin{bmatrix} \Re\big(T(s)\big) & -\gamma \Im\big(T(s)\big) \\ \gamma^{-1} \Im\big(T(s)\big) & \Re\big(T(s)\big) \end{bmatrix} \right)$$

with T as defined before and $\sigma_2(\cdot)$ the second largest singular value of its matrix argument. This characterization allows again for a level-set approach to compute the corresponding distance to instability [174] and a criss-cross approach for the pseudospectral abscissa [123] (with an extension to delay

differential equations in [29]). As in the complex-valued case, there exists local methods for large and sparse A [78, 74]. In this case, the search space can be restricted to perturbations Δ with rank two. These large-scale methods have also been extended to perturbations measured in the Frobenius norm [75] and to delay differential equations [28].

2.2.2 H-infinity norm

Consider the continuous-time system depicted in Figure 2.3, with $w : [0, \infty) \mapsto \mathbb{R}^p$ and $z : [0, \infty) \mapsto \mathbb{R}^q$ input and output channels used to characterize the performance or robustness of the system. Furthermore, we assume that the system is causal and linear time-invariant. This system can be characterized in the Laplace domain by means of its transfer function $T : \mathbb{C} \mapsto \mathbb{C}^{q \times p}$. Assuming the internal state of the system is initially zero, this transfer matrix describes the input-to-output behavior of the system. (Or, assuming the system is internally stable, this transfer matrix describes the *asymptotic* input-to-output behavior of the system.)

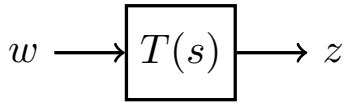

Figure 2.3: The standard open-loop configuration.

If the transfer function T is analytic in the open right-half plane and essentially bounded on the imaginary axis, it belongs to Hardy space H_∞ and the associated norm is defined as follows

$$\begin{aligned} \|T\|_{H_\infty} &:= \sup_{s \in \mathbb{C}^+} \sigma_1\big(T(s)\big) \\ &= \operatorname{ess\,sup}_{\omega \in \mathbb{R}} \sigma_1\big(T(\jmath\omega)\big) \end{aligned} \tag{2.18}$$

with $\sigma_1(\cdot)$ as defined before and $\mathbb{C}^+$ the open right half-plane. The equality follows from the maximum modulus principle. Intuitively, if $T \in H_\infty$ then its H_∞-norm corresponds to the highest peak in the singular value plot of its frequency response, i.e., the transfer function evaluated at the imaginary axis.

Chapter 4 discusses the H_∞-norm for time-delay systems in more detail. We will see that for such systems, the characterization of the H_∞-norm is more complex, as it might be sensitive to arbitrarily small delay perturbations (similarly as the spectral abscissa of a neutral delay differential equation).

Applications

Below we will see that the H_∞-norm offers a framework for quantifying both various performance criteria, such as noise attenuation or disturbance rejection, as well as robust stability.

We start with an interpretation of the H_∞-norm as an induced system norm. To this end, let us denote the space of input signals $w : [0, \infty) \mapsto \mathbb{R}^p$ for which

$$\|w\|_{L_2^p} = \left(\int_0^{+\infty} \|w(t)\|_2^2 \, \mathrm{d}t \right)^{1/2} < \infty$$

by L_2^p, i.e., L_2^p is the space of square-integrable (finite-energy) real-valued vector functions of dimensions p. Similarly, the space for finite-energy output signals z will be denoted by L_2^q with as corresponding norm $\| \cdot \|_{L_2^q}$. The H_∞-norm now quantifies the maximal amplification between these two spaces, in the sense that

$$\|T\|_{H_\infty} = \sup_{w \in L_2^p} \frac{\|z\|_{L_2^q}}{\|w\|_{L_2^p}}$$

with z the output of the system for an input w and a zero initial state. Or in other words, the H_∞-norm is equal to the maximal input-to-output energy amplification of the system.

Remark 2.8. A similar result can be obtained when working with the space of power signals, which allow us to consider more realistic signals such as sines and cosines.

Now, consider the closed-loop system depicted in Figure 2.4, that consists of the feedback interconnection of a plant P and a controller C. In this figure, r denotes the reference signal, e the tracking error, u the output of the controller, d_i the input disturbance, u_p the plant's input signal, d_o the output disturbance, y the output and n the sensor noise. Besides stability, a closed-loop system must typically satisfy certain performance criteria, such as good noise attenuation, good disturbance rejection, avoiding (input) saturation, robustness against model errors, and good tracking, which can be expressed in terms of the transfer functions between the various signals in Figure 2.4. For example, to achieve a good attenuation of the disturbance d_o at the output y, the magnitude of the output sensitivity matrix

$$S_o(\jmath\omega) := \big(I + P(\jmath\omega)C(\jmath\omega)\big)^{-1}$$

with $P(\cdot)$ and $C(\cdot)$ the transfer functions of the plant and the controller respectively, must be small at frequencies for which the disturbance is active

(typically at low frequencies). On the other hand, good robustness against model uncertainty and good noise attenuation require that the magnitude of the output complementary sensitivity matrix

$$T_o(\jmath\omega) := I - S_o(\jmath\omega) = P(\jmath\omega)C(\jmath\omega)\big(I + P(\jmath\omega)C(\jmath\omega)\big)^{-1}$$

is small at frequencies for which the uncertainty and the noise signal are significant (typically at high frequencies). However, when optimizing multiple objectives, typically a waterbed effect is observed, meaning that improving one objective leads to a deterioration of another one. For example, the magnitude of the output sensitivity matrix S_o is small when the loop gain $P(\jmath\omega)C(\jmath\omega)$ is large, i.e.,

$$\sigma_{\min}\big(P(\jmath\omega)C(\jmath\omega)\big) \gg 1$$

with $\sigma_{\min}(\cdot)$ the smallest singular value of its matrix argument. Yet, a large loop gain implies that T_o almost becomes the identity matrix which means that noise is "passed through" to the output. To balance these conflicting design requirements, the following objective function

$$\left\| \begin{bmatrix} W_1 S_o \\ W_2 C S_o \\ W_3 T_o \end{bmatrix} \right\|_{H_\infty} \tag{2.19}$$

with W_1, W_2, and W_3 frequency-dependent weighting functions that allow make a trade-off between the different design objectives at each frequency, is considered. The so called *mixed-sensitivity H_∞-control problem* consists of finding the controller that minimizes this objective function.

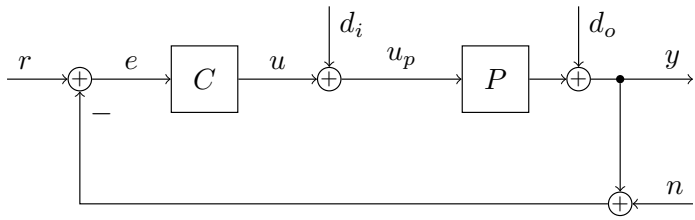

Figure 2.4: The standard feedback configuration. Based on [207, Figure 5.1].

The H_∞-norm also plays an important role in examining uncertain dynamical systems. For example, the celebrated small gain theorem induces a necessary and sufficient condition for the robust stability of the feedback interconnection in Figure 2.5 with respect to a class of unstructured uncertainties.

Theorem 2.4 (Small-gain theorem for robust stability)**.** Let $T(s) \in H_\infty$, then the feedback loop of $T(s)$ and $\Delta(s)$ (as depicted in Figure 2.5) is stable for all

$\Delta(s) \in H_\infty$ with $\|\Delta\|_{H_\infty} \leq 1$ if and only if

$$\|T\|_{H_\infty} < 1.$$

Remark 2.9. The condition $\Delta(s) \in H_\infty$ implies that the dynamic perturbation $\Delta(s)$ is stable.

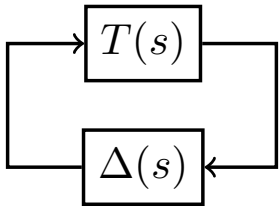

Figure 2.5: Feedback configuration for small-gain theorem.

Furthermore, in certain situations the H_∞-norm gives an exact characterization for the distance to instability, as shown in the following theorem.

Theorem 2.5. The distance to instability of the uncertain differential equation (2.12) for $\mathbb{K} = \mathbb{C}$ and $\|\cdot\| = \|\cdot\|_2$ (assuming the matrix A is Hurwitz), is equal to the reciprocal of the H_∞-norm of the transfer function of (2.14) from w to z, i.e.,

$$r_{\mathbb{C},\|\cdot\|_2}(A, B, C) = (\|T\|_{H_\infty})^{-1}$$

with $T(s) = C(sI_n - A)^{-1}B$.

Proof. For a given perturbation Δ, the differential equation (2.12) has a characteristic root at $\lambda_0 \notin \Lambda(A)$, if there exists a vector $y \in \mathbb{C}^n \setminus \{0\}$ such that

$$(A + B\Delta C)\, y = \lambda_0 y.$$

Because $\lambda_0 \notin \Lambda(A)$, this condition is equivalent with

$$(\lambda_0 I_n - A)^{-1} B\Delta C y = y.$$

Multiplying this equation from the left with ΔC and introducing the variable $\hat{y} = \Delta C y$, we get

$$\Delta T(\lambda_0)\hat{y} = \hat{y}$$

with $(\lambda_0 I_n - A)^{-1} B\hat{y} = y \neq 0$, meaning that $\hat{y} \neq 0$. The equality above is thus equivalent with

$$\det\left(I_p - \Delta T(\lambda_0)\right) = 0. \tag{2.20}$$

It is clear that in order for (2.20) to be satisfied, the following inequality must hold

$$1 \leq \|\Delta\, T_{zw}(\lambda_0)\|_2 \,(\leq \|\Delta\|_2 \, \|T_{zw}(\lambda_0)\|_2)\,.$$

Any destabilizing perturbation Δ must thus satisfy $\|\Delta\|_2 \geq \|T(\lambda_0)\|_2^{-1}$. Next, consider the perturbation $\Delta^\star = \sigma_1^{-1} v_1 u_1^H$ with $\sigma_1 = \|T(\lambda_0)\|_2$ the maximal singular value of $T(\lambda_0)$ and u_1 and v_1, respectively, the corresponding left and right singular vectors with unit norm. It now holds that

$$\begin{aligned}\det\left(I_p - \Delta^\star T(\lambda_0)\right) &= \det\left(I_p - \sigma_1^{-1} v_1 u_1^H T(\lambda_0)\right) \\ &= \det\left(I_p - v_1 v_1^H\right) = \det\left(1 - v_1^H v_1\right) = 0.\end{aligned}$$

The norm of the smallest perturbation Δ such that (2.12) has a characteristic root at λ_0 is thus $\|T(\lambda_0)\|_2^{-1}$.

Due to the continuity of the spectrum of (2.12) with respect to the entries of the perturbation Δ a transition to instability is characterized by a root crossing the imaginary axis. The distance to instability is thus equal to

$$\inf_{\omega\in\mathbb{R}} \|T(\jmath\omega)\|_2^{-1} = \left(\sup_{\omega\in\mathbb{R}} \sigma_1\big(T(\jmath\omega)\big)\right)^{-1} = \left(\|T\|_{H_\infty}\right)^{-1}.$$

□

Computing the H_∞-norm

There exist several methods for computing the H_∞-norm. Below we will briefly introduce two popular approaches and discuss their (dis)advantages. For other methods, such as subspace methods [4] or the implicit determinant method [65], we refer the interested reader to the relevant literature.

In the discussion below we will assume that T is the transfer function of

$$\left\{\begin{array}{rcl} \dot{x}(t) &=& A\,x(t) + B\,w(t), \\ z(t) &=& C\,x(t) \end{array}\right. \tag{2.21}$$

with the state variable $x(t) \in \mathbb{R}^n$, the performance input $w(t) \in \mathbb{R}^p$, and performance output $z(t) \in \mathbb{R}^q$ for all $t \geq 0$, the matrices A, B, and C real-valued and A Hurwitz. The associated transfer function is thus $T(s) = C(sI - A)^{-1}B$.

Level set methods Let us introduce this method by means of an example. Consider the following multiple-input multiple output system

$$\begin{cases} \dot{x}(t) &= \begin{bmatrix} -0.15 & 1.55 & -0.1 & -1.55 \\ 2.3 & -0.2 & -2.3 & -3.8 \\ -1.45 & 0.05 & 1.2 & -0.05 \\ 5.3 & 1.5 & -5.3 & -5.5 \end{bmatrix} x(t) + \begin{bmatrix} -29/3 & 0 \\ 101/3 & 1 \\ -29/3 & 1 \\ 101/3 & -1 \end{bmatrix} w(t), \\ z(t) &= \begin{bmatrix} -1 & -0.2 & 1.2 & 1 \\ -3.2 & 0.4 & 3.2 & -0.4 \end{bmatrix} x(t). \end{cases} \tag{2.22}$$

(It is easy to verify that this system is exponentially stable as the corresponding spectral abscissa is equal to -0.2.) Figure 2.6 shows the singular values of the associated frequency response for $\omega \in [0, 8]$. (As all matrices in (2.22) are real, the singular value plot of the frequency response is symmetric with respect to $\omega = 0$.) The H_∞-norm is equal to 11.9959 and is attained at $\omega = \pm 1.5052$ (both rounded to four decimal places, indicated by the red cross).

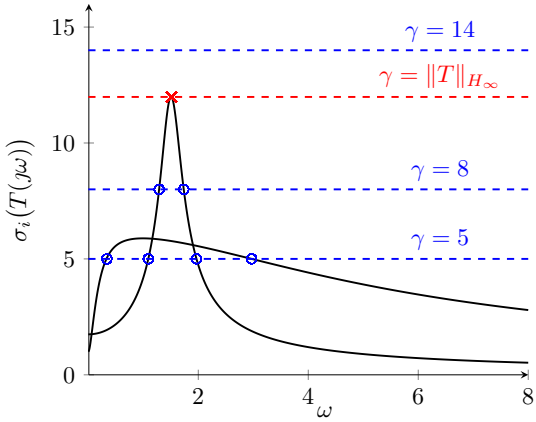

Figure 2.6: The singular values of the frequency response associated with (2.22).

A first method to compute the H_∞-norm was the bisection method presented in [31]. In this method, one keeps track of a lower estimate γ_l and an upper estimate γ_u for the H_∞-norm. These bounds are iteratively updated by checking whether the singular value plot intersects the level $\gamma_{new} = \frac{\gamma_l + \gamma_u}{2}$, i.e., checking if there exist angular frequencies $\omega \in \mathbb{R}$ such that γ_{new} is a singular value of $T(j\omega)$. If such an intersection exists then the lower estimate is set to this new value. Otherwise, the upper estimate is updated. This process is repeated until the distance between the upper and lower bound is sufficiently small. To check for intersections the following theorem can be used.

Theorem 2.6. Given a constant $\gamma > 0$, then γ is a singular value of $T(\jmath\omega)$ with $\omega \in \mathbb{R}$ if and only if $\jmath\omega$ is an eigenvalue of the parameterized Hamiltonian matrix[3] H_γ with

$$H_\gamma := \begin{bmatrix} A & \gamma^{-1}BB^T \\ -\gamma^{-1}C^TC & -A^T \end{bmatrix}. \tag{2.23}$$

Proof. See for example [31, Theorem 1]. □

The angular frequencies ω at which a level γ intersects the singular value plot thus correspond to the purely imaginary eigenvalues of the matrix H_γ. This relation is illustrated in Figures 2.6 and 2.7. For $\gamma = 5$, the matrix H_γ has four characteristic roots $\jmath\omega$ on the imaginary axis with $\omega \geq 0$, which correspond to the four circles in Figure 2.6 at the level $\gamma = 5$. Similarly, at $\gamma = 8$ there are two intersections with the singular value plot for $\omega \geq 0$ corresponding to the two purely imaginary eigenvalues of H_γ. At $\gamma = \|T\|_{H_\infty}$, the matrix H_γ has only one pair of purely imaginary roots at $\omega = \pm 1.5052$, corresponding with the red cross in Figure 2.6. (Furthermore, closer inspection learns that these purely imaginary eigenvalues are multiple and defective.) Finally, for $\gamma = 14$, the matrix H_γ has no purely imaginary eigenvalues, as there is no intersection with the singular value plot. Intersections of a level γ and the singular value plot can thus be found by checking whether the Hamiltonian matrix H_γ has purely imaginary eigenvalues.

To speed-up convergence, the BBBS algorithm [30, 38] was devised. This method only keeps track of a lower estimate γ_l. In each iteration it checks for intersections of the singular value plot with the level $\gamma_{new} = \gamma_l(1 + \epsilon_{\text{tol}})$ (with ϵ_{tol} the desired relative tolerance) by computing the eigenvalues of $H_{\gamma_{new}}$. If no intersection is found, γ_l is returned as an estimate for the H_∞-norm. Otherwise, the purely imaginary eigenvalues of $H_{\gamma_{new}}$ are used to determine the frequency intervals for which $\sigma_1(T(\jmath\omega)) \geq \gamma_{new}$. Subsequently, $\sigma_1(T(\jmath\omega))$ is evaluated at the midpoints (using either an arithmetic or a geometric mean) of these intervals. The maximum of these function evaluations is then used as the new lower estimate for the H_∞-norm. It can be shown this approach converges quadratically to the H_∞-norm. An extension to time-delay systems is presented in [137, 82] and will be discussed in more detail in Section 6.1.

Large and sparse systems The level-set approach discussed above is computationally too demanding when A is large, as it involves solving eigenvalue problems with dimension $2n$. Therefore, when A is large and sparse, the methods

[3] A matrix $H \in \mathbb{C}^{2n\times 2n}$ is Hamiltonian if $JH = (JH)^H$ with $J = \begin{bmatrix} 0 & I_n \\ -I_n & 0 \end{bmatrix}$.

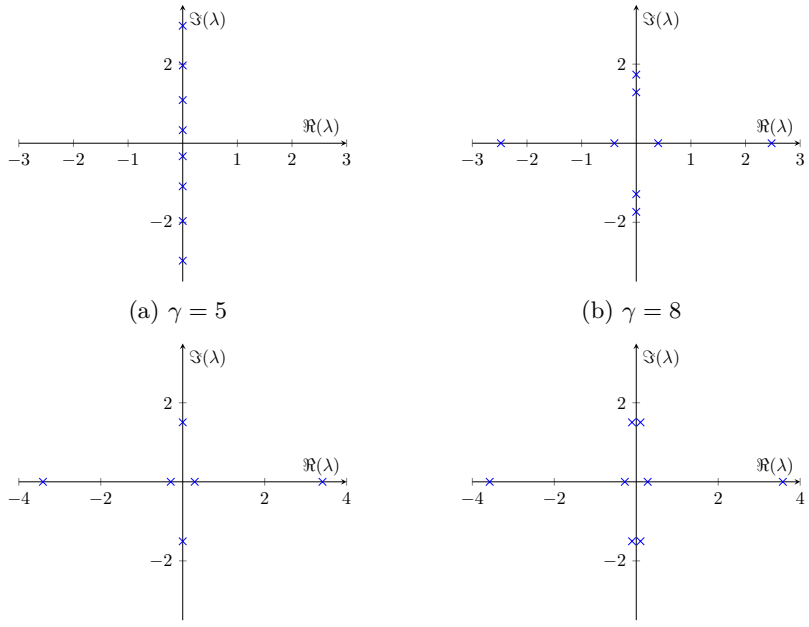

(a) $\gamma = 5$ (b) $\gamma = 8$

(c) $\gamma = \|T_{zw}\|_{H_\infty}$ (d) $\gamma = 14$

Figure 2.7: The eigenvalues of H_γ as defined in (2.23) for several value of γ.

developed in [26, 76] are preferred. These methods exploit the equivalence between the distance to instability $r_{\mathbb{C},\|\cdot\|_2}(A, B, C)$ and the H_∞-norm of T given in Theorem 2.5. To compute $r_{\mathbb{C},\|\cdot\|_2}(A, B, C)$ these methods use the observation that the distance to instability corresponds to the unique zero crossing of the function $\epsilon \mapsto c^{\text{ps}}_{\mathbb{C},\|\cdot\|_2}(\epsilon; A, B, C)$ (a consequence of Definition 2.8 and Remark 2.7), which can be computed efficiently using the Newton(-bisection) method. Below we will therefore briefly sketch (an extension[4] of) the method proposed in [77], which allows to efficiently compute the ϵ-pseudospectral abscissa $c^{\text{ps}}_{\mathbb{C},\|\cdot\|_2}(\epsilon; A, B, C)$ of a large and sparse matrix A.

The method in [77] computes the ϵ-pseudospectral abscissa by directly seeking a solution for the optimization problem in (2.15). The key observation underlying this method is that the ϵ-pseudospectral abscissa remains unchanged if we restrict the perturbation Δ to be a rank one matrix (see the first part of the proof of Theorem 2.5). This allows to reduce the search space to the manifold of rank one matrices whose spectral norm is equal to ϵ. To this end, let us

[4] In [77], it is assumed that $B = C = I_n$. However, the presented algorithm can easily be extended to the case with B and C arbitrary.

consider the following ordinary differential equation on the manifold of rank one matrices with unit norm:

$$\dot{\Delta}_n(t) = P_{\Delta_n(t)}\Big(B^T x(t) y(t)^H C^T\Big) \text{ for } t \geq 0, \tag{2.24}$$

in which $x(t)$ and $y(t)$ are, respectively, the left and right eigenvectors associated with $\lambda(t)$, the rightmost eigenvalue of $A + \epsilon B\Delta_n(t)\, C$, normalized such that $\|x(t)\|_2 = \|y(t)\|_2 = 1$ and $x(t)^H y(t) > 0$. The operator $P_{\Delta_n(t)}(\cdot)$ ensures that $\Delta_n(t)$ remains on the manifold. Assuming that $\lambda(t)$ is a simple eigenvalue of $A+\epsilon B\Delta_n(t)\, C$ with corresponding left and right eigenvectors $x(t)$ and $y(t)$ such that $B^T x(t) \neq 0$ and $Cy(t) \neq 0$ for all $t \geq 0$, then along this path

$$\frac{\mathrm{d}}{\mathrm{d}t}\Re\big(\lambda(t)\big) \geq 0,$$

i.e., $\lambda(t)$ is monotonically increasing. Furthermore, the attractive stationary points of (2.24) correspond to critical perturbations $\Delta_n^\star$ in the sense that one of the eigenvalues of $A + \epsilon B\Delta_n^\star\, C$ is a (locally) rightmost point of the ϵ-pseudospectrum.

In a practical implementation, the matrix differential equation in (2.24) should be avoid. Instead, by considering the explicit decomposition $\Delta_n(t) = u(t)v(t)^H$ with $u(t) \in \mathbb{C}^p$, $v(t) \in \mathbb{C}^q$ and $\|u(t)\|_2 = \|v(t)\|_2 = 1$, (2.24) can equivalently be characterized by the following system of differential equations:

$$\left\{\begin{array}{rcl} \dot{u} &=& \frac{1}{2}\Im\left(u^H B^T x y^H C^T v\right) u + (I - uu^H) B^T x y^H C^T v, \\ \dot{v} &=& \frac{1}{2}\Im\left(v^H C y x^H B u\right) v + (I - vv^H) C y x^H B u \end{array}\right. \tag{2.25}$$

in which the explicit dependency on t is dropped for notational convenience. The attractive stationary points of this differential equation (which correspond to locally rightmost points of the ϵ-pseudospectrum), can be found by forward simulating the differential equation from an initial point. To this end, [77] proposes to use the exponential forward Euler method. Note however that we are not interested in finding a good approximation for the solution of (2.25) but rather in solving (2.15). The step size should therefore not chosen to bound the discretization error but to guarantee a monotonic increase of $\Re\big(\lambda(t)\big)$.

If $n \gg p, q$, the main computation cost in each Euler step consists of calculating the rightmost eigenvalue of $A + \epsilon B u(t) v(t)^H C$ (i.e., a rank one perturbation of A). If A is sparse, this eigenvalue can be computed efficiently using an iterative eigenvalue method [161], as implemented in the `eigs` function of MATLAB [115], and the Sherman-Morrison formula.

Remark 2.10. Note that the proposed approach might fail to find the global maximum of (2.15). To alleviate this problem, one can restart the optimization

procedure from different initial perturbations. Good candidates are $\frac{(B^T x)(Cy)^H}{\|B^T x\|_2 \|Cy\|_2}$ with x and y the left and right eigenvectors associated with rightmost eigenvalues of A.

Now that we have presented an algorithm to compute the ϵ-pseudospectral abscissa, we can use the Newton-bisection algorithm [156] to find the unique zero of $\epsilon \mapsto c^{\text{ps}}_{\mathbb{C},\|\cdot\|_2}(\epsilon; A, B, C)$. To this end, we need the derivative of the ϵ-pseudospectral abscissa with respect to ϵ as given in the following lemma.

Lemma 2.1. Assume that $\Lambda^{\text{ps}}_{\mathbb{C},\|\cdot\|_2}(\epsilon; A, B, C)$ has a unique rightmost point $\lambda_\star$ in the half plane $\{\lambda \in \mathbb{C} : \Im(\lambda) \geq 0\}$ [5] such that $\lambda_\star$ is a simple, rightmost eigenvalue of $A + \epsilon B u_\star {v_\star}^H C$ with $\|u_\star\|_2 = \|v_\star\|_2 = 1$ and corresponding left and right eigenvectors $x_\star$ and $y_\star$ (with $B^T x_\star \neq 0$ and $Cy_\star \neq 0$), then the derivative of the ϵ-pseudospectral abscissa with respect to ϵ is equal to

$$\frac{d}{d\epsilon} c^{\text{ps}}_{\mathbb{C},\|\cdot\|_2}(\epsilon; A, B, C) = \Re\left(\frac{{x_\star}^H B u_\star {v_\star}^H C y_\star}{{x_\star}^H y_\star}\right).$$

2.3 Controller design

In the discussion above we focused on **analyzing** the (robust) stability and performance of a given (uncertain) system. Engineers, however, want to go further than just analysis. They are also interested in **designing control systems** that steer the system in such a way that it exhibits some favorable behavior. The most common control set-up is the feedback loop (also known as closed-loop control), in which the control action at the inputs is based on measurements at the outputs. An example of such a controller is the automatic cruise control system in your car, which maintains a given speed by applying the necessary throttle or brake input based on measurements of the current speed and acceleration. A simplified feedback configuration is sketched in Figure 2.8, in which u represents the input signals that govern the actuators and y the available measurements. The exogenous input w and exogenous output z are introduced to quantify the performance and robust stability of the closed-loop system. (For example, via the H_∞-norm of the corresponding transfer function.)

[5] It is easy to verify that $\Lambda^{\text{ps}}_{\mathbb{C},\|\cdot\|_2}(\epsilon; A, B, C)$ with A, B, and C real-valued, is symmetric with respect to the real axis.

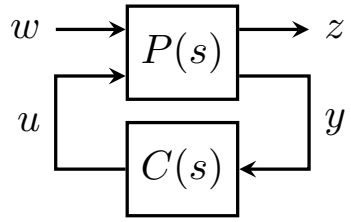

Figure 2.8: Simplified feedback configuration.

2.3.1 Controller architectures

Nowadays, there exists a wide variety of (feedback) control architectures. Below we will introduce some structures that are relevant for the discussions in the remainder of this thesis.
The most simple feedback controller is the static feedback law, in which the input signal is a linear combination of the measurements, i.e.,

$$C \leftrightarrow u(t) = Ky(t) \tag{2.26}$$

with $u(t) \in \mathbb{R}^{p_1}$, $y(t) \in \mathbb{R}^{q_1}$ and K a real-valued matrix of appropriate dimensions. For certain applications such a static feedback controller might not be sufficient to achieve the desired performance. In that case, one can consider a dynamic feedback controller, i.e., a controller which itself is a dynamical system,

$$C \leftrightarrow \left\{ \begin{array}{rcl} \dot{x}_c(t) & = & A_c\, x_c(t) + B_c\, y(t), \\ u(t) & = & C_c\, x_c(t) + D_c\, y(t) \end{array} \right. \tag{2.27}$$

with the control input $u(t) \in \mathbb{R}^{p_1}$, the measured output $y(t) \in \mathbb{R}^{q_1}$, the controller state $x_c(t) \in \mathbb{R}^{n_c}$, n_c the order of the controller and A_c, B_c, C_c, and D_c real-valued matrices of appropriate dimensions.

Another popular controller structure is proportional-integral-derivative feedback, in which the input signal is a linear combination of the output signal, its integral, and its derivative, i.e.,

$$C \leftrightarrow u(t) = K_p\, y(t) + K_i \int_0^t y(s)\, \mathrm{d}s + K_d\, \dot{y}(t) \tag{2.28}$$

with $u(t) \in \mathbb{R}^{p_1}$, $y(t) \in \mathbb{R}^{q_1}$ and K_p, K_i, and K_d real-valued matrices of appropriate dimensions. Compared to a static feedback controller, the integral term allows eliminate a steady state error, while the derivative term anticipates future behavior of the system and as such allows to improve the responsiveness of the controller and avoid overshoot. PID-controllers are popular in industrial applications due to their robustness and their relative ease to tune [148, 19].

In the controller architectures discussed above, it was assumed that all output measurements are centrally available and can be used to compute a global feedback signal. In networked systems, that consist of multiple interacting subsystems, this assumption is often no longer valid as collecting all measurements centrally would be too time-consuming, too expensive or even impossible. In such systems the computation of the control action is therefore divided over different local controllers, giving rise to decentralized, overlapping, and distributed control architectures. Such controllers can still be represented in the mathematical frameworks given above, but require that a sparsity pattern is imposed on the matrices, meaning that only certain entries are allowed to be non-zero.

2.3.2 Direct optimization framework

Once a suitable control architecture is chosen, one needs to derive appropriate values for the controller parameters, i.e., the entries of the matrices in (2.26), (2.27), and (2.28). Depending on the structure of the controller, one of the following techniques can be applied. For PID controllers, for example, there exists an extensive literature on heuristic tuning rules [148, 19]. However, in most cases one wants to rely on a more rigorous, computer-aided control system design (CACSD) paradigm. In this work we will use a direct optimization approach [42, 8, 152, 186]. The main idea behind this framework is to formulate the design objective as an optimization problem in the controller parameters. For example, a stabilizing controller can be found by minimizing the closed-loop spectral abscissa. As such, this approach allows to consider a wide variety of control architectures, including dynamic output feedback controllers for which the order of the controller is be smaller than the order of the plant. Such low-order controllers are preferred in certain applications, such as embedded aerospace control systems [173]. The direct optimization approach was, for example, successfully applied to save the Rosetta space mission [10]. Furthermore, within the direct optimization framework it is also easy to impose a certain structure on the controller, e.g., multiple feedback loops, decentralized or distributed control, or PID control. This comes however often at the cost of having to solve a nonsmooth, nonconvex optimization problem. Yet, as discussed in the next subsection, there exist well-established tools for solving such problems. In contrast, Lyapunov-based techniques, which we will briefly discuss in more detail below, are typically limited to state feedback controllers or full-order dynamic output feedback controllers (in which the order of the controller is equal to or larger than the order of the plant) but result in convex optimization problems.

To conclude this subsection, we will briefly compare the direct optimization approach with an alternative CACSD framework based on linear matrix inequalities (LMIs), as presented in (among others) [33, 68, 67, 163]. This framework is based on (extensions of) Lyapunov's second method and involves checking the feasibility of an LMI or solving a semidefinite programming problem. Although in some cases there exists a "closed-form" solution for these problems, one generally needs to rely on a reformulation in terms of a convex optimization problem (which can be solved efficiently using an interior-point method). However, compared to the nonsmooth, nonconvex optimization problems arising in the direct optimization approach, the number of the optimization variables is typically much larger due to the introduction of Lyapunov matrices (whose dimensions grow quadratically with the number of states) [183]. Furthermore, for output feedback control, the convex-optimization framework is typically restricted to controllers of the form (2.27) with n_c equal to or larger than the order of the plant. For example, the design of fixed-order output feedback controllers, such as static output feedback controllers, typically results in a set of bilinear matrix inequalities (BMIs) which are much harder to solve than LMIs [179, 180, 162]. Alternatively, these BMIs can be approximated by sufficient LMIs, see [183, 91] and the references therein. Similar difficulties arise when certain constraints on the structure of the controller are imposed. Finally, especially in the context of time-delay systems, the LMI framework introduces conservatism, in the sense that the derived LMIs only give sufficient conditions for stability. In contrast, the direct optimization approach allows to directly optimize the quantities of interest such as the spectral abscissa or the H_∞-norm, and is therefore not conservative.

2.3.3 Nonsmooth, nonconvex optimization

As mentioned above, the optimization problems that arise in the direct optimization framework are typically nonsmooth and nonconvex. Next, we illustrate the potential difficulties encountered when optimizing nonsmooth, nonconvex functions. To this end, let us consider the stabilization of the following dynamical system

$$P \leftrightarrow \begin{cases} \dot{x}(t) = \begin{bmatrix} -5.1 & 6 & 0 & 0 & 0 \\ 0 & -5.1 & 6 & 0 & 0 \\ 0 & 0 & -5.1 & 6 & 0 \\ 0 & 0 & 0 & -5.1 & 6 \\ -47.76 & -36.39 & 51.1 & -49.5 & 4.39 \end{bmatrix} x(t) + \begin{bmatrix} 0 \\ 0 \\ 0 \\ 0 \\ 1 \end{bmatrix} u(t), \\ y(t) = \begin{bmatrix} -18.78 & -15.32 & 19.48 & -22.31 & 5.29 \end{bmatrix} x(t) \end{cases} \tag{2.29}$$

with the static output feedback law

$$C \leftrightarrow u(t) = k\, y(t). \tag{2.30}$$

To this end, we will look for the (scalar) feedback gain k that minimizes the closed-loop spectral abscissa. Figure 2.9 shows this quantity in function of k. Although the objective function is almost everywhere differentiable, it is neither convex nor smooth. For example, at $k \approx 1.53$ (indicated by a red circle) its first derivative is discontinuous. This discontinuity is related to a switch in the dominant (rightmost) characteristic root as k is varied, see Figure 2.10a. Furthermore, at $k \approx -2.43$ (indicated by a blue square) the objective function is even not Lipschitz continuous. Taking a look at Figure 2.10b, we see that at $k = -2.45$ the two rightmost characteristic roots are real-valued. However, when increasing k to -2.4, these two characteristic roots come together and form a complex conjugate pair. At the k-value for which this transition happens, the rightmost characteristic root becomes defective, causing the discontinuity (in a Lipschitz sense) in the spectral abscissa function. Finally, remark that the objective function has two local minima. However, only one of these corresponds to a stable closed-loop system. Notice furthermore that these local minimizers coincide with the "special" points considered before.

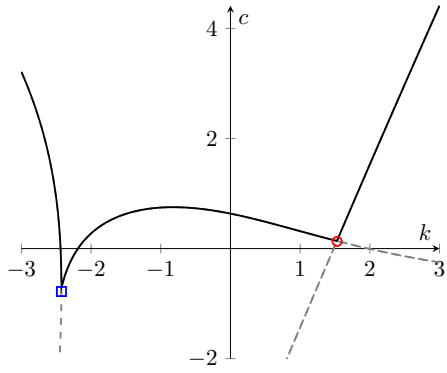

Figure 2.9: The spectral abscissa of the closed loop of (2.29) and (2.30) in function of the (scalar) feedback gain k. The gray dashed line, indicates the real part of the non-dominant characteristic roots in function of k.

More generally, in the direct optimization framework a suitable controller is designed by solving a minimization problem of the form

$$\min_{\vec{p}} f(\vec{p}), \tag{2.31}$$

in which $\vec{p}$ is a vector containing the tunable control parameters and f is a certain property of the closed-loop system such as the spectral abscissa, the

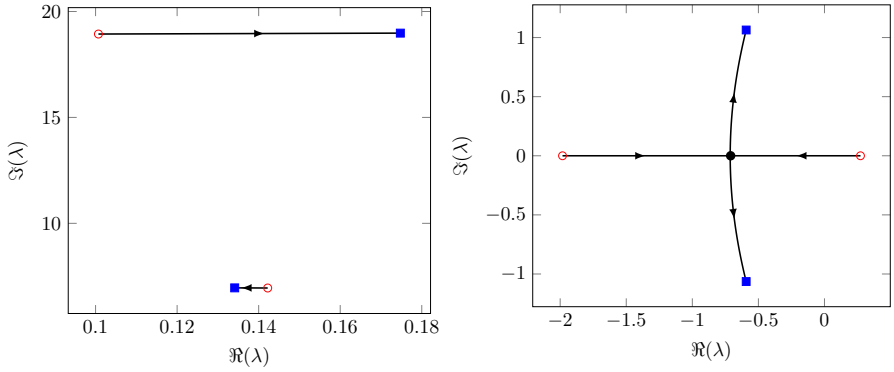

(a) k from 1.515 to 1.54

(b) k from -2.45 to -2.4

Figure 2.10: The root loci of the rightmost characteristic roots of the closed loop of (2.29) and (2.30) in function of k. The red circle indicates the starting value of k and the blue square indicates the final value of k.

pseudospectral abscissa, the distance to instability, or the H_∞-norm. The function f can be nonsmooth and nonconvex, but is assumed to be continuous and almost everywhere differentiable, in the sense that for a randomly chosen parameter vector f is differentiable with probability one. For example, the spectral abscissa function considered before is differentiable at all parameter values for which there is a unique, simple rightmost characteristic root (or a unique pair of simple complex conjugate roots).

As the objective function f is nonsmooth and nonconvex, traditional routines for smooth, convex optimization are likely to fail. For example, the steepest descent method typically gets jammed near points for which the gradient is discontinuous, resulting in tiny steps before eventually terminating prematurely at a point that is far from optimal. Consider for example the minimization of the spectral abscissa and assume that for the current parameter vector there are multiple characteristic roots with real part almost equal to the spectral abscissa. Assuming that the rightmost root is unique and simple, one can compute the gradient of spectral abscissa with respect to the control parameters. However, taking a step in the negative gradient direction, may induce a waterbed effect in which one of the nearly rightmost characteristic roots moves to the right and becomes dominant, resulting in the aforementioned jamming problem. To minimize nonsmooth functions, gradient bundle methods, which approximate the nonsmooth steepest descend direction near parameter values for which the gradient is discontinuous, are therefore preferred [186].

In this work, we will use the Hybrid Algorithm for Non-Smooth Optimization (HANSO), available from [150] to solve optimization problems of the form (2.31). This algorithm will first try to minimize the objective function using a traditional quasi-Newton method, such as BFGS, combined with inexact line search using the Armijo and weak Wolfe conditions. It is shown in [116] that such an approach typically works effectively even for nonsmooth functions (that may not be locally Lipschitz). Subsequently, HANSO tries to improve the obtained result using a bundle method, namely the gradient sampling method [45, 44]. In this phase, the algorithm will compute the gradients in randomly sampled points near the current parameter vector. These samples are subsequently used to compute a new search direction by solving a quadratic optimization problem. This typically results in a good approximation for the nonsmooth steepest descend direction. After completing these two stages, HANSO will typically return a parameter vector that locally minimizes the objective function. However, recall from the example above that such a local optimum might not be stabilizing or might be far from the global optimal value. It is therefore advisable to restart the optimization procedure from different initial values. HANSO is well-established for optimization problems arising in the context of controller design as it underlies the MATLAB package HIFOO [42, 80, 18]. This last package allows to design structured low-order controllers for LTI dynamical systems without delays.

An alternative approach for solving nonsmooth optimization problems is presented in [8]. This method underlies the MATLAB function `hinfstruct` for the H_∞-design of fixed-structure controllers [9]. As for the spectral abscissa, the H_∞-norm is typically a nonsmooth, nonconvex function of the control parameters but is almost everywhere differentiable. More specifically, the H_∞-norm is differentiable if the singular value plot attains a unique maximum and the corresponding singular value is simple. The method underlying `hinfstruct` is also based on a bundle method. However, instead of randomly sampling the gradient for nearby parameter values, a new nonsmooth search direction is found by also taking into account frequencies at which the H_∞-norm is almost attained, thereby anticipating the effect of nearly dominant peaks in the frequency response. In contrast to the gradient sampling method, the approach underlying `hinfstruct` is thus fully deterministic.

CHAPTER

3 Analysis and Design of Strongly Stabilizing PID Controllers for Time-Delay Systems

Abstract

This chapter presents the closed-loop stability analysis of time-delay systems with multiple pointwise state delays controlled using PID feedback, thereby focusing on a well-posedness problem. First it will be shown that under certain conditions on the derivative feedback gain, closed-loop stability may be destroyed by introducing arbitrarily small parametric perturbations, such as an arbitrarily small feedback delay, an arbitrarily accurate finite difference approximation of the derivative action or adding a low-pass filter with an arbitrarily large cut-off frequency. We therefore introduce a 'robustified' notion of stability called *strong exponential stability*, inspired by the corresponding notion for neutral functional differential equations. We prove that strong exponential stability can be achieved by adding a low-pass filter with a sufficiently large cut-off frequency to the control loop on the condition that the filter itself does not destabilize the nominal closed-loop system. Besides this analysis, a computational procedure for designing strongly stabilizing PID controllers is provided. This design method is illustrated using several case-studies. Finally, we discuss some extensions of the presented results for systems with relative degree larger than one, systems with an input delay and systems with bounded uncertainties on the system matrices and the state delays.

The results of this chapter were originally presented in [15] and [16].

3.1 Introduction

As mentioned in Section 2.3.1, PID controllers are a popular choice in many control applications due to their implementation simplicity, in the sense that they are determined by a limited number of parameters (for which good tuning procedures are available). This is particularly apparent for time-delay systems, for which a full-order controller would be infinite-dimensional. On the other hand, the structured, low-order nature of PID controllers imposes limitations on stabilizability and performance. An alternative for PID control is proportional-integral-retarded (PIR) control, in which the derivative signal is replaced by a purposely delayed version of the output signal [51, 159]. This approach is

motivated by the sensitivity of derivative control with respect to high-frequency noise. Furthermore, note that by using a finite-difference interpretation for the derivative, i.e., $\dot{y}(t) \approx \frac{y(t)-y(t-\tau)}{\tau}$, derivative feedback can be seen as a limit case of delayed feedback in which the size of the delay τ goes to zero. Finally, we briefly discuss the existing literature on the PID control of time-delay systems. Most of these works focus on systems with feedback delay, in which case an analytic characterization of stabilization and stabilizability is still possible, as witnessed by a plentiful recent literature including, among others, [169, 83, 151, 142, 63, 209, 208, 147, 125, 117] and the references therein.

Central in this chapter is the study of a well-posedness problem, namely the sensitivity of exponential stability with respect to a class of modeling errors, which include neglected feedback delay, a finite-difference approximation of the derivative and neglected high-frequency behavior. Similar sensitivity problems are examined in [70], which introduces the concept of *w-stability*. w-Stability requires that closed-loop stability is preserved for sufficiently small perturbations, in which the considered perturbation class consists of approximate identities (see [203, Section V.C]). Of interest for this chapter, is Section 4 which examines the control of rational (finite-dimensional) plants using non-proper, rational controllers, such as PID controllers. More specifically, [70, Theorem 2] suggests that in certain cases w-stability can be induced by adding a low-pass filter with a sufficiently large cut-off frequency to the control loop. However, as indicated in Theorem 3 of the same paper, such a low-pass filter can itself destroy closed-loop stability. In this work, we will derive similar results but we will focus on time-delay systems, which are infinite dimensional, and PID control. Furthermore, we will consider a (slightly) different perturbation class and allow for modeling errors inside the (derivative part of the) controller, to account for an implementation of the derivative control action using a finite-difference approximation.

Another important starting point is the article [140], which examines the stabilizability of a controllable LTI system without delays using state-derivative feedback, i.e., using a control law of the form $u(t) = K\dot{x}(t)$ instead of the conventional state feedback law $u(t) = Kx(t)$. While the nominal system can be stabilized if (and only if) the open-loop state matrix has no zero eigenvalue, closed-loop stability can be destroyed by infinitesimal perturbations if the open-loop state matrix has an odd number of eigenvalues in the open right half-plane (the so-called odd number limitation). On the other hand, if the number of right half-plane eigenvalues is even, then robustness against sufficiently small perturbations can always be achieved by adding a low-pass filter to the feedback loop.

Finally, there exists an abundant literature addressing fragility with respect

to infinitesimal perturbations. In [120, 52, 86, 143, 119] (and the references therein), the effect of feedback delay on the stability of a controlled system is discussed. In [90, 135, 121] (and the references therein) the sensitivity of stability of neutral functional differential equations with respect to infinitesimal (changes on the) delays is investigated. Finally, [172] examines the fragility of a gradient play dynamics model against a derivative approximation.

Below we will extend the theoretical framework of [140] to systems with state delays controlled by PID output feedback, and complement it with an algorithm for the design of the controller gain matrices. After introducing the considered set-up and illustrating the aforementioned sensitivity problems in Section 3.2, we derive conditions on the derivative gain matrix under which a stable closed-loop system is destabilized by introducing an arbitrarily small feedback delay (Section 3.3.1) and an arbitrary close finite-difference approximation of the derivative (Section 3.3.2). In Section 3.4, we introduce the notion of *strong stability*, in analogy with the corresponding notion for neutral functional differential equations (see Section 2.1.3). As in [140], we will show that a strongly stable closed-loop system can be obtained by including a low-pass filter in the control law, under the condition that this low-pass filter itself does not destabilize the system. It is shown that this last condition induces an algebraic constraint on the derivative gain matrix. Subsequently, Section 3.5 presents a computational procedure for the design of strongly stabilizing PID controllers, which consists of minimizing the spectral abscissa of closed-loop system in function of the feedback matrices under the aforementioned constraint on the derivative gain matrix. The presented method thus fits in the direct optimization framework as discussed in Section 2.3.2. Section 3.6 presents some remarks on systems with a relative degree larger than one and on how to generalize the presented results to systems with input delay and to systems with bounded uncertainties on the system matrices and the delays. Finally, Section 3.7 concludes the chapter.

3.2 Problem statement

Consider the following LTI system with pointwise state delays:

$$\left\{\begin{array}{rcl} \dot{x}(t) & = & A_0\,x(t) + \sum\limits_{k=1}^{m} A_k\,x(t-\tau_k) + B\,u(t), \\ y(t) & = & C\,x(t) \end{array}\right. \tag{3.1}$$

with the state variable $x(t) \in \mathbb{R}^n$, the control input $u(t) \in \mathbb{R}^{p_1}$, and the measured output $y(t) \in \mathbb{R}^{q_1}$. The delays satisfy $0 < \tau_1 < \cdots < \tau_m < +\infty$ and the matrices A_0, A_1, …, A_m, B and C are real-valued and have appropriate

dimension. Furthermore, without loss of generality, we assume that the matrix B is of full column rank and the matrix C is of full row rank. The goal is to design a PID output feedback control law, which can be denoted by

$$u(t) = K_p\, y(t) + K_d\, \dot{y}(t) + K_i \int_0^t y(s)\, \mathrm{d}s \tag{3.2}$$

with K_p, K_d and K_i real-valued $p_1 \times q_1$ matrices, that exponentially stabilizes the closed-loop system. The corresponding characteristic function is given by

$$\begin{aligned} H_0(\lambda) := \det \Bigg(\lambda \begin{bmatrix} I_n - BK_dC & 0 \\ 0 & I_{r_i} \end{bmatrix} - \\ \begin{bmatrix} A_0 + BK_pC & BU_i \\ V_iC & 0 \end{bmatrix} - \sum_{k=1}^{m} \begin{bmatrix} A_k & 0 \\ 0 & 0 \end{bmatrix} e^{-\lambda \tau_k} \Bigg) \end{aligned} \tag{3.3}$$

with $r_i = \mathrm{rank}(K_i)$ and $K_i = U_iV_i$, a rank revealing decomposition of K_i with $U_i \in \mathbb{R}^{p_1 \times r_i}$ of full column rank and $V_i \in \mathbb{R}^{r_i \times q_1}$ of full row rank. Recall from Section 2.1 that the closed-loop system is exponentially stable if and only if all roots of (3.3) lie inside the open left half-plane bounded away from the imaginary axis. However, the following example illustrates that closed-loop stability might be fragile with respect to introducing arbitrarily small implementation errors.

Example 3.1. Consider the following second-order system:

$$\begin{cases} \dot{x}(t) &= \begin{bmatrix} 0 & \omega_0 \\ \omega_0 & 0 \end{bmatrix} x(t) + \begin{bmatrix} -1 \\ 0 \end{bmatrix} u(t), \\ y(t) &= \begin{bmatrix} 1 & 0 \end{bmatrix} x(t) \end{cases} \tag{3.4}$$

with $\omega_0 \in \mathbb{R}$ and the feedback law

$$u(t) = k_p\, y(t) + k_d\, \dot{y}(t) \tag{3.5}$$

with k_p and k_d both belonging to $\mathbb{R}$. The corresponding open-loop transfer function is given by $-s/(s^2 - \omega_0^2)$, while the considered feedback law is nothing else than a PD controller. For this set-up, the characteristic function (3.3) reduces to a second-order polynomial:

$$(1 + k_d)\lambda^2 + k_p\, \lambda - \omega_0^2.$$

It follows from the Routh-Hurwitz stability criterion that the roots of this polynomial lie inside the open left half-plane if (and only if) $k_d < -1$ and $k_p < 0$. As a consequence, neither proportional nor derivative feedback can exponentially stabilize (3.4) on its own.

Let us now examine the effect of implementation errors on the exponential stability of the closed-loop system. Firstly, we consider delayed feedback, i.e., replacing $u(t)$ with $u(t-r)$ in (3.4) (in which $r > 0$). In this case, the exponential stability of the closed-loop system is characterized by the roots of the following quasi-polynomial

$$\left(1 + k_d\, e^{-\lambda r}\right)\, \lambda^2 + k_p\, e^{-\lambda r}\, \lambda - \omega_0^2. \tag{3.6}$$

It follows from [139, Proposition 1.28] that (3.6) has a sequence of zeros $\{\lambda_k\}_{k=1}^{\infty}$ which satisfies

$$\lim_{k\to\infty} |\Im(\lambda_k)| = +\infty \text{ and } \lim_{k\to\infty} \Re(\lambda_k) = \frac{1}{r} \ln\left(|k_d|\right).$$

For any $k_d < -1$ and $r > 0$, the characteristic function (3.6) thus has (infinitely many) roots in the closed right half-plane, meaning that the closed-loop system is destabilized by introducing a feedback delay, no matter how small. Secondly, we consider a finite-difference approximation of the derivative action, i.e., replacing (3.5) by

$$u(t) = k_p\, y(t) + k_d\, \frac{y(t) - y(t-r)}{r}$$

with $r > 0$. Such an approximation might be necessary if there is no sensor to measure the actual derivative. For the considered example, the exponential stability of the closed-loop system is now characterized by the roots of

$$f(\lambda) := \lambda^2 + \left(k_p + k_d \frac{1 - e^{-\lambda r}}{r}\right) \lambda - \omega_0^2. \tag{3.7}$$

This characteristic function can be rewritten as $f(\lambda) = \lambda^2\Big(f_1(\lambda) - f_2(\lambda)\Big)$ with

$$f_1(\lambda) := 1 + \frac{k_p}{\lambda} - \frac{\omega_0^2}{\lambda^2} \quad \text{and} \quad f_2(\lambda) := -k_d \frac{1 - e^{-\lambda r}}{\lambda r}.$$

As $\lambda = 0$ is not a root of $f(\cdot)$, the roots of (3.7) thus correspond to the intersections of $f_1(\cdot)$ and $f_2(\cdot)$ in the complex plane. Figure 3.1 shows these functions for λ real-valued and positive, $k_d < -1$, $k_p < 0$ and $r > 0$. For the considered parameter region it is clear that the characteristic function (3.7) has a real-valued root in the right half-plane. Furthermore, notice that this root moves to $+\infty$ as $r \to 0+$. So also under an arbitrary accurate finite-difference approximation of the derivative, the closed-loop system loses exponential stability. ◇

Remark 3.1. We consider the characteristic function (3.3) instead of

$$\det\left(\lambda \begin{bmatrix} I_n - BK_dC & 0 \\ 0 & I_{p_1} \end{bmatrix} - \begin{bmatrix} A_0 + BK_pC & B \\ K_iC & 0 \end{bmatrix} - \sum_{k=1}^{m} \begin{bmatrix} A_k & 0 \\ 0 & 0 \end{bmatrix} e^{-\lambda\tau_k}\right),$$

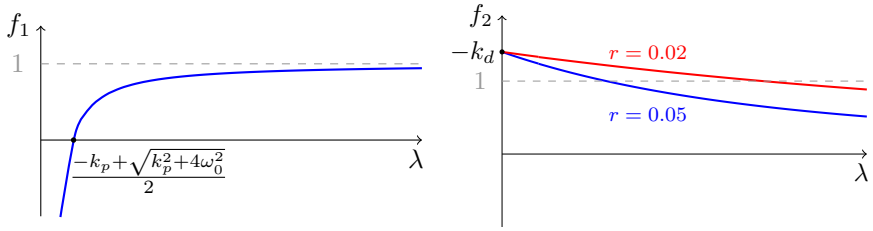

Figure 3.1: The functions $f_1(\lambda)$ and $f_2(\lambda)$ for λ real-valued and positive, $k_d < -1$, $k_p < 0$ and $r > 0$.

which one would naively obtain by bringing closed-loop system to linear form. This is motivated by the fact that this last equation might introduce "spurious" roots at the origin that have no relation with the actual asymptotic behavior of the closed loop system. Furthermore, note that $r_i\big(= \operatorname{rank}(K_i)\big)$ corresponds to the minimal number of integrators needed to implement the (integral) control action.

3.3 Losing stability under arbitrarily small implementation errors

Motivated by Example 3.1, this section will derive conditions on the spectrum of BK_dC under which exponential stability is lost by introducing an arbitrarily small feedback delay (Section 3.3.1) or an arbitrarily accurate finite-difference approximation of the derivative (Section 3.3.2).

3.3.1 Feedback delay

To study the effect of a feedback delay, we now consider the following system

$$\begin{cases} \dot{x}(t) &= A_0\, x(t) + \sum_{k=1}^{m} A_k\, x(t-\tau_k) + B\, u(t-r), \\ y(t) &= C\, x(t) \end{cases} \tag{3.8}$$

which is derived from (3.1) by including a delay $r > 0$ in the input. The following proposition gives a *sufficient condition* on the spectral radius of BK_dC under which an exponentially stable closed-loop interconnection of (3.1) and (3.2) is destabilized by introducing an arbitrarily small feedback delay.

Proposition 3.1. Assume that the gain matrices K_p, K_d, and K_i exponentially stabilize the closed-loop system consisting of (3.1) and (3.2). If the spectral radius of BK_dC is larger than one, then the feedback interconnection of (3.8) and (3.2) is unstable for all $r > 0$.

Proof. Under delayed feedback, the closed-loop system is unstable if

$$H_1(\lambda; r) := \det\left(\lambda\left(\begin{bmatrix} I_n & 0 \\ 0 & I_{r_1} \end{bmatrix} - \begin{bmatrix} BK_dC & 0 \\ 0 & 0 \end{bmatrix} e^{-\lambda r}\right) - \begin{bmatrix} A_0 & 0 \\ V_iC & 0 \end{bmatrix} - \begin{bmatrix} BK_pC & BU_i \\ 0 & 0 \end{bmatrix} e^{-\lambda r} - \sum_{k=1}^{m} \begin{bmatrix} A_k & 0 \\ 0 & 0 \end{bmatrix} e^{-\lambda \tau_k}\right) \tag{3.9}$$

has at least one root inside the right half-plane. Note that (3.9) corresponds to the characteristic function of a neutral delay eigenvalue problem (Section 2.1.3). It follows therefore from [139, Proposition 1.28] that for non-zero BK_dC, the characteristic function (3.9) has a sequence of zeros $\{\lambda_k\}_{k=1}^{\infty}$ for which

$$\lim_{k\to\infty} |\Im(\lambda_k)| = +\infty \text{ and } \lim_{k\to\infty} \Re(\lambda_k) = \frac{1}{r} \ln\big(\rho(BK_dC)\big)$$

with $\rho(\cdot)$ the spectral radius of its matrix argument. If $\rho(BK_dC) > 1$, then the characteristic function $H_1(\cdot; r)$ thus has (infinitely many) characteristic roots in the right half-plane for all $r > 0$. □

3.3.2 Finite-difference approximation of the derivative

Next, we derive a similar condition for the effect of using a finite-difference approximation instead of the actual derivative in the feedback signal. The control law now becomes:

$$u(t) = K_p\, y(t) + K_d\, \frac{y(t) - y(t-r)}{r} + K_i \int_0^t y(s)\, \mathrm{d}s. \tag{3.10}$$

Proposition 3.2. Assume that the gain matrices K_p, K_d, and K_i exponentially stabilize the closed-loop system consisting of (3.1) and (3.2). If at least one of the eigenvalues of BK_dC lies outside $\mathrm{clos}(S)$, with

$$S := \left\{ \begin{array}{l} \lambda \in \mathbb{C} :\ \Im(\lambda) \in (-\pi,\ \pi) \text{ and} \\ \qquad \Re(\lambda) < \left\{ \begin{array}{ll} \Im(\lambda)\ \mathrm{cotan}(\Im(\lambda)), & \Im(\lambda) \in (-\pi,\ 0) \cup (0,\ \pi) \\ 1, & \Im(\lambda) = 0 \end{array} \right. \end{array} \right\},$$

then there exists a $\hat{r} > 0$ such that the feedback interconnection of (3.1) and (3.10) is unstable for all $r \in (0, \hat{r})$.

Proof. The exponential stability of the closed-loop system consisting of (3.1) and (3.10) is characterized by the zeros of

$$H_2(\lambda; r) := \det\left(\lambda\left(\begin{bmatrix} I_n & 0 \\ 0 & I_{r_i} \end{bmatrix} - \begin{bmatrix} BK_dC & 0 \\ 0 & 0 \end{bmatrix} \frac{1 - e^{-\lambda r}}{\lambda r}\right) - \begin{bmatrix} A_0 + BK_pC & BU_i \\ V_iC & 0 \end{bmatrix} - \sum_{k=1}^{m} \begin{bmatrix} A_k & 0 \\ 0 & 0 \end{bmatrix} e^{-\lambda \tau_k}\right). \tag{3.11}$$

Multiplying $H_2(\cdot; r)$ with r^{n+r_i} and introducing the change of variables $\widehat{\lambda} = \lambda r$, we obtain

$$G_2(\widehat{\lambda}; r) := \det\left(\widehat{\lambda}\begin{bmatrix} I_n & 0 \\ 0 & I_{r_i} \end{bmatrix} - \begin{bmatrix} BK_dC & 0 \\ 0 & 0 \end{bmatrix}\left(1 - e^{-\widehat{\lambda}}\right) - r\begin{bmatrix} A_0 + BK_pC & BU_i \\ V_iC & 0 \end{bmatrix} - \sum_{k=1}^{m} r\begin{bmatrix} A_k & 0 \\ 0 & 0 \end{bmatrix} e^{-\widehat{\lambda}(\tau_k/r)}\right).$$

As $r \searrow 0$, $G_2(\cdot; r)$ uniformly converges to

$$\widetilde{G}_2(\widehat{\lambda}) := \det\left(\widehat{\lambda}\begin{bmatrix} I_n & 0 \\ 0 & I_{r_i} \end{bmatrix} - \begin{bmatrix} BK_dC & 0 \\ 0 & 0 \end{bmatrix}\left(1 - e^{-\widehat{\lambda}}\right)\right)$$

on compact regions in the open right half-plane. The function $\widetilde{G}_2(\cdot)$ has a root of multiplicity (at least) r_i at the origin; the remaining roots are the solutions of one of the following n equations

$$\widehat{\lambda} - \mu_i\left(1 - e^{-\widehat{\lambda}}\right) = 0 \quad \text{for } i = 1, \ldots, n$$

in which $\{\mu_i\}_{i=1}^n$ are the eigenvalues of BK_dC. It follows from [140, Lemma A.1] that $\widetilde{G}_2(\cdot)$ has a root in the open right half-plane if (and only if) BK_dC has an eigenvalue outside $\mathrm{clos}(S)$. As $G_2(\cdot; r)$ uniformly converges to $\widetilde{G}_2(\cdot)$ on compact regions in the open right half plane, it follows from a similar argument as in [140, Proposition 3.1 - Case 1] that there exist $c > 0$ and $\hat{r} > 0$ such that the function $G_2(\cdot; r)$ has at least one root in the right half-plane $\{\lambda \in \mathbb{C} : \Re(\lambda) > c\}$ for all $r \in (0, \hat{r})$. Because the zeros of $H_2(\cdot; r)$ correspond to the roots of $G_2(\cdot; r)$ divided by r, $H_2(\cdot; r)$ has at least one root in the right half plane $\{\lambda \in \mathbb{C} : \Re(\lambda) > c/r\}$. □

3.4 Strong stability

The previous section demonstrated that, under certain conditions on the spectrum of BK_dC, there exist arbitrarily small implementation errors that render an exponentially stable closed-loop interconnection of (3.1) and (3.2) unstable. Or in other words, under certain conditions on the derivative gain matrix, the exponential stability of the closed-loop interconnection of (3.1) and (3.2) is *sensitive* with respect to infinitesimal perturbations. As observed in the proofs of the previous section, these perturbations introduce characteristic roots in the right half-plane that move to $+\infty$ (without leaving the right half-plane) as the perturbation size goes to zero. An intuitive way to avoid such right half-plane roots is to apply a low-pass filter to the derivative signal, leading to the following control law:

$$u(t) = K_p\, y(t) + K_d\, \zeta(t) + K_i \int_0^t y(s)\, \mathrm{d}s \tag{3.12}$$

with

$$T\, \dot{\zeta}(t) + \zeta(t) = \dot{y}(t)$$

and $1/T$ the cut-off frequency. However, as observed in [70, Theorem 3] and [140, Secion 4.1] such a low-pass filter might itself be destabilizing.

The following subsection shows that this low-pass filter does not destroy stability for sufficiently large cut-off frequencies if a certain algebraic constraint on K_d is fulfilled. Subsequently, Section 3.4.2 introduces the notion of strong exponential stability, which requires the closed-loop system to remain exponentially stable under sufficiently small perturbations. Furthermore, it will be shown that if the aforementioned constraint on K_d is fulfilled, then the closed-loop interconnection of (3.1) and (3.12) is strongly exponentially stable. Finally, these theoretical results and those of the previous section are illustrated using an example in Section 3.4.3.

3.4.1 Losing stability under low-pass filtering

The following proposition shows that, under a particular condition on the spectrum of BK_dC, the exponential stability of the closed-loop system consisting of (3.1) and (3.2) can be destroyed by low-pass filtering the derivative signal. However, this proposition also shows that if all eigenvalues of BK_dC have real part smaller than 1, then the exponential stability of the closed-loop system is preserved when replacing control law (3.2) by (3.12) for T sufficiently small.

Proposition 3.3. Assume that the gain matrices K_p, K_d, and K_i exponentially stabilize the closed-loop system consisting of (3.1) and (3.2). If BK_dC has an eigenvalue with real part larger than one, then there exists a $\widehat{T} > 0$ such that the feedback interconnection of (3.1) and (3.12) is unstable for all $T \in (0, \widehat{T})$. On the other hand, if $BK_dC - I_n$ is Hurwitz (i.e., all eigenvalues of BK_dC have real part smaller than 1) then there exists a $\widetilde{T} > 0$ such that the feedback interconnection of (3.1) and (3.12) is exponentially stable for all $T \in (0, \widetilde{T})$.

Proof. The exponentially stability of the closed-loop system consisting of (3.1) and (3.12) is characterized by the roots of

$$H_3(\lambda; T) := \det \left(\lambda \left(\begin{bmatrix} I_n & 0 \\ 0 & I_{r_i} \end{bmatrix} - \frac{1}{\lambda T + 1} \begin{bmatrix} BK_dC & 0 \\ 0 & 0 \end{bmatrix} \right) - \begin{bmatrix} A_0 + BK_pC & BU_i \\ V_iC & 0 \end{bmatrix} - \sum_{k=1}^{m} \begin{bmatrix} A_k & 0 \\ 0 & 0 \end{bmatrix} e^{-\lambda \tau_k} \right). \tag{3.13}$$

If BK_dC has an eigenvalue with real part larger than one, then a similar derivation as in the proof of Proposition 3.2 shows that there exist $c > 0$ and $\widehat{T} > 0$ such that $H_3(\cdot; T)$ has a root in the right half plane $\{\lambda \in \mathbb{C} : \Re(\lambda) > c/T\}$ for all $T \in (0, \widehat{T})$.

On the other hand, if $BK_dC - I_n$ is Hurwitz, then for each $c > 0$ there exists a $\widehat{T} > 0$ such that $I_n - (BK_dC)/(\lambda T + 1)$ is invertible for all λ inside the right half-plane $V := \{\lambda \in \mathbb{C} : \Re(\lambda) > -c\}$ and all $T \in (0, \widehat{T})$. This means that for λ inside V and all $T \in (0, \widehat{T})$, the equation $H_3(\lambda; T) = 0$ is equivalent with

$$\det \left(\lambda \begin{bmatrix} I_n & 0 \\ 0 & I_{r_i} \end{bmatrix} - \left[\begin{matrix} \left(I_n - \frac{BK_dC}{\lambda T + 1} \right)^{-1} & 0 \\ 0 & I_{r_i} \end{matrix} \right] \times \left(\begin{bmatrix} A_0 + BK_pC & BU_i \\ V_iC & 0 \end{bmatrix} + \sum_{k=1}^{m} \begin{bmatrix} A_k & 0 \\ 0 & 0 \end{bmatrix} e^{-\lambda \tau_k} \right) \right) = 0.$$

A root, λ, of $H_3(\cdot; T)$ for $T \in (0, \widehat{T})$ inside V is thus bounded in modulus by

$$|\lambda| \leq \sup_{\substack{z \in V \\ T \in (0, \widehat{T})}} \left\| \left[\begin{matrix} \left(I_n - \frac{BK_dC}{zT + 1} \right)^{-1} & 0 \\ 0 & I_{r_i} \end{matrix} \right] \right\| \times \left(\left\| \begin{bmatrix} A_0 + BK_pC & BU_i \\ V_iC & 0 \end{bmatrix} \right\| + \sum_{k=1}^{m} \|A_k\| e^{-\Re(z)\tau_k} \right) := \Xi < \infty.$$

Because $H_3(\cdot;T)$ uniformly converges to $H_0(\cdot)$ on compact regions in the complex plane as $T \searrow 0$, there exists a $\widetilde{T} \leq \widehat{T}$ such that for all $T \in (0, \widetilde{T})$

$$\max_{\lambda \in \partial\Omega} |H_3(\lambda;T) - H_0(\lambda)| < \min_{\lambda \in \partial\Omega} |H_0(\lambda)|$$

with Ω the intersection of V and $\{\lambda \in \mathbb{C} : |\lambda| \leq \Xi\}$ if $H_0(\cdot)$ has no root on $\partial\Omega$. It then follows from Rouché's theorem [178, pages 116-117] that $H_3(\cdot;T)$ and $H_0(\cdot)$ have the same number of zeros in Ω for all $T \in (0, \widetilde{T})$. The proposition now follows by choosing $-c$ larger than the real part of the rightmost zero of $H_0(\cdot)$. □

3.4.2 Strong stability framework

In this subsection, we will show that if the low-pass filter itself is not destabilizing, then the closed-loop system consisting of (3.1) and (3.12) does not suffer from the same sensitivity problems as encountered in Section 3.3. Furthermore, instead of restricting ourselves to delayed feedback and a finite-difference approximation of the derivative, we will consider all perturbations that fit the framework given in Figure 3.2, in which perturbation functions $R_1(\cdot;\cdot) : \mathbb{C} \times [0, +\infty) \mapsto \mathbb{C}^{p_1 \times p_1}$, $R_2(\cdot;\cdot) : \mathbb{C} \times [0, +\infty) \mapsto \mathbb{C}^{q_1 \times q_1}$, and $R_3(\cdot;\cdot) : \mathbb{C} \times [0, +\infty) \mapsto \mathbb{C}^{q_1 \times q_1}$ fulfill the following assumptions:

Assumption 3.1.

1. for $i = 1, 2, 3$, the function $\lambda \mapsto R_i(\lambda; r)$ is meromorphic for every $r \geq 0$ and the function $r \mapsto R_i(\lambda; r)$ is continuous for every $\lambda \in \mathbb{C}$;
2. the matrices $R_1(\lambda; r)$ and $R_3(\lambda; r)$ have full rank for all $\lambda \in \mathbb{C}$ and all $r \geq 0$;
3. $\lambda \mapsto R_i(\lambda; 0) \equiv I$ for $i = 1, 2, 3$;
4. for every compact set $\Omega \subset \mathbb{C}$, we have

   $$\lim_{r \to 0+} \max_{\lambda \in \Omega} \|R_i(\lambda; r) - I\| = 0 \text{ for } i = 1, 2, 3$$

   i.e., the function $\lambda \mapsto R_i(\lambda; r)$ uniformly converge to the identity matrix on compact regions in the complex plane as r goes to zero;
5. there exist constants $M, N, \hat{r} > 0$ such that for all $\lambda \in \mathbb{C}$ with $\Re(\lambda) \geq -N$ and for all $r \in (0, \hat{r})$

   $$\|R_i(\lambda; r)\| \leq M \text{ for } i = 1, 2, 3.$$

The implementation errors studied in Section 3.3 fit this framework:

- the feedback delay in (3.8) can be represented by

$$R_1(\lambda; r) = e^{-\lambda r} I_{p_1} \text{ and } R_2(\lambda; r) = R_3(\lambda; r) = I_{q_1};$$

- the finite-difference approximation of the derivative control action in (3.11) can be represented by

$$R_1(\lambda; r) = I_{p_1},\ R_2(\lambda; r) = \begin{cases} \frac{1-e^{-\lambda r}}{\lambda r} I_{q_1} & \lambda r \neq 0 \\ I_{q_1} & \lambda r = 0, \end{cases} \text{ and } R_3(\lambda; r) = I_{q_1};$$

Also the low-pass filter in (3.12) can be interpreted in terms of this perturbation framework:

- $R_1(\lambda; r) = I_{p_1}$, $R_2(\lambda; T) = I_{q_1} / (\lambda T + 1)$, and $R_3(\lambda; r) = I_{q_1}$.

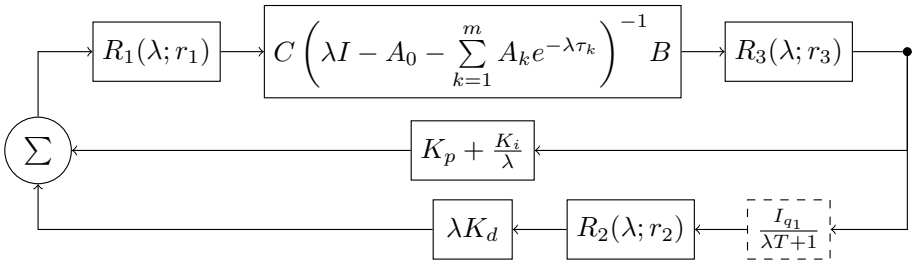

Figure 3.2: Closed loop description of the considered perturbation framework.

Next, in analogy with neutral delay differential equations, we define strong exponential stability as follows.

Definition 3.1. A closed-loop system as depicted in Figure 3.2, is strongly exponentially stable if for every set $\{R_i(\lambda; r_i)\}_{i=1}^{3}$ that satisfies the five assumptions given in Assumption 3.1, there exists a $\hat{r} > 0$ such that the corresponding perturbed closed-loop system is exponentially stable for all r_1, r_2 and r_3 in the half-open interval $[0, \hat{r})$.

Remark 3.2. The notion of strong stability introduced above should not be confused with the one used in [190, Section 5.3], which refers to stabilization with controllers that are themselves stable.

In the following proposition, it is shown that an exponentially stable closed-loop interconnection of (3.1) and (3.2) can be made strongly exponentially stable

by including a low-pass filter with a sufficiently large cut-off frequency on the condition that this low-pass filter itself does not destabilize the system.

Proposition 3.4. Assume that the gain matrices K_p, K_d, and K_i exponentially stabilize the closed-loop system consisting of (3.1) and (3.2). If $BK_dC - I_n$ is Hurwitz, then the feedback interconnection of (3.1) and (3.12) is strongly exponentially stable for sufficiently small T.

Proof. By incorporating the perturbations $R_i(\lambda; r_i)$ for $i = 1, 2, 3$ in (3.13), the characteristic function becomes

$$H_4(\lambda; T, r_1, r_2, r_3) := \det\left(\lambda \begin{bmatrix} I_n & 0 \\ 0 & I_{r_i} \end{bmatrix} - \begin{bmatrix} A_0 & 0 \\ 0 & 0 \end{bmatrix} - \sum_{k=1}^{m} \begin{bmatrix} A_k & 0 \\ 0 & 0 \end{bmatrix} e^{-\lambda\tau_k} - \begin{bmatrix} BR_1(\lambda; r_1) & 0 \\ 0 & I_{r_i} \end{bmatrix} \times \begin{bmatrix} K_p + \frac{\lambda}{\lambda T+1} K_d R_2(\lambda; r_2) & U_i \\ V_i & 0 \end{bmatrix} \begin{bmatrix} R_3(\lambda; r_3)C & 0 \\ 0 & I_{r_i} \end{bmatrix}\right).$$

Next, we choose numbers N and $\hat{r}$ according to item 5 of Assumption 3.1. Furthermore, it follows from Proposition 3.3 that if $BK_dC - I_p$ is Hurwitz and the closed-loop interconnection of (3.1) and (3.2) is stable, that we can choose a sufficiently small T such that there exists a $c \in (0, N]$ for which $H_3(\lambda; T)$ has no root in the right half-plane $V := \{\lambda \in \mathbb{C} : \Re(\lambda) > -c\}$. Subsequently, for all r_1, r_2, and r_3 in the interval $(0, \hat{r})$, the characteristic roots of $H_4(\cdot; T, r_1, r_2, r_3)$ in V are bounded in modulus by

$$|\lambda| \leq \sup_{\substack{z \in V \\ r_1, r_2, r_3 \in (0, \hat{r})}} \|A_0\| + \sum_{k=1}^{m} \|A_k\| e^{-\Re(z)\tau_k} + \left\| \begin{bmatrix} BR_1(z; r_1) & 0 \\ 0 & I_{r_i} \end{bmatrix} \times \begin{bmatrix} K_p + \frac{z}{zT+1} K_d R_2(z; r_2) & U_i \\ V_i & 0 \end{bmatrix} \begin{bmatrix} R_3(z; r_3)C & 0 \\ 0 & I_{r_i} \end{bmatrix} \right\| := \Xi < \infty.$$

By using Rouché's theorem as in Proposition 3.3 and the uniform convergence of $H_4(\cdot; T, r_1, r_2, r_3)$ to $H_3(\cdot; T)$ on compact regions for r_1, r_2, and r_3 going to zero, it follows that for sufficiently small r_1, r_2, and r_3 the functions $H_4(\cdot; T, r_1, r_2, r_3)$ and $H_3(\cdot; T)$ have the same number of roots in the right half-plane V, namely zero. □

The time-delay system in (3.1) is thus strongly exponentially stabilizable with a control law of the form (3.12) and a sufficiently large cut-off frequency, if there exists gain matrices K_p, K_d, and K_i for which the characteristic function

$H_0(\cdot)$ has no right half-plane roots and K_d satisfies the algebraic constraint in Proposition 3.4. Next, we introduce a condition that allows to verify for given matrices K_p and K_i, whether there exists a feedback matrix K_d such that both these conditions can be satisfied.

Proposition 3.5. If for given gain matrices K_p and K_i, the function

$$\det\left(\lambda\begin{bmatrix} I_n & 0 \\ 0 & I_{r_i} \end{bmatrix} - \begin{bmatrix} A_0 + BK_pC & BU_i \\ V_iC & 0 \end{bmatrix} - \sum_{k=1}^{m} \begin{bmatrix} A_k & 0 \\ 0 & 0 \end{bmatrix} e^{-\lambda\tau_k}\right),$$

i.e., $H_0(\cdot)$ with $K_d = 0_{p_1\times q_1}$, has an odd number of roots in the closed right half-plane then there does not exist a matrix K_d such that all zeros of $H_0(\cdot)$ lie in the open left half-plane and $BK_dC - I$ is Hurwitz. As a consequence, there does not exist a matrix K_d such that the feedback interconnection of (3.1) with (3.12) is strongly exponentially stable for sufficiently small T.

Proof. We use a similar continuation argument as in [140, Theorems 5.1]. More specifically, assume that there exists a derivative feedback gain $K_d^\star$ such that all zeros of $H_0(\cdot)$ lie in the open left half-plane. Consider now the feedback law: $u(t) = K_py(t) + kK_d^\star\dot{y}(t) + K_i\int_0^t y(s)\,\mathrm{d}s$ for $k \in [0,1]$. For $k = 0$ the corresponding characteristic function has an odd number of roots in right half-plane, while for $k = 1$ there are no right half-plane roots. By increasing k from 0 to 1, all roots are thus moved to the left half-plane. Furthermore, as all matrices in the characteristic function are real-valued, these characteristic roots move in complex conjugate pairs. Therefore, to bring an odd number of characteristic roots to the left half-plane, at least one root has to pass through either the origin or infinity. The first option is however impossible as a characteristic root at the origin is invariant with respect to k. On the other hand, a root crossing through infinity means that there exists a $\hat{k} \in (0,1)$ such that $\det(I - \hat{k}BK_d^\star C) = 0$, which implies that $BK_d^\star C$ has a real-valued eigenvalue $1/\hat{k} > 1$. □

3.4.3 Illustration

In this subsection, we illustrate the results of Sections 3.3 and 3.4.2 by means of an example.

Example 3.2. Let us consider the following third-order, single-input single-output system:

$$\begin{cases} \dot{x}(t) &= \begin{bmatrix} 0 & 1 & 0 \\ 0 & 0 & 1 \\ -1 & 0 & 0 \end{bmatrix} x(t) + \begin{bmatrix} 0 & 0 & 0 \\ 0 & 0 & 0 \\ 2.15 & 0 & 0 \end{bmatrix} x(t-6) + \begin{bmatrix} 0 \\ 0 \\ -1 \end{bmatrix} u(t), \\ y(t) &= \begin{bmatrix} 8.7 & 0 & 1 \end{bmatrix} x(t) \end{cases} \tag{3.14}$$

with corresponding transfer function

$$T(s) = -\frac{8.7 + s^2}{s^3 + (1 - 2.15e^{-6s})}.$$

It can be verified that the open-loop system is unstable as the associated characteristic function has five roots in the closed right half-plane[1]. To stabilize this system, we consider the PD feedback law

$$u(t) = k_p\, y(t) + k_d\, \dot{y}(t). \tag{3.15}$$

The corresponding closed-loop characteristic function is given by

$$h_0(\lambda) = (1 + k_d)\lambda^3 + k_p\lambda^2 + 8.7k_d\lambda + 8.7k_p + 1 - 2.15e^{-6\lambda}. \tag{3.16}$$

Figure 3.3 shows the number of right half-plane roots of this quasi-polynomial in function of k_p and k_d (encircled). This figure can be derived as follows. When k_d is decreased from $k_d > -1$ to $k_d < -1$ a right half-plane root either appears (for $k_p > 0$) or disappears (for $k_p < 0$) via infinity (dot-dashed line). Other changes in the number of right half-plane roots are caused by crossings via the imaginary axis and correspond to complex numbers $\lambda = \jmath\omega$ for which

$$-\jmath(1 + k_d)\omega^3 - k_p\omega^2 + \jmath 8.7k_d\omega + 1 \\ + 8.7k_p - 2.15\cos(6\omega) + \jmath 2.15\sin(6\omega) = 0.$$

By grouping the real and imaginary terms in this expression, we obtain the following nonlinear system in k_p, k_d, and ω:

$$\begin{cases} -k_p\omega^2 + 1 + 8.7k_p - 2.15\cos(6\omega) = 0, \\ -(1 + k_d)\omega^3 + 8.7k_d\omega + 2.15\sin(6\omega) = 0. \end{cases}$$

It is clear that for $k_p = 1.15/8.7$ and $k_d \in \mathbb{R}$ there is a crossing at the origin ($\omega = 0$ - dash-dot-dot-dash line) and for

$$\begin{aligned} \omega \in &(0, \infty), \\ k_p = &(2.15\cos(6\omega) - 1)/(8.7 - \omega^2), \\ k_d = &(\omega^3 - 2.15\sin(6\omega))/(8.7\omega - \omega^3) \end{aligned}$$

there is a complex conjugate pair crossing the imaginary axis at $\pm\jmath\omega$ (full line). Now we only need determine the crossing directions. To this end we use the derivative of the real part of a (simple) zero of (3.16) with respect to k_p:

$$\left.\frac{\partial \Re(\lambda)}{\partial k_p}\right|_{\lambda=\jmath\omega} = \Re\left(\frac{\omega^2 - 8.7}{-3(1 + k_d)\omega^2 + 2k_p\jmath\omega + 8.7k_d + 12.9e^{-6\jmath\omega}}\right).$$

[1] For example using the `TDS-CONTROL` package presented in Chapter 7.

We observe that there are two parameter regions for which the closed-loop system is exponentially stable. A large one in the left bottom corner of Figure 3.3a with $k_d < -1$ (light gray) and a smaller one in the parameter region on which Figure 3.3b focuses (dark gray). For parameter pairs (k_p, k_d) inside the light gray region, the feedback interconnection of (3.14) with (3.15) is exponentially stable, but the closed-loop system is destabilized by introducing an (arbitrarily small) feedback delay ($\rho(BK_dC) = |k_d| > 1$) or a finite-difference approximation of the derivative ($\Lambda(BK_dC) = \{-k_d\} \notin \text{clos}(S)$). Furthermore, the closed-loop system can not be made strongly exponentially stable by low-pass filtering the derivative as the filter is itself destabilizing ($c(BK_dC) = -k_d > 1$). On the other hand, for feedback parameters in the dark gray region, low-pass filtering of the derivative does not destabilize the closed-loop system ($c(BK_dC) = -k_d < 1$) and hence strong exponential stability can be achieved by adding a low-pass filter of the form (3.12) with a sufficiently large cut-off frequency to the control loop. Note furthermore that for parameter pairs inside the darkest gray area in Figure 3.3b, it can be shown that exponential stability of the closed-loop interconnection of (3.14) and (3.15) (i.e., PD control without low-pass filtering) is preserved under a sufficiently small feedback delay or a sufficiently accurate finite-difference approximation of the derivative.

Finally, we illustrate Proposition 3.5 and its proof. To this end, we take a look at the number of unstable roots for $k_d = 0$. For $k_p < 1.15/8.7$ this number is always odd. To remove these right half-plane roots while keeping k_p fixed (i.e., moving vertically from the horizontal axis to the light gray area) one of the roots needs to disappear via infinity. As a consequence, any stabilizing pair (k_p, k_d) left of the line $k_p < 1.15/8.7$ does not satisfy $c(BK_dC) = -k_d < 1$ and closed-loop stability can therefore be destroyed by introducing a low-pass filter with a sufficiently large cut-off frequency. ◇

3.5 Design of strongly stabilizing PID controllers

In this section, we describe a computational procedure to find gain matrices K_p, K_d, and K_i such that the closed-loop interconnection of (3.1) and (3.12) is strongly exponentially stable for sufficiently small T. To this end, we will use a direct optimization approach, as described in Section 2.3.2. More specifically, the proposed design procedure can be summarized as follows:

1. choose initial controller matrices K_p, K_d, and K_i;
2. if $c(BK_dC) > 0.9$, then re-scale K_d by $0.9/c(BK_dC)$;

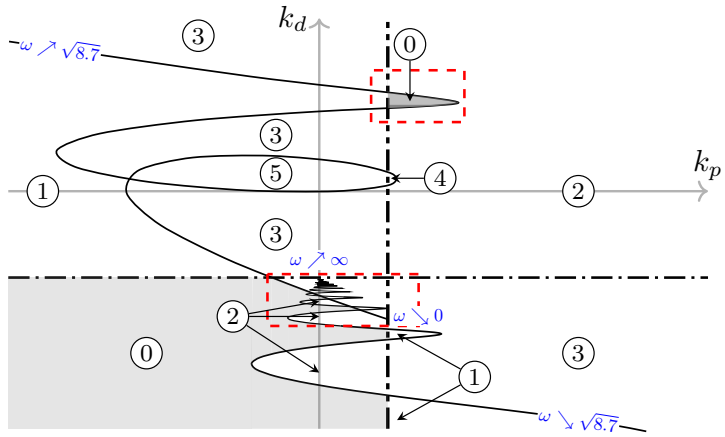

(a) $(k_p, k_d) \in [-0.6, 0.75] \times [-4.4, 2]$

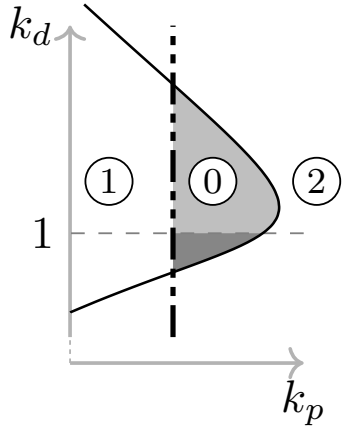

(b) $(k_p, k_d) \in [0, 0.3] \times [0.8, 1.3]$

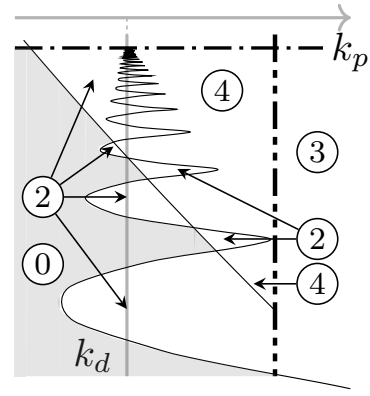

(c) $(k_p, k_d) \in [-0.1, 0.2] \times [0.96, -1.6]$

Crossing via infinity

Crossing via imaginary axis

Crossing via the origin

PD controller is stabilizing but not robust against the perturbations of Section 3.3 or low-pass filtering.

PD controller with low-pass filtering is strongly stabilizing.

PD controller without low-pass filtering is stabilizing and robust against the perturbations of Section 3.3 and the PD controller with low-pass filtering is strongly stabilizing.

Figure 3.3: Number of right half-plane roots (encircled) of (3.16) in function of k_p and k_d.

3. minimize the spectral abscissa of (3.3) as function of the entries of K_p, K_d, and K_i under the constraint that $c(BK_dC) < 1$;

4. choose a sufficiently small T such that the feedback interconnection of (3.1) and (3.12) is strongly exponentially stable.

The constraint in step 3 ensures that introducing the low-pass filter does not destabilize the closed-loop system. This constraint is handled using a penalty method. More precisely, we consider the objective function

$$c(K_p, K_d, K_i) + \gamma \max\{0, c(BK_dC) - 1\} \tag{3.17}$$

with $c(K_p, K_d, K_i)$ the spectral abscissa of (3.3) for the given feedback gains and $\gamma > 0$ a weighting parameter. The goal of the term $\max\{0, c(BK_dC) - 1\}$ is to penalize feedback gains that do not satisfy $c(BK_dC) < 1$. If the final K_d does not fulfill this constraint then γ is increased and the minimization procedure is restarted. This process is repeated until the resulting K_d fulfills the constraint. As the objective function is generally nonconvex and nonsmooth, one must use the nonsmooth, nonconvex optimization approach described in Section 2.3.3.

Next, we illustrate the effectiveness of this method on three example problems. All experiments were performed in MATLAB R2018b (version 9.5.0.944444) on a Dell Latitude 7490 with a Intel(R) Core(TM) i7-8650U CPU @ 1.90GHz eight core processor and 16GB of RAM running Ubuntu 20.04.4 LTS. All results are rounded to four digits accuracy.

Example 3.3. We start with designing a controller for the system examined in Example 3.2. Starting from the zero controller $(K_p, K_d) = (0, 0)$ and γ equal to 100, we obtain the stabilizing feedback parameters $(K_p, K_d) = (0.2378, 1.019)$. As $c(BK_dC) = -1.019 < 1$, it follows from Proposition 3.4 that the closed-loop system with low-pass filtering of the derivative signal is strongly exponentially stable for sufficiently small T. For example, choosing $T = 10^{-4}$s, the closed-loop system with low-pass filtering is strongly exponentially stable and has an exponential decay rate of 3.792×10^{-2}. ◇

Example 3.4. Secondly, we consider a system of form (3.1) with $n = 6$, $p = 3$, $q = 2$ and $m = 3$. The system matrices and delays are given in [16, Appendix B]. The open-loop plant has 5 right half-plane roots and the spectral abscissa is equal to 2.607. After running the design procedure starting from a zero initial controller and $\gamma = 10^5$ we obtain a stable closed-loop system. The corresponding feedback matrices are given in [16, Appendix B]. As the real part of all eigenvalues of BK_dC is smaller than one, the closed-loop system with low-pass filtering is strongly exponentially stable for a sufficiently large cut-off

frequency. For example, for $T = 10^{-4}$ s the exponential decay rate is equal to 0.10031. ◇

Example 3.5. As a last example, we consider the stabilization of a quadcopter around its equilibrium point, i.e., hovering at a fixed position with a fixed orientation of the principal axes. We use the twelve dimensional linearized model given in [103, Equations (6.4-6.7)] for the parameters given in [103, Section 4]. By choosing an appropriate output matrix C we obtain the following system of the form (3.1):

$$\begin{cases} \dot{x}(t) = \begin{bmatrix} 0_{3\times3} & I_3 & 0_{3\times3} & 0_{3\times3} \\ 0_{3\times3} & 0_{3\times3} & G & 0_{3\times3} \\ 0_{3\times3} & 0_{3\times3} & 0_{3\times3} & I_3 \\ 0_{3\times3} & 0_{3\times3} & 0_{3\times3} & 0_{3\times3} \end{bmatrix} x(t) + \begin{bmatrix} 0_{3\times4} \\ T \\ 0_{3\times4} \\ R \end{bmatrix} u(t), \\ y(t) = \begin{bmatrix} I_3 & 0_{3\times1} & 0_{3\times1} & 0_{3\times1} & 0_{3\times3} & 0_{3\times1} & 0_{3\times1} & 0_{3\times1} \\ 0_{1\times3} & 1 & 1 & 1 & 0_{1\times3} & 0 & 0 & 0 \\ 0_{3\times3} & 0_{3\times1} & 0_{3\times1} & 0_{3\times1} & I_3 & 0_{3\times1} & 0_{3\times1} & 0_{3\times1} \\ 0_{1\times3} & 0 & 0 & 0 & 0_{1\times3} & 0 & 0 & 1 \end{bmatrix} x(t) \end{cases} \tag{3.18}$$

with

$$G = \begin{bmatrix} 0 & -g & 0 \\ g & 0 & 0 \\ 0 & 0 & 0 \end{bmatrix}, \; T = \begin{bmatrix} 0 & 0 & 0 & 0 \\ 0 & 0 & 0 & 0 \\ \frac{-\theta}{m} & \frac{-\theta}{m} & \frac{-\theta}{m} & \frac{-\theta}{m} \end{bmatrix},$$

$$R = \begin{bmatrix} 0 & \frac{l\,\theta}{I_x} & 0 & \frac{-l\,\theta}{I_x} \\ \frac{l\,\theta}{I_y} & 0 & \frac{-l\,\theta}{I_y} & 0 \\ \frac{-2d\Omega_0}{I_z} & \frac{2d\Omega_0}{I_z} & \frac{-2d\Omega_0}{I_z} & \frac{2d\Omega_0}{I_z} \end{bmatrix},$$

$\theta = 2b\Omega_0$, $g = 9.8\,\mathrm{m/s^2}$, $m = 1.32\,\mathrm{kg}$, $b = 1.5108 \cdot 10^{-5}\,\mathrm{kg\,m}$, $l = 0.214\,\mathrm{m}$, $I_x = 9.3 \cdot 10^{-3}\,\mathrm{kg\,m^2}$, $I_y = 9.2 \cdot 10^{-3}\,\mathrm{kg\,m^2}$, $I_z = 151 \cdot 10^{-2}\,\mathrm{kg\,m^2}$, $d = 4.406 \cdot 10^{-7}\,\mathrm{kg\,m^2/s}$ and $\Omega_0 = \sqrt{(mg/(4b))}$. We run the optimization procedure with γ equal to 100 for ten random initial parameter values. Next, we select the controller for which closed-loop spectral abscissa is the smallest (see [16, Appendix C]). As for these controller parameters the constraint $c(BK_dC) < 1$ is satisfied, introducing a low-pass filter with a sufficiently large cut-off frequency (e.g., with $T = 10^{-6}$ s) does not destabilize the closed-loop system and assures strong exponential stability. Figure 3.4 shows the corresponding characteristic roots. Note that four of these characteristic roots almost correspond to the eigenvalues of $(K_dCB - I_4)/T$. ◇

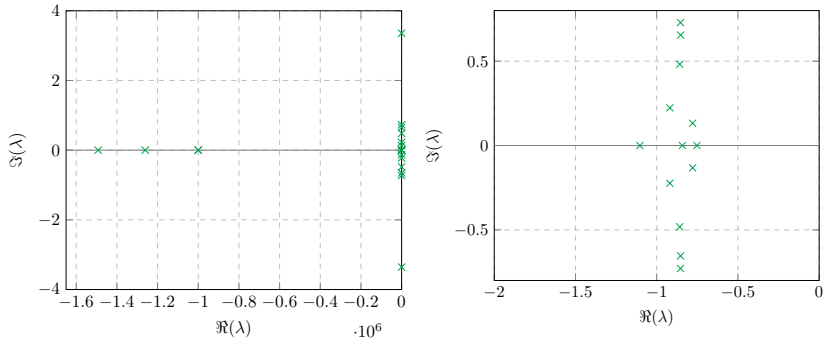

Figure 3.4: The characteristic roots of the resulting closed-loop quadcopter system with low-pass filtering of the derivative. The right-hand panel zooms in on the rightmost characteristic roots.

3.6 Extensions

We present three extensions of the previous results. Firstly, we examine systems for which $CB = 0_{q_1 \times p_1}$. Secondly, we consider systems with an input delay in the nominal model. Finally, we briefly comment on incorporating bounded (non-vanishing) perturbations on the system matrices and delays as so far we dealt with analyzing and resolving the sensitivity of exponential stability with respect to perturbations that can be made sufficiently small.

3.6.1 Systems with relative degree larger than one

Note that if $CB = 0_{q_1 \times p_1}$, i.e., the relative degree[2] of each input-output channel of system (3.1) is larger than one, then exponential stability implies strong exponential stability even without low-pass filtering of the derivative signal, as shown in the following proposition.

Proposition 3.6. Assume that the gain matrices K_p, K_d, and K_i exponentially stabilize the closed-loop system consisting of (3.1) and (3.2). If $CB = 0_{p_1 \times q_1}$, then the feedback interconnection of (3.1) with (3.2) is strongly exponentially stable.

[2]By interpreting the system (3.1) as an infinite dimensional system on the head-tail state space $H := \mathbb{R}^n \times \mathcal{C}([-\tau_K, 0], \mathbb{R}^n)$ equipped with the inner product $\left\langle (x_1, \phi_1), (x_2, \phi_2) \right\rangle_H = x_1^T x_2 + \int_{-\tau_m}^0 \phi_1(s)^T \phi_2(s)\, \mathrm{d}s$, the relative degree of each input-output channel is defined as in [144, Definition 1.3].

Proof. By incorporating the perturbations $R_i(\lambda; r_i)$ for $i = 1, 2, 3$ in (3.3), the characteristic function becomes

$$H_5(\lambda; r_1, r_2, r_3) := \det \left(\lambda \begin{bmatrix} I_n - Q(\lambda; r_1, r_2, r_3) & 0 \\ 0 & I_{r_i} \end{bmatrix} - \begin{bmatrix} A_0 & 0 \\ 0 & 0 \end{bmatrix} - \right.$$

$$\left. \sum_{k=1}^{m} \begin{bmatrix} A_k & 0 \\ 0 & 0 \end{bmatrix} e^{-\lambda \tau_k} - \begin{bmatrix} BR_1(\lambda; r_1) & 0 \\ 0 & I_{r_i} \end{bmatrix} \begin{bmatrix} K_p & U_i \\ V_i & 0 \end{bmatrix} \begin{bmatrix} R_3(\lambda; r_3)C & 0 \\ 0 & I_{r_i} \end{bmatrix} \right)$$

with

$$Q(\lambda; r_1, r_2, r_3) := BR_1(\lambda; r_1) K_d R_2(\lambda; r_2) R_3(\lambda; r_3) C.$$

Because $CB = 0_{q_1 \times p_1}$, the Weinstein–Aronszajn identity implies that $I_n - Q(\lambda; r_1, r_2, r_3)$ is invertible for all $\lambda \in \mathbb{C}$.[3] Further, by the last item of Assumption 3.1 there exist $\hat{r} > 0$ and $N > 0$ such that the norm of $\big(I - Q(\lambda; r_1, r_2, r_3)\big)^{-1}$ is finite in the right half-plane $V := \{\lambda \in \mathbb{C} : \Re(\lambda) > -N\}$ for all r_1, r_2, and r_3 in the interval $(0, \hat{r})$. Using a similar approach as in the proof of Proposition 3.3, one can show that the modulus of a characteristic root of $H_5(\cdot; r_1, r_2, r_3)$ in the right half plane V is finite for r_1, r_2, and r_3 in $(0, \hat{r})$. Furthermore, because $H_5(\cdot; r_1, r_2, r_3)$ uniformly converges to $H_0(\cdot)$ on compact regions in the complex plane for r_1, r_2 and r_3 going to zero, the proposition now follows from a similar argument as in the proof of Proposition 3.4. □

Remark 3.3. Let us consider the following single-input, single-output system with relative degree $\nu > 1$ and no state delay:

$$\begin{cases} \dot{x}(t) = & A\,x(t) + b\,u(t), \\ y(t) = & c^T x(t) \end{cases}$$

in which $b \in \mathbb{R}^n$, $c \in \mathbb{R}^n$, $c^T b = 0$, $c^T Ab = 0, \ldots, c^T A^{\nu-2} b = 0$ and $c^T A^{\nu-1} b \neq 0$. In this case the presented results can be generalized to extended PID control (in the sense of [94, 205]). In extended PID control not only the first derivative is fed back but also higher order derivatives. More specifically, for a system with relative degree ν the feedback signal now becomes,

$$u(t) = K_p\, y(t) + K_i \int_0^t y(s)\, \mathrm{d}s + \sum_{i=1}^{\nu} K_{d,i} y^{(i)}(t).$$

[3] For two matrices $U \in \mathbb{R}^{n \times m}$ and $V \in \mathbb{R}^{m \times n}$, the equality $\det(I_n + UV) = \det(I_m + VU)$ holds. By choosing $U = -BR_1(\lambda; r_1) K_d R_2(\lambda; r_2) R_3(\lambda; r_3)$ and $V = C$, it follows that $\det(I_n - Q(\lambda; r_1, r_2, r_3)) = \det(I_{q_1}) \neq 0$.

The strong exponential stability analysis can now be addressed by defining a new output y_e and recasting the control law:

$$\begin{aligned} y_e(t) = &\begin{bmatrix} c & \left(c^\top A\right)^\top & \dots & \left(c^\top A^{\nu-1}\right)^\top \end{bmatrix}^\top x(t), \\ u(t) = &\begin{bmatrix} K_p & K_{d,1} & \dots & K_{d,\nu-1} \end{bmatrix} y_e(t) + \begin{bmatrix} 0 & \dots & 0 & K_{d,\nu} \end{bmatrix} \dot{y}_e(t) \\ &+ \begin{bmatrix} K_i & 0 & \dots & 0 \end{bmatrix} \int_0^t y_e(s)\,\mathrm{d}s \end{aligned}$$

meaning that the previously obtained results hold when BK_dC is replaced with $bK_{d,\nu}c^\top A^{\nu-1}$. Furthermore, note that the controller synthesis algorithm in Section 3.5 can easily be adapted to handle this sparsity pattern on the gain matrices. However, such a direct extension is not possible for the general system class introduced in (3.1), as it relies on the concepts of relative degree and normal form (in which output (derivatives) take the role of state variables). More specifically, for time-delay systems the relative degree may be sensitive to infinitesimal delay perturbations and the normal form may not exist [141].

3.6.2 Systems with input delay

This subsection considers systems with a fixed input delay $\tau_u > 0$,

$$\begin{cases} \dot{x}(t) = A_0\, x(t) + \sum_{k=1}^{m} A_k\, x(t-\tau_k) + B\, u(t-\tau_u), \\ y(t) = C\, x(t). \end{cases} \tag{3.19}$$

The exponential stability of the nominal closed-loop system is now characterized by the roots of (3.9) with r fixed to τ_u. It follows from a similar argument as in the proof of Proposition 3.1, that $\rho(BK_dC) < 1$ is a necessary condition for the exponential stability of the nominal system. In the following proposition, we examine strong exponential stability for systems with input delay. In contrast to systems without input delay, there is now no additional constraint (besides stabilizing the system) on K_d to achieve strong exponential stability using a low-pass filter with a sufficiently large cut-off frequency.

Proposition 3.7. Assume that the gain matrices K_p, K_d, and K_i exponentially stabilize the closed-loop system consisting of (3.19) and (3.2), then the feedback interconnection of (3.19) and (3.12) is strongly exponentially stable.

Proof. By incorporating the low-pass filter and the perturbations $R_i(\lambda; r_i)$ for $i = 1, 2, 3$, the characteristic function becomes:

$$H_6(\lambda; T, r_1, r_2, r_3) := \det \Bigg(\lambda \begin{bmatrix} I_n & 0 \\ 0 & I_{r_i} \end{bmatrix} - \begin{bmatrix} A_0 & 0 \\ 0 & 0 \end{bmatrix} - \sum_{k=1}^{m} \begin{bmatrix} A_k & 0 \\ 0 & 0 \end{bmatrix} e^{-\lambda \tau_k} + \begin{bmatrix} BR_1(\lambda; r_1) e^{-\lambda \tau_u} & 0 \\ 0 & I_{r_i} \end{bmatrix} \times \begin{bmatrix} K_p + \frac{\lambda}{\lambda T + 1} K_d R_2(\lambda; r_2) & U_i \\ V_i & 0 \end{bmatrix} \begin{bmatrix} R_3(\lambda; r_3) C & 0 \\ 0 & I_{r_i} \end{bmatrix} \Bigg).$$

We have already established that the exponential stability of the closed-loop system of (3.19) and (3.2) requires $\rho(BK_dC) < 1$. Next, we will show that this condition implies that the low-pass filter is not destabilizing for $R_1(\lambda; r_1) = R_2(\lambda; r_2) = R_3(\lambda; r_3) = I$. If $\rho(BK_dC) < 1$, there exist $c > 0$ and $\widehat{T} > 0$ such that $\rho\left(BK_dCe^{-\lambda\tau_u} \frac{1}{\lambda T+1}\right) < 1$ for all $\lambda \in V := \{\lambda \in \mathbb{C} : \Re(\lambda) > -c\}$ and all $T \in (0, \widehat{T})$. This implies that $I - BK_dCe^{-\lambda\tau_u} \frac{1}{\lambda T+1}$ is invertible on V for $T \in (0, \widehat{T})$. It now follows from a similar argument as in Proposition 3.3 that the low-pass filter does not destabilize the system for sufficiently small T. Strong exponential stability follows from a similar argument as in Proposition 3.4. □

The proposition above shows that if a PID controller stabilizes the system (3.19), then including a low-pass filter with a sufficiently large cut-off frequency makes the closed-loop system strongly exponentially stable. Such stabilizing controller matrices can, for instance, be obtained using the method presented in [134], in which suitable controller matrices are derived by minimizing the spectral abscissa of the closed-loop system under the constraint that $\rho(BK_dC) < 1$ (which assures stability of the underlying delay differential equation). As in Section 3.5, this constraint is incorporated in the cost function. However, instead of including a penalty term, a logbarier method is used to enforce that the constraint is fulfilled at each iteration step.

Example 3.6. We revisit Example 3.5 with a (fixed) feedback delay of $\tau_u = 0.1$s. Although $\rho(BK_dC) = 0.4925 < 1$ for the controller obtained in Section 3.5, the closed-loop system is unstable for $\tau_u = 0.1$s, both with and without filtering. (Recall that the preservation of exponential stability is only guaranteed for a sufficiently small feedback delay.) Next, we will therefore look for a new controller that takes this fixed input delay into account. To this end, we apply the procedure of [134] starting from this controller, we arrive at a stable closed-loop system with an exponentially decay rate (with $T = 10^{-6}$s) of less than 0.0100 and $\rho(BK_dC) = 0.9990 < 1$. However, when starting from another

initial controller, created by swapping the initial K_i and K_d matrices, we arrived at an exponentially decay rate (for $T = 10^{-6}$s) of 1.1797, illustrating the non-convexity of the optimization problem at hand and the influence of the chosen starting values. The corresponding controller matrices are given in [16, Appendix C]. ◇

3.6.3 Bounded uncertainties on system matrices and state delays

We conclude the section with a comment on parametric uncertainty. Firstly, it follows from the proof of Proposition 3.4, that strong exponential stability not only guarantees robustness against sufficiently small perturbations within the framework presented in Section 3.4.2 but also against (sufficiently) small perturbations on the system matrices and the delays. Secondly, the algorithm presented in Section 3.5 can be generalized to systems with bounded (i.e., non-vanishing) uncertainties on the system matrices and the delays. More specifically, consider the uncertain system

$$\begin{cases} \dot{x}(t) = \widetilde{A}_0(\delta)\, x(t) + \sum\limits_{k=1}^{m} \widetilde{A}_k(\delta)\, x\big(t - (\tau_k + \delta\tau_k)\big) + \widetilde{B}(\delta)\, u(t), \\ y(t) = \widetilde{C}(\delta)\, x(t) \end{cases} \tag{3.20}$$

with $\delta = (\delta_1, \ldots, \delta_L)$ a set of L real-valued matrix uncertainties such that

$$\delta_1 \in \mathbb{R}^{\varrho_1 \times \varsigma_1}, \ldots, \delta_L \in \mathbb{R}^{\varrho_L \times \varsigma_L} \text{ and } \|\delta_1\|_F \leq 1, \ldots, \|\delta_L\|_F \leq 1.$$

These uncertainties affect the system matrices in an affine way, for example $\tilde{A}_0(\delta)$ is given by:

$$\widetilde{A}_0(\delta) = A_0 + \sum_{l=1}^{L} G_{A_0,l}\delta_l H_{A_0,l}$$

with A_0 the nominal value of the system matrix and $G_{R,l}$ and $H_{R,l}$ real-valued shape matrices that allow to target specific blocks or parameters in the system matrices. The other uncertain matrices are defined in a similar way. The uncertainties on the state delays, $\delta\tau_1, \ldots, \delta\tau_m$, are real-valued and bounded in absolute value. The goal is now to design a PID controller with low-pass filtering of the derivative signal that strongly stabilizes the system for all admissible uncertainty values. To this end, the design procedure of Section 3.5 has to be modified in the following way. Firstly, the constraint $c(\widetilde{B}(\delta)K_d\widetilde{C}(\delta)) < 1$ now has to hold for all admissible uncertainty values, i.e., $c^{\text{ps}}(\widetilde{B}(\delta)K_d\widetilde{C}(\delta)) < 1$. Secondly, instead of minimizing the spectral abscissa, we now have to minimize the pseudospectral abscissa of the closed-loop interconnection of (3.20) and

(3.2). Both these quantities can be computed using a slight modification of the method presented in [28]. Furthermore, explicit expressions for the derivative of these quantities with respect to the elements of K_p, K_d, and K_i, which are required in the optimization process, can be obtained.

3.7 Conclusion

This chapter analyzed the exponential stability of the closed-loop interconnection of dynamical systems with multiple state delays and a PID controller. More specifically, we saw that under certain conditions on the derivative feedback gain, such systems can be fragile, in the sense that they can be destabilized by arbitrarily small modeling errors. We therefore introduced the notion of *strong exponential stability*, which requires the preservation of exponential stability under sufficiently small perturbations. We showed that an exponential stable closed-loop system can be made strongly exponentially stability by adding a low-pass filter with a sufficiently large cut-off frequency to the control loop, under a certain algebraic constraint on the derivative gain matrix K_d. This result led to a computational procedure for designing strongly exponentially stabilizing PID controllers. A MATLAB implementation of this algorithm is available from `http://twr.cs.kuleuven.be/research/software/delay-control/strong-stability`. The code used to generate Examples 3.3 to 3.5 is available from the same location.

CHAPTER

4 The robust strong H-infinity norm of time-delay systems with real-valued and structured uncertainties

Abstract

This chapter provides a mathematical characterization for the robust (strong) H_∞-norm of an uncertain linear time-invariant time-delay system with discrete delays and real-valued, structured, Frobenius norm bounded uncertainties on the system matrices. The robust H_∞-norm is defined as the worst-case value of the H_∞-norm over all admissible uncertainty values. For the considered system class, the robust H_∞-norm is however a fragile measure as for a particular instance of the uncertainties the H_∞-norm might be sensitive to arbitrarily small perturbations on the delays. We therefore introduce the robust strong H_∞-norm, which takes into account both the uncertainties on the system matrices and infinitesimal delay perturbations. This quantity is a continuous function of both the elements of the system matrices and the delays. The main contribution of this chapter is a relation between the robust strong H_∞-norm of an uncertain time-delay system and the robust distance to instability of an associated uncertain delay differential algebraic equation. This relation is subsequently employed in a novel algorithm for computing the robust strong H_∞-norm of an uncertain time-delay system.

The results of this chapter were originally presented in [11] and [12].

4.1 Introduction

As we have seen in Section 2.2.2, the H_∞-norm is an important quantity in the robust control framework. For uncertain dynamical systems, one is typically interested in the worst-case (maximal) value of the H_∞-norm over all admissible uncertainty values, the so-called robust H_∞-norm [202]. For systems with pointwise delays, the robust H_∞-norm has already been examined in, among others, [118, 107, 54, 127] and [101], which are all based on (extension of) Lyapunov theory. More specifically, these papers derive linear matrix inequalities that guarantee that the H_∞-norm of an uncertain (closed-loop) system is below a certain specified bound for all admissible uncertainty values. However, as the derived conditions are typically only sufficient, this upper bound may be an overestimate for the actual robust H_∞-norm of the system. Furthermore, these papers are mostly limited to systems with one delay. In contrast, we will

consider dynamical systems with multiple pointwise delays and derive an exact characterization for the robust H_∞-norm. Also, the uncertainties considered in this chapter are real-valued as the system itself is real-valued.

As an additional distinctive feature, we consider systems of which the direct feed-through part includes multiple delays. For such systems, the robust H_∞-norm might be *fragile* with respect to infinitesimal delay changes. This fragility problem originates from the sensitivity of the H_∞-norm of a particular instance of the uncertain system with respect to arbitrary small delay changes [82]. This work will therefore introduce the novel notion of the robust strong H_∞-norm, which is defined as the worst-case value of the strong H_∞-norm[1] over all admissible uncertainty values. This robust strong H_∞-norm takes both the uncertainties on the system matrices and infinitesimal perturbations on the delay values into account. Within this framework, the main technical contribution of this chapter is a relation between the robust strong H_∞-norm and the robust distance to instability of an associated uncertain delay differential algebraic equation with both real- and complex-valued perturbations. This relation can be seen as an extension of Theorem 2.5 to uncertain time-delay systems with multiple delays in the direct feed-through part.

The mathematical characterization of the robust strong H_∞-norm will be accompanied by a numerical algorithm for computing this quantity, inspired by recent developments in numerical linear algebra [28] that allow to efficiently calculate the distance to instability of a delay differential equation with real-valued and structured uncertainties.

The remainder of this chapter is organized as follows. In Section 4.2 we recall some important preliminary results. Next, we introduce the considered class of uncertain time-delay systems and define the robust strong H_∞-norm. Thereafter, we introduce the notion of the robust distance to instability of a particular class of uncertain delay differential algebraic equations. Section 4.5 contains the main theoretical result of the paper as it gives the relation between the robust strong H_∞-norm of an uncertain time-delay system and the robust distance to instability of an uncertain delay differential algebraic equation. This relationship is illustrated in Section 4.6 using four examples. Next, Section 4.7 presents a numerical algorithm to compute the robust strong $\mathcal{H}_\infty$-norm, based on the theory developed in Section 4.5. Finally, Section 4.8 gives some concluding remarks.

[1] As defined in [82, Definition 4.4]

4.2 Preliminaries

Firstly, we examine the H_∞-norm of a nominal time-delay system with multiple delays in the direct feed-through part. We will see that for such systems the H_∞-norm might be a discontinuous function of the delay values. We will therefore recall the notion of the strong H_∞-norm and some related properties from [82]. Secondly, we will extend Theorem 2.5 to systems with direct feed-through. This will motivate the stability analysis of a class of linear time-invariant delay differential algebraic equations (DDAEs) in Section 4.2.2.

4.2.1 The strong H_∞-norm

Consider the following LTI system with discrete delays:

$$\begin{cases} \dot{x}(t) = \sum\limits_{k=0}^{m} A_k\, x(t-\tau_k) + \sum\limits_{k=0}^{m} B_k\, w(t-\tau_k), \\ z(t) = \sum\limits_{k=0}^{m} C_k\, x(t-\tau_k) + \sum\limits_{k=0}^{m} D_k\, w(t-\tau_k) \end{cases} \tag{4.1}$$

with $x(t) \in \mathbb{R}^n$ the state variable, $w(t) \in \mathbb{R}^p$ the performance input and $z(t) \in \mathbb{R}^q$ the performance output. The matrices A_k, B_k, C_k, and D_k for $k = 0, \ldots, m$ are real-valued and have appropriate dimension. Finally, without loss of generality we assume $0 = \tau_0 < \tau_1 < \cdots < \tau_m < \infty$. The corresponding transfer function from w to z is given by:

$$T(s;\vec{\tau}) = \Big(\sum_{k=0}^{m} C_k e^{-s\tau_k}\Big)\Big(sI - \sum_{k=0}^{m} A_k e^{-s\tau_k}\Big)^{-1}\Big(\sum_{k=0}^{m} B_k e^{-s\tau_k}\Big) + \sum_{k=0}^{m} D_k e^{-s\tau_k}$$

with $\vec{\tau} = (\tau_1, \ldots, \tau_m)$[2]. Recall from (2.18) that for an (internally) exponentially stable system, the H_∞-norm is equal to the supremum of the spectral norm of its frequency response:

$$\|T(\cdot;\vec{\tau})\|_{\mathcal{H}_\infty} := \operatorname{ess\,sup}_{\omega\in\mathbb{R}^+} \sigma_1\big(T(\jmath\omega;\vec{\tau})\big).$$

For systems of the form (4.1), the H_∞-norm continuously depends on the entries of the system matrices at values for which the system is exponentially stable. However, similar as the spectral abscissa of a neutral DDE (see Section 2.1.3) the function $\vec{\tau} \mapsto \|T(\cdot;\vec{\tau})\|_{\mathcal{H}_\infty}$ might be discontinuous, even if the system remains stable. Let us illustrate this sensitivity by means of an example.

[2]Note that τ_0 is not included in $\vec{\tau}$ as it is fixed to 0.

Example 4.1. Consider the following system

$$\begin{cases} \dot{x}(t) = -2x(t) + x(t-\tau_1) - \ \ w(t) - 0.5w(t-\tau_2), \\ z(t) = -2x(t) + x(t-\tau_2) + 5w(t) + 1.5w(t-\tau_1) - 3w(t-\tau_2). \end{cases} \tag{4.2}$$

It can be verified that the underlying DDE is (strongly) exponentially stable for $\tau_1 = 1$ and $\tau_2 = 2$. The corresponding frequency response is given by

$$T(\jmath\omega; (\tau_1, \tau_2)) = \frac{2 - 0.5e^{-\jmath\omega 2\tau_2}}{\jmath\omega + 2 - e^{-\jmath\omega\tau_1}} + 5 + 1.5e^{-\jmath\omega\tau_1} - 3e^{-\jmath\omega\tau_2}.$$

Figure 4.1a plots the magnitude of the frequency response in function of ω for $\tau_1 = 1$ and $\tau_2 = 2$. We observe that a maximum of approximately 8.4907 is attained at $\omega \approx 1.5865$. Figure 4.1b shows the effect of a small change in the delay parameters, $\tau_1 = 1$ and $\tau_2 = 2 + \pi/100$. Now the H_∞-norm is equal to approximately 9.5. Even if we further decrease the size of the perturbation on the delays, e.g., $\tau_1 = 1$ and $\tau_2 = 2 + \pi/1000$, we observe a similar effect, see Figure 4.1c. ◇

Remark 4.1. We can draw several parallels with Example 2.2. As the spectral abscissa of a NDDE, the H_∞-norm of a time-delay system that has multiple delays in its direct feed-through part might be discontinuous with respect to delay perturbations, even if the system remains strongly exponentially stable. However, if we look at a fixed angular frequency, the magnitude of the frequency response changes in a continuous way when the delay parameters are varied. Nonetheless, we observe from Figures 4.1b and 4.1c that the larger the angular frequency, the larger its sensitivity (i.e., derivative) to perturbations on the delays. It can be shown that in the example above, this derivative grows unbounded as ω goes to infinity. Furthermore, as we will see below for any bound (no matter how small), there exists a delay perturbation smaller than this bound for which the H_∞-norm of (4.2) jumps to at least 9.5. If this perturbation bound is decreased, the frequencies at which such a peak in the magnitude can be attained, moves to the right (as indicated with the arrow in Figure 4.1c). Below, we will therefore introduce the strong H_∞-norm and the asymptotic frequency response.

To examine the behavior of the frequency response for ω going to infinity, we consider the asymptotic frequency response (denoted by T_a), which for (4.1) is equal to

$$T_a(\jmath\omega; \vec{\tau}) = D_0 + \sum_{k=1}^{m} D_k e^{-\jmath\omega\tau_k}.$$

Remark 4.2. The name asymptotic frequency response stems from the observation that

$$\lim_{\bar{\omega}\to\infty} \sup_{\omega\geq\bar{\omega}} \sigma_1\big(T(\jmath\omega) - T_a(\jmath\omega)\big) = 0.$$

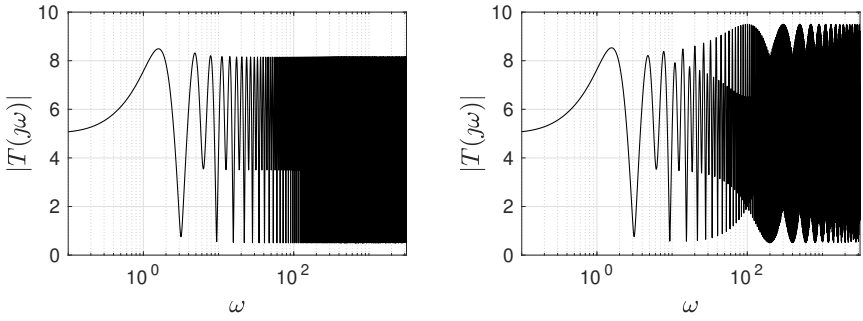

(a) $(1, 2)$ (b) $(1, 2 + \pi/100)$

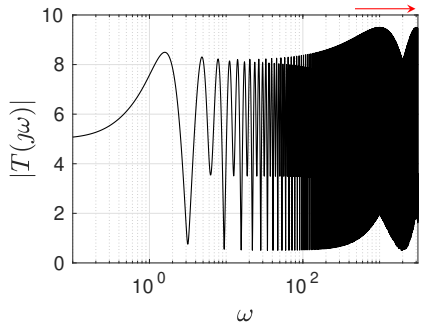

(c) $(1, 2 + \pi/1000)$

Figure 4.1: The magnitude of the frequency response of system (4.2) in function of ω for different values of the delays (τ_1, τ_2).

Inspired by the strong spectral abscissa of a NDDE, [82, Definition 4.4] introduced the *strong* H_∞-norm as the smallest upper bound for the H_∞-norm that is insensitive to infinitesimal delay changes:

$$|||T(\cdot;\vec{\tau})|||_{H_\infty} := \limsup_{\epsilon\to 0+} \left\{ \|T(\cdot;\vec{\tau}_\gamma)\|_{H_\infty} : \vec{\tau}_\gamma \in \mathcal{B}(\vec{\tau},\gamma) \cap (\mathbb{R}^+)^m \right\} \tag{4.3}$$

with $\mathcal{B}(\vec{\tau},\gamma)$ a ball in $\mathbb{R}^m$ with radius γ and centered at $\vec{\tau}$. In contrast to the nominal H_∞-norm, the strong H_∞-norm is continuous as a function of both the entries of the system matrices and the delays at values for which the system is exponentially stable [82, Theorem 4.5].

Below we will recall some important properties from [82]. We start with a characterization of the strong H_∞-norm that is amenable for numerical computation.

Proposition 4.1. [82, Theorem 4.5 & Proposition 4.3] The strong $\mathcal{H}_\infty$-norm of (4.1) satisfies

$$|||T(\cdot;\vec{\tau})|||_{H_\infty} = \max\left\{\|T(\cdot;\vec{\tau})\|_{H_\infty}, |||T_a(\cdot;\vec{\tau})|||_{H_\infty}\right\}$$

with $|||T_a(\cdot;\vec{\tau})|||_{H_\infty}$ the strong H_∞-norm of the associated asymptotic frequency response. Furthermore, it holds that

$$|||T_a(\cdot;\vec{\tau})|||_{H_\infty} = \max_{\vec{\theta}\in[0,2\pi)^m} \sigma_1\Big(D_0 + \sum_{k=1}^{m} D_k e^{\jmath\theta_k}\Big). \tag{4.4}$$

The following proposition states that the H_∞-norm and the strong H_∞-norm coincide for rationally independent delays[3].

Proposition 4.2. [82, Proposition 4.3] If the delays in $\vec{\tau}$ are rationally independent, then

$$|||T_a(\cdot;\vec{\tau})|||_{H_\infty} = \|T_a(\cdot;\vec{\tau})\|_{H_\infty},$$

and, as a consequence

$$|||T(\cdot;\vec{\tau})|||_{H_\infty} = \|T(\cdot;\vec{\tau})\|_{H_\infty}.$$

Example 4.2. Let us revisit Example 4.1. It follows from Propositions 4.1 and 4.2 that for every $i \in \mathbb{N}_{>0}$

$$\begin{aligned}
\|T(\cdot;(1,2+\pi/i))\|_{\mathcal{H}_\infty} &= |||T(\cdot;(1,2+\pi/i))|||_{\mathcal{H}_\infty} \\
&\geq |||T_a(\cdot;(1,2+\pi/i))|||_{\mathcal{H}_\infty} \\
&= \max_{\vec{\theta}\in[0,2\pi)^2} \sigma_1\left(5 + 1.5e^{\jmath\theta_1} - 3e^{\jmath\theta_2}\right) \\
&= 9.5.
\end{aligned}$$

One can thus choose delay values arbitrarily close to $(1,2)$ for which the $\mathcal{H}_\infty$-norm jumps to at least 9.5. ◇

By considering the strong H_∞-norm we remove a *fragility* problem of the H_∞-norm, namely being potentially sensitive to infinitesimal perturbations on the delays. Note however that the strong $\mathcal{H}_\infty$-norm is still a property of the nominal model (and infinitesimal perturbations of the delays). The strong H_∞-norm of a time-delay system with discrete time-delays can be computed using the method presented in [82], which is an extension the well-known BBBS algorithm (see Section 2.2.2).

[3] A collection of real numbers is rationally independent if no member can be written as a linear combination of the other elements with rational coefficients.

4.2.2 Delay differential algebraic equations

Recall from Theorem 2.5 that for a delay-free system without direct feed-through, the H_∞-norm is equal to the reciprocal of the distance to instability of an uncertain ordinary differential equation. The following proposition generalizes this result to systems with direct feed-through.

Proposition 4.3. The H_∞-norm of

$$\begin{cases} \dot{x}(t) = Ax(t) + Bw(t), \\ z(t) = Cx(t) + Dw(t) \end{cases} \tag{4.5}$$

with corresponding transfer function

$$T(s) = C(Is - A)^{-1}B + D,$$

is equal to the distance to instability of the following uncertain differential algebraic equation (DAE):

$$\begin{bmatrix} I_n & 0 & 0 \\ 0 & 0 & 0 \\ 0 & 0 & 0 \end{bmatrix} \dot{x}_e(t) = \left(\begin{bmatrix} A & B & 0 \\ 0 & -I_p & 0 \\ C & D & -I_q \end{bmatrix} + \begin{bmatrix} 0 \\ I_p \\ 0 \end{bmatrix} \Delta \begin{bmatrix} 0 & 0 & I_q \end{bmatrix} \right) x_e(t) \tag{4.6}$$

with $x_e(t) \in \mathbb{R}^{(n+p+q)}$ and $\Delta \in \mathbb{C}^{p\times q}$ a complex-valued full-block uncertainty whose size is measured in the spectral norm. The distance to instability of (4.6) is defined as the smallest $\epsilon \geq 0$ for which there exists a $\Delta \in \mathbb{C}^{p\times q}$ with $\|\Delta\|_2 \leq \epsilon$ such that $I_p - \Delta D$ is not invertible[4] or (4.6) has (a) characteristic root(s) in the closed right half-plane.

Proof. By introducing slack variables ζ_w and ζ_z, system (4.5) can be rewritten as a descriptor system:

$$\begin{cases} \begin{bmatrix} I & 0 & 0 \\ 0 & 0 & 0 \\ 0 & 0 & 0 \end{bmatrix} \begin{bmatrix} \dot{x}(t) \\ \dot{\zeta}_w(t) \\ \dot{\zeta}_z(t) \end{bmatrix} = \begin{bmatrix} A & B & 0 \\ 0 & -I & 0 \\ C & D & -I \end{bmatrix} \begin{bmatrix} x(t) \\ \zeta_w(t) \\ \zeta_z(t) \end{bmatrix} + \begin{bmatrix} 0 \\ I \\ 0 \end{bmatrix} w(t), \\ z(t) = \begin{bmatrix} 0 & 0 & I \end{bmatrix} \begin{bmatrix} x(t) \\ \zeta_w(t) \\ \zeta_z(t) \end{bmatrix}. \end{cases}$$

The proposition now follows from [26, Proposition 3.2] by noting that

$$\min\{\|\Delta\|_2 : \Delta \in \mathbb{C}^{p\times q} \text{ s.t. } \det(I_p - \Delta D) = 0\} = \sigma_1(D) = \lim_{\omega\to\infty} \sigma_1(T(\jmath\omega)).$$

□

[4] The invertibility of $I_p - \Delta D$ assures that (4.6) is regular and that its index is at most one, see the discussion below.

The proposition above shows that Theorem 2.5 can be generalized to systems with direct feed-through by a reformulation in terms of a descriptor system (sometimes also referred to as an implicit or singular system). In the following, we will derive a similar relation between the robust strong H_∞-norm of an uncertain time-delay system and the robust distance to instability of an uncertain delay differential algebraic equation. However, the stability analysis of such DDAEs is not trivial. We will therefore give a detailed discussion below.

Consider the following DDAE

$$E\dot{x}(t) = A_0\dot{x}(t) + \sum_{k=1}^{m} A_k x(t-\tau_k) \tag{4.7}$$

with the state variable $x(t) \in \mathbb{R}^n$, the matrices E, A_0,...,A_m belonging to $\mathbb{R}^{n\times n}$ and $0 < \tau_1 < \cdots < \tau_m < \infty$. A DDAE differs from an implicit DDE in that the matrix E is allowed to be singular. As a consequence, (4.7) can consists of both delay differential and delay algebraic equations.

First, we discuss the existence and uniqueness of the solutions of initial value problems associated with (4.7). As discussed in [49, 50, 66], (4.7) may be of advanced type[5] or admit impulsive solutions. To avoid such problems, we will introduce the notions of regularity and index below. To this end, let us first define these concepts for the following DAE:

$$E\dot{x}(t) = A_0 x(t) \tag{4.8}$$

and the associated (characteristic) matrix pencil

$$E\lambda - A_0. \tag{4.9}$$

The DAE (4.8) (or equivalently the matrix pencil (4.9)) is regular when the polynomial $\mathbb{C} \ni \lambda \mapsto \det\left(E\lambda - A_0\right)$ does not vanish identically. If regular, the matrix pencil (4.9) can be brought in Weierstrass-Kronecker canonical form by invertible matrices W and T [69, Chapter XII]:

$$W\left(E\lambda - A_0\right)T = \begin{bmatrix} I & 0 \\ 0 & N \end{bmatrix}\lambda - \begin{bmatrix} J & 0 \\ 0 & I \end{bmatrix}$$

with J in Jordan form and N a nilpotent matrix. The index of (4.8) is defined as zero if N is void and as the smallest integer ν such that $N^\nu = 0$ for non-void N. As in [66, Section 2.1], the DDAE (4.7) is said to be regular if the corresponding DAE (4.8) is regular and (if regular) its index is defined as the index of the DAE (4.8). Based on these notions of regularity and index, we define well-posedness in the remainder of this chapter in the following way.

[5] A FDE is of advanced type if the evolution of the state variable depends on its value in the future.

Definition 4.1. The DDAE (4.7) is called well-posed when it is regular and has at most index one.

By restricting ourselves to well-posed DDAEs, we avoid systems of advanced type and impulsive solutions. Furthermore, as shown in [66, Proposition 1], under certain conditions on the initial function there exists a unique solution to the initial value problem associated with an index one DDAE.

The following lemma allows us to easily verify whether the aforementioned well-posedness condition is satisfied. To this end let us introduce the matrices U and V (both belonging to $\mathbb{R}^{n\times n_E}$) whose columns form a (minimal) basis for the left and right null space of E, respectively, or in other words,

$$n_E := n - \operatorname{rank}(E),\ U^\top E = 0_{n_E\times n} \text{ and } EV = 0_{n\times n_E}. \tag{4.10}$$

Lemma 4.1. The DDAE (4.7) is well-posed if and only if $U^\top A_0 V$ is invertible.

Proof. The lemma follows from [41, Lemma 2]. □

Next we examine the exponential stability (as defined in Definition 2.1) of well-posed DDAEs. As in Section 2.1, exponential stability can be assessed by looking at the characteristic function associated with (4.7):

$$\mathbb{C} \ni \lambda \mapsto F_D(\lambda;\vec{\tau}) := \det\Big(\lambda E - A_0 - \sum_{k=1}^{m} A_k e^{-\lambda\tau_k}\Big).$$

More specifically, the DDAE (4.7) is exponential stable if and only if its spectral abscissa is strictly negative (or equivalently if all its characteristic roots lie in the open left half-plane, bounded away from imaginary axis). However, the considered class of well-posed DDAEs encompasses both retarded and neutral delay differential equations [134, Section 1]. As a consequence, the exponential stability of (4.7) might be sensitive to infinitesimal delay perturbations. To resolve this fragility problem, we will again consider strong exponential stability (as defined in Definition 2.4) and the strong spectral abscissa (Definition 2.5).

In the remainder of this chapter, we will need the following properties from [134]. We start with a characterization of the strong spectral abscissa of the DDAE (4.7) that is amenable for numerical computations.

Proposition 4.4. [134, Propostition 3] For well-posed DDAEs, the strong spectral abscissa satisfies

$$C(\vec{\tau}) = \max\big\{C_D(\vec{\tau}), c(\vec{\tau})\big\}$$

with $C_D(\vec{\tau})$ the strong spectral abscissa of the following delay algebraic equation:

$$0 = U^\top A_0 V\, x(t) + \sum_{k=1}^{m} U^\top A_k V\, x(t-\tau_k)$$

with U and V as defined in (4.10). Furthermore, the quantity $C_D(\vec{\tau})$ is equal to the unique zero crossing of the monotonically decreasing function

$$\mathbb{R} \ni \varsigma \mapsto \max_{\vec{\theta}\in[0,2\pi)^m} \rho\left(\sum_{k=1}^{m} \left(U^\top A_0 V\right)^{-1} \left(U^\top A_k V\right) e^{-\varsigma\tau_k + \jmath\theta_k}\right) - 1, \qquad (4.11)$$

in which $\rho(\cdot)$ denotes the spectral radius of its matrix argument, if such a crossing exists and otherwise $C_D(\vec{\tau})$ equals $-\infty$.

The following proposition states that (4.7) has a vertical chain of characteristic roots (as we encountered in Example 2.2 for a NDDE) whose real part approaches $C_D(\vec{\tau})$ or that there exists an arbitrarily small perturbation on the delays for which such a chain exists.

Proposition 4.5. If $C_D(\vec{\tau}) \neq -\infty$ then for each $\gamma > 0$ there exist $\vec{\tau}_\gamma \in \mathcal{B}(\vec{\tau},\gamma) \cap (\mathbb{R}^+)^m$ such that the spectrum of (4.7) with the delay values replaced by $\vec{\tau}_\gamma$ contains a chain of characteristic roots $\{\lambda_i\}_{i\in\mathbb{N}}$ that satisfies

$$\lim_{i\to\infty} \Re(\lambda_i) = C_D(\vec{\tau}) \text{ and } \lim_{i\to\infty} |\Im(\lambda_i)| = +\infty.$$

Proof. For each $\vec{\tau} \in (\mathbb{R}^+)^m$ and $\gamma > 0$ there exists a $\vec{\tau}_\gamma \in \mathcal{B}(\vec{\tau},\gamma) \cap (\mathbb{R}^+)^m$ such that the elements of $\vec{\tau}_\gamma$ are rationally independent. The assertion now follows from [134, Proposition 2.3 and Lemma 1]. □

Finally, the following proposition shows that if $C_D(\vec{\tau})$ is strictly negative then there does not exist a vertical root chain approaching the imaginary axis and the closed right half-plane only contains finitely many characteristic roots, even when sufficiently small delay perturbations are considered.

Proposition 4.6. If $C_D(\vec{\tau}) < 0$, there exist $\epsilon_1 > 0$ and $\epsilon_2 > 0$ such that for any $\vec{\tau}_{\epsilon_1} \in \mathcal{B}(\vec{\tau},\epsilon_1) \cap (\mathbb{R}^+)^m$ the number of roots of $F_D(\lambda;\vec{\tau}_{\epsilon_1})$ that lie to the right of $-\epsilon_2$ is finite.

Proof. If $C_D(\vec{\tau}) < 0$ then by the definition of $C_D(\vec{\tau})$ there exist $\epsilon_1 > 0$ and $\epsilon_2 > 0$ such that $C_D(\vec{\tau}_{\epsilon_1}) \leq -\epsilon_2 < 0$ for all $\vec{\tau}_{\epsilon_1} \in \mathcal{B}(\vec{\tau},\epsilon_1) \cap (\mathbb{R}^+)^m$. The proposition now follows from [134, Lemma 2]. □

4.3 The robust strong H_∞-norm

In this section we introduce the notion of the robust strong H_∞-norm. We start with describing the considered class of uncertain time-delay systems. The nominal systems are of the form (4.1) which are affected by L real-valued full-block uncertainties bounded in Frobenius norm:

$$\delta_l \in \mathbb{R}^{s_l \times r_l} \text{ with } \|\delta_l\|_F \leq \bar{\delta}_l \text{ for } l = 1, \ldots, L.$$

For notational convenience, we denote $\delta = (\delta_1, \ldots, \delta_L)$ as the collection of uncertainties and $\mathcal{D}$ as the set of admissible uncertainty values:

$$\mathcal{D} = \{\delta \in \mathbb{R}^{s_1 \times r_1} \times \cdots \times \mathbb{R}^{s_L \times r_L} : \|\delta_l\|_F \leq \bar{\delta}_l \text{ for } l = 1, \ldots, L\}.$$

The uncertain system now becomes

$$\left\{ \begin{array}{rcl} \dot{x}(t) & = & \sum\limits_{k=0}^{m} \tilde{A}_k(\delta)\, x(t-\tau_k) + \sum\limits_{k=0}^{m} \tilde{B}_k(\delta)\, w(t-\tau_k), \\ z(t) & = & \sum\limits_{k=0}^{m} \tilde{C}_k(\delta)\, x(t-\tau_k) + \sum\limits_{k=0}^{m} \tilde{D}_k(\delta)\, w(t-\tau_k) \end{array} \right. \tag{4.12}$$

with $\tilde{A}_k(\delta)$, $\tilde{B}_k(\delta)$, $\tilde{C}_k(\delta)$, and $\tilde{D}_k(\delta)$ (for $k = 0, \ldots, m$) the uncertain system matrices. More specifically, given the collection of uncertainties δ, the matrix-valued function $\tilde{A}_k(\delta)$ is defined as

$$\tilde{A}_k(\delta) := A_k + \sum_{l=1}^{L} \sum_{s=1}^{S_l^{A_k}} G_{l,s}^{A_k} \delta_l H_{l,s}^{A_k},$$

in which A_k is the nominal value of the matrix and $G_{l,s}^{A_k}$ and $H_{l,s}^{A_k}$ are real-valued shape matrices of appropriate dimension that allow to target specific blocks or entries in the uncertain system matrices. The other uncertain system matrices are defined in the same way. Note that this definition allows a single uncertainty to affect multiple blocks in the same system matrix and even multiple system matrices as the same uncertainty may be present at multiple locations.

To assure that the H_∞-norm is well-defined (finite) for all admissible instances of (4.12), we make the following assumption.

Assumption 4.1. System (4.12) is internally exponentially stable for all admissible uncertainty values, i.e., for all $\delta \in \mathcal{D}$.

The robust H_∞-norm of (4.12) is defined as the maximal value of the H_∞-norm over all admissible values of the uncertainties:

$$\|T(\cdot;\cdot)\|_{H_\infty}^{\mathcal{D}} := \max_{\delta \in \mathcal{D}} \|T(\cdot;\delta)\|_{H_\infty},$$

in which $T(s;\delta)$ is the transfer function associated with (4.12) for a given instance of the uncertainties. Next we give an equivalent definition in terms of the worst-case gain function, which we define as follows

$$\Upsilon(\omega) := \max_{\delta\in\mathcal{D}} \sigma_1\big(T(\jmath\omega;\delta)\big). \tag{4.13}$$

More specifically, the robust H_∞-norm is equal to the smallest upper bound of this function:

$$\|T(\cdot;\cdot)\|_{\mathcal{H}_\infty}^{\mathcal{D}} = \operatorname{ess\,sup}_{\omega\in\mathbb{R}^+} \Upsilon(\omega).$$

Note however that the potential discontinuity of the nominal H_∞-norm with respect to the delay values carries over to the robust H_∞-norm. Let us therefore introduce the robust *strong* H_∞-norm as the worst-case value of the strong H_∞-norm over all admissible uncertainty values:

$$|||T(\cdot;\cdot)|||_{H_\infty}^{\mathcal{D}} := \max_{\delta\in\mathcal{D}} |||T(\cdot;\delta)|||_{H_\infty}.$$

Furthermore, it follows from Proposition 4.1 that

$$|||T(\cdot;\cdot)|||_{H_\infty}^{\mathcal{D}} = \max\left\{|||T_a(\cdot;\cdot)|||_{H_\infty}^{\mathcal{D}}, \|T(\cdot;\cdot)\|_{H_\infty}^{\mathcal{D}}\right\}$$

with

$$|||T_a(\cdot;\cdot)|||_{H_\infty}^{\mathcal{D}} := \max_{\delta\in\mathcal{D}} |||T_a(\cdot;\delta)|||_{H_\infty}.$$

In the remainder of this chapter, this last quantity will be referred to as the robust strong asymptotic H_∞-norm.

We thus can thus distinguish two cases. In the first case, the robust strong H_∞-norm is equal to the robust strong asymptotic H_∞-norm. In the second case

$$|||T(\cdot;\cdot)|||_{H_\infty}^{\mathcal{D}} > \max_{\delta\in\mathcal{D}} |||T_a(\cdot;\delta)|||_{H_\infty},$$

which means that

$$|||T(\cdot;\cdot)|||_{H_\infty}^{\mathcal{D}} = \|T(\cdot;\cdot)\|_{H_\infty}^{\mathcal{D}} = \max_{\omega\in\mathbb{R}^+} \Upsilon(\omega),$$

in which the supremum operator is replaced by the maximum operator as in this case the maximum is attained at at least one finite ω. We will come back to this characterization in Section 4.5.

4.4 The robust distance to instability of an uncertain DDAE

In this section we will introduce the notion of the robust distance to instability for an uncertain DDAE. We restrict our attention to uncertain DDAEs with a

specific structure which is chosen to facilitate the discussion in Section 4.5. More specifically, inspired by Proposition 4.3 and its proof, we focus on uncertain DDAEs of the following form:

$$E_e\,\dot{x}_e(t) = (\tilde{A}_{e,0}(\delta) + B_e\Delta C_e)\,x_e(t) + \sum_{k=1}^{m} \tilde{A}_{e,k}(\delta)\,x_e(t-\tau_k) \tag{4.14}$$

with

$$E_e = \begin{bmatrix} I_n & 0 & 0 \\ 0 & 0 & 0 \\ 0 & 0 & 0 \end{bmatrix},\ \tilde{A}_{e,0}(\delta) = \begin{bmatrix} \tilde{A}_0(\delta) & \tilde{B}_0(\delta) & 0 \\ 0 & -I_p & 0 \\ \tilde{C}_0(\delta) & \tilde{D}_0(\delta) & -I_q \end{bmatrix},$$

$$\tilde{A}_{e,k}(\delta) = \begin{bmatrix} \tilde{A}_k(\delta) & \tilde{B}_k(\delta) & 0 \\ 0 & 0 & 0 \\ \tilde{C}_k(\delta) & \tilde{D}_k(\delta) & 0 \end{bmatrix},\ B_e = \begin{bmatrix} 0 \\ I_p \\ 0 \end{bmatrix},\ \text{and } C_e = \begin{bmatrix} 0 & 0 & I_q \end{bmatrix}.$$

in which the uncertain matrices $\tilde{A}_k(\delta)$, $\tilde{B}_k(\delta)$, $\tilde{C}_k(\delta)$, and $\tilde{D}_k(\delta)$ (for $k = 0,\ldots,m$) are as defined above and $\Delta \in \mathbb{C}^{p\times q}$ is a full-block uncertainty whose size is measured in the spectral norm. Observe that this DDAE shares some similarities with the uncertain DAE (4.6) but there are two main differences. Firstly, (4.14) contains delay terms and secondly it has both real and complex-valued perturbations. The real-valued perturbations, δ, originate from the uncertainties in (4.12) and are therefore confined to the set $\mathcal{D}$. The complex-valued perturbation, Δ, on the other hand plays a similar role as in Proposition 4.3: we are interested in the smallest ϵ such that there exists a $\Delta \in \mathbb{C}^{p\times q}$ with $\|\Delta\|_2 \leq \epsilon$ for which (4.14) is either not well-posed (Definition 4.1) or not strongly stable for at least one $\delta \in \mathcal{D}$. This critical ϵ will be called the *robust* distance to instability of (4.14), where the specifier "robust" is used to indicate that we take the worst-case value over all $\delta \in \mathcal{D}$. In the following section it will be shown that there exists a relation between the robust distance to instability of (4.14) and the robust strong H_∞-norm of system (4.12). The remainder of this subsection therefore characterizes the robust distance to instability of (4.14) in greater detail.

To determine the robust distance to instability, we first need to find the smallest ϵ for which there exists a $\delta \in \mathcal{D}$ and a $\Delta \in \mathbb{C}^{p\times q}$ with $\|\Delta\|_2 \leq \epsilon$ such that (4.14) is not well-posed. To this end, let us introduce the notion of the robust distance to non well-posedness:

$$\mathrm{r}^{\mathrm{nwp}}_{\mathbb{C},\|\cdot\|_2}(\mathcal{D}) := \begin{cases} +\infty, \text{ if (4.7) is well-posed for all } \Delta \in \mathbb{C}^{p\times q} \text{ and } \delta \in \mathcal{D} \\ \min\limits_{\substack{\delta\in\mathcal{D} \\ \Delta\in\mathbb{C}^{p\times q}}} \{\|\Delta\|_2 : \text{(4.7) is not well-posed}\}, \text{ otherwise.} \end{cases}$$

If we restrict ϵ to the half-open interval $\left[0, \mathrm{r}^{\mathrm{nwp}}_{\mathbb{C},\|\cdot\|_2}(\mathcal{D})\right)$, all instances of (4.14) with $\delta \in \mathcal{D}$ and $\|\Delta\|_2 \leq \epsilon$ are well-posed. If well-posed, an instance of (4.14) is

not strongly stable if its strong spectral abscissa is non-negative. Therefore we study the strong pseudospectral abscissa of (4.14), which for $\epsilon \in \left[0, \mathrm{r}^{\mathrm{nwp}}_{\mathbb{C},\|\cdot\|_2}(\mathcal{D})\right)$ is defined as the maximal strong spectral abscissa over all $\delta \in \mathcal{D}$ and all $\Delta \in \mathbb{C}^{p\times q}$ with $\|\Delta\|_2 \leq \epsilon$:

$$C^{\mathrm{ps}}(\mathcal{D},\epsilon) := \max\left\{C(\delta,\Delta) : \delta \in \mathcal{D}, \Delta \in \mathbb{C}^{p\times q}, \text{ and } \|\Delta\|_2 \leq \epsilon\right\}$$

with $C(\delta,\Delta)$ the strong spectral abscissa of the particular instance of (4.14). It follows from Proposition 4.4 that:

$$C^{\mathrm{ps}}(\mathcal{D},\epsilon) = \max\left\{C_D^{\mathrm{ps}}(\mathcal{D},\epsilon), c^{\mathrm{ps}}(\mathcal{D},\epsilon)\right\} \tag{4.15}$$

with

$$C_D^{\mathrm{ps}}(\mathcal{D},\epsilon) := \max\left\{C_D(\delta,\Delta) : \delta \in \mathcal{D}, \Delta \in \mathbb{C}^{p\times q}, \text{ and } \|\Delta\|_2 \leq \epsilon\right\}$$

and

$$c^{\mathrm{ps}}(\mathcal{D},\epsilon) := \max\left\{c(\delta,\Delta) : \delta \in \mathcal{D}, \Delta \in \mathbb{C}^{p\times q}, \text{ and } \|\Delta\|_2 \leq \epsilon\right\}.$$

Remark 4.3. The quantity $c^{\mathrm{ps}}(\mathcal{D},\epsilon)$ can alternatively be characterized using the pseudospectrum of (4.14) which we define as the set containing the characteristic roots of (4.14) for all admissible instances of δ and Δ, i.e.,

$$\Lambda^{\mathrm{ps}}(\mathcal{D},\epsilon) := \bigcup_{\substack{\delta\in\mathcal{D} \\ \Delta\in\mathbb{C}^{p\times q},\|\Delta\|_2\leq\epsilon}} \left\{\lambda \in \mathbb{C} : \tilde{F}_D(\lambda;\delta,\Delta)\right) = 0\right\} \tag{4.16}$$

with

$$\tilde{F}_D(\lambda;\delta,\Delta) = \det\left(\lambda E_e - (\tilde{A}_{e,0}(\delta) + B_e\Delta C_e) - \sum_{k=1}^{m} \tilde{A}_{e,k}(\delta)e^{-\lambda\tau_k}\right).$$

The pseudospectral abscissa, $c^{\mathrm{ps}}(\mathcal{D},\epsilon)$, is now equal to the supremum of the real parts of the points in this pseudospectrum:

$$c^{\mathrm{ps}}(\mathcal{D},\epsilon) = \sup\{\Re(\lambda) : \lambda \in \Lambda^{\mathrm{ps}}(\mathcal{D},\epsilon)\}.$$

Remark 4.4. Both $C_D^{\mathrm{ps}}(\mathcal{D},\epsilon)$ and $c^{\mathrm{ps}}(\mathcal{D},\epsilon)$ continuously depend on ϵ for $\epsilon \in \left[0, \mathrm{r}^{\mathrm{nwp}}_{\mathbb{C},\|\cdot\|_2}(\mathcal{D})\right)$. This follows from the fact that both $C_D(\delta,\Delta)$ and $c(\delta,\Delta)$ continuously depend on the elements of Δ for $\|\Delta\|_2 < \mathrm{r}^{\mathrm{nwp}}_{\mathbb{C},\|\cdot\|_2}(\mathcal{D})$.

Based on (4.15), we now introduce two new distance measures. Firstly, the robust distance to a characteristic root chain crossing is defined as

$$\mathrm{r}^{\mathrm{chain}}_{\mathbb{C},\|\cdot\|_2}(\mathcal{D}) := \begin{cases} +\infty, \text{ if } C_D^{\mathrm{ps}}(\mathcal{D},\epsilon) < 0 \quad \forall\epsilon \in \left[0, \mathrm{r}^{\mathrm{nwp}}_{\mathbb{C},\|\cdot\|_2}(\mathcal{D})\right) \\ \min\{\varepsilon \in \left[0, \mathrm{r}^{\mathrm{nwp}}_{\mathbb{C},\|\cdot\|_2}(\mathcal{D})\right) : C_D^{\mathrm{ps}}(\mathcal{D},\epsilon) \geq 0\}, \text{ otherwise.} \end{cases} \tag{4.17}$$

Secondly, the robust distance to a finite root crossing is defined as

$$\mathrm{r}^{\mathrm{fin}}_{\mathbb{C},\|\cdot\|_2}(\mathcal{D}) := \begin{cases} +\infty, \text{ if } c^{\mathrm{ps}}(\mathcal{D},\epsilon,\vec{\tau}) < 0 \\ \qquad \text{for all } \epsilon \in \left[0, \min\{\mathrm{r}^{\mathrm{nwp}}_{\mathbb{C},\|\cdot\|_2}(\mathcal{D}), \mathrm{r}^{\mathrm{chain}}_{\mathbb{C},\|\cdot\|_2}(\mathcal{D})\}\right) \\ \min\{\epsilon \in \left[0, \min\{\mathrm{r}^{\mathrm{nwp}}_{\mathbb{C},\|\cdot\|_2}(\mathcal{D}), \mathrm{r}^{\mathrm{chain}}_{\mathbb{C},\|\cdot\|_2}(\mathcal{D})\}\right) : \\ \qquad\qquad c^{\mathrm{ps}}(\mathcal{D},\epsilon) \geq 0\}, \text{ otherwise.} \end{cases} \tag{4.18}$$

Remark 4.5. Because both $C_D^{\mathrm{ps}}(\mathcal{D},\epsilon)$ and $c^{\mathrm{ps}}(\mathcal{D},\epsilon)$ continuously depend on ϵ for $\epsilon \in \left[0, \mathrm{r}^{\mathrm{nwp}}_{\mathbb{C},\|\cdot\|_2}(\mathcal{D})\right)$, both $\mathrm{r}^{\mathrm{chain}}_{\mathbb{C},\|\cdot\|_2}(\mathcal{D})$ and $\mathrm{r}^{\mathrm{fin}}_{\mathbb{C},\|\cdot\|_2}(\mathcal{D})$, when finite, are characterized by critical $\epsilon^\star_{\mathrm{chain}}$ and $\epsilon^\star_{\mathrm{fin}}$ for which $C_D^{\mathrm{ps}}(\mathcal{D},\epsilon^\star_{\mathrm{chain}}) = 0$ and $c^{\mathrm{ps}}(\mathcal{D},\epsilon^\star_{\mathrm{fin}}) = 0$, respectively.

The names of these two distances can be understood using Proposition 4.5. If the function $\epsilon \mapsto C_D^{\mathrm{ps}}(\mathcal{D},\epsilon)$ has a zero crossing in the interval $\left[0, \mathrm{r}^{\mathrm{nwp}}_{\mathbb{C},\|\cdot\|_2}(\mathcal{D})\right)$, this zero crossing corresponds to the smallest ϵ such that for each $\gamma > 0$ there exist a $\delta \in \mathcal{D}$, a $\Delta \in \mathbb{C}^{p\times q}$ with $\|\Delta\|_2 \leq \epsilon$ and a $\vec{\tau}_\gamma \in \mathcal{B}(\vec{\tau},\gamma) \cap (\mathbb{R}^+)^m$ for which the spectrum of (4.14) contains a chain of characteristic roots, as introduced in Proposition 4.5, with the imaginary axis as vertical asymptote. At the same time, for $\epsilon < \min\left\{\mathrm{r}^{\mathrm{chain}}_{\mathbb{C},\|\cdot\|_2}(\mathcal{D}), \mathrm{r}^{\mathrm{nwp}}_{\mathbb{C},\|\cdot\|_2}(\mathcal{D})\right\}$ the number of characteristic roots of any admissible instance of (4.14) in the closed right half-plane is finite and the vertical chains of characteristic roots are bounded away from the imaginary axis, even for infinitesimal delay perturbations. A zero crossing of $\epsilon \mapsto c^{\mathrm{ps}}(\mathcal{D},\epsilon)$ in the interval $\left[0, \min\{\mathrm{r}^{\mathrm{nwp}}_{\mathbb{C},\|\cdot\|_2}(\mathcal{D}), \mathrm{r}^{\mathrm{chain}}_{\mathbb{C},\|\cdot\|_2}(\mathcal{D})\}\right)$ thus corresponds to the smallest ϵ for which there exist a $\delta \in \mathcal{D}$ and a $\Delta \in \mathbb{C}^{p\times q}$ with $\|\Delta\|_2 \leq \epsilon$ such that (4.14) has (finitely many) characteristic roots on the imaginary axis. The motivation behind these names will (hopefully) become more clear in Section 4.6.

Remark 4.6. Based on this information and the alternative definition of $c^{\mathrm{ps}}(\mathcal{D},\epsilon)$ in terms of the pseudospectrum $\Lambda^{\mathrm{ps}}(\mathcal{D},\epsilon)$, we can introduce the following equivalent definition for the robust distance to a finite root crossing:

$$\mathrm{r}^{\mathrm{fin}}_{\mathbb{C},\|\cdot\|_2}(\mathcal{D}) := \begin{cases} +\infty, \text{ if } c^{\mathrm{ps}}(\mathcal{D},\epsilon) < 0 \\ \qquad \text{for all } \epsilon \in \left[0, \min\{\mathrm{r}^{\mathrm{nwp}}_{\mathbb{C},\|\cdot\|_2}(\mathcal{D}), \mathrm{r}^{\mathrm{chain}}_{\mathbb{C},\|\cdot\|_2}(\mathcal{D})\}\right) \\ \min\{\epsilon \in \left[0, \min\{\mathrm{r}^{\mathrm{nwp}}_{\mathbb{C},\|\cdot\|_2}(\mathcal{D}), \mathrm{r}^{\mathrm{chain}}_{\mathbb{C},\|\cdot\|_2}(\mathcal{D})\}\right) : \\ \quad \exists \omega \in \mathbb{R} \text{ such that } \jmath\omega \in \Lambda^{\mathrm{ps}}(\mathcal{D},\epsilon,\vec{\tau})\}, \text{ otherwise,} \end{cases} \tag{4.19}$$

i.e., the robust distance to a finite root crossing is equal to the smallest ϵ for which the ϵ-pseudospectrum touches the imaginary axis.

To conclude this section we define the robust distance to instability as follows.

Definition 4.2. The robust distance to instability of (4.14) is equal to the minimum of the three distance measures introduced above:

$$\mathrm{r}_{\mathbb{C},\|\cdot\|_2}(\mathcal{D}) := \min\left\{\mathrm{r}^{\mathrm{nwp}}_{\mathbb{C},\|\cdot\|_2}(\mathcal{D}),\, \mathrm{r}^{\mathrm{chain}}_{\mathbb{C},\|\cdot\|_2}(\mathcal{D}),\, \mathrm{r}^{\mathrm{fin}}_{\mathbb{C},\|\cdot\|_2}(\mathcal{D})\right\}. \tag{4.20}$$

4.5 Relation between the robust strong H_∞-norm and the robust distance to instability

This section establishes the relation between the robust strong H_∞-norm of (4.12) and the robust distance to instability of the uncertain DDAE (4.14) and is structured as follows. Section 4.5.1 reviews some preliminary results. Section 4.5.2 focuses on the relation between the robust strong asymptotic H_∞-norm $\left(|||T_a(\cdot;\cdot,\vec{\tau})|||^{\mathcal{D}}_{H_\infty}\right)$ on the one hand and the robust distances to non well-posedness ($\mathrm{r}^{\mathrm{nwp}}_{\mathbb{C},\|\cdot\|_2}$) and a characteristic root chain crossing ($\mathrm{r}^{\mathrm{chain}}_{\mathbb{C},\|\cdot\|_2}$) on the other hand. Next, Section 4.5.3 investigates the link between the worst-case gain function, $\omega \mapsto \Upsilon(\omega)$, and the robust distance to a finite root crossing ($\mathrm{r}^{\mathrm{fin}}_{\mathbb{C},\|\cdot\|_2}$). Finally, Section 4.5.4 combines these results in the central theorem of this work.

4.5.1 Preliminary results

We start with some technical lemmas.

Lemma 4.2. For a matrix $M \in \mathbb{C}^{q\times p}$ it holds that

$$\sigma_1(M)^{-1} = \min_{\Delta\in\mathbb{C}^{p\times q}} \{\|\Delta\|_2 : \det(I_p - \Delta M) = 0\}$$

and

$$\sigma_1(M)^{-1} vu^H \in \mathrm{argmin}_{\Delta\in\mathbb{C}^{p\times q}}\{\|\Delta\|_2 : \det(I_p - \Delta M) = 0\},$$

in which u and v are normalized left and right singular vectors of M associated with $\sigma_1(M)$, respectively.

Proof. This is a standard result. See for example [153, Section 3]. □

Lemma 4.3. The robust distance to instability of (4.14) is strictly positive if and only if the characteristic roots of

$$\dot{x}(t) = \tilde{A}_0(\delta)x(t) + \sum_{k=1}^{m} \tilde{A}_k(\delta)e^{-\lambda\tau_k}$$

lie in the open left half-plane for all $\delta \in \mathcal{D}$.

Proof. Because

$$U^\top \tilde{A}_{e,0}(\delta)V = \begin{bmatrix} -I & 0 \\ \tilde{D}_0(\delta) & -I \end{bmatrix}$$

is invertible for all $\delta \in \mathcal{D}$, it follows from Lemma 4.1 that the robust distance to non well-posedness is strictly positive. Furthermore, from (4.11) it is easy to verify that

$$C_D^{\text{ps}}(\mathcal{D}, 0) = -\infty$$

and thus also the robust distance to a characteristic root chain crossing is strictly positive. Finally, it holds that

$$c^{\text{ps}}(\mathcal{D}, 0) = \max_{\lambda \in \mathbb{C}} \Big\{ \Re(\lambda) : \exists \delta \in \mathcal{D} \text{ such that } \det\left(I\lambda - \tilde{A}_0(\delta) - \sum_{k=1}^{m} \tilde{A}_k(\delta) e^{-\lambda \tau_k} \right) = 0 \Big\},$$

from which the lemma follows. □

By Assumption 4.1 this means that all characteristic matrices examined in the remainder of this chapter have a strictly positive robust distance to instability.

Lemma 4.4. For a given $\delta^\star \in \mathcal{D}$, an $\epsilon > 0$ and a complex number s such that

$$\det\left(Is - \tilde{A}_0(\delta^\star) - \sum_{k=1}^{m} \tilde{A}_k(\delta^\star) e^{-s\tau_k} \right) \neq 0,$$

there exists a $\Delta^\star \in \mathbb{C}^{p \times q}$ with $\|\Delta^\star\|_2 \leq \epsilon$ such that s is a characteristic root of (4.14) with $\delta = \delta^\star$ and $\Delta = \Delta^\star$ if and only if

$$\sigma_1\big(T(s; \delta^\star)\big) \geq \epsilon^{-1}.$$

Proof. By definition, a complex number s is a characteristic root of (4.14) with $\delta = \delta^\star$ and $\Delta = \Delta^\star$ if and only if

$$\det\left(\left[\begin{array}{c|c|c} Is - \sum_{k=0}^{m} \tilde{A}_k(\delta^\star) e^{-s\tau_k} & -\sum_{k=0}^{m} \tilde{B}_k(\delta^\star) e^{-s\tau_k} & 0 \\ \hline 0 & I_p & -\Delta^\star \\ \hline -\sum_{k=0}^{m} \tilde{C}_k(\delta^\star) e^{-s\tau_k} & -\sum_{k=0}^{m} \tilde{D}_k(\delta^\star) e^{-s\tau_k} & I_q \end{array} \right] \right) = 0.$$

Because the matrix $sI - \tilde{A}_0(\delta^\star) - \sum_{k=1}^{m} \tilde{A}_k(\delta^\star) e^{-s\tau_k}$ is invertible, it follows from Schur's determinant formula for block partitioned matrices, see [164] and [157,

Equation 0.3.2], that this equation is equivalent with

$$\det\left(\begin{bmatrix} I_p & -\Delta^\star \\ -T(s;\delta^\star) & I_q \end{bmatrix}\right) = 0.$$

By applying Schur's determinant formula once again, we find

$$\det\big(I_p - \Delta^\star T(s;\delta^\star)\big) = 0.$$

From Lemma 4.2 it follows that there exists a $\Delta \in \mathbb{C}^{p\times q}$ with $\|\Delta\|_2 \leq \epsilon$ such that this condition is met if and only if

$$\sigma_1\big(T(s;\delta^\star)\big) \geq \epsilon^{-1}.$$

□

4.5.2 Link between the robust strong asymptotic H_∞-norm and the robust distances to non well-posedness and a characteristic root chain crossing

We start with a characterization of the robust distance to non well-posedness ($\mathrm{r}^{\mathrm{nwp}}_{\mathbb{C},\|\cdot\|_2}$) in terms of the undelayed direct feed-through term of system (4.12).

Proposition 4.7. It holds that

$$\mathrm{r}^{\mathrm{nwp}}_{\mathbb{C},\|\cdot\|_2}(\mathcal{D})^{-1} = \max_{\delta\in\mathcal{D}} \sigma_1\big(\tilde{D}_0(\delta)\big).$$

Proof. It follows from Lemma 4.1 that a particular instance of (4.14) is not well-posed if and only if the matrix

$$U^\top\left(\tilde{A}_{e,0}(\delta) + B_e\Delta C_e\right)V = \begin{bmatrix} -I_p & \Delta \\ \tilde{D}_0(\delta) & -I_q \end{bmatrix}$$

is singular. As a consequence of the Schur's determinant formula for block partitioned matrices, this condition is equivalent with $I_p - \Delta\tilde{D}_0(\delta)$ being singular. The robust distance to non well-posedness is thus equal to

$$\mathrm{r}^{\mathrm{nwp}}_{\mathbb{C},\|\cdot\|_2}(\mathcal{D}) = \begin{cases} +\infty, \text{ if } \det\big(I_p - \Delta\tilde{D}_0(\delta)\big) \neq 0 \text{ for all } \Delta\in\mathbb{C}^{p\times q} \text{ and } \delta\in\mathcal{D} \\ \min\limits_{\substack{\delta\in\mathcal{D} \\ \Delta\in\mathbb{C}^{p\times q}}} \big\{\|\Delta\|_2 : \det\big(I_p - \Delta\tilde{D}_0(\delta)\big) = 0\big\}, \text{ otherwise.} \end{cases}$$

Using Lemma 4.2, one finds

$$\mathrm{r}^{\mathrm{nwp}}_{\mathbb{C},\|\cdot\|_2}(\mathcal{D}) = \begin{cases} +\infty, \text{ if } \sigma_1\big(\tilde{D}_0(\delta)\big) = 0 \text{ for all } \delta \in \mathcal{D} \\ \min\limits_{\delta\in\mathcal{D}} \sigma_1\big(\tilde{D}_0(\delta)\big)^{-1}, \text{ otherwise} \end{cases}$$

$$= \begin{cases} +\infty, \text{ if } \sigma_1\big(\tilde{D}_0(\delta)\big) = 0 \text{ for all } \delta \in \mathcal{D} \\ \Big(\max\limits_{\delta\in\mathcal{D}} \sigma_1\big(\tilde{D}_0(\delta)\big)\Big)^{-1}, \text{ otherwise} \end{cases}$$

which completes the proof. □

The following lemma gives a lower bound for the robust strong asymptotic H_∞-norm.

Lemma 4.5. It holds that

$$\max_{\delta\in\mathcal{D}} \sigma_1\big(\tilde{D}_0(\delta)\big) \leq |||T_a(\cdot;\cdot)|||^{\mathcal{D}}_{H_\infty}.$$

Proof. Consider the matrix-valued function $s \mapsto D_0 + \sum\limits_{k=1}^{m} D_k e^{-s}$, of which every entry is an analytic function bounded from above for s in the closed right half-plane, $\overline{\mathbb{C}}^+ = \{s \in \mathbb{C} : \Re(s) \geq 0\}$. From [32, Theorem 2.1 and Equation 2.3] it follows that the function $s \mapsto \sigma_1\left(D_0 + \sum\limits_{k=1}^{m} D_k e^{-s}\right)$ attains its maximum over $\overline{\mathbb{C}}^+$ on the imaginary axis, $\jmath\mathbb{R}$. Thus

$$\begin{aligned} \sigma_1(D_0) = \lim_{\Re(s)\to\infty} \sigma_1\left(D_0 + \sum_{k=1}^{m} D_k e^{-s}\right) &\leq \sup_{s\in\overline{\mathbb{C}}^+} \sigma_1\left(D_0 + \sum_{k=1}^{m} D_k e^{-s}\right) \\ &= \operatorname*{ess\,sup}_{\omega\in\mathbb{R}} \sigma_1\left(D_0 + \sum_{k=1}^{m} D_k e^{-\jmath\omega}\right) \\ &\leq \max_{\vec{\theta}\in[0,2\pi)^m} \sigma_1\left(D_0 + \sum_{k=1}^{m} D_k e^{\jmath\theta_k}\right). \end{aligned}$$

The lemma now follows from (4.4). □

Next we show that the robust distance to a characteristic root chain crossing is finite if and only if the above mentioned lower bound is not attained.

Lemma 4.6. The robust distance to a characteristic root chain crossing of (4.14) is finite if and only if

$$\max_{\delta\in\mathcal{D}} \sigma_1\big(\tilde{D}_0(\delta)\big) < |||T_a(\cdot;\cdot)|||^{\mathcal{D}}_{\mathcal{H}_\infty}.$$

Proof. First we prove sufficiency. It follows from the definition of the robust strong asymptotic H_∞-norm and (4.4) that

$$\max_{\delta\in\mathcal{D}} \sigma_1\big(\tilde{D}_0(\delta)\big) < |||T_a(\cdot;\cdot)|||^{\mathcal{D}}_{H_\infty}$$

implies that there exist a $\vec{\theta}^\star \in [0, 2\pi)^m$ and a $\delta^\star \in \mathcal{D}$ such that

$$\max_{\delta\in\mathcal{D}} \sigma_1\big(\tilde{D}_0(\delta)\big) < \sigma_1\left(\tilde{D}_0(\delta^\star) + \sum_{k=1}^{m} \tilde{D}_k(\delta^\star)e^{\jmath\theta_k^\star}\right).$$

By Lemma 4.2 and Proposition 4.7, this means that there exists a $\Delta^\star$ with

$$\begin{aligned}\|\Delta^\star\|_2 &= \sigma_1\left(\tilde{D}_0(\delta^\star) + \sum_{k=1}^{m} \tilde{D}_k(\delta^\star)e^{\jmath\theta_k^\star}\right)^{-1} \\ &< \left(\max_{\delta\in\mathcal{D}} \sigma_1\big(\tilde{D}_0(\delta)\big)\right)^{-1} = \mathrm{r}^{\mathrm{nwp}}_{\mathbb{C},\|\cdot\|_2}(\mathcal{D}),\end{aligned}$$

such that

$$\det\left(I - \Delta^\star\left(\tilde{D}_0(\delta^\star) + \sum_{k=1}^{m} \tilde{D}_k(\delta^\star)e^{\jmath\theta_k^\star}\right)\right) = 0. \tag{4.21}$$

Because $I - \Delta^\star\tilde{D}_0(\delta^\star)$ is invertible, this last equation is equivalent to

$$\det\left(I - \Big(I - \Delta^\star\tilde{D}_0(\delta^\star)\Big)^{-1}\Delta^\star\left(\sum_{k=1}^{m} \tilde{D}_k(\delta^\star)e^{\jmath\theta_k^\star}\right)\right) = 0. \tag{4.22}$$

Furthermore, using the Shur-Banachiewicz inversion formula [157, Equation 0.8.1] one finds that for (4.14),

$$\begin{aligned}&\rho\left(\sum_{k=1}^{m} \big(U^\top\big(\tilde{A}_{e,0}(\delta^\star) + B_e\Delta^\star C_e\big)V\big)^{-1}\big(U^H\tilde{A}_{e,k}(\delta^\star)V\big)e^{\jmath\theta_k^\star}\right) \\ &\qquad = \rho\left(\Big(I - \Delta^\star\tilde{D}_0(\delta^\star)\Big)^{-1}\Delta^\star\left(\sum_{k=1}^{m} \tilde{D}_k(\delta^\star)e^{\jmath\theta_k^\star}\right)\right).\end{aligned} \tag{4.23}$$

Equation (4.22) thus implies that

$$\rho\left(\sum_{k=1}^{m} \big(U^\top(\tilde{A}_{e,0}(\delta^\star) + B_e\Delta^\star C_e)V\big)^{-1}\big(U^\top\tilde{A}_{e,k}(\delta^\star)V\big)e^{\jmath\theta_k^\star}\right) \geq 1.$$

It now follows from Proposition 4.4 that $C_D(\delta^\star, \Delta^\star) \geq 0$, and hence $C_D^{\mathrm{ps}}(\mathcal{D}, \|\Delta^\star\|_2) \geq 0$. This means that $\mathrm{r}^{\mathrm{chain}}_{\mathbb{C},\|\cdot\|_2}(\mathcal{D}) \leq \|\Delta^\star\|_2 < \mathrm{r}^{\mathrm{nwp}}_{\mathbb{C},\|\cdot\|_2}(\mathcal{D})$.

To prove necessity, we use an argument by contradiction and assume $\max_{\delta\in\mathcal{D}} \sigma_1\big(\tilde{D}_0(\delta)\big) \geq |||T_a(\cdot;\cdot,\vec{\tau})|||^{\mathcal{D}}_{\mathcal{H}_\infty}$. This implies that there do not exist values $\delta \in \mathcal{D}$, $\vec{\theta} \in [0, 2\pi)^m$ and $\Delta \in \mathbb{C}^{p\times q}$ with $\|\Delta\|_2 < \mathrm{r}^{\mathrm{nwp}}_{\mathbb{C},\|\cdot\|_2}(\mathcal{D})$ such that (4.22) holds. This implies that the matrix

$$\sum_{k=1}^{m} \big(U^\top\big(\tilde{A}_{e,0}(\delta) + B_e\Delta C_e\big)V\big)^{-1}\big(U^\top \tilde{A}_{e,k}(\delta)V\big)e^{\jmath\theta_k}$$

has no eigenvalue with unit modulus for all $\delta \in \mathcal{D}$, $\vec{\theta} \in [0, 2\pi)^m$ and $\Delta \in \mathbb{C}^{p\times q}$ with $\|\Delta\|_2 < \mathrm{r}^{\mathrm{nwp}}_{\mathbb{C},\|\cdot\|_2}(\mathcal{D})$. Because 0 is the only eigenvalue of $\sum_{k=1}^{m} \big(U^\top \tilde{A}_{e,0}(\delta)V\big)^{-1}\big(U^\top \tilde{A}_{e,k}(\delta)V\big)e^{\jmath\theta_k}$ and by the continuity of (4.23) with respect to the elements of Δ for $\|\Delta\|_2 < \mathrm{r}^{\mathrm{nwp}}_{\mathbb{C},\|\cdot\|_2}(\mathcal{D})$ this implies that

$$\rho\left(\sum_{k=1}^{m} \Big(U^\top\big(\tilde{A}_{e,0}(\delta) + B_e\Delta C_e\big)V\Big)^{-1}\big(U^\top \tilde{A}_{e,k}(\delta)V\big)e^{\jmath\theta_k}\right) < 1$$

for all $\delta \in \mathcal{D}$, $\vec{\theta} \in [0, 2\pi)^m$ and $\Delta \in \mathbb{C}^{p\times q}$ with $\|\Delta\|_2 < \mathrm{r}^{\mathrm{nwp}}_{\mathbb{C},\|\cdot\|_2}(\mathcal{D})$. It follows that $C_D^{\mathrm{ps}}(\mathcal{D}, \epsilon) < 0$ for all $\epsilon \in \Big[0, \mathrm{r}^{\mathrm{nwp}}_{\mathbb{C},\|\cdot\|_2}(\mathcal{D})\Big)$ and hence $\mathrm{r}^{\mathrm{chain}}_{\mathbb{C},\|\cdot\|_2}(\mathcal{D}) = +\infty$.

□

Lemma 4.7. For $\epsilon \in \Big[0, \mathrm{r}^{\mathrm{nwp}}_{\mathbb{C},\|\cdot\|_2}(\mathcal{D})\Big)$, the inequality $\epsilon \geq \big(|||T_a(\cdot;\cdot)|||^{\mathcal{D}}_{H_\infty}\big)^{-1}$ is a necessary and sufficient condition for $C_D^{\mathrm{ps}}(\mathcal{D}, \epsilon) \geq 0$.

Proof. Sufficiency follows from the fact that $\epsilon \geq \big(|||T_a(\cdot;\cdot)|||^{\mathcal{D}}_{H_\infty}\big)^{-1}$ implies that there exist $\delta^\star \in \mathcal{D}$, $\Delta^\star \in \mathbb{C}^{p\times q}$ with $\|\Delta^\star\|_2 \leq \epsilon$ and $\vec{\theta^\star} \in [0, 2\pi)^m$ such that (4.21) holds and a similar argument as in the sufficiency part of Lemma 4.6. We use an argument by contradiction to prove necessity. Assume $\epsilon < \big(|||T_a(\cdot;\cdot)|||^{\mathcal{D}}_{H_\infty}\big)^{-1}$. By Lemma 4.2 this means that there do not exist $\delta \in \mathcal{D}$, $\Delta \in \mathbb{C}^{p\times q}$ with $\|\Delta\|_2 \leq \epsilon$ and $\theta \in [0, 2\pi)^m$ such that (4.21) holds. The lemma now follows from a similar argument as the necessity part of the proof of Lemma 4.6. □

By combining these results we arrive at an expression for the robust strong asymptotic H_∞-norm in terms of the robust distances to non well-posedness and a characteristic root chain crossing.

Proposition 4.8. The robust strong asymptotic H_∞-norm of (4.12) is equal to the reciprocal of the minimum of the robust distance to non well-posedness and the robust distance to a characteristic root chain crossing, i.e.,

$$|||T_a(\cdot;\cdot)|||_{H_\infty}^{\mathcal{D}} = \min\left\{\mathrm{r}^{\mathrm{nwp}}_{\mathbb{C},\|\cdot\|_2}(\mathcal{D}), \mathrm{r}^{\mathrm{chain}}_{\mathbb{C},\|\cdot\|_2}(\mathcal{D})\right\}^{-1}.$$

Proof. First we consider the case where $\mathrm{r}^{\mathrm{chain}}_{\mathbb{C},\|\cdot\|_2}(\mathcal{D})$ is finite and hence

$$\mathrm{r}^{\mathrm{chain}}_{\mathbb{C},\|\cdot\|_2}(\mathcal{D}) < \mathrm{r}^{\mathrm{nwp}}_{\mathbb{C},\|\cdot\|_2}(\mathcal{D}).$$

Lemma 4.7 shows that $\epsilon \geq \left(|||T_a(\cdot;\cdot)|||_{H_\infty}^{\mathcal{D}}\right)^{-1}$ is a necessary and sufficient condition for $C_D^{\mathrm{ps}}(\mathcal{D},\epsilon) \geq 0$, thus

$$|||T_a(\cdot;\cdot)|||_{H_\infty}^{\mathcal{D}} = \mathrm{r}^{\mathrm{chain}}_{\mathbb{C},\|\cdot\|_2}(\mathcal{D})^{-1}.$$

Next we consider the case where $\mathrm{r}^{\mathrm{chain}}_{\mathbb{C},\|\cdot\|_2}(\mathcal{D})$ is not finite. In this case it follows from Lemma 4.6 that $\max_{\delta\in\mathcal{D}} \sigma_1\big(\tilde{D}_0(\delta)\big) \geq |||T_a(\cdot;\cdot)|||_{H_\infty}^{\mathcal{D}}$. But by Lemma 4.5 we have $\max_{\delta\in\mathcal{D}} \sigma_1\big(\tilde{D}_0(\delta)\big) \leq |||T_a(\cdot;\cdot)|||_{H_\infty}^{\mathcal{D}}$, thus

$$|||T_a(\cdot;\cdot)|||_{H_\infty}^{\mathcal{D}} = \max_{\delta\in\mathcal{D}} \sigma_1\big(\tilde{D}_0(\delta)\big) = \mathrm{r}^{\mathrm{nwp}}_{\mathbb{C},\|\cdot\|_2}(\mathcal{D})^{-1}.$$

□

4.5.3 Link between the worst-case gain function and the robust distance to a finite root crossing

The previous subsection established a relation between the robust strong asymptotic H_∞-norm and the robust distances to non well-posedness and a characteristic root chain crossing. In this subsection the link between the worst-case gain function $\omega \mapsto \Upsilon(\omega)$ and the robust distance to a finite root crossing is examined.

Lemma 4.8. Under Assumption 4.1, the robust distance to a finite root crossing is finite if and only if

$$||T(\cdot;\cdot)||_{H_\infty}^{\mathcal{D}} > |||T_a(\cdot;\cdot)|||_{H_\infty}^{\mathcal{D}}.$$

Furthermore, if this condition is fulfilled it holds that

$$\mathrm{r}^{\mathrm{fin}}_{\mathbb{C},\|\cdot\|_2}(\mathcal{D}) = \Big(\max_{\omega\in\mathbb{R}} \Upsilon(\omega)\Big)^{-1}.$$

Proof. We first prove necessity. If the robust distance to a finite root crossing is finite, it follows from Remark 4.6 that there exist $\delta^\star \in \mathcal{D}$, $\Delta^\star \in \mathbb{C}^{p\times q}$ with $\|\Delta^\star\|_2 = \epsilon < \min\left\{\mathrm{r}^{\mathrm{nwp}}_{\mathbb{C},\|\cdot\|_2}(\mathcal{D}), \mathrm{r}^{\mathrm{chain}}_{\mathbb{C},\|\cdot\|_2}(\mathcal{D})\right\}$ and an $\omega \in \mathbb{R}$ such that $\jmath\omega$ is a characteristic root of (4.14). By Lemma 4.4, this means that

$$\sigma_1\big(T(\jmath\omega;\delta^\star)\big) \geq \epsilon^{-1} > \min\left\{\mathrm{r}^{\mathrm{nwp}}_{\mathbb{C},\|\cdot\|_2}(\mathcal{D}), \mathrm{r}^{\mathrm{chain}}_{\mathbb{C},\|\cdot\|_2}(\mathcal{D})\right\}^{-1}.$$

Using the definition of $\|T(\cdot;\cdot)\|^{\mathcal{D}}_{H_\infty}$ and Proposition 4.8 one finds that

$$\|T(\cdot;\cdot)\|^{\mathcal{D}}_{H_\infty} \geq \sigma_1(T(\jmath\omega;\delta^\star)) \geq \epsilon^{-1} > |||T_a(\cdot;\cdot)|||^{\mathcal{D}}_{H_\infty}.$$

Next, we prove sufficiency. If $||T(\cdot;\cdot)||^{\mathcal{D}}_{H_\infty} > |||T_a(\cdot;\cdot)|||^{\mathcal{D}}_{H_\infty}$, then there exist $\delta^\star \in \mathcal{D}$ and $\omega^\star \in \mathbb{R}$ such that $\sigma_1(T(\jmath\omega^\star;\delta^\star)) > |||T_a(\cdot;\cdot)|||^{\mathcal{D}}_{H_\infty}$. From Lemma 4.4 and Proposition 4.8 it follows that there exists a $\Delta^\star$ with

$$\begin{aligned}\|\Delta^\star\|_2 &= \sigma_1(T(\jmath\omega^\star;\delta^\star,\vec{\tau}))^{-1}\\ &< \big(|||T_a(\cdot;\cdot,\vec{\tau})|||^{\mathcal{D}}_{H_\infty}\big)^{-1} = \min\left\{\mathrm{r}^{\mathrm{nwp}}_{\mathbb{C},\|\cdot\|_2}(\mathcal{D}), \mathrm{r}^{\mathrm{chain}}_{\mathbb{C},\|\cdot\|_2}(\mathcal{D})\right\},\end{aligned}$$

such that $\jmath\omega^\star$ is a characteristic root of (4.14) for $\delta = \delta^\star$ and $\Delta = \Delta^\star$ and hence $\mathrm{r}^{\mathrm{fin}}_{\mathbb{C},\|\cdot\|_2}(\mathcal{D})$ is finite.

Finally, we prove the equality $\mathrm{r}^{\mathrm{fin}}_{\mathbb{C},\|\cdot\|_2}(\mathcal{D}) = \big(\max_{\omega\in\mathbb{R}} \Upsilon(\omega)\big)^{-1}$ when $\mathrm{r}^{\mathrm{fin}}_{\mathbb{C},\|\cdot\|_2}(\mathcal{D})$ is finite. It follows from Lemma 4.4 that $\jmath\omega \in \Lambda^{\mathrm{ps}}(\mathcal{D},\epsilon)$ if and only if $\epsilon \geq \left(\max_{\delta\in\mathcal{D}} \sigma_1\left(T(\jmath\omega;\delta)\right)\right)^{-1}$. Using the alternative definition of $\mathrm{r}^{\mathrm{fin}}_{\mathbb{C},\|\cdot\|_2}(\mathcal{D})$ in (4.19), we obtain

$$\mathrm{r}^{\mathrm{fin}}_{\mathbb{C},\|\cdot\|_2}(\mathcal{D}) = \min_{\omega\in\mathbb{R}^+}\Big(\max_{\delta\in\mathcal{D}} \sigma_1(T(\jmath\omega;\delta^\star))\Big)^{-1} = \Big(\max_{\omega\in\mathbb{R}^+} \Upsilon(\omega)\Big)^{-1}.$$

□

4.5.4 Main theoretical result

This subsection combines the results of the two previous subsections to characterize the robust strong H_∞-norm of the uncertain time-delay system (4.12) in terms of the robust distance to instability of the uncertain delay differential algebraic equation (4.14).

Theorem 4.1. Under Assumption 4.1, the robust strong H_∞-norm of (4.12) is equal to the reciprocal of the robust distance to instability of (4.14), i.e.,

$$|||T(\cdot;\cdot)|||^{\mathcal{D}}_{H_\infty} = \mathrm{r}_{\mathbb{C},\|\cdot\|_2}(\mathcal{D})^{-1}.$$

Proof. As mentioned in Section 4.1, we have to consider two cases. If $|||T(\cdot;\cdot)|||_{H_\infty}^{\mathcal{D}} = |||T_a(\cdot;\cdot)|||_{H_\infty}^{\mathcal{D}}$, the theorem follows from Proposition 4.8. If $|||T(\cdot;\cdot)|||_{H_\infty}^{\mathcal{D}} > |||T_a(\cdot;\cdot)|||_{H_\infty}^{\mathcal{D}}$, then the theorem follows from Lemma 4.8. □

4.6 Illustration theoretical results

In Section 4.4 we encountered three ways in which the uncertain DDAE (4.14) can loose strong stability. Thereafter in Section 4.5, we established the relation between the robust distance to instability of this uncertain DDAE and the robust strong H_∞-norm of the uncertain system (4.12). This section presents 4 examples to illustrate these distance measures and their relation with the robust strong H_∞-norm in more details.

4.6.1 Robust distance to non well-posedness

Example 4.3. Consider the following uncertain system:

$$\begin{cases} \dot{x}(t) = -(10+\delta_1)\,x(t) + (2+3\delta_1)\,x(t-1) + (4-\delta_1+\delta_2)\,w(t), \\ z(t) = (-8-3\delta_1+2\delta_2)\,x(t) + 4\,w(t) \end{cases} \tag{4.24}$$

in which the scalar uncertainties δ_1 and δ_2 are confined to $|\delta_1| \leq 0.2$ and $|\delta_2| \leq 0.1$. The corresponding frequency response is given by

$$T(\jmath\omega;\delta) = \frac{(4-\delta_1+\delta_2)(-8-3\delta_1+2\delta_2)}{\jmath\omega + (10+\delta_1) - (2+3\delta_1)e^{-\jmath\omega}} + 4$$

and the asymptotic frequency response is equal to

$$T_a(\jmath\omega;\delta) = 4.$$

Hence, it follows from (4.4) that the robust strong asymptotic H_∞-norm ($|||T_a(\cdot;\cdot,\vec{\tau})|||_{H_\infty}^{\mathcal{D}}$) equals 4. Figure 4.2 shows the worst-case gain function $\omega \mapsto \Upsilon(\omega)$ for $\omega \in [10^{-2}, 10^3]$. It can be verified that $\Upsilon(\omega)$ lies below the robust strong asymptotic H_∞-norm (indicated by the dashed line) for all finite ω. It thus holds that

$$|||T(\cdot;\cdot)|||_{H_\infty}^{\mathcal{D}} = |||T_a(\cdot;\cdot)|||_{H_\infty}^{\mathcal{D}} = \max_{\delta\in\mathcal{D}} \sigma_1\big(\tilde{D}_0(\delta)\big) = 4.$$

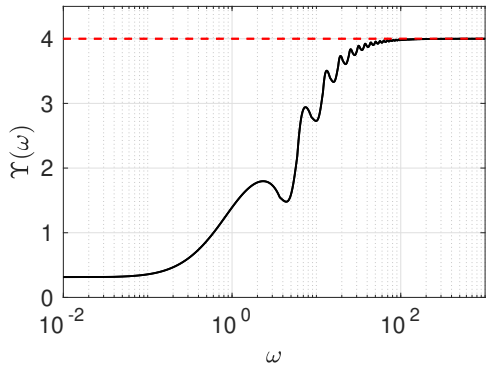

Figure 4.2: The worst-case gain function $\omega \mapsto \Upsilon(\omega)$ associated with the uncertain system (4.24) (black full line) and $|||T_a(\cdot;\cdot,\vec{\tau})|||_{H_\infty}^{\mathcal{D}}$ (red dashed line).

Next we consider the associated uncertain DDAE of the form (4.14):

$$\begin{bmatrix} 1 & 0 & 0 \\ 0 & 0 & 0 \\ 0 & 0 & 0 \end{bmatrix} \dot{x}_e(t) = \begin{bmatrix} -(10+\delta_1) & 4-\delta_1+\delta_2 & 0 \\ 0 & -1 & \Delta \\ -8-3\delta_1+2\delta_2 & 4 & -1 \end{bmatrix} x_e(t) + \begin{bmatrix} 2+3\delta_1 & 0 & 0 \\ 0 & 0 & 0 \\ 0 & 0 & 0 \end{bmatrix} x_e(t-1). \quad (4.25)$$

As the robust strong H_∞-norm is in this case equal to $\max_{\delta\in\mathcal{D}} \sigma_1\big(\tilde{D}_0(\delta)\big)$ it follows from the theory developed in Section 4.5, that

$$\mathrm{r}_{\mathbb{C},\|\cdot\|_2}(\mathcal{D}) = \mathrm{r}^{\mathrm{nwp}}_{\mathbb{C},\|\cdot\|_2}(\mathcal{D}) = 0.25,$$

meaning that the loss of stability corresponds to a realization of (4.25) that is not well-posed. Indeed, Lemma 4.1 implies that (4.25) is non well-posed for $\Delta = 0.25$.

To conclude this section, Figure 4.3 shows the pseudospectrum of (4.25) for ϵ close to 0.25. For $\epsilon = 0.249$, the pseudospectrum consists of closed regions around the nominal characteristic roots (i.e., $\delta_1 = \delta_2 = \Delta = 0$) and lies completely in the open left half-plane. However, if we increase ϵ to 0.251, the pseudospectrum includes almost the complete right half-plane apart the points inside the black contour. ◇

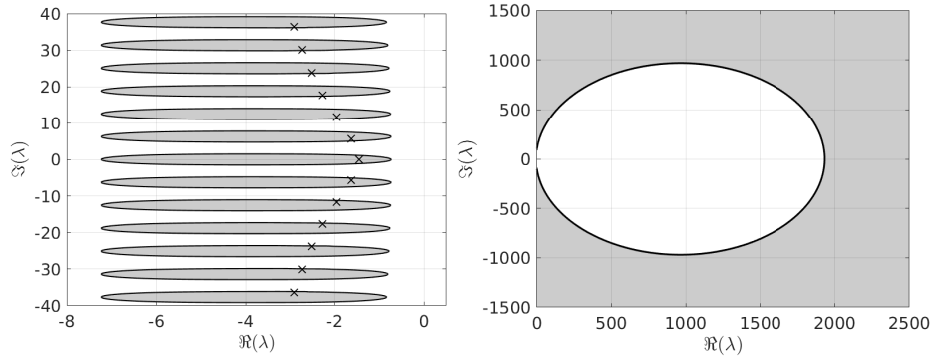

(a) $\epsilon = 0.249$ (b) $\epsilon = 0.251$

Figure 4.3: The nominal characteristic roots (black crosses) and part of the pseudospectrum of (4.25) for different values of ϵ (gray shading).

4.6.2 Robust distance to characteristic root chain crossing

Example 4.4. Next we consider the following uncertain system:

$$\begin{cases} \dot{x}(t) = (-3+\delta_2)\,x(t) + (-1+3\delta_1)\,x(t-1) + 4\,w(t), \\ z(t) = (-2-3\delta_1+2\delta_2)\,x(t) + (3+\delta_1)\,w(t) + (1+\delta_1+\delta_2)\,w(t-1) \end{cases} \tag{4.26}$$

with $|\delta_1| \leq 0.1$ and $|\delta_2| \leq 0.25$. The corresponding frequency response and asymptotic frequency response are respectively given by

$$T(\jmath\omega;\delta) = \frac{4(-2-3\delta_1+2\delta_2)}{\jmath\omega + (3-\delta_2) + (1-3\delta_1)e^{-\jmath\omega}} + (3+\delta_1) + (1+\delta_1+\delta_2)e^{-\jmath\omega}$$

and

$$T_a(\jmath\omega;\delta) = (3+\delta_1) + (1+\delta_1+\delta_2)e^{-\lambda}.$$

It follows from (4.4) the robust strong asymptotic H_∞-norm is equal to

$$\max_{\substack{|\delta_1|\leq 0.1 \\ |\delta_2|\leq 0.25}} \max_{\theta\in[0,2\pi)} \left|3+\delta_1+(1+\delta_1+\delta_2)e^{j\theta}\right| = 4.45.$$

Figure 4.4 shows the worst-case gain function for $\omega \in [10^{-1}, 10^{2.5}]$ and the robust strong asymptotic H_∞-norm (dashed line). Also in this example, the worst-case gain function lies below this line for all finite ω. As a consequence,

$$|||T(\cdot;\cdot)|||^{\mathcal{D}}_{H_\infty} = |||T_a(\cdot;\cdot)|||^{\mathcal{D}}_{H_\infty}.$$

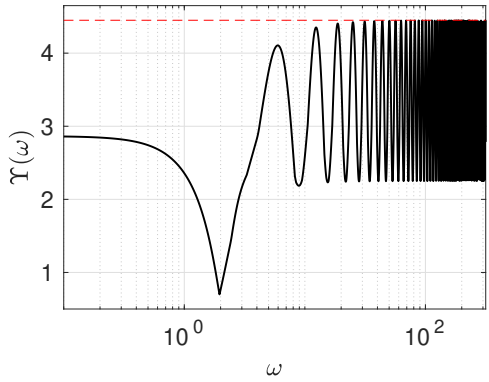

Figure 4.4: The worst-case gain function $\omega \mapsto \Upsilon(\omega)$ associated with the uncertain system (4.26) (black full line) and $|||T_a(\cdot;\cdot,\vec{\tau})|||_{H_\infty}^{\mathcal{D}}$ (red dashed line).

However, the robust strong asymptotic H_∞-norm is now strictly larger than $\max_{\delta\in\mathcal{D}} \sigma_1\big(\tilde{D}(\delta)\big) = 3.1$.

Next, we examine the associated uncertain DDAE:

$$\begin{bmatrix} 1 & 0 & 0 \\ 0 & 0 & 0 \\ 0 & 0 & 0 \end{bmatrix} \dot{x}_e(t) = \begin{bmatrix} -3+\delta_2 & 4 & 0 \\ 0 & -1 & \Delta \\ -2-3\delta_1+2\delta_2 & 3+\delta_1 & -1 \end{bmatrix} x_e(t) + \begin{bmatrix} -1+3\delta_1 & 0 & 0 \\ 0 & 0 & 0 \\ 0 & 1+\delta_1+\delta_2 & 0 \end{bmatrix} x_e(t-1). \quad (4.27)$$

It follows from Section 4.5 that the robust distance to instability is equal to the robust distance to a characteristic root chain crossing, which on its turn is equal to $\big(|||T_a(\cdot;\cdot,\vec{\tau})|||_{H_\infty}^{\mathcal{D}}\big)^{-1} = 1/4.45$. This is illustrated in Figure 4.5, which shows the pseudospectral abscissa (c^{ps}) and the strong pseudospectral abscissa of the underlying delay difference equation (C_D^{ps}) for the uncertain DDAE (4.27) in function of ϵ. We observe that the zero-crossings of these two quantities coincide, meaning that stability is lost due to a vertical chain of characteristic roots crossing the imaginary axis. This is shown in Figure 4.6 which plots the characteristic roots of (4.27) for the critical perturbations $\delta_1 = 0.1$, $\delta_2 = 0.25$ and $\Delta = 1/4.45$ associated with $C^{\mathrm{ps}}(\mathcal{D}, \mathrm{r}_{\mathbb{C},\|\cdot\|_2}(\mathcal{D})) = 0$. ◇

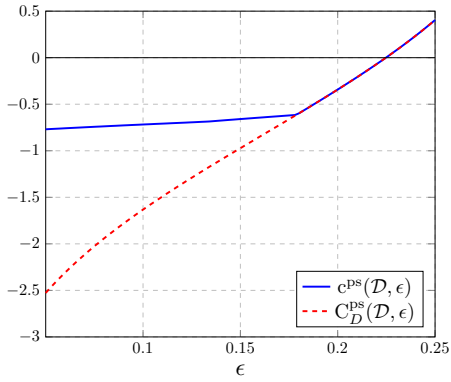

Figure 4.5: The functions $\epsilon \mapsto c^{\mathrm{ps}}(\mathcal{D}, \epsilon)$ (blue full line) and $\epsilon \mapsto C_D^{\mathrm{ps}}(\mathcal{D}, \epsilon)$ (red dashed) for the uncertain DDAE (4.27).

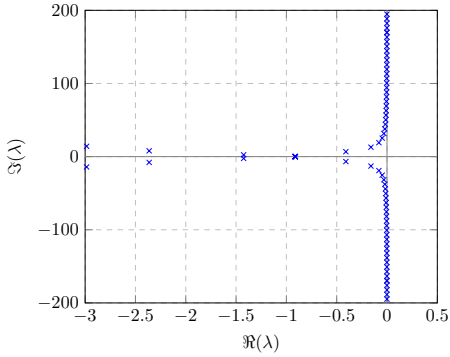

Figure 4.6: Characteristic roots of (4.27) for $\delta_1 = 0.1$, $\delta_2 = 0.25$, and $\Delta = 1/4.45$.

Example 4.5. As a third example we consider the following uncertain system:

$$\begin{cases} \dot{x}(t) = (-2+\delta_1)\,x(t) + (1+\delta_2)\,x(t-1) \\ \qquad\qquad\qquad\qquad -w(t) + (-0.5+\delta_1)\,w(t-2), \\ z(t) = (-2+2\delta_2)\,x(t) + x(t-2) + (5+4\delta_1)\,w(t) \\ \qquad\qquad\qquad\qquad +1.5\,w(t-1) + (-3+\delta_1)\,w(t-2) \end{cases} \tag{4.28}$$

in which the scalar uncertainties δ_1 and δ_2 are confined to $|\delta_1| \leq 0.2$ and $|\delta_2| \leq 0.3$. The corresponding frequency response and asymptotic frequency

response are given by

$$T(\jmath\omega;\delta) = \frac{\big[-1+(-0.5+\delta_1)e^{-2\jmath\omega}\big]\big[(-2+2\delta_2)+e^{-2\jmath\omega}\big]}{\jmath\omega-(-2+\delta_1)-(1+\delta_2)e^{-\jmath\omega}}+$$
$$(5+4\delta_1)+1.5e^{-\jmath\omega}+(-3+\delta_1)e^{-2\jmath\omega}$$

and

$$T_a(\jmath\omega;\delta) = (5+4\delta_1)+1.5e^{-\jmath\omega}+(-3+\delta_1)e^{-2\jmath\omega},$$

respectively. We start again with a characterization of the robust strong asymptotic H_∞-norm, which in this case is equal to

$$\max_{|\delta_1|\leq 0.2}\ \max_{\vec{\theta}\in[0,2\pi)^2} |5+4\delta_1+1.5e^{\jmath\theta_1}+(-3+\delta_1)e^{\jmath\theta_2}| = 10.1.$$

In Figure 4.7a, we again plot the worst-case gain function $\omega \mapsto \Upsilon(\omega)$ and indicate the robust strong asymptotic H_∞-norm with a dashed line. Also in this example, the worst-case gain function lies below this line for all ω. In contrast to the two previous examples, it holds however that $\limsup_{\omega\to+\infty}\Upsilon(\omega) < |||T_a(\cdot;\cdot,\vec{\tau})|||^{\mathcal{D}}_{H_\infty}$. This means that the robust asymptotic H_∞-norm is strictly smaller than the robust **strong** asymptotic H_∞-norm and that, as in Example 4.1, the asymptotic behavior of the transfer function is sensitive to infinitesimal perturbations on the delays, as illustrated in Figure 4.7b.

Next, we examine the associated uncertain DDAE:

$$\begin{bmatrix}1&0&0\\0&0&0\\0&0&0\end{bmatrix}\dot{x}_e(t) = \begin{bmatrix}-2+\delta_1 & -1 & 0\\ 0 & -1 & \Delta\\ -2+2\delta_2 & 5+4\delta_1 & -1\end{bmatrix}x_e(t)+$$
$$\begin{bmatrix}1+\delta_2&0&0\\0&0&0\\0&1.5&0\end{bmatrix}x_e(t-1)+\begin{bmatrix}0&-0.5+\delta_1&0\\0&0&0\\1&-3+\delta_1&0\end{bmatrix}x_e(t-2). \quad (4.29)$$

Using the theory of Section 4.5 we conclude that

$$\mathrm{r}_{\mathbb{C},\|\cdot\|_2}(\mathcal{D}) = \mathrm{r}^{\mathrm{chain}}_{\mathbb{C},\|\cdot\|_2}(\mathcal{D}) = 1/10.1.$$

Figure 4.8 shows the pseudospectral abscissa and the strong pseudospectral abscissa of the underlying delay difference equation for the uncertain DDAE (4.29). In contrast to the previous example, the zero-crossing of $\epsilon \mapsto C_D^{\mathrm{ps}}(\mathcal{D},\epsilon)$ lies strictly to the left of the zero-crossing of $\epsilon \mapsto c^{\mathrm{ps}}(\mathcal{D},\epsilon)$. As a consequence, the spectrum of (4.29) is bounded away from the imaginary

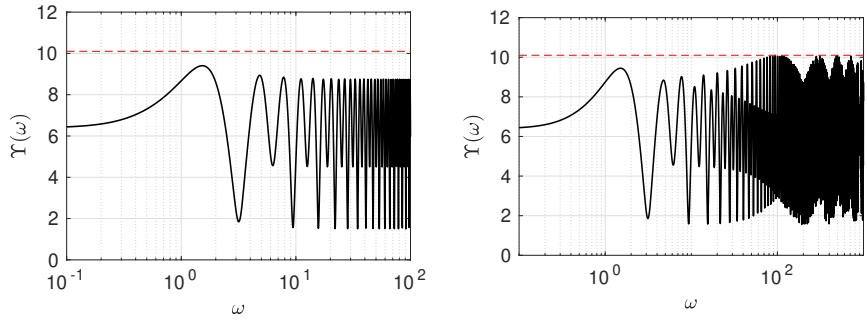

(a) $\vec{\tau} = (1, 2)$ (b) $\vec{\tau} = (1, 2 + \frac{\pi}{100})$

Figure 4.7: The worst-case gain function $\omega \mapsto \Upsilon(\omega)$ associated with the uncertain system (4.28) (black full line) for the nominal delays and a small perturbation on the delays and $|||T_a(\cdot;\cdot,\vec{\tau})|||_{H_\infty}^{\mathcal{D}}$ (red dashed line).

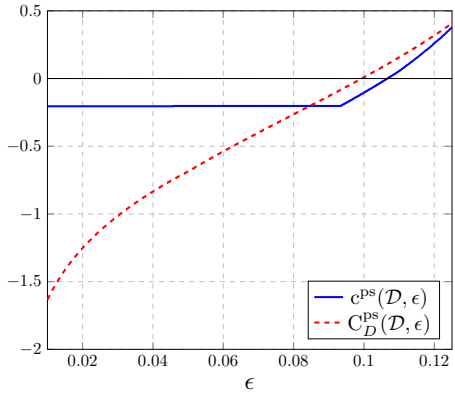

Figure 4.8: The functions $\epsilon \mapsto c^{\mathrm{ps}}(\mathcal{D}, \epsilon)$ (blue full line) and $\epsilon \mapsto C_D^{\mathrm{ps}}(\mathcal{D}, \epsilon)$ (red dashed) for the uncertain DDAE (4.29).

axis for all $\delta \in \mathcal{D}$ and $\|\Delta\|_2 \leq \mathrm{r}_{\mathbb{C},\|\cdot\|_2}(\mathcal{D})$. Yet, for any $\gamma > 0$ there exist $\delta \in \mathcal{D}$, $\Delta \in \mathbb{C}^{p\times q}$ with $\|\Delta\|_2 \leq \mathrm{r}_{\mathbb{C},\|\cdot\|_2}(\mathcal{D})$ and $\vec{\tau}_\gamma \in \mathcal{B}\big((1,2),\gamma\big) \cap (\mathbb{R}^+)^m$ such that the spectrum of (4.29) with the delay values $(1, 2)$ replaced by $\vec{\tau}_\gamma$ contains a chain of characteristic roots with the imaginary axis as vertical asymptote. This is illustrated in Figure 4.9, which shows the spectrum of (4.29) for $\Delta = 1/10.1$, $\delta_1 = 0.2$ and $\delta_2 = 0$ for the nominal delays $\vec{\tau} = (1, 2)$ and a small perturbation on the delays $\vec{\tau}_\gamma = (1, 2 + \pi/100)$, where the chosen δ and Δ correspond to $C^{\mathrm{ps}}\big(\mathcal{D}, \mathrm{r}_{\mathbb{C},\|\cdot\|_2}(\mathcal{D})\big)$. ◇

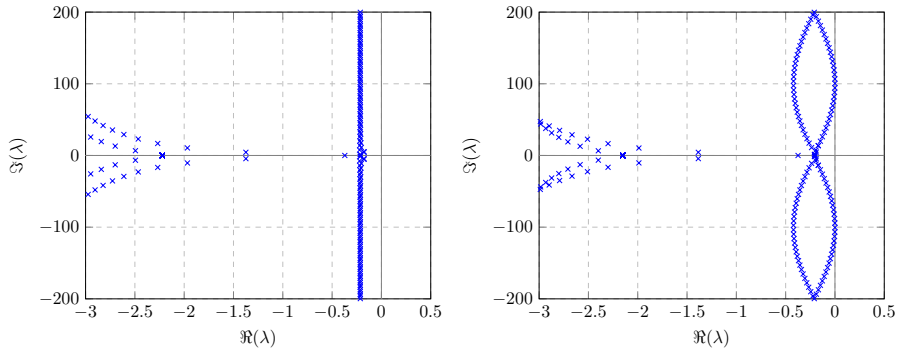

(a) $\vec{\tau} = (1, 2)$ (b) $\vec{\tau} = (1, 2 + \pi/100)$

Figure 4.9: The spectrum of (4.29) for $\delta_1 = 0.2$, $\delta_2 = 0$, and $\Delta = 1/10.1$ for the nominal delay values and a small perturbation on the delays.

4.6.3 Robust distance to a finite root crossing

Example 4.6. In this final example we consider the following uncertain system

$$\begin{cases} \dot{x}(t) = (-7 + 3\delta_1)\, x(t) + (-5 + 2\delta_2)\, x(t-1) + 4\, w(t), \\ z(t) = (2 - 2\delta_2)\, x(t) + (1 + \delta_1)\, w(t) + w(t-1) \end{cases} \tag{4.30}$$

with $|\delta_1| \leq 0.15$ and $|\delta_2| \leq 0.2$. The corresponding frequency response and asymptotic frequency response are now given by

$$T(\jmath\omega; \delta) = \frac{4(2 - 2\delta_2)}{\jmath\omega - (-7 + 3\delta_1) - (-5 + 2\delta_2)e^{-\jmath\omega}} + (1 + \delta_1) + e^{-\jmath\omega}$$

and

$$T_a(\jmath\omega; \delta) = (1 + \delta_1) + e^{-\jmath\omega},$$

respectively. For this final example the robust strong asymptotic H_∞-norm is equal to

$$\max_{|\delta_1| \leq 0.15} \max_{\theta \in [0, 2\pi)} \left| (1 + \delta_1) + 1e^{\jmath\theta} \right| = 2.15.$$

Figure 4.10 shows the worst-case gain function $\omega \mapsto \Upsilon(\omega)$ for $\omega \in [10^{-1}, 10^{2.5}]$ which attains a maximum of approximately 6.012 at $\omega \approx 2.734$. In this case the robust strong H_∞-norm is thus equal to the peak of the worst-case gain function which is attained at a finite frequency.

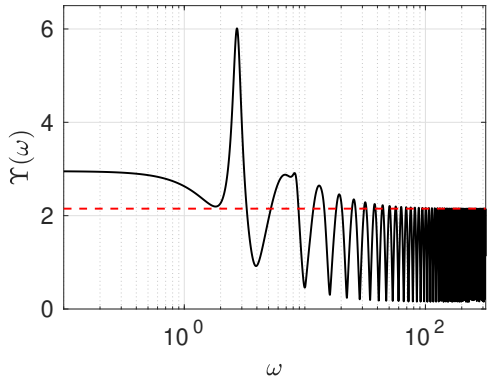

Figure 4.10: The worst-case gain function $\omega \mapsto \Upsilon(\omega)$ associated with the uncertain system (4.30) (black full line) and $|||T_a(\cdot;\cdot,\vec{\tau})|||^{\mathcal{D}}_{H_\infty}$ (red dashed line).

Next we examine the corresponding uncertain DDAE:

$$\begin{bmatrix} 1 & 0 & 0 \\ 0 & 0 & 0 \\ 0 & 0 & 0 \end{bmatrix} \dot{x}_e(t) = \begin{bmatrix} (-7+3\delta_1) & 4 & 0 \\ 0 & -1 & \Delta \\ (2-2\delta_2) & (1+\delta_1) & -1 \end{bmatrix} x_e(t) + \begin{bmatrix} (-5+2\delta_2) & 0 & 0 \\ 0 & 0 & 0 \\ 0 & 1 & 0 \end{bmatrix} x_e(t-1). \quad (4.31)$$

It follows from Lemma 4.8 that $\mathrm{r}_{\mathbb{C},\|\cdot\|_2}(\mathcal{D}) = \mathrm{r}^{\mathrm{fin}}_{\mathbb{C},\|\cdot\|_2}(\mathcal{D}) = \left(\max_{\omega\in\mathbb{R}^+} \Upsilon(\omega)\right)^{-1}$ ≈ 0.1663. This is illustrated in Figure 4.11 which shows $c^{\mathrm{ps}}(\mathcal{D},\epsilon)$ and $C^{\mathrm{ps}}_D(\mathcal{D},\epsilon)$ in function of ϵ. From this figure it is clear that the robust distance to a finite root crossing is indeed smaller than the robust distance to a characteristic root chain crossing. To conclude this example, we return to the alternative definition of the robust distance to a finite root crossing in Remark 4.6. Figure 4.12, shows the pseudospectrum of (4.31) for ϵ smaller than, equal to, and larger than the robust distance to instability. We observe that for ϵ equal to the robust distance to instability the pseudospectrum touches the imaginary axis at approximately $\pm\jmath 2.734$. ◇

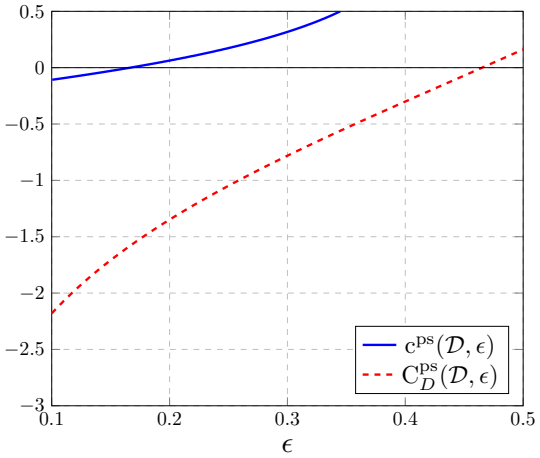

Figure 4.11: The functions $\epsilon \mapsto c^{\text{ps}}(\mathcal{D},\epsilon)$ (blue full line) and $\epsilon \mapsto C_D^{\text{ps}}(\mathcal{D},\epsilon)$ (red dashed) for the uncertain system (4.31).

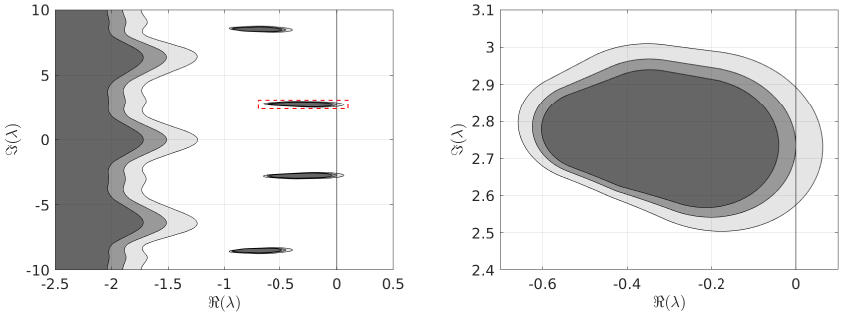

(a) $[-2.5,\ 0.5] \times \jmath[-10,\ 10]$ (b) $[-0.7,\ 0.1] \times \jmath[2.4,\ 3.1]$

Figure 4.12: The pseudospectrum $\Lambda^{\text{ps}}(\mathcal{D},\epsilon)$ of (4.31) for ϵ equal to 1/7 (dark gray), $\text{r}_{\mathbb{C},\|\cdot\|_2}(\mathcal{D})$ (gray) and 1/5 (light gray) in different regions of the complex plane.

4.7 Numerical algorithm for computing the robust strong H_∞-norm

This section introduces a numerical algorithm to compute the robust strong H_∞-norm. This algorithm exploits the relation of the robust strong H_∞-norm of uncertain system (4.12) with the robust distance to instability of the uncertain DDAE (4.14). First we give a high-level description of the algorithm. Next, we briefly describe the projected gradient flow method, which allows to solve the constrained optimization problems encountered in the algorithm. Thereafter, we briefly sketch how it is used in the presented algorithm.

4.7.1 High-level description

In a preliminary step, we have to check that the uncertain system (4.12) is internally exponentially stable for all admissible uncertainties. To this end we use the method presented in [28]. Next we compute the robust strong asymptotic H_∞-norm ($|||T_a(\cdot;\cdot,\vec{\tau})|||^{\mathcal{D}}_{H_\infty}$) by solving the following (constrained) optimization problem:

$$\begin{array}{ll} \underset{\delta,\vec{\theta}}{\text{maximise}} & \sigma_1\left(\tilde{D}_0(\delta)+\sum_{k=1}^{m}\tilde{D}_k(\delta)e^{\jmath\theta_k}\right), \\ \text{subject to} & \delta\in\mathcal{D}, \text{ and} \\ & \vec{\theta}\in[0,2\pi)^m. \end{array} \tag{4.32}$$

Subsequently, we compute $\mathrm{r}^{\mathrm{fin}}_{\mathbb{C},\|\cdot\|_2}(\mathcal{D})$ by looking for a zero-crossing of the function $\epsilon \mapsto c^{\mathrm{ps}}(\mathcal{D},\epsilon)$ in the interval $\left[0,\left(|||T_a(\cdot;\cdot,\vec{\tau})|||^{\mathcal{D}}_{\mathcal{H}_\infty}\right)^{-1}\right)$ using the Newton-bisection method (see [156, Section 9] for a reference implementation). This root finding method combines the robustness of the bisection method (if the initial search bracket contains a unique root then the algorithm will converge to this root) with the fast (local) convergence of Newton's method (quadratic when close to the root) and requires the evaluation of both $c^{\mathrm{ps}}(\mathcal{D},\epsilon)$ and $\frac{d}{d\epsilon}c^{\mathrm{ps}}(\mathcal{D},\epsilon)$ for given ϵ. The quantity $c^{\mathrm{ps}}(\mathcal{D},\epsilon)$ is found by solving the following optimization problem:

$$\begin{array}{ll} \underset{\delta,\Delta}{\text{maximise}} & \Re\big(\lambda_{RM}(\delta,\Delta)\big), \\ \text{subject to} & \delta\in\mathcal{D}, \\ & \Delta\in\mathbb{C}^{p\times q} \text{ and } \|\Delta\|_2\leq\epsilon \end{array} \tag{4.33}$$

with $\lambda_{RM}(\delta,\Delta)$ the right-most characteristic root of a particular instance of (4.14). Below we will discuss how this optimization problem can be solved using

the projected gradient flow method and give an expression for the derivative of $c^{\mathrm{ps}}(\mathcal{D}, \epsilon)$ with respect to ϵ, which follows readily from the result of the above optimization problem.

Once $|||T_a(\cdot;\cdot,\vec{\tau})|||_{H_\infty}^{\mathcal{D}}$ and $\mathrm{r}^{\mathrm{fin}}_{\mathbb{C},\|\cdot\|_2}(\mathcal{D})$ are computed, it follows from Theorem 4.1 that:

$$\begin{aligned} |||T(\cdot;\cdot,\vec{\tau})|||_{H_\infty} &= \mathrm{r}(\mathcal{D})^{-1} = \min\left\{\mathrm{r}^{\mathrm{nwp}}_{\mathbb{C},\|\cdot\|_2}(\mathcal{D}), \mathrm{r}^{\mathrm{chain}}_{\mathbb{C},\|\cdot\|_2}(\mathcal{D}), \mathrm{r}^{\mathrm{fin}}_{\mathbb{C},\|\cdot\|_2}(\mathcal{D})\right\}^{-1} \\ &= \max\left\{|||T_a(\cdot;\cdot,\vec{\tau})|||_{H_\infty}^{\mathcal{D}}, \mathrm{r}^{\mathrm{fin}}_{\mathbb{C},\|\cdot\|_2}(\mathcal{D})^{-1}\right\}. \end{aligned}$$

4.7.2 Projected gradient flow method

The projected gradient flow method is a continuous variant of the well-known steepest ascend method for solving constrained optimization problems. It looks for a flow in the space of admissible variables along which the objective function monotonically increases. This flow is defined in such a way that the (local) optima of the objective function appear as attractive stationary points. These optimizers can be found by choosing an initial point and discretizing the resulting path till convergence to a stationary point using Euler's forward method with an adaptive step size. As the goal is not to accurately solve the differential equation but rather converge to a local optimum, the step size is not chosen to satisfy an error bound but rather to guarantee a monotonic increase of objective function. The path following algorithm is stopped when the objective function can no longer be increased. However, because the algorithm can end up in a local optimum, one needs to restart the optimization procedure from several initial values. For more details on using the projected gradient flow method for computing extremal points of pseudospectra we refer to the extensive literature [28, 77, 78] (see also Section 2.2.2). Below, we will restrict ourselves to give the resulting flows for the two optimization problems encountered above.

4.7.3 Computing the robust strong asymptotic H_∞-norm

This subsection briefly describes how to use the projected gradient flow method for optimization problem (4.32). In this case we are looking for a path $t \mapsto \big(\delta(t), \theta(t)\big) \in \mathcal{D} \times [0, 2\pi)^m$ such that the function

$$t \mapsto \sigma_1\Big(\tilde{D}_0(\delta(t)) + \sum_{k=1}^{m} \tilde{D}_k(\delta(t)) e^{\jmath\theta_k(t)}\Big)$$

is monotonically increasing and that the (local) optimizers of (4.32) appear as attractive stationary points. It can be verified that the following path fulfills

these requirements:

$$\begin{cases} \delta_l(t) = \bar{\delta}_l \delta_l^n(t) & \text{for } l = 1, \ldots, L, \\ \theta_k(t) = \vartheta_k(t) \bmod 2\pi & \text{for } k = 1, \ldots m \end{cases}$$

with mod the modulo operator[6], which assures that $\theta_k(t)$ remains bounded to the half-open interval $[0, 2\pi)$, and

$$\begin{cases} \dot{\vartheta}_k(t) = -\Im\left(u(t)^H \tilde{D}_k(\delta(t)) v(t) e^{\jmath\theta_k(t)}\right), \\ \Xi_l(t) = \bar{\delta}_l \sum_{k=0}^{m} \sum_{s=1}^{S_l^{D_k}} {G_{l,s}^{D_k}}^T \Re\left(u(t) v(t)^H e^{-\jmath\theta_k(t)}\right) {H_{l,s}^{D_k}}^T, \\ \dot{\delta}_l^n(t) = \begin{cases} \Xi_l(t) - \left\langle \delta_l^n(t), \Xi_l(t) \right\rangle_F \delta_l^n(t) & \text{if } \|\delta_l^n(t)\|_F = 1 \text{ and} \\ & \left\langle \delta_l^n(t), \Xi_l(t) \right\rangle_F > 0 \\ \Xi_l(t) & \text{otherwise,} \end{cases} \end{cases} \tag{4.34}$$

where $u(t)$ and $v(t)$ are the left and right singular vectors of unit norm associated with the largest singular value of $\tilde{D}_0(\delta(t)) + \sum_{k=1}^{m} \tilde{D}_k(\delta(t)) e^{\jmath\theta_k(t)}$ and $\langle A, B \rangle_F = \sum_{i,j} A_{i,j} B_{i,j}$, the Frobenius inner product of two matrices A and B.

Remark 4.7. The right-hand side of (4.34) can be seen as the projection of the gradient of $\sigma_1\left(\tilde{D}_0(\delta) + \sum_{k=1}^{m} \tilde{D}_k(\delta) e^{\jmath\theta_k}\right)$ with respect to the elements of δ_l and θ_k onto the search space. The projection ensures that the constraints are fulfilled for all t.

4.7.4 Computing the pseudospectral abscissa

For a given ϵ, the pseudospectral abscissa, $c^{\text{ps}}(\mathcal{D}, \epsilon)$, can be computed by solving (4.33). Note however that for an arbitrary ϵ the maximum of (4.33) might not be attained, as for $\Delta \neq 0$ the dominant characteristic root of (4.14) might be part of a vertical root chain (as encountered in Proposition 4.5). To guarantee that the maximum of (4.33) is defined, we add an additional constraint to the optimization problem:

$$\lambda_{RM}(\delta, \Delta) \in \{\lambda \in \mathbb{C} : \Im(\lambda) \in [-\beta, \beta]\}$$

[6]The modulo operator is defined as follows: $a \bmod b = a - \left\lfloor \frac{a}{b} \right\rfloor b$ in which the floor function $\lfloor \cdot \rfloor$ returns the greatest integer smaller than or equal to its argument.

with β sufficiently large. This may lead to an underestimate for $c^{\text{ps}}(\mathcal{D},\epsilon)$ for a given ϵ. However for $\epsilon \in \left[0, \min\{\mathrm{r}^{\text{nwp}}_{\mathbb{C},\|\cdot\|_2}(\mathcal{D}), \mathrm{r}^{\text{chain}}_{\mathbb{C},\|\cdot\|_2}(\mathcal{D})\}\right)$, the transition to $c^{\text{ps}}(\mathcal{D},\epsilon) \geq 0$ is caused by a (finite) characteristic root crossing the imaginary axis, and thus if β is sufficiently large this additional constraint does not influence the result of the overall root finding procedure to compute $\mathrm{r}^{\text{fin}}_{\mathbb{C},\|\cdot\|_2}(\mathcal{D})$.

In this case we are looking for a path $t \mapsto (\delta(t), \Delta(t))$ such that $\delta(t) \in \mathcal{D}$, $\|\Delta(t)\|_2 \leq \epsilon$ and the spectral abscissa of (4.14) monotonically increases. To end, we start with stating the derivative of $\Re\big(\lambda_{RM}(\delta(t),\Delta(t))\big)$ along this path:

$$\frac{1}{\xi(t)}\Bigg(\Re\left(\left\langle B_e^T\phi(t)\psi(t)^H C_e^T, \dot{\Delta}(t)\right\rangle_F\right) + \sum_{l=1}^{L}\left\langle \sum_{k=0}^{m}\sum_{s=1}^{S_l^k} {G_{l,s}^k}^T \Phi(t)\Gamma_k(t)\Psi(t)^T {H_{l,s}^k}^T, \dot{\delta}_l(t)\right\rangle_F\Bigg), \tag{4.35}$$

in which $\phi(t)$ and $\psi(t)$ are respectively the left and right eigenvectors associated with $\lambda_{RM}(\delta(t),\Delta(t))$ normalized such that

$$\xi(t) := \phi(t)^H\left(E_e + \sum_{k=1}^{m}\tau_k\tilde{A}_{e,k}(\delta(t))e^{-\lambda_{RM}(t)\tau_k}\right)\psi(t) > 0, \tag{4.36}$$

$$\Phi(t) := \begin{bmatrix}\Re(\phi(t)) & \Im(\phi(t))\end{bmatrix},$$

$$\Psi(t) := \begin{bmatrix}\Re(\psi(t)) & \Im(\psi(t))\end{bmatrix},$$

$$\Gamma_k(t) := \begin{bmatrix}\Re(e^{-\lambda_{RM}(t)\tau_k}) & -\Im(e^{-\lambda_{RM}(t)\tau_k})\\ \Im(e^{-\lambda_{RM}(t)\tau_k}) & \Re(e^{-\lambda_{RM}(t)\tau_k})\end{bmatrix},$$

and $\langle X, Y\rangle_F = \sum_{i,j}\bar{A}_{i,j}B_{i,j}$ the complex Frobenius inner product.

Before defining the resulting paths, we note that we can limit the search space for the complex perturbation Δ to the manifold of rank one matrices of norm ϵ (see [26, 77]):

$$\Delta(t) = \epsilon u(t)v(t)^H$$

with $u(t) \in \mathbb{C}^p$, $v(t) \in \mathbb{C}^q$ and $\|u(t)\|_2 = \|v(t)\|_2 = 1$. In [28] a similar low rank structure for the real-valued matrix perturbation was discussed; however, here we will not exploit this low rank structure because the targeted real uncertainties are scalar or low dimensional for which working with the low rank factorisation is not advantageous.

Let us consider the following path:

$$\begin{cases} \dot{u}(t) &= \frac{\jmath}{2}\Im\big(u(t)^H B_e^T \phi(t)\psi(t)^H C_e^T v(t)\big)u(t) + \\ & \qquad\qquad (I - u(t)u(t)^H)B^{eT}\phi(t)\psi(t)^H C_e^T v(t), \\ \dot{v}(t) &= \frac{\jmath}{2}\Im\left(v(t)^H C_e\psi(t)\phi(t)^H B_e u(t)\right)v(t) + \\ & \qquad\qquad (I - v(t)v(t)^H)C_e\psi(t)\phi(t)^H B_e u(t), \\ \dot{\delta}_l(t) &= \begin{cases} \Theta_l(t) - \dfrac{\langle \delta_l(t), \Theta_l(t)\rangle_F \, \delta_l}{\|\delta_l(t)\|_F^2} & \|\delta_l(t)\|_F = \bar{\delta}_l \text{ and } \langle \delta_l(t), \Theta_l(t)\rangle_F > 0, \\ \Theta_l(t) & \text{otherwise} \end{cases} \end{cases}$$

with

$$\Theta_l(t) = \sum_{k=1}^{m}\sum_{s=1}^{S_l^k} {G_{l,s}^k}^T \Phi(t)\Gamma_k(t)\Psi(t)^T {H_{l,s}^k}^T.$$

By plugging this path into (4.35), one observes that $\delta(t) \in \mathcal{D}$, $\|\Delta(t)\|_2 \leq \epsilon$ and the objective function monotonically increases. Furthermore, this path can be seen as a combination of the paths presented in [28] (computing the pseudospectral abscissa for real-valued Frobenius norm bounded uncertainties) and [77] (computing the pseudospectral abscissa for complex-valued spectral norm bounded uncertainties).

Once the pseudospectral abscissa $c^{\mathrm{ps}}(\mathcal{D}, \epsilon)$ is known, its derivative with respect to ϵ can easily be calculate with almost no additional cost (whenever it exists). Let $\delta^\star$ and $\Delta^\star = \epsilon u^\star {v^\star}^H$ be maximizers of (4.33) obtained by the projected gradient flow method and assume that the corresponding rightmost eigenvalue of (4.14) is unique and simple with left and right eigenvectors $\phi^\star$ and $\psi^\star$ normalized such that $\xi^\star$ (as defined in (4.36)) is real and positive, then

$$\frac{\mathrm{d}}{\mathrm{d}\epsilon} c^{\mathrm{ps}}(\mathcal{D}, \epsilon) = \frac{1}{\xi^\star}\Re\left((\phi^{\star H} B_e u^\star)(v^{\star H} C_e \psi^\star)\right). \tag{4.37}$$

4.8 Conclusion

In this chapter we examined uncertain time-delay systems of the form (4.12) and introduced the notion of the robust H_∞-norm as the worst-case value of the H_∞-norm over all admissible uncertainty values. Similar as the nominal H_∞-norm, the robust H_∞-norm might be a discontinuous function of the delay values for systems with multiple direct feedthrough terms. We therefore introduced the robust strong H_∞-norm as the worst-case value of the strong H_∞-norm. Next,

we demonstrated that there exists a relation between the robust strong H_∞-norm of an uncertain time-delay system and the robust distance to instability of the uncertain DDAE (4.14). Based on this relation, Section 4.7 introduced a novel numerical algorithm to compute this robust strong H_∞-norm.

The presented theory and algorithm can be generalized to systems with uncertainties on the delays. Because the robust strong asymptotic H_∞-norm, the robust distance to non well-posedness and the robust distance to a characteristic root chain crossing are independent of the delay values, the proofs in Section 4.5.2 can be reused without modification. The results from Section 4.5.3 trivially generalize to the uncertain delay case by extending the definitions of the worst-case gain function and the robust distance to a finite root crossing to include the uncertainties on the delays. Also the algorithm presented in Section 4.7 only needs minor modifications.

Finally, a reference MATLAB implementation of the algorithm described in Section 4.7 is available from `http://twr.cs.kuleuven.be/research/software/delay-control/rb_hinf/`.

CHAPTER

5 A scalable controller design method for the robust control of networked systems

Abstract

This chapter presents a scalable controller design method for networked systems with a large number of subsystems based on the robust H_∞-control framework. The dynamics of the individual subsystems are assumed to be described by identical linear time-invariant delay differential equations and the effect of transport and communication delay is explicitly taken into account. The proposed controller architecture consists of identical local controllers that each control a single subsystem but are allowed to communicate with neighboring systems. The control objective is to minimize the H_∞-norm of the overall system. However the cost of computing the H_∞-norm of the overall system scales poorly with respect to the number of subsystems. To achieve scalability, the presented method is therefore based on the result that, under a particular assumption on the graph describing the interconnections between the subsystems, the H_∞-norm of the overall system is upper bounded by the robust H_∞-norm of a single subsystem with an additional (scalar) uncertainty. The proposed design method consists of finding suitable controller parameters by directly minimizing this upper bound instead of the actual H_∞-norm.

The results in this chapter are based on [14].

5.1 Introduction

A networked system is a system that consist of a large number of subsystems that interact with each other. Examples of such systems are the power grid, the internet-of-things, or cooperative cruise control systems. The control of networked systems is challenging due to their large dimension and the presence of delays, originating from the time needed to transfer matter, energy or information between the subsystems. As a consequence, the traditional approach of using one global controller for the complete system is typically not feasible. Furthermore, the assumption that all measurements are centrally available, does often not hold. Therefore, decentralized and distributed control approaches, in which the task of computing the control action is divided over multiple (local) controllers, are preferred [20, 168].

In this chapter we consider networked systems in which the dynamics of the individual subsystems are described by identical linear time-invariant delay differential equations. Furthermore, the transport and communication delays between the individual subsystems are explicitly taken into account. To control the system, we propose a controller architecture that consists of identical local controllers that each steer a single subsystem. To guarantee robustness against uncertainties, such as model mismatch or external disturbances, we want to select the controller parameters in such a way that the H_∞-norm of the overall network is minimized. However, the computation cost of the standard algorithms for calculating the H_∞-norm of dynamical systems with discrete delays, such as [82], scales cubically with respect to the number of states (and hence the number of subsystems). For certain networked systems with identical subsystems this cost can be decreased significantly using the decoupling transformation presented in [128] and [57]. More specifically, if the adjacency matrix of the graph describing the interconnections between the subsystems is unitarily diagonalizable, then the H_∞-norm of the complete system is equal to the maximal H_∞-norm of a single parametrized subsystem where the allowable values of the parameter correspond to the eigenvalues of the adjacency matrix. The computation cost now scales linearly with respect to the number of subsystems. Moreover, if these eigenvalues are confined to an interval on the real-axis, we can consider this parameter as a real-valued scalar uncertainty. The robust H_∞-norm of this uncertain subsystem then gives an upper bound for the H_∞-norm of the complete network, which can be computed using the method presented in the previous chapter. Furthermore, the computation cost of this upper bound only depends on the dimension of an individual subsystem and not on the number of subsystems. The proposed design approach consists of minimizing this upper bound with respect to the controller parameters. A similar idea is applied in [56] which presents a scalable method to design stabilizing decentralized controllers for networked systems with identical subsystems.

The remainder of this chapter is structured as follows. First, Section 5.2 introduces the considered class of networked systems. Next, Section 5.3 shows that under a particular assumption on the interconnection graph, the aforementioned decoupling transformation can be used to compute an upper bound for the H_∞-norm of the system that does not depend on the number of subsystems. Thereafter, a direct optimization approach to synthesize the controller is outlined in Section 5.4. Finally, the resulting design methodology is illustrated using an example problem in Section 5.5. Section 5.6 gives some concluding remarks.

5.2 System description and control objective

In this chapter, we consider networked systems with N subsystems. The dynamics of the individual subsystems are identical and described by a state-space representation of the following form:

$$S_j \leftrightarrow \begin{cases} \dot{x}_j(t) = \sum_{k=0}^{m} A_k\, x_j(t-\tau_k) + B_u\, u_j(t-\tau_u) \\ \qquad\qquad\qquad\qquad + B_{u_n}\, u_{n,j}(t) + B_w\, w_j(t), \\ y_j(t) = C_y\, x_j(t), \\ y_{n,j}(t) = C_{y_n}\, x_j(t), \\ z_j(t) = C_z\, x_j(t) \qquad\qquad \text{for } j = 1, \ldots, N \end{cases} \tag{5.1}$$

with $x_j(t) \in \mathbb{R}^n$ the state vector of subsystem j, $u_j(t) \in \mathbb{R}^{p_c}$ its control input, $y_j(t) \in \mathbb{R}^{q_c}$ its measured output, $w_j(t) \in \mathbb{R}^p$ its performance input, and $z_j(t) \in \mathbb{R}^q$ its performance output. The pointwise state delays are assumed to satisfy $0 = \tau_0 < \tau_1 < \cdots < \tau_m$ and the input delay $\tau_u \geq 0$. The matrices A_k (for $k = 0, \ldots, m$), B_u, B_{u_n}, B_w, C_y, C_{y_n} and C_z are real-valued and have appropriate dimension. The input $u_{n,j}(t) \in \mathbb{R}^{p_n}$ and the output $y_{n,j}(t) \in \mathbb{R}^{q_n}$ model the interactions between the subsystems:

$$u_{n,j}(t) = \sum_{i=1}^{N} [P_N]_{j,i}\, y_{n,i}(t-\tau_n)$$

with $\tau_n \geq 0$ the interaction delay and $[P_N]_{j,i}$ the entry on the jth row and i^{th} column of $P_N \in \mathbb{R}^{N\times N}$, the adjacency matrix of the interconnection graph of the network. (An entry $[P_N]_{j,i}$ is non-zero if the dynamics of subsystem j are influenced by the network output $y_{n,i}(t)$ of subsystem i.)

The considered control architecture consists of local controllers that each steer one subsystem. These local controllers are identical dynamic output feedback controllers of order n_c:

$$C_j \leftrightarrow \begin{cases} \dot{\xi}_j(t) = J_{\mathbf{p}}\, \xi_j(t) + F_{\mathbf{p}}\, y_j(t) + F_{n,\mathbf{p}}\, y_{nc,j}(t), \\ u_j(t) = L_{\mathbf{p}}\, \xi_j(t) + K_{\mathbf{p}}\, y_j(t) + K_{n,\mathbf{p}}\, y_{nc,j}(t) \quad \text{for } j = 1, \ldots, N \end{cases} \tag{5.2}$$

with $\xi_j(t) \in \mathbb{R}^{n_c}$ the state of the local controller associated with subsystem j. The matrices $J_{\mathbf{p}}$, $F_{\mathbf{p}}$, $F_{n,\mathbf{p}}$, $L_{\mathbf{p}}$, $K_{\mathbf{p}}$ and $K_{n,\mathbf{p}}$ are real-valued and have appropriated dimension. The subscript $\mathbf{p}$ is used to indicate that these matrices depend on some tunable control parameters $\mathbf{p}$. If $F_{n,\mathbf{p}} \not\equiv 0$ and/or $K_{n,\mathbf{p}} \not\equiv 0$, the local controllers have access to the sensor measurements of neighboring

subsystems. It is however required that the communication graph is same as the interaction graph:

$$y_{nc,j}(t) = \sum_{i=1}^{N} [P_N]_{j,i}\, y_i(t - \tau_{nc})$$

with $\tau_{nc} \geq 0$ a communication delay.

Remark 5.1. In the remainder of this chapter we restrict our attention to controller architectures in which the local controllers can only share sensor measurements. Note however that the results can easily be extended to distributed control architectures in which the local controllers also share their internal state.

By eliminating the control and coupling variables, we find the following state-space description for the complete networked system:

$$\begin{cases} \dot{x}(t) = \sum_{k=0}^{m} (I_N \otimes A_k)\, x(t-\tau_k) + (I_N \otimes B_u K_{\mathbf{p}} C_y)\; x(t-\tau_u) + \\ \qquad\qquad (P_N \otimes B_{u_n} C_{y_n})\; x(t-\tau_n) + \big(I_N \otimes B_u L_{\mathbf{p}}\big)\, \xi(t-\tau_u) + \\ \qquad\qquad (P_N \otimes B_u K_{n,\mathbf{p}} C_y)\; x(t-\tau_u-\tau_{nc}) + (I_N \otimes B_w)\; w(t), \\ \dot{\xi}(t) = (I_N \otimes J_{\mathbf{p}})\; \xi(t) + (I_N \otimes F_{\mathbf{p}} C_y)\, x(t) + \\ \qquad\qquad\qquad\qquad (P_N \otimes F_{n,\mathbf{p}} C_y)\; x(t-\tau_{nc}), \\ z(t) = (I_N \otimes C_z)\, x(t) \end{cases} \tag{5.3}$$

with $\otimes$ the Kronecker product, I_N the identity matrix of size N, $x(t) = [x_1(t)^\top \cdots\; x_N(t)^\top]^\top$ the combined state vector of the complete system, $\xi(t) = [\xi_1(t)^\top \cdots\; \xi_N(t)^\top]^\top$ the combined controller state vector, $w(t) = [w_1(t)^\top \cdots\; w_N(t)^\top]^\top$ the combined performance input and $z(t) = [z_1(t)^\top \cdots z_N(t)^\top]^\top$ the combined performance output. The corresponding transfer function from w to z is equal to:

$$T(s;\mathbf{p},N) = \big(I_N \otimes \begin{bmatrix} C_z & 0 \end{bmatrix}\big)\, \big(I_{N(n+n_c)} s - I_N \otimes Q_{\mathbf{p}}(s) - P_N \otimes R_{\mathbf{p}}(s)\big)^{-1} \times \Big(I_N \otimes \begin{bmatrix} B_w \\ 0 \end{bmatrix}\Big) \tag{5.4}$$

with

$$Q_{\mathbf{p}}(s) = \begin{bmatrix} A_0 & 0 \\ F_{\mathbf{p}} C_y & J_{\mathbf{p}} \end{bmatrix} + \sum_{k=1}^{m} \begin{bmatrix} A_k & 0 \\ 0 & 0 \end{bmatrix} e^{-s\tau_k} + \begin{bmatrix} B_u K_{\mathbf{p}} C_y & B_u L_{\mathbf{p}} \\ 0 & 0 \end{bmatrix} e^{-s\tau_u}$$

and

$$R_{\mathbf{p}}(s) = \begin{bmatrix} B_{u_n} C_{y_n} & 0 \\ 0 & 0 \end{bmatrix} e^{-s\tau_n} + \begin{bmatrix} B_u K_{n,\mathbf{p}} C_y & 0 \\ 0 & 0 \end{bmatrix} e^{-s(\tau_u+\tau_{nc})} + \begin{bmatrix} 0 & 0 \\ F_{n,\mathbf{p}} C_y & 0 \end{bmatrix} e^{-s\tau_{nc}}.$$

5.3 Upper bound for the H-infinity norm

In this subsection we show that under the following assumption on the adjacency matrix P_N, there exists a decoupling transformation that allows to compute an upper bound for the H_∞-norm of (5.4) at a computation cost that does not depend on the number of subsystems N.

Assumption 5.1. The matrix P_N has real-valued eigenvalues confined to an interval $[a,\, b]$ and is diagonalizable by a unitary matrix $V_N \in \mathbb{C}^{n\times n}$, i.e.,

$$V_N{}^H P_N V_N = \Lambda_N$$

with $\Lambda_N = \mathrm{diag}(\lambda_1, \lambda_2, \ldots, \lambda_N)$ and $\lambda_j \in [a,\, b]$ for $j = 1, \ldots, N$.

If we apply the following change of variables to the state variables, the controller state variables, the performance input and the performance output of system (5.3)

$$\begin{aligned}
\bar{x}(t) &:= (V_N{}^H \otimes I_n)\, x(t),\\
\bar{\xi}(t) &:= (V_N{}^H \otimes I_{n_c})\, \xi(t),\\
\bar{w}(t) &:= (V_N{}^H \otimes I_p)\, w(t), \text{ and}\\
\bar{z}(t) &:= (V_N{}^H \otimes I_q)\, z(t)
\end{aligned}$$

we obtain

$$\begin{cases}
\dot{\bar{x}}(t) = \sum_{k=0}^{m} (I_N \otimes A_k)\, \bar{x}(t-\tau_k) + (I_N \otimes B_u K_{\mathbf{p}} C_y)\, \bar{x}(t-\tau_u) + \\
\qquad\qquad (\Lambda_N \otimes B_{u_n} C_{y_n})\, \bar{x}(t-\tau_n) + (I_N \otimes B_u L_{\mathbf{p}})\, \bar{\xi}(t-\tau_u) + \\
\qquad\qquad (\Lambda_N \otimes B_u K_{n,\mathbf{p}} C_y)\, \bar{x}(t-\tau_u-\tau_{nc}) + (I_N \otimes B_w)\, \bar{w}(t),\\
\dot{\bar{\xi}}(t) = (I_N \otimes J_{\mathbf{p}})\, \bar{\xi}(t) + (I_N \otimes F_{\mathbf{p}} C_y)\, \bar{x}(t) + \\
\qquad\qquad\qquad\qquad (\Lambda_N \otimes F_{n,\mathbf{p}} C_y)\, \bar{x}(t-\tau_{nc}),\\
\bar{z}(t) = (I_N \otimes C_z)\, \bar{x}(t).
\end{cases} \tag{5.5}$$

Notice that all matrices in (5.5) are block diagonal and hence the behavior of this transformed system is fully characterized by its N independent subsystems. This leads to the following theorem.

Theorem 5.1. For a networked system of the form (5.3) whose adjacency matrix fulfills Assumption 5.1, it holds that

$$\|T(\cdot;\mathbf{p},N)\|_{H_\infty} = \|\bar{T}_{\bar{z}\bar{w}}(\cdot;\mathbf{p},N)\|_{H_\infty} = \max_{\lambda\in\{\lambda_1,\ldots,\lambda_N\}} \|\hat{T}_{\hat{z}\hat{w}}(\cdot;\mathbf{p},\lambda)\|_{H_\infty}$$

with $\bar{T}_{\bar{z}\bar{w}}(\cdot;\mathbf{p},N)$ the transfer function from $\bar{w}$ to $\bar{z}$ of system (5.5) and $\hat{T}_{\hat{z}\hat{w}}(\cdot;\mathbf{p},\lambda)$ the transfer function from $\hat{w}$ to $\hat{z}$ of the following system parameterized in λ:

$$\begin{cases} \dot{\hat{x}}(t) = \sum_{k=0}^{m} A_k\,\hat{x}(t-\tau_k) + B_u K_{\mathbf{p}} C_y\,\hat{x}(t-\tau_u) + \lambda B_{u_n} C_{y_n}\,\hat{x}(t-\tau_n) \\ \qquad\qquad +\lambda B_u K_{n,\mathbf{p}} C_y\,\hat{x}(t-\tau_u-\tau_{nc}) + B_u L_{\mathbf{p}}\,\hat{\xi}(t-\tau_u) + B_w\,\hat{w}(t), \\ \dot{\hat{\xi}}(t) = J_{\mathbf{p}}\,\hat{\xi}(t) + F_{\mathbf{p}} C_y\,\hat{x}(t) + \lambda F_{n,\mathbf{p}} C_y\,\hat{x}(t-\tau_{nc}), \\ \hat{z}(t) = C_z\,\hat{x}(t). \end{cases} \tag{5.6}$$

Proof. The provided proof is added for self-containedness and is similar to the ones given in [128] and [57]. We refer to these papers for more details.
The relation between $T(\jmath\omega;\mathbf{p},N)$ and $\bar{T}_{\bar{z}\bar{w}}(\jmath\omega;\mathbf{p},N)$ is given by

$$T(\jmath\omega;\mathbf{p},N) = (V_N \otimes I_q)\ \bar{T}_{\bar{z}\bar{w}}(\jmath\omega;N)\ \left({V_N}^H \otimes I_p\right).$$

Because $(V_N \otimes I_q)$ and $({V_N}^H \otimes I_p)$ are unitary matrices it follows that,

$$\begin{aligned}\sigma_1\big(T(\jmath\omega;\mathbf{p},N)\big) &= \sigma_1\Big(\ (V_N \otimes I_q)\ \bar{T}_{\bar{z}\bar{w}}(\jmath\omega;\mathbf{p},N)\ \left({V_N}^H \otimes I_p\right)\Big) \\ &= \sigma_1\left(\bar{T}_{\bar{z}\bar{w}}(\jmath\omega;\mathbf{p},N)\right).\end{aligned}$$

The second equality follows from the fact that

$$\bar{T}_{\bar{z}\bar{w}}(\jmath\omega;\mathbf{p},N) = \mathrm{blkdiag}_{j=1,\ldots,N}\left(\hat{T}_{\hat{z}\hat{w}}(\jmath\omega;\mathbf{p},\lambda_j)\right),$$

and hence

$$\sigma_1\left(\bar{T}_{\bar{z}\bar{w}}(\jmath\omega;\mathbf{p},N)\right) = \max_{\lambda\in\{\lambda_1,\ldots,\lambda_N\}} \sigma_1\big(\hat{T}_{\hat{z}\hat{w}}(\jmath\omega;\mathbf{p},\lambda)\big),$$

which concludes the proof. □

Note that system (5.6) corresponds to a single subsystem in (5.3) where the network connections are replaced by a parameter. By treating λ in (5.6) as an uncertainty confined to the interval $[a,\,b]$, the robust H_∞-norm of (5.6), denoted by

$$\|\hat{T}_{\hat{z}\hat{w}}(\cdot;\mathbf{p},\cdot)\|_{H_\infty}^{[a,\,b]} = \max_{\lambda\in[a,\,b]} \|\hat{T}_{\hat{z}\hat{w}}(\cdot;\mathbf{p},\lambda)\|_{H_\infty}, \tag{5.7}$$

can be used as an upper bound for the H_∞-norm of the complete network (5.3), as stated in the following corollary.

Corollary 5.1. The H_∞-norm of a networked system of the form (5.3) whose adjacency matrix fulfills Assumption 5.1, is upper bounded by the robust H_∞-norm of $\hat{T}_{\hat{z}\hat{w}}(\cdot; \mathbf{p}, \lambda)$, with λ an uncertain parameter confined to $[a,\, b]$:

$$\|T(\cdot; \mathbf{p}, N)\|_{H_\infty} \leq \|\hat{T}_{\hat{z}\hat{w}}(\cdot; \mathbf{p}, \cdot)\|_{H_\infty}^{[a,\, b]}.$$

Furthermore, if Assumption 5.1 holds with a and b independent of N, then $\|\hat{T}_{\hat{z}\hat{w}}(\cdot; \mathbf{p}, \cdot)\|_{H_\infty}^{[a,\, b]}$ is also an upper bound for the supremum of $\|T(\cdot; \mathbf{p}, N)\|_{H_\infty}$ over the number of subsystems:

$$\sup_{N=1,\ldots,+\infty} \|T(\cdot; \mathbf{p}, N)\|_{H_\infty} \leq \|\hat{T}_{\hat{z}\hat{w}}(\cdot; \mathbf{p}, \lambda)\|_{H_\infty}^{[a,\, b]}.$$

Finally, if the (Hausdorff) distance between $\bigcup_{N=1}^{+\infty} \{\lambda \in \mathbb{C} : \det(I_N \lambda - P_N) = 0\}$ and $[a,\, b]$ goes to zero then

$$\sup_{N=1,\ldots,+\infty} \|T(\cdot; \mathbf{p}, N)\|_{H_\infty} = \|\hat{T}_{\hat{z}\hat{w}}(\cdot; \mathbf{p}, \lambda)\|_{H_\infty}^{[a,\, b]}.$$

Example 5.1. To illustrate the applicability of this result, we consider the following adjacency matrices:

$$P_N^{\text{ring}} = \begin{bmatrix} 0 & 0.5 & & & & & 0.5 \\ 0.5 & 0 & 0.5 & & & & \\ & 0.5 & 0 & 0.5 & & & \\ & & \ddots & \ddots & \ddots & & \\ & & & 0.5 & 0 & 0.5 & \\ 0.5 & & & & 0.5 & 0 & \end{bmatrix} \text{ and } P_N^{\text{line}} = \begin{bmatrix} 0 & 0.5 & & & & & \\ 0.5 & 0 & 0.5 & & & & \\ & 0.5 & 0 & 0.5 & & & \\ & & \ddots & \ddots & \ddots & & \\ & & & 0.5 & 0 & 0.5 & \\ & & & & 0.5 & 0 & \end{bmatrix}.$$

The first adjacency matrix, P_N^{ring}, corresponds to a bidirectional ring topology, see Figure 5.1; the second one corresponds to a bidirectional line topology, see Figure 5.2. The eigenvalues of these adjacency matrices are

$$\left\{\cos\left(\tfrac{2\pi(j-1)}{N}\right)\right\}_{j=1}^{\lfloor \frac{N+2}{2} \rfloor} \text{ and } \left\{\cos\left(\tfrac{j\pi}{N+1}\right)\right\}_{j=1}^{N},$$

respectively. The eigenvalues of both matrices are thus confined to the interval $[a,\ b] = [-1,\ 1]$ for all $N > 1$. As both adjacency matrices are symmetric and hence unitary diagonalizable, we can apply Corollary 5.1 to compute an upper bound for the H_∞-norm of (5.4) that holds for all $N > 1$ at a computation cost that only depends on the dimension of a single subsystem. Furthermore, this upper bound is the same for both topologies. ◇

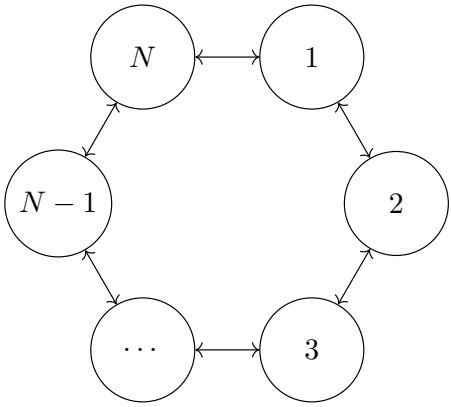

Figure 5.1: Bidirectional ring topology

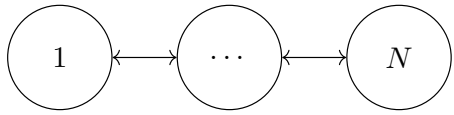

Figure 5.2: Bidirectional line topology

5.4 A scalable H-infinity controller synthesis method

In this section we will describe a controller synthesis method for networked systems of the form (5.3) whose associated adjacency matrix fulfills Assumption 5.1. The idea behind the presented method is to find a suitable controller by directly minimizing the upper bound (5.7) in the controller parameters $\mathbf{p}$. Or in other words, we look for controller parameters $\mathbf{p}^\star$ that fulfill

$$\mathbf{p}^\star \in \arg\min_{\mathbf{p}} \|\hat{T}_{\hat{z}\hat{w}}(\cdot;\mathbf{p},\cdot)\|_{H_\infty}^{[a,\,b]}. \tag{5.8}$$

Note however that $\|\hat{T}_{\hat{z}\hat{w}}(\cdot;\mathbf{p},\cdot)\|_{H_\infty}^{[a,\,b]}$ is only an upper bound for the actual H_∞-norm of (5.4). The resulting control parameters will therefore in most cases not minimize the actual H_∞-norm of the system, but this methodology has the advantage that its computation cost does not depend on the number of subsystems. Furthermore, if Assumption 5.1 remains valid with a and b independent of the number of subsystems, then the resulting controller guarantees a level of disturbance rejection even if the number of subsystems is unknown.

The minimization of (5.8) is however not trivial, as the robust H_∞-norm may be a nonsmooth and nonconvex function of the controller parameters even if the controller matrices are analytic functions of the controller parameters. We therefore use the optimization approach described in Section 2.3.2, which requires the evaluation of both the objective function and its derivative with respect to the control parameters whenever this derivative exists. To evaluate

the objective function, we use the method presented in Chapter 4. The derivative with respect to the control parameters follows from the following proposition.

Proposition 5.1. If for a given set of control parameters $\mathbf{p}$ system (5.6) is internally exponentially stable for all $\lambda \in [a, b]$, there exists a unique pair

$$(\omega^\star, \lambda^\star) \in \arg \max_{\substack{\lambda \in [a,\, b], \\ \omega \in \mathbb{R}^+}} \sigma_1 \left(T(\jmath\omega; \mathbf{p}, \lambda) \right)$$

and $\sigma_1 \left(T(\jmath\omega^\star; \mathbf{p}, \lambda^\star) \right)$ is simple, then the function $\mathbf{p} \mapsto \|\hat{T}_{\hat{z}\hat{w}}(\cdot; \mathbf{p}, \cdot)\|_{H_\infty}^{[a,\, b]}$ is differentiable at $\mathbf{p}$, with

$$\frac{\mathrm{d}}{\mathrm{d}\mathbf{p}} \|T(\cdot; \mathbf{p}, \cdot)\|_{H_\infty}^{[a,\, b]} = \Re \left(u^H \left(\frac{\partial}{\partial \mathbf{p}} T(\jmath\omega^\star; \mathbf{p}, \lambda^\star) \right) v \right),$$

in which u and v are the normalized left and right singular vectors associated with $\sigma_1\big(T(\jmath\omega^\star; \mathbf{p}, \lambda^\star)\big)$, respectively.

To start the optimization process we need initial controller parameters $\mathbf{p}$ for which the system is internally exponentially stable for all $\lambda \in [a, b]$. To find such a starting point, we use the method presented in [56].

5.5 Example

In this example we consider a networked system that consists of N frictionless carts that are interconnected using identical springs and that each balance an inverted pendulum. Furthermore, the first and the last cart are connected to the wall using additional (but identical) springs. This set-up is illustrated in Figure 5.3 for N equal to 3. The dynamics of an individual cart-pendulum subsystem are governed by the following nonlinear delay differential equations

$$\begin{cases} (M+m)\ddot{d}_j(t) + \ ml\cos\big(\theta_j(t)\big)\ddot{\theta}_j(t) - ml\sin\big(\theta_j(t)\big)\big(\dot{\theta}_j(t)\big)^2 + \\ \quad k\big(d_j(t) - d_{j+1}(t)\big) + k\big(d_j(t) - d_{j-1}(t)\big) - u_j(t-\tau_u) - w_{j,1}(t) = 0, \\ l\ddot{\theta}_j(t) - g\sin\big(\theta_j(t)\big) + \ddot{d}_j(t)\cos\big(\theta_j(t)\big) - w_{j,2}(t) = 0 \text{ for } j = 1, \ldots, N \end{cases}$$

with M the mass of the individual carts, m the mass of the pendulum's bob which is connected to the cart using a massless rod of length l, k the spring constant, u_j a controllable force that acts on the cart with an input delay τ_u, $w_{j,1}$ and $w_{j,2}$ external disturbances, θ_j the angular displacement of the pendulum of cart j, d_j the horizontal displacement of the jth cart's centre of mass with respect to its equilibrium position and

$d_0(t) = d_{N+1}(t) = 0$. By a linearization around the equilibrium point $(d_j, \dot{d}_j, \theta_j, \dot{\theta}_j) = (0,0,0,0)$ for $j = 1, \ldots, N$ and choosing $\begin{bmatrix} d_j(t) & \theta_j(t) \end{bmatrix}^\top$ as both measured and exogenous output, we obtain the following linear state-space model of the form (5.1):

$$\begin{aligned} \dot{x}_j(t) = &\begin{bmatrix} 0 & 1 & 0 & 0 \\ -\frac{2k}{M} & 0 & -\frac{mg}{M} & 0 \\ 0 & 0 & 0 & 1 \\ \frac{2k}{Ml} & 0 & \frac{g}{l} + \frac{mg}{Ml} & 0 \end{bmatrix} x_j(t) + \begin{bmatrix} 0 \\ \frac{1}{M} \\ 0 \\ \frac{-1}{Ml} \end{bmatrix} u_j(t - \tau_u) + \\ &\begin{bmatrix} 0 \\ \frac{k}{M} \\ 0 \\ \frac{-k}{Ml} \end{bmatrix} u_{n,j}(t) + \begin{bmatrix} 0 & 0 \\ \frac{1}{M} & \frac{-m}{M} \\ 0 & 0 \\ \frac{-1}{Ml} & \frac{1}{l} + \frac{m}{Ml} \end{bmatrix} w_j(t), \end{aligned} \tag{5.9}$$

$$y_j(t) = \begin{bmatrix} 1 & 0 & 0 & 0 \\ 0 & 0 & 1 & 0 \end{bmatrix} x_j(t), \quad y_{n,j}(t) = \begin{bmatrix} 2 & 0 & 0 & 0 \end{bmatrix} x_j(t), \text{ and } z_j(t) = \begin{bmatrix} 1 & 0 & 0 & 0 \\ 0 & 0 & 1 & 0 \end{bmatrix} x_j(t)$$

with

$$u_{n,j}(t) = \sum_{i=1}^{N} [P_N^{\text{line}}]_{j,i} \; y_{n,i}(t).$$

We use an overlapping controller architecture of the form (5.2) with n_c equal to 2. The vector $\mathbf{p}$ containing the control parameters consists of the entries of the control matrices. As mentioned in Section 5.4, suitable values for these parameters can be obtained by minimizing the robust H_∞-norm of an uncertain system of the form (5.6) with λ bounded to the inteval $[-1, 1]$. As the eigenvalues of P_N^{line} are restricted to the interval $[-1, 1]$, it follows from Corollary 5.1 that this quantity is an upper bound for the H_∞-norm of the overall network that holds independently of N.

For the parameter values: $M = 1\,\text{kg}$, $m = 0.05\,\text{kg}$, $k = 1\,\text{N/m}$, $l = 1\,\text{m}$, $g = 9.8\,\text{m/s}^2$, $\tau_u = 0.1\,\text{s}$, and $\tau_{u_{nc}} = 0.2\,\text{s}$, we obtained the following controller matrices (rounded to four digits accuracy):

$$\begin{aligned} J_{\mathbf{p}^\star} &= \begin{bmatrix} -67.92 & -313.2 \\ -52.15 & -306.8 \end{bmatrix}, & F_{\mathbf{p}^\star} &= \begin{bmatrix} -407.4 & 1139 \\ 141.8 & 1519 \end{bmatrix}, \\ F_{n,\mathbf{p}^\star} &= \begin{bmatrix} -33.74 & -112.6 \\ -91.45 & -147.9 \end{bmatrix}, & L_{\mathbf{p}^\star} &= \begin{bmatrix} -143.3 & -834.4 \end{bmatrix}, \\ K_{\mathbf{p}^\star} &= \begin{bmatrix} 349.9 & 4172 \end{bmatrix}, \text{ and } & K_{n,\mathbf{p}^\star} &= \begin{bmatrix} -246.5 & -406.9 \end{bmatrix}, \end{aligned} \tag{5.10}$$

in which the subscript $\mathbf{p}^\star$ is used to indicate that these matrices correspond to (locally) minimizing control parameters. The corresponding upper bound for

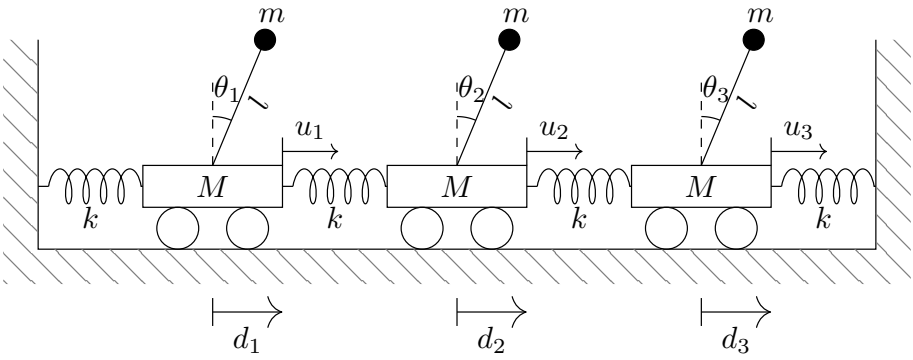

Figure 5.3: Schematic representation of the considered set-up for $N = 3$.

the H_∞-norm equals 0.512249 (rounded to 6 digits). Table 5.1 gives the actual H_∞-norm of the closed-loop system with controller matrices (5.10) for several N. We observe that these values lie close to the computed upper bound. This table also gives the time required by the algorithm described in [82] to compute these values. As expected, the computation time grows roughly cubically with respect to N. For comparison, the computation time of the robust H_∞-norm of the associated uncertain subsystem equals 75.70 s. For system with large number of subsystems, it is thus beneficiary to minimize this upper bound instead of the actual H_∞-norm.

The experiment was carried out in MATLAB R2018b (version 9.5.0.944444) on a Dell Latitude 7490 with a Intel(R) Core(TM) i7-8650U CPU @ 1.90GHz eight core processor with 16GB of RAM running Ubuntu 20.04.4 LTS.

Table 5.1: The H_∞-norm (rounded to 6 digits accuracy) of the closed-loop networked system for several N and the computation time required by the algorithm described in [82] to compute these values.

N	3	5	10	15
$\|T(\cdot;\mathbf{p}^\star,N)\|_{H_\infty}$	0.512228	0.512239	0.512246	0.512247
Computation time (s)	17.39	91.56	806.3	2961

To conclude this section, Figure 5.4 shows the worst-case gain function, as defined in (4.13), of the corresponding uncertain subsystem of the form (5.6) for $\omega \in [10^{-1}, 10^2]$. The robust H_∞-norm, which is equal to the maximal value of this worst-case gain function, is indicated with a dashed line. Observe that

the worst-case gain function is flat and almost equal to the robust H_∞-norm for $\omega \in [0, 1]$. This phenomenon is typical for the direct optimization framework.

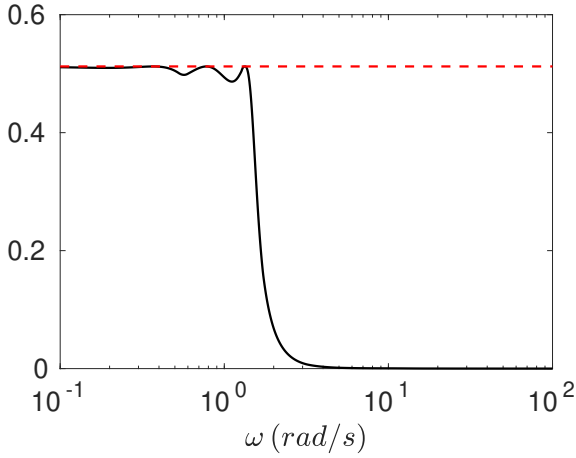

Figure 5.4: The worst-case gain function of the associated uncertain subsystem of the form (5.6) for $\omega \in [10^{-1}, 10^2]$ (full black line) and the robust H_∞-norm, $\|\hat{T}_{\hat{z}\hat{w}}(\cdot; \mathbf{p}^\star, \cdot)\|_{H_\infty}^{[-1,\,1]}$ (red dashed line).

5.6 Conclusion

In this chapter we introduced a scalable controller synthesis method for networked systems with identical subsystems and an interconnection topology that fulfills Assumption 5.1. Using the decoupling transformation of Section 5.3 we arrived at an upper bound for the H_∞-norm which can be computed at a cost that does not depend on the number of subsystems, namely the robust H_∞-norm of a single subsystem with an additional scalar uncertainty. Next, in Section 5.4 we proposed a controller design strategy that consists of minimizing this upper bound with respect to the controller parameters. This approach was illustrated for an example in Section 5.5. To conclude, we note that the presented method can be extended to networked systems for which the subsystems have direct feed-through terms. As mentioned in the previous section, the H_∞-norm of such systems is sensitive to infinitesimal delay changes and the strong H_∞-norm is a more appropriate performance measure. As in Section 5.3, one can show that the strong H_∞-norm of the overall system is upper bounded by the robust strong H_∞-norm of a single uncertain subsystem.

CHAPTER

6 A structure preserving shift-invert infinite Arnoldi algorithm for a class of delay eigenvalue problems with Hamiltonian symmetry

Abstract

This chapter considers a class of delay eigenvalue problems that admit a spectrum similar to that of a Hamiltonian matrix, in the sense that the spectrum is symmetric with respect to both the real and imaginary axis. We propose a method to iteratively approximate the eigenvalues closest to a given purely real or imaginary shift, while preserving the symmetries of the spectrum. To this end, our method exploits the equivalence between the considered delay eigenvalue problem and the eigenvalue problem associated with a linear but infinite-dimensional operator. To compute the eigenvalues closest to the given shift, we apply a specifically chosen shift-invert transformation, such that the spectrum of the transformed operator has a "real skew-Hamiltonian"-like structure. Furthermore, it is proven that the Krylov subspace constructed by applying this operator satisfies an orthogonality property in terms of a specifically chosen bilinear form. By taking this property into account during the orthogonalization process, it is ensured that, even in the presence of rounding errors, the obtained approximation for, e.g., a simple, purely imaginary eigenvalue is typically simple and purely imaginary. The presented work can thus be seen as an extension of [V. Mehrmann and D. Watkins, *Structure-Preserving Methods for Computing Eigenpairs of Large Sparse Skew-Hamiltonian/Hamiltonian Pencils*, SIAM J. Sci. Comput. (22.6), 2001], to the considered class of delay eigenvalue problems. Although the presented method is initially defined on function spaces, it can be implemented using finite-dimensional linear algebra operations. The performance of the resulting numerical algorithm is verified for two example problems: the first example illustrates the advantage of the proposed approach in preserving purely imaginary eigenvalues when working in finite precision, while the second one demonstrates its applicability to a large scale problem.

The contents of this chapter were originally presented in [13].

6.1 Introduction

In this chapter, we consider nonlinear eigenvalue problems (NEPs) of the form

$$M(\lambda)v = 0 \tag{6.1}$$

with $\lambda \in \mathbb{C}$ an eigenvalue and $v \in \mathbb{C}^{2n} \setminus \{0\}$ a right eigenvector, for which the matrix-valued function $M : \mathbb{C} \mapsto \mathbb{C}^{2n\times 2n}$ has the following structure:

$$M(\lambda) := \lambda I_{2n} - H_0 - \sum_{k=1}^{m} \left(H_{-k}e^{-\lambda\tau_k} + H_k e^{\lambda\tau_k}\right) \tag{6.2}$$

with $0 < \tau_1 < ... < \tau_m < \infty$ discrete delays and I_{2n} the identity matrix of size $2n$. The matrices $H_0, H_1, H_{-1}, \ldots, H_m$ and H_{-m} belong to $\mathbb{R}^{2n\times 2n}$ and satisfy the following assumption.

Assumption 6.1. Firstly, the matrix H_0 is Hamiltonian meaning that

$$\left(JH_0\right)^\top = JH_0, \tag{6.3}$$

in which the matrix J is defined as

$$J := \begin{bmatrix} 0 & I_n \\ -I_n & 0 \end{bmatrix}.$$

Secondly, the matrices H_k and H_{-k} are related via

$$\left(JH_{-k}\right)^\top = JH_k \text{ for } k = 1, \ldots, m \tag{6.4}$$

with J as defined above.

Recall from Section 2.2.2 that Hamiltonian eigenvalue problems typically arise in the context of level-set methods for computing the H_∞-norm. In [137, 82] it is shown that the results of Theorem 2.6 can be generalized to the following dynamical system with delays,

$$\begin{cases} \dot{x}(t) &= A_0x(t) + \sum_{k=1}^{m} A_kx(t-\tau_k) + Bw(t), \\ z(t) &= Cx(t) \end{cases} \tag{6.5}$$

with $0 < \tau_1 < ... < \tau_m < \infty$ discrete delays. More specifically, let T be the transfer function of (6.5) from w to z, then $\|T(\cdot)\|_{H_\infty} \geq \gamma$ if (and only if) the NEP associated with the following matrix-valued function has purely imaginary eigenvalues

$$\lambda \begin{bmatrix} I_n & 0 \\ 0 & I_n \end{bmatrix} - \begin{bmatrix} A_0 & \gamma^{-1}BB^\top \\ -\gamma^{-1}C^\top C & -A_0^\top \end{bmatrix} - \sum_{k=1}^{m} \left(\begin{bmatrix} A_k & 0 \\ 0 & 0 \end{bmatrix} e^{-\lambda\tau_k} + \begin{bmatrix} 0 & 0 \\ 0 & -A_k^\top \end{bmatrix} e^{\lambda\tau_k} \right). \tag{6.6}$$

Notice that (6.6) fits the structure given in (6.2). A method to efficiently compute the purely imaginary eigenvalues of (6.6) is thus an important prerequisite for developing a level-set method to compute the H_∞-norm of large-scale systems of the form (6.5).

The spectrum of the considered NEP has some interesting features. Firstly, notice that (6.1) bears some similarities with a retarded delay eigenvalue problem (see Section 2.1.2), but in contrast has both positive and negative delays. Secondly, due to the structure of the matrix-valued function $M(\lambda)$ in (6.2) and Assumption 6.1, the considered class of NEPs can be seen as an extension of the eigenvalue problem associated with a Hamiltonian matrix, i.e.,

$$(I_{2n}\lambda - H)\, v = 0 \tag{6.7}$$

with $H \in \mathbb{R}^{2n\times 2n}$ and $(JH)^\top = JH$, as studied in, among others, [24, 184, 132]. It is well known that the spectrum of such eigenvalue problems is symmetric with respect to both the real and imaginary axis, meaning that eigenvalues appear either in quadruplets (λ, $\bar{\lambda}$, $-\lambda$ and $-\bar{\lambda}$) or in purely real or imaginary pairs (λ and $-\lambda$) [130].

The goal of this chapter is to develop a method to accurately compute the eigenvalues of (6.1) in the neighborhood of a given shift σ that is either purely real or imaginary. We are particularly interested in the case for which n is large. For large-scale linear eigenvalue problems, Krylov subspace methods, such as the (shift-invert) Arnoldi method, are well-established [161]. These methods have recently been generalized to NEPs, see for example [99, 98, 84, 193, 100]. In the case of retarded DEPs, the method in [99] can be interpreted in two ways: either as applying the Arnoldi method to a sufficiently large linearisation of the NEP with vectors of increasing length or as applying the Arnoldi method to an associated linear but infinite-dimensional operator, resulting in a Krylov subspace spanned by functions instead of vectors, hence its name, the infinite Arnoldi method. As a main benefit, this method is in some sense discretization-free as the error made by approximating the nonlinear delay term can be reduced by applying more Arnoldi iterations. Here we want to apply a similar approach. However, for eigenvalue problems with a Hamiltonian structure, as considered here, the regular shift-invert (infinite) Arnoldi method destroys the particular structure of the spectrum. For linear finite-dimensional eigenvalue problems, a modified, structure-preserving, shift-invert Arnoldi approach was therefore developed in [132] and subsequently generalized to both matrix pencils and polynomial eigenvalue problems in [131] and [133], respectively. The goal of this chapter is to extend this structure-preserving method to the considered class of NEPs.

More specifically, the adopted approach can be interpreted as the algorithm of [132] applied to a linear (but infinite dimensional) operator whose spectrum

corresponds to that of (6.1). An alternative approach could consist of constructing a rational or polynomial approximation of the matrix-valued function (6.2), followed by a direct application of the algorithm of [133] (a so-called discretize-and-solve approach). As we are interested in computing selected eigenvalues close to a shift σ (on the real or imaginary axis) this would require an approximation that preserves the Hamiltonian symmetry of the spectrum while being accurate around $\pm\sigma$, precluding an approximation around zero if $|\sigma| \gg 0$. As we shall see, the latter property is naturally embedded in the presented shift-invert transformation. Furthermore, when using the discretize-and-solve framework, it is not trivial to a priori determine the degree of the discretization for which the approximation error is sufficiently small (e.g., such that the imaginary axis eigenvalues are preserved for the H_∞-norm computation). It should be noted, though, that the discretize-and-solve framework does not exclude dynamic methods, for which the degree of the discretisation does not need to be specified beforehand and can change during the Arnoldi process (see, for example the dynamic variants of NLEIGS [85]). These methods are however closely related to the adopted infinite Arnoldi approach.

The remainder of this chapter is structured as follows. Section 6.2 recalls some preliminary results: first some properties of the spectrum of (6.1) are highlighted, next the most important components of the structure preserving shift-invert Arnoldi method from [132] are reviewed and finally the equivalence of the considered NEP and the eigenvalue problems associated with two linear but infinite-dimensional operators (one related to the left eigenspace and one related to the right eigenspace) is demonstrated. In Section 6.3, the structure preserving shift-invert Arnoldi method from [132] is generalized to the considered NEP based on the aforementioned equivalence with a linear infinite-dimensional eigenvalue problem, giving rise to an algorithmic implementation of the structure preserving shift-invert *infinite* Arnoldi method. Subsequently Sections 6.4 and 6.5 discuss how this method can be implemented using finite-dimensional operations for the shift σ employed in the shift-invert Arnoldi method equal to zero and different from zero, respectively. Next, Section 6.6 applies the resulting numerical implementations on two example problems. The first example illustrates that the presented method indeed preserves the Hamiltonian structure of the spectrum, while the second example demonstrates its applicability to large-scale problems. Finally, Section 6.7 draws some concluding remarks.

6.2 Preliminary results

In this section we will recall some important preliminary results. First, we introduce the notion of a left eigenvector. Next, we highlight two important properties of the considered NEP. Thereafter, we briefly review the method presented in [132], to get a good understanding of the existing results in the finite-dimensional case. Next, we introduce two linear but infinite-dimensional operators (one related to the left eigenspace and one related to the right eigenspace) whose eigenvalues correspond to those of the considered DEP. Finally, we introduce a bilinear form that relates these two infinite-dimensional operators and that will play an important role in the results of Section 6.3.

6.2.1 Properties of the considered DEP

Throughout the paper a nonzero column vector $w \in \mathbb{C}^{2n} \setminus \{0\}$ is a left eigenvector associated with the eigenvalue $\lambda \in \mathbb{C}$ if it satisfies

$$w^\top M(\lambda) = 0.$$

Note that our definition differs from the traditional one, namely, a nonzero column vector w is a left eigenvector associated with λ if $w^H M(\lambda) = 0$. The definition used here is however common for real Hamiltonian eigenvalue problems and simplifies the notation in the remainder of this text.

It can be shown that the considered NEP generally has infinitely many eigenvalues. However the number of eigenvalues in any vertical strip around the imaginary axis is finite, as stated in the following proposition.

Proposition 6.1. For any $\alpha > 0$, the characteristic matrix (6.2) has only a finite number of eigenvalues in the vertical strip $\{z \in \mathbb{C} : -\alpha < \Re(z) < \alpha\}$.

Proof. This result follows from a similar argument as in [137, Corollary 2.6]. □

Next, we show that its spectrum is symmetric with respect to both the real and imaginary axis. Symmetry with respect to the real axis follows from the fact that all matrices and delays in (6.2) are real-valued, while symmetry with respect to the origin follows from the following proposition.

Proposition 6.2. If $\lambda \in \mathbb{C}$ is an eigenvalue of (6.2) with associated right eigenvector v_+ and left eigenvector w_+, then $-\lambda$ is also an eigenvalue of (6.2) and the corresponding right and left eigenvectors are Jw_+ and Jv_+, respectively.

Proof. Since (λ, w_+) is a left eigenpair of (6.2) and J is nonsingular, we have that $w_+^\top M(\lambda)J = 0$. Transposing this equation and using Assumption 1.1 leads to $M(-\lambda)Jw_+ = 0$, meaning that $(-\lambda, Jw_+)$ is a right eigenpair of (6.2). In a similar way it can be shown that if (λ, v_+) is a right eigenpair of (6.2) then $(-\lambda, Jv_+)$ is a left eigenpair of (6.2). □

6.2.2 A structure preserving shift-invert Arnoldi method for linear finite-dimensional Hamiltonian eigenvalue problems

As demonstrated below, the method in [132] allows to compute the eigenvalues of (6.7) closest to a given purely real or imaginary shift σ while preserving the Hamiltonian structure of the spectrum. For simplicity, we will assume σ purely imaginary (the discussion for σ real is however similar).

Let us first examine the traditional shift-invert Arnoldi method. A natural way to compute the eigenvalues of H closest to the shift σ is to apply the Arnoldi method to the matrix

$$H_\sigma^{-1} := (H - \sigma I_{2n})^{-1}.$$

Note that this matrix is no longer real nor Hamiltonian. A purely imaginary eigenvalue $\jmath\omega$ of H is mapped to the purely imaginary eigenvalue $\mu = (\jmath\omega - \sigma)^{-1}$ of H_σ^{-1}. Thus, if $\jmath\omega$ lies sufficiently close to σ, the Hessenberg matrix constructed by applying the Arnoldi procedure to H_σ^{-1} will typically contain a Ritz value approximating μ after sufficiently many iterations. However, as the standard Arnoldi procedure does not preserve the eigenvalue symmetry with respect to the imaginary axis, the Ritz value approximating μ typically does not lie on the imaginary axis. Furthermore, even if this Ritz value would lie on the imaginary axis, then computing the eigenvalues of the Hessenberg matrix in finite precision would typically introduce a small real component due to rounding errors inside the eigenvalue solver. As a consequence, the approximations for purely imaginary eigenvalues of H obtained using this approach typically have a small but non-zero real part. This means that in applications for which the detection of purely imaginary eigenvalues is important, additional postprocessing is necessary.

Let us now examine why the structure preserving shift-invert Arnoldi method from [132] is preferred. In this method, the Arnoldi procedure is applied to the matrix

$$R_\sigma^{-1} := (H + \sigma I_{2n})^{-1} (H - \sigma I_{2n})^{-1}. \tag{6.8}$$

It is easy to verify that the matrix R_σ^{-1} is real-valued and skew-Hamiltonian[1]. Furthermore, both the eigenvalues λ and $-\lambda$ of H are mapped to the eigenvalue $\mu = (\lambda^2 - \sigma^2)^{-1}$ of R_σ^{-1} (which consequently has multiplicity two). For the traditional Arnoldi method such multiple eigenvalues would hamper the convergence behavior. Yet, as we will see below, each eigenvalue of R_σ^{-1} will only appear once in the Hessenberg matrix obtained by applying the Arnoldi procedure to R_σ^{-1}. More specifically, consider the following Krylov subspace generated by R_σ^{-1},

$$\mathrm{K}_r\left(R_\sigma^{-1}, q_1\right) = \mathrm{span}\left\{q_1, R_\sigma^{-1}q_1, R_\sigma^{-2}q_1, \ldots, R_\sigma^{-(r-1)}q_1\right\} \tag{6.9}$$

with $q_1 \in \mathbb{R}^{2n}$ an arbitrary real-valued starting vector. It can be shown that this subspace is J-neutral (sometimes also referred to as isotropic), meaning that for each pair of vectors x and y in this subspace, the equality $x^\top Jy = 0$ holds, see [132, Proposition 3.3]. This has the following important consequence.

Proposition 6.3. Let q_1 be an arbitrary real-valued vector of length $2n$ and let $\lambda \neq 0$ be a simple eigenvalue of H with corresponding right eigenvector v_+ and let v_- be a right eigenvector associated with the eigenvalue $-\lambda$, then the dimension of the intersection of $\mathrm{span}\{v_+, v_-\}$ and $\mathrm{K}_r\left(R_\sigma^{-1}, q_1\right)$ is at most 1.

Proof. The result follows from a similar argument as in [131, Lemma 2.3], which is repeated here to ease the derivations for the infinite-dimensional case. It follows from Proposition 6.2 that if (λ, v_+) is a right eigenpair of H, then $(-\lambda, w_-)$ with $w_- := Jv_+$ is a left eigenpair of H. This implies that $v_-^\top Jv_+ = v_-^\top w_- \neq 0$, in which the last inequality follows from the fact that $-\lambda$ is a simple eigenvalue of H. Thus the intersection of $\mathrm{span}\{v_+, v_-\}$ and $\mathrm{K}_r\left(R_\sigma^{-1}, q_1\right)$ can not have dimension 2 (which implies that both v_+ and v_- are in $\mathrm{K}_r\left(R_\sigma^{-1}, q_1\right)$) as this would contradict the J-neutrality of the constructed Krylov subspace. □

This proposition has an important effect on the obtained Ritz values as demonstrated below. For sake of simplicity, assume that all eigenvalues of H are simple and different from zero. In this case, all eigenvalues of R_σ^{-1} have multiplicity two and the right eigenspace corresponding to the eigenvalue $\mu = (\lambda^2 - \sigma^2)^{-1}$ is spanned by v_+ and v_-, the right eigenvectors of H associated with λ and $-\lambda$, respectively. Now let us introduce the matrix $Q_r = \begin{bmatrix} q_1 & \ldots & q_r \end{bmatrix}$, with $r \leq n$, whose columns $q_1, \ldots, q_r \in \mathbb{R}^{2n}$ form an orthonormal basis for $\mathrm{K}_r\left(R_\sigma^{-1}, q_1\right)$. Using this notation, the Arnoldi recurrence

[1] A matrix S is skew-Hamiltonian if $(JS)^\top = -JS$.

relation can be written as

$$R_\sigma^{-1} Q_r = Q_r \Psi_r + \Psi_{[r+1,r]} q_{r+1} e_r^\top \tag{6.10}$$

with $\Psi_r \in \mathbb{R}^{r\times r}$ a reduced Hessenberg matrix, $\Psi_{[r+1,r]}$ a real-valued scalar, $q_{r+1} \in \mathbb{R}^{2n}$ and $e_r \in \mathbb{R}^r$ the rth Euclidean basis vector. When the Arnoldi procedure breaks down, i.e., $\Psi_{[r+1,r]} = 0$, let $\Psi_r V_r = V_r \Sigma_r$ be an eigenvalue decomposition of Ψ_r with $\Sigma_r = \operatorname{diag}(s_1, \ldots, s_r)$ a diagonal matrix containing the eigenvalues of Ψ_r (the so called Ritz values) and $V_r \in \mathbb{C}^{r\times r}$ a matrix containing the associated right eigenvectors. It then follows from (6.10) that $R_\sigma^{-1}(Q_r V_r) = (Q_r V_r)\Sigma_r$, meaning that $s_1, \ldots, s_r$ are also eigenvalues of R_σ^{-1} with as corresponding right eigenvectors the columns of $Q_r V_r$. However, although each eigenvalue of R_σ^{-1} has multiplicity two, there appear no doubles in $s_1, \ldots, s_r$ as this would imply that there exist two linear independent vectors in $\operatorname{span}\{v_+, v_-\}$ that lie in the column space of Q_r what would contradict Proposition 6.3.

Thus, if the eigenvalues $\pm\jmath\omega$ lie sufficiently close to the shifts $\pm\sigma$, it follows from the reasoning above and the convergence behavior of the Arnoldi method that for sufficiently large r the corresponding real eigenvalue $\mu = (-\omega^2 - \sigma^2)^{-1}$ of R_σ^{-1} will be approximated by a **real and simple Ritz value** of the **real-valued** Hessenberg matrix Ψ_r. Thus even when the eigenvalues of Ψ_r are computed in finite precision, the approximations for $\pm\jmath\omega$ obtained via the transformation $\pm\sqrt{\frac{1}{s} + \sigma^2}$, with s the computed eigenvalues of Ψ_r, are typically strictly imaginary.

Note however that to ensure that only one component of the space $\operatorname{span}\{v_+, v_-\}$ appears in the Krylov subspace, it is important that the Krylov subspace remains J-neutral. Although this property is satisfied by construction in exact arithmetic, it is typically lost when working in finite precision. [132, Section 5] therefore suggests to use the following orthogonalization procedure,

$$\Psi_{[r+1,r]} q_{r+1} = R_\sigma^{-1} q_r - Q_r \Psi_{[:,r]} - J Q_r \Upsilon_{[:,r]} \tag{6.11}$$

with $\Psi_{[:,r]} = Q_r^\top R_\sigma^{-1} q_r$, $\Upsilon_{[:,r]} = (JQ_r)^\top R_\sigma^{-1} q_m$ and $\Psi_{[r+1,r]}$ a normalisation factor such that $\|q_{r+1}\|_2 = 1$, i.e., orthogonalise the new basis vector not only with respect to Q_r but also to JQ_r. (Note that the last term in (6.11) is zero when working in exact arithmetic.)

Remark 6.1. The transformation in (6.8) assumed that σ is either purely real or purely imaginary. However, similar results for a more general shift σ can be obtained by choosing

$$R_\sigma^{-1} = \Big((H - \sigma I_{2n})(H + \sigma I_{2n})(H - \bar\sigma I_{2n})(H + \bar\sigma I_{2n})\Big)^{-1},$$

see [131, Equation 3.2].

6.2.3 Two equivalent eigenvalue problems on an infinite-dimensional space

In this subsection we examine the relation between the considered NEP and two linear but infinite-dimensional eigenvalue problems. To this end, we consider the space X_H of continuous functions that map the interval $[-\tau_m, \tau_m]$ to $\mathbb{C}^{2n}$, denoted by $X_H := C\big([-\tau_m, \tau_m], \mathbb{C}^{2n}\big)$, and define the linear operator $\mathcal{H} : D(\mathcal{H}) \subseteq X_H \mapsto X_H$ as

$$\mathcal{H}\varphi := \varphi', \tag{6.12}$$

in which the domain of this operator, $D(\mathcal{H})$, consists of the functions φ in X_H that are continuously differentiable and fulfill the condition

$$\varphi'(0) = H_0\varphi(0) + \sum_{k=1}^{m} \Big(H_{-k}\varphi(-\tau_k) + H_k\varphi(\tau_k) \Big), \tag{6.13}$$

or in other words

$$D(\mathcal{H}) := \{\varphi \in X_H : \varphi' \in X_H \ \text{ and } \ \varphi \text{ satisfies (6.13)}\}.$$

It can be shown that the operator $\mathcal{H}$ only features a point spectrum and a complex number λ is an eigenvalue of this operator if (and only if) there exists a non-trivial eigenfunction $\varphi \in D(\mathcal{H})$ such that

$$\mathcal{H}\varphi = \lambda\varphi.$$

From (6.12), it is clear that these eigenfunctions must have the form $ve^{\lambda \cdot}$ with $v \in \mathbb{C}^{2n}$. By plugging this result into (6.13) it is evident that there exists a correspondence between a right eigenpair (λ, v) of (6.2) and an eigenpair (λ, φ) of $\mathcal{H}$. This relation is stated more rigorously in the following proposition.

Proposition 6.4. It holds that

1. if (λ, v) is a right eigenpair of the NEP associated with (6.2), then $(\lambda, ve^{\lambda \cdot})$ is an eigenpair of $\mathcal{H}$, and
2. if (λ, φ) is an eigenpair of $\mathcal{H}$, then the eigenfunction φ is of the form $ve^{\lambda \cdot}$ with (λ,v) a right eigenpair of the NEP associated with (6.2).

Proof. The result follows from a similar argument as in [137, Proposition 2.2]. □

As seen in Proposition 6.4, the right eigenpairs of the considered NEP are connected with the eigenpairs of the operator $\mathcal{H}$. Now we will look for an

operator which has a similar connection with the left eigenpairs of the considered NEP. To this end, let us introduce another operator $\mathcal{G} : D(\mathcal{G}) \subseteq X_H \mapsto X_H$:

$$\mathcal{G}\psi := -\psi'$$

with

$$D(\mathcal{G}) := \{\psi \in X_H : \psi' \in X_H \text{ and } -\psi'(0) = H_0^\top \psi(0) + \sum_{k=1}^{m} \left(H_k^\top \psi(-\tau_k) + H_{-k}^\top \psi(\tau_k) \right) \Big\}.$$

The infinite-dimensional eigenvalue problem associated with this operator has the following relation with the left eigenpairs of the considered NEP.

Proposition 6.5. It holds that,

1. if (λ, w) is a left eigenpair of the NEP associated with (6.2), then $(\lambda, we^{-\lambda \cdot})$ is an eigenpair of $\mathcal{G}$.
2. if (λ, ψ) is an eigenpair of $\mathcal{G}$, then the eigenfunction ψ has the form $we^{-\lambda \cdot}$ with (λ, w) a left eigenpair of the NEP associated with (6.2).

Proof. As before, the assertions follow from a similar argument as in [137, Proposition 2.2]. □

Combined with Proposition 6.2, these two propositions imply that the following relation between the eigenpairs of $\mathcal{H}$ and those of $\mathcal{G}$ holds.

Corollary 6.1. If $\big(\lambda, \varphi\big)$ is an eigenpair of $\mathcal{H}$, then $\big(-\lambda, \psi\big)$, with $\psi(\theta) = J\varphi(\theta)$ for $\theta \in [-\tau_m, \tau_m]$, is an eigenpair of $\mathcal{G}$ and visa versa.

Finally, let us introduce the bilinear form $\mathbf{B} : X_H \times X_H \mapsto \mathbb{C}$ with

$$\mathbf{B}\left(\varphi, \psi\right) := \psi(0)^\top \varphi(0) + \sum_{k=1}^{m} \left(\int_0^{\tau_k} \psi(\theta)^\top H_{-k} \varphi(\theta - \tau_k) \, \mathrm{d}\theta - \int_0^{\tau_k} \psi(\theta - \tau_k)^\top H_k \varphi(\theta) \, \mathrm{d}\theta \right). \quad (6.14)$$

Notice that this bilinear form does not define an inner product as it is neither Hermetian symmetric nor positive definite. However, this bilinear form does induce two important relations between the operators $\mathcal{H}$ and $\mathcal{G}$. Firstly, borrowing terminology from [87, Chapters 7], $\mathcal{G}$ can be seen as the *formal adjoint* of $\mathcal{H}$ with respect to the bilinear form (6.14), since the following result holds.

Proposition 6.6. For $\varphi \in D(\mathcal{H})$ and $\psi \in D(\mathcal{G})$ the equality

$$\mathbf{B}\left(\mathcal{H}\varphi, \psi\right) = \mathbf{B}\left(\varphi, \mathcal{G}\psi\right)$$

holds.

Proof. Using the definition of both operators and partial integration, we find that

$$\begin{aligned}
\mathbf{B}\left(\varphi, \mathcal{G}\psi\right) = & -\psi'(0)^\top \varphi(0) - \sum_{k=1}^{m} \Bigg(\int_0^{\tau_k} \psi'(\theta)^\top H_{-k} \varphi(\theta - \tau_k)\, \mathrm{d}\theta - \\
& \qquad \int_0^{\tau_k} \psi'(\theta - \tau_k)^\top H_k \varphi(\theta)\, \mathrm{d}\theta \Bigg) \\
= & \, \psi(0)^\top \underbrace{\Bigg(H_0 \varphi(0) + \sum_{k=1}^{m} \left(H_{-k} \varphi(-\tau_k) + H_k \varphi(\tau_k) \right) \Bigg)}_{\varphi'(0)} + \\
& \sum_{k=1}^{m} \Bigg(\int_0^{\tau_k} \psi(\theta)^\top H_{-k} \varphi'(\theta - \tau_k)\, \mathrm{d}\theta - \int_0^{\tau_k} \psi(\theta - \tau_k)^\top H_k \varphi'(\theta)\, \mathrm{d}\theta \Bigg) \\
= & \, \mathbf{B}\left(\mathcal{H}\varphi, \psi\right).
\end{aligned}$$

□

Secondly, under the bilinear form (6.14) the eigenfunctions of $\mathcal{G}$ are complementary to the eigenfunctions of $\mathcal{H}$, as spelled out in the following proposition.

Proposition 6.7. If φ_λ is an eigenfunction of $\mathcal{H}$ associated with an eigenvalue λ and if ψ_μ is an eigenfunction of $\mathcal{G}$ associated with a different eigenvalue $\mu \neq \lambda$ then $\mathbf{B}\left(\varphi_\lambda, \psi_\mu\right) = 0$.

Proof. It follows from the result above that $\mathbf{B}\left(\mathcal{H}\varphi_\lambda, \psi_\mu\right) = \mathbf{B}\left(\varphi_\lambda, \mathcal{G}\psi_\mu\right)$. Using the properties of a bilinear form one finds that

$$\begin{aligned}
0 &= \mathbf{B}\left(\mathcal{H}\varphi_\lambda, \psi_\mu\right) - \mathbf{B}\left(\varphi_\lambda, \mathcal{G}\psi_\mu\right) \\
&= \mathbf{B}\left(\lambda\varphi_\lambda, \psi_\mu\right) - \mathbf{B}\left(\varphi_\lambda, \mu\psi_\mu\right) \\
&= (\lambda - \mu)\, \mathbf{B}\left(\varphi_\lambda, \psi_\mu\right).
\end{aligned}$$

As $\lambda - \mu \neq 0$, $\mathbf{B}\left(\varphi_\lambda, \psi_\mu\right)$ must equal zero. □

6.3 The structure preserving shift-invert infinite Arnoldi method for Hamiltonian delay eigenvalue problems

In the previous section we saw that the eigenvalues of the considered NEP correspond to those of the linear but infinite-dimensional operator $\mathcal{H}$. To compute the eigenvalues of this operator in the neighborhood of some purely real or imaginary shift σ, a modification of the infinite Arnoldi method for RDEPs will be introduced in this section. The presented method differs from the traditional shift-invert infinite Arnoldi method in that it preserves the Hamiltonian structure of the spectrum. As such, it can be seen as an extension of [132] to linear (infinite-dimensional) operators.

Let us start by deriving an adequate shift-invert transformation. Inspired by (6.8), we consider the following linear operator:

$$\mathcal{R}_\sigma := (\mathcal{H} - \sigma\mathcal{I}_{X_H})\,(\mathcal{H} + \sigma\mathcal{I}_{X_H})$$

with $\mathcal{I}_{X_H}$ the identity operator on X_H. By plugging in the definition of $\mathcal{H}$ we find that

$$\mathcal{R}_\sigma\varphi = \varphi'' - \sigma^2\varphi$$

with the domain of $\mathcal{R}_\sigma$ consisting of the functions $\varphi \in X_H$ which are twice continuously differentiable and fulfill the following two conditions

$$\varphi'(0) = H_0\varphi(0) + \sum_{k=1}^{m} \left(H_{-k}\varphi(-\tau_k) + H_k\varphi(\tau_k)\right) \text{ and} \tag{6.15}$$

$$\varphi''(0) = H_0\varphi'(0) + \sum_{k=1}^{m} \left(H_{-k}\varphi'(-\tau_k) + H_k\varphi'(\tau_k)\right), \tag{6.16}$$

or in other words

$$D\left(\mathcal{R}_\sigma\right) = \left\{\varphi \in X_H : \varphi' \in X_H \ ,\ \varphi'' \in X_H \ \text{ and } \ \varphi \text{ satisfies (6.15) and (6.16)}\right\}.$$

If σ is not an eigenvalue of $\mathcal{H}$, then the operator $\mathcal{R}_\sigma$ is invertible. For $\sigma \neq 0$ one finds:

$$\mathcal{R}_\sigma^{-1}\phi\,(\theta) = \left(\int_0^\theta \tfrac{\phi(\eta)}{2\sigma} e^{-\sigma\eta} d\eta + \mathrm{C}_\sigma[\phi]\right) e^{\sigma\theta} + \left(-\int_0^\theta \tfrac{\phi(\eta)}{2\sigma} e^{\sigma\eta} d\eta + \mathrm{C}_{-\sigma}[\phi]\right) e^{-\sigma\theta}, \tag{6.17}$$

in which the constants $\mathrm{C}_\sigma[\phi]$ and $\mathrm{C}_{-\sigma}[\phi]$ are uniquely defined by conditions (6.15) and (6.16). After some straight forward (but tedious) calculations we find

$$2\sigma M(\sigma)\,\mathrm{C}_\sigma[\phi] = -\phi(0) + \sum_{k=1}^{m}\left[H_k\int_0^{\tau_k}\phi(\eta)e^{-\sigma(\eta-\tau_k)}\,\mathrm{d}\eta - H_{-k}\int_0^{\tau_k}\phi(\eta-\tau_k)e^{-\sigma\eta}\,\mathrm{d}\eta\right] \tag{6.18}$$

and

$$2\sigma M(-\sigma)\,\mathrm{C}_{-\sigma}[\phi] = \phi(0) - \sum_{k=1}^{m}\left[H_k\int_0^{\tau_k}\phi(\eta)e^{\sigma(\eta-\tau_k)}\,\mathrm{d}\eta - H_{-k}\int_0^{\tau_k}\phi(\eta-\tau_k)e^{\sigma\eta}\,\mathrm{d}\eta\right] \tag{6.19}$$

with $M(\cdot)$ the characteristic matrix as introduced in (6.2). Note that to determine the integration constants $C_\sigma[\phi]$ and $C_{-\sigma}[\phi]$, one has to solve a linear system with both $M(\sigma)$ and $M(-\sigma)$ to preserve the symmetries in the spectrum. For $\sigma = 0$, one finds

$$\mathcal{R}_0^{-1}\phi\,(\theta) = \int_0^\theta\int_0^{\eta_2}\phi(\eta_1)\,\mathrm{d}\eta_1\,\mathrm{d}\eta_2 + \mathrm{C}_1[\phi]\theta + \mathrm{C}_0[\phi], \tag{6.20}$$

in which $\mathrm{C}_1[\phi]$ and $\mathrm{C}_0[\phi]$ again follow from (6.15) and (6.16).

Proposition 6.8. If $\phi \in X_H$ is a real-valued function and σ is purely real or purely imaginary and not an eigenvalue of $\mathcal{H}$, then $\mathcal{R}_\sigma^{-1}\phi$ is a real function.

Proof. For $\sigma \neq 0$, this assertion follows directly from (6.17), (6.18) and (6.19) by noting that $\mathrm{C}_\sigma[\phi]$ and $\mathrm{C}_{-\sigma}[\phi]$ are real if σ is real and that $\mathrm{C}_{-\sigma}[\phi]$ is the complex conjugate of $\mathrm{C}_\sigma[\phi]$ if σ is purely imaginary. For $\sigma = 0$ this result follows from (6.20) and the expressions for $C_1[\phi]$ and $C_0[\phi]$. □

Lemma 6.1. For σ not an eigenvalue of $\mathcal{H}$, the operator $\mathcal{R}_\sigma^{-1}$ is self-adjoint with respect to $\mathbf{B}\,(\cdot, J\cdot)$ meaning that the equality $\mathbf{B}\left(\mathcal{R}_\sigma^{-1}\varphi, J\psi\right) = \mathbf{B}\left(\varphi, J{\mathcal{R}_\sigma}^{-1}\psi\right)$ holds.

Proof. See Appendix B.1. □

Next, we introduce some properties of the (infinite-dimensional) eigenvalue problem associated with this operator:

$$\mathcal{R}_\sigma^{-1}\phi = \mu\phi. \tag{6.21}$$

Proposition 6.9. For σ not an eigenvalue of $\mathcal{H}$, the infinite-dimensional eigenvalue problem in (6.21) satisfies the following three properties .

1. If λ is an eigenvalue of $\mathcal{H}$ then $\mu = (\lambda^2 - \sigma^2)^{-1}$ is an eigenvalue of $\mathcal{R}_\sigma^{-1}$ and visa versa, if μ is an eigenvalue of $\mathcal{R}_\sigma^{-1}$ then $\pm\sqrt{\mu^{-1} + \sigma^2}$ are eigenvalues of $\mathcal{H}$.
2. Let $\lambda \neq 0$ and $-\lambda$ be simple eigenvalues of $\mathcal{H}$ with eigenfunctions φ_+ and φ_-, respectively, then the eigenspace of $\mu = (\lambda^2 - \sigma^2)^{-1}$ is span $\{\varphi_+, \varphi_-\}$.
3. The eigenvalues of $\mathcal{R}_\sigma^{-1}$ have even multiplicity.

Proof. First we show that if $\varphi \in D(\mathcal{H})$ is an eigenfunction of $\mathcal{H}$ associated with λ, i.e., $\mathcal{H}\varphi = \lambda\varphi$, then this function is also an eigenfunction of $\mathcal{R}_\sigma^{-1}$ associated with $\mu = (\lambda^2 - \sigma^2)^{-1}$:

$$\mathcal{R}_\sigma\varphi = (\mathcal{H} - \sigma I_{X_H})(\mathcal{H} + \sigma I_{X_H})\varphi = (\lambda + \sigma)(\mathcal{H} - \sigma I_{X_H})\varphi = (\lambda^2 - \sigma^2)\varphi,$$

which implies that $\mathcal{R}_\sigma^{-1}\varphi = (\lambda^2 - \sigma^2)^{-1}\varphi$. Visa versa, if there exists a $\phi \not\equiv 0$ such that $\mathcal{R}_\sigma^{-1}\phi = \mu\phi$, then $\left(\mathcal{H} - \sqrt{\mu^{-1} + \sigma^2}\mathcal{I}_{X_H}\right)\left(\mathcal{H} + \sqrt{\mu^{-1} + \sigma^2}\mathcal{I}_{X_H}\right)\phi = 0$, meaning that either $\mathcal{H} - \sqrt{\mu^{-1} + \sigma^2}\mathcal{I}_{X_H}$ or $\mathcal{H} + \sqrt{\mu^{-1} + \sigma^2}\mathcal{I}_{X_H}$ has a non-trivial null space. The fact that both $\pm\sqrt{\mu^{-1} + \sigma^2}$ are eigenvalues of $\mathcal{H}$ follows from Proposition 6.2.

Thus if $\lambda \neq 0$ is an eigenvalue of $\mathcal{H}$, then both λ and $-\lambda$ are mapped together to $\mu = (\lambda^2 - \sigma^2)^{-1}$ and the eigenspace associated with μ is spanned by their eigenfunctions.

If $\lambda = 0$ is an eigenvalue of $\mathcal{H}$, then it has even multiplicity. As a consequence, $-\sigma^{-2}$ is an eigenvalue of $\mathcal{R}_\sigma^{-1}$ with the same multiplicity. □

Next we examine the following Krylov subspace generated by $\mathcal{R}_\sigma^{-1}$:

$$\mathrm{K}_r\left(\mathcal{R}_\sigma^{-1}, \phi_1\right) = \mathrm{span}\left\{\phi_1, \mathcal{R}_\sigma^{-1}\phi_1, \mathcal{R}_\sigma^{-2}\phi_1, \ldots, \mathcal{R}_\sigma^{-(r-1)}\phi_1\right\} \subseteq X_H$$

with $\phi_1 \in X_H$ an arbitrary real-valued starting function. This subspace has the following important property.

Proposition 6.10. Let σ not be an eigenvalue of $\mathcal{H}$ and let $\phi_1 \in X_H$ be a real-valued function, then for any two functions φ and ψ in the Krylov subspace $\mathrm{K}_r\left(\mathcal{R}_\sigma^{-1}, \phi_1\right)$ the equality $\mathbf{B}(\varphi, J\psi) = 0$ holds, with $\mathbf{B}(\cdot, \cdot)$ as defined in (6.14).

Proof. Each function in $\mathrm{K}_r\left(\mathcal{R}_\sigma^{-1}, \phi_1\right)$ can be written as $P_{r-1}(\mathcal{R}_\sigma^{-1})\phi_1$ with $P_{r-1}(\cdot)$ a polynomial of degree (at most) $r-1$. Due to the bilinearity of $\mathbf{B}\left(\cdot, J\cdot\right)$, it thus suffices to prove that $\mathbf{B}\left(\mathcal{R}_\sigma^{-i}\phi_1, J\mathcal{R}_\sigma^{-j}\phi_1\right) = 0$ for $i, j = 0, \ldots, r-1$.

By Lemma 6.1 we have

$$\mathbf{B}\left(\mathcal{R}_\sigma^{-i}\phi_1, J\mathcal{R}_\sigma^{-j}\phi_1\right) = \mathbf{B}\left(\mathcal{R}_\sigma^{-(j+i)}\phi_1, J\phi_1\right) = \mathbf{B}\left(\phi_1, J\mathcal{R}_\sigma^{-(j+i)}\phi_1\right).$$

However, due to the fact that $\mathbf{B}\left(\varphi, J\psi\right) = -\mathbf{B}\left(\psi, J\varphi\right)$, i.e., $\mathbf{B}\left(\cdot, J\cdot\right)$ is anti-symmetric (see Appendix B.2), we also have

$$\mathbf{B}\left(\mathcal{R}_\sigma^{-(j+i)}\phi_1, J\phi_1\right) = -\mathbf{B}\left(\phi_1, J\mathcal{R}_\sigma^{-(j+i)}\phi_1\right),$$

which implies that $\mathbf{B}\left(\mathcal{R}_\sigma^{-i}\phi_1, J\mathcal{R}_\sigma^{-j}\phi_1\right) = 0$. □

This proposition has the following important consequence.

Theorem 6.1. For σ not an eigenvalue of $\mathcal{H}$ and $\phi_1 \in X_H$ a real-valued function, let $\lambda \neq 0$ be a simple eigenvalue of $\mathcal{H}$ (or equivalently of the NEP (6.1)) with associated eigenfuction φ_+ and let φ_- be the eigenfunction associated with the eigenvalue $-\lambda$, then the dimension of the intersection of $\mathrm{span}\{\varphi_+, \varphi_-\}$ and $\mathrm{K}_r(\mathcal{R}_\sigma^{-1}, \phi_1)$ is at most 1.

Proof. Recall from Proposition 6.4 that $\varphi_+(\theta) = v_+ e^{\lambda\theta}$ and $\varphi_-(\theta) = v_- e^{-\lambda\theta}$, with v_+ and v_- right eigenvectors of the NEP (6.1) associated with λ and $-\lambda$, respectively. Furthermore, from Proposition 6.2 it follows that there exists a vector w_+ which is a left eigenvector of (6.2) associated with λ, such that $v_- = Jw_+$. Combing these properties with the definition of the bilinear form in (6.14), we find that

$$\begin{aligned}\mathbf{B}\left(\varphi_+, J\varphi_-\right) &= -w_+^\top \left[I + \sum_{k=1}^{K}\left(H_{-k}e^{-\lambda\tau_k}\tau_k - H_k e^{\lambda\tau_k}\tau_k\right)\right] v_+ \\ &= -w_+^\top \frac{\partial M(\lambda)}{\partial\lambda} v_+ \neq 0,\end{aligned}$$

in which the last inequality follows from the fact that λ is a simple eigenvalue of the eigenvalue problem associated with (6.2). Thus if the intersection of $\mathrm{span}\{\varphi_+, \varphi_-\}$ and $\mathrm{K}_r(\mathcal{R}_\sigma^{-1}, \phi_1)$ has dimension two, then both φ_+ and φ_- must lie inside this Krylov subspace, which would contradict Proposition 6.10. □

Combining this result with Proposition 6.9, we have the following important result.

Corollary 6.2. Under the conditions of Theorem 6.1 and assuming that $\lambda \neq 0$ is a simple eigenvalue of $\mathcal{H}$, the dimension of the intersection of the eigenspace of $\mathcal{R}_\sigma^{-1}$ associated with $\mu = (\lambda^2 - \sigma^2)^{-1}$ and the Krylov subspace $\mathrm{K}_r\left(\mathcal{R}_\sigma^{-1}, \phi_1\right)$ is at most 1.

We conclude this section with Algorithm 1, which gives a high-level description of the structure preserving shift-invert infinite Arnoldi method operating on the infinite-dimensional space X_H. In this algorithm $\Psi_{[i,j]}$ denotes the element on the ith row and j^{th} column of the matrix Ψ, $\Psi_{[1:r,:]}$ is the submatrix of Ψ consisting of its first r rows, $\langle \cdot, \cdot \rangle_{X_H}$ is an appropriate inner product on X_H (which we will define later on), and $\| \cdot \|_{X_H}$ is the norm associated with this inner product.

The algorithm works as follows. Starting from a real initial function ϕ_1, an orthonormal basis for the Krylov subspace $\mathrm{K}_r(\mathcal{R}_\sigma^{-1}, \phi_1)$ is constructed iteratively. After obtaining this orthonormal basis, the eigenvalues of $\mathcal{R}_\sigma^{-1}$ are approximated by the eigenvalues of its orthogonal projection onto the Krylov subspace, i.e., the submatrix $\Psi_{[1:r,:]}$, which has a reduced Hessenberg structure. Finally, the approximations for the eigenvalues of $\mathcal{H}$ can be obtained using the transformation from Proposition 6.9. Each iteration in Algorithm 1 consists of the following steps. First the Krylov subspace is extended with the candidate function $\varphi_{i+1} = \mathcal{R}_\sigma^{-1}\phi_i$. Next, this function is orthogonalized against the already obtained basis functions and subsequently normalized to have norm 1. Note that in contrast to the traditional infinite Arnoldi method, one now has to ensure that ϕ_{i+1} is also *orthogonal* against $\phi_1, \ldots, \phi_i$ with respect to the bilinear functional $\mathbf{B}(\cdot, J\cdot)$. Although this last orthogonality constraint holds by construction in exact arithmetic (see Proposition 6.10), this typically is no longer the case when working in finite precision, as we shall illustrate in Section 6.6.1.

Inspired by [99], we define the following inner product on X_H based on the scaled Chebyshev expansion. More precisely, let $\phi \in X_H$ and $\psi \in X_H$ be Lipschitz continuous functions, then for each of these functions there exists a unique Chebyshev expansion series that is absolute and uniformly convergent [182]:

$$\varphi(\theta) = \sum_{l=0}^{\infty} c_l T_l\left(\tfrac{\theta}{\tau_m}\right) \text{ and } \psi(\theta) = \sum_{l=0}^{\infty} d_l T_l\left(\tfrac{\theta}{\tau_m}\right) \text{ for } \theta \in [-\tau_m, \tau_m]$$

with $T_l(\cdot) := \cos\left(l \arccos(\cdot)\right)$ the lth Chebyshev polynomial of the first kind. The inner product of these two functions is then defined as

$$\langle \psi, \varphi \rangle_{X_H} := \sum_{l=0}^{\infty} c_l^\top d_l. \tag{6.22}$$

Furthermore, it can be shown, see [99, Equation 4.10], that this inner product is equivalent with the following expression

$$\langle \psi, \varphi \rangle_{X_H} = \tfrac{2}{\pi} I\left[\varphi^\top \psi\right] - \tfrac{1}{\pi^2} I[\varphi^\top] I[\psi]$$

with $I[f] = \int_{-\tau_m}^{\tau_m} \frac{f(\theta)}{\sqrt{\tau_m^2 - \theta^2}} \, \mathrm{d}\theta$.

As in the finite-dimensional case (see Section 6.2.2), Theorem 6.1 and Corollary 6.2 have an important consequence for the obtained approximations of purely imaginary eigenvalues of (6.1). More specifically, since ϕ_1 is chosen real-valued, Proposition 6.8 and the definition of the inner product in (6.22), imply that $\mathrm{K}_r\left(\mathcal{R}_\sigma^{-1}, \phi_1\right)$ consists of real-valued functions and that the matrix Ψ is real-valued. Now, let $\pm \jmath\omega$ be simple eigenvalues of $\mathcal{H}$ sufficiently close to $\pm\sigma$ and r sufficiently large. These two eigenvalues are mapped together to the purely real eigenvalue $\mu = (-\omega^2 - \sigma^2)^{-1}$ of $\mathcal{R}_\sigma^{-1}$. However, as long as the Krylov subspace satisfies Proposition 6.10 (which is always the case in exact arithmetic), only a single component of the two-dimensional eigenspace associated with μ will be approximated in the Krylov subspace and hence the multiple eigenvalue μ will be approximated by a simple, real Ritz value in the reduced Hessenberg matrix $\Psi[1:r,:]$. After re-transformation the obtained approximations for $\pm\jmath\omega$ are thus typically purely imaginary. However, if orthogonality with respect to $\mathbf{B}\left(\cdot, J\cdot\right)$ is lost (due to rounding errors), the Krylov subspace will eventually also approximate a second component in the eigenspace of μ. As a consequence, the double eigenvalue μ will be approximated by a pair of Ritz values: either two nearby real Ritz values or a pair of complex conjugate Ritz values. In the latter case, after re-transformation the obtained approximations for the purely imaginary eigenvalues $\pm\jmath\omega$ of $\mathcal{H}$ thus have a small real part.

Algorithm 1 High-level description of the structure preserving shift-invert infinite Arnoldi method for NEP (6.1).

Choose a **real-valued** initial function ϕ_1 with $\|\phi_1\|_{X_H} = 1$.
Define a $(r+1) \times r$ matrix Ψ with all elements equal to zero.
for $i = 1, \ldots, r$ **do**
  Extend the Krylov subspace with $\varphi_{i+1} = \mathcal{R}_\sigma^{-1}\phi_i$.
  Orthogonalize φ_{i+1} against the already obtained orthogonal basis for the Krylov subspace and normalize the result:

$$\Psi_{[i+1,i]}\phi_{i+1} = \varphi_{i+1} - \Psi_{[1,i]}\,\phi_1 - \cdots - \Psi_{[i,i]}\,\phi_i$$

  with $\Psi_{[j,i]} = \langle \phi_j, \varphi_{i+1} \rangle_{X_H}$ for $j = 1, \ldots, i$ and $\Psi_{[i+1,i]}$ such that $\|\phi_{i+1}\|_{X_H} = 1$.

  Ensure orthogonality of ϕ_{i+1} against $\phi_1, \ldots, \phi_i$ with respect to $\mathbf{B}(\cdot, J\cdot)$.
end for
Compute the eigenvalues μ of $\Psi_{[1:r,:]}$.
Return the approximations for the eigenvalues of (6.1): $\pm\sqrt{\frac{1}{\mu} + \sigma^2}$.

The algorithm introduced above is described in terms of functions and therefore not directly implementable using finite-dimensional operations. The following two sections will therefore describe how this algorithm can be implemented using finite-dimensional linear algebra operations and how one can ensure that the built up Krylov subspace satisfies Proposition 6.10, even in the presence of rounding errors.

6.4 Numerical implementation for the shift equal to zero

We start with the case $\sigma = 0$. First we will see that by choosing an appropriate initial function ϕ_1, a natural finite-dimensional representation for the functions and operations in Algorithm 1 appears. To this end, observe from (6.17) that if $\mathcal{R}_0^{-1}$ is applied on a vector-valued polynomial of degree N, the result is a polynomial of degree $N + 2$. As a consequence, when choosing a vector-valued polynomial as initial function, the constructed Krylov subspace consists entirely of polynomials. By choosing an appropriate basis for the space of polynomials, Algorithm 1 can thus be carried out using finite-dimensional operations on the coefficient vectors of these polynomials. Due to our choice for the inner product in (6.22), it makes sense to work with scaled Chebyshev functions. The

extension step in Algorithm 1 can now be computed using straightforward linear algebra operations, as demonstrated in the following theorem.

Theorem 6.2. Let

$$\phi_i(\theta) = \sum_{l=0}^{N_i} q_l^{(i)} T_l\left(\frac{\theta}{\tau_m}\right)$$

with $q_l^{(i)} \in \mathbb{R}^{2n}$ for $l = 0, \ldots, N_i$, then

$$\varphi_{i+1}(\theta) = \mathcal{R}_0^{-1}\phi_i(\theta) = \sum_{l=0}^{N_i+2} v_l^{(i+1)} T_l\left(\frac{\theta}{\tau_m}\right),$$

in which the coefficient vectors $v_2^{(i+1)}, \ldots, v_{N_i+2}^{(i+1)}$ follow from

$$\left[v_2^{(i+1)} \ \cdots \ v_{N_i+2}^{(i+1)}\right] = \tau_m^2 \left[q_0^{(i)} \ \cdots \ q_{N_i}^{(i)}\right] \begin{bmatrix} \frac{1}{4} & & & & & \\ & \frac{1}{24} & & & & \\ \frac{-1}{6} & & \frac{1}{48} & & & \\ & \frac{-1}{16} & & \frac{1}{80} & & \\ \frac{1}{24} & & \frac{-1}{30} & & \frac{1}{120} & \\ & \ddots & & \ddots & & \ddots \\ & \frac{1}{4(N_i-1)(N_i-2)} & & \frac{-1}{2(N_i-1)(N_i+1)} & & \frac{1}{4(N_i+1)(N_i+2)} \end{bmatrix}, \quad (6.23)$$

while $v_1^{(i+1)}$ and $v_0^{(i+1)}$ follow from (6.15) and (6.16):

$$M(0)\, v_1^{(i+1)} = \sum_{l=2}^{N_i+2} \Bigg(H_0 T_l'(0) - I_{2n} \frac{T_l''(0)}{\tau_m} + \sum_{k=1}^{m} \left(H_k T_l'\left(\frac{\tau_k}{\tau_m}\right) + H_{-k} T_l'\left(\frac{-\tau_k}{\tau_m}\right)\right)\Bigg) v_l^{(i+1)}$$

and

$$M(0)\, v_0^{(i+1)} = \sum_{l=1}^{N_i+2} \Bigg(H_0 T_l(0) - I_{2n} \frac{T_l'(0)}{\tau_m} + \sum_{k=1}^{m} \left(H_k T_l\left(\frac{\tau_k}{\tau_m}\right) + H_{-k} T_l\left(\frac{-\tau_k}{\tau_m}\right)\right)\Bigg) v_l^{(i+1)}$$

with $M(\cdot)$ as defined in (6.2).

Proof. We refer to Appendix B.3 for more details on this result. □

Notice that for large n, the main computation cost consists of solving the systems for $v_0^{(i+1)}$ and $v_1^{(i+1)}$. However, because the same matrix $M(0)$ is used in each iteration, its factorization needs only to be computed once, which greatly reduces the computation time.

Secondly, due to the chosen initial function, also the orthogonalisation step can be carried out using standard linear algebra operations. More specifically, as a consequence of Theorem 6.2, the functions encountered in the ith orthogonalisation step of Algorithm 1 can be written as

$$\phi_j(\theta) = \sum_{l=0}^{N_j} q_l^{(j)} T_l\left(\frac{\theta}{\tau_m}\right) \text{ for } j = 1, \ldots, i+1 \tag{6.24}$$

and

$$\varphi_{i+1}(\theta) = \sum_{l=0}^{N_{i+1}} v_l^{(i+1)} T_l\left(\frac{\theta}{\tau_m}\right). \tag{6.25}$$

By introducing $v^{(i+1)}$ as the vector containing the stacked coefficients of φ_{i+1}, $q^{(j,i+1)}$ the vector containing the stacked coefficients of ϕ_j padded with zeros to length $2n(N_{i+1}+1)$ and $Q_{(i,i+1)} = \begin{bmatrix} q^{(1,i+1)} & \ldots & q^{(i,i+1)} \end{bmatrix}$, the orthogonalisation step reduces to

$$\Psi_{[i+1,i]} q^{(i+1,i+1)} = v^{(i+1)} - Q_{(i,i+1)} Q_{(i,i+1)}^\top v^{(i+1)} \tag{6.26}$$

with $\Psi_{[i+1,i]}$ a normalisation constant such that $\|q^{(i+1,i+1)}\|_2 = 1$.

Up till now, the presented approach closely resembles the classic infinite Arnoldi method from [99], but with the degree of the polynomials in the Krylov subspace increasing with two instead of one in each iteration. Recall however that it is important that the build-up Krylov subspace satisfies the condition in Proposition 6.10. Although this condition holds automatically in exact arithmetic, rounding errors cause a loss of orthogonality when working in finite precision. We therefore introduce an *additional orthogonalisation step*, which ensures orthogonality with respect to $\mathbf{B}(\cdot, J\cdot)$. To this end, note that for $\phi_1, \ldots, \phi_i$ and φ_{i+1} in form (6.24) and (6.25) the bilinear form $\mathbf{B}(\cdot, J\cdot)$ can be evaluated using matrix-vector operations:

$$\mathbf{B}(\phi_j, J\varphi_{i+1}) = {v^{(i+1)}}^\top S_{N_{i+1}} q^{(j,i+1)}$$

with

$$S_{N_{i+1}} = S_{N_{i+1}}^0 \otimes J + \sum_{k=1}^{m} \left(S_{N_{i+1}}^{-k} \otimes JH_{-k} + S_{N_{i+1}}^{k} \otimes JH_k \right)$$

in which $\otimes$ is the Kronecker product. The elements on position (l_1, l_2) of $S^0_{N_{i+1}}$, $S^{-k}_{N_{i+1}}$, and $S^k_{N_{i+1}}$ are equal to

$$-T_{l_1}(0)T_{l_2}(0), -\int_0^{\tau_k} T_{l_1}\Big(\frac{\theta}{\tau_m}\Big)T_{l_2}\Big(\frac{\theta-\tau_k}{\tau_m}\Big)\,\mathrm{d}\theta \text{ and } \int_0^{\tau_k} T_{l_1}\Big(\frac{\theta-\tau_k}{\tau_m}\Big)T_{l_2}\Big(\frac{\theta}{\tau_m}\Big)\,\mathrm{d}\theta,$$

respectively.

In the ith iteration step, the vector $q^{(i+1,i+1)}$ must thus be orthogonal with respect to the columns of both $Q_{(i,i+1)}$ and $S_{N_{i+1}}Q_{(i,i+1)}$. Moreover, because

$$q^{(j,i+1)^\top} S_{N_{i+1}} q^{(j,i+1)} = 0 \text{ for } j = 1, \ldots, i$$

due to the skew-symmetry of $S_{N_{i+1}}$ and

$$q^{(j_1,i+1)^\top} S_{N_{i+1}} q^{(j_2,i+1)} = 0 \text{ for } j_1, j_2 = 1, \ldots, i$$

due to the orthogonality conditions in the previous iteration, the product $Q^\top_{(i,i+1)} S_{N_{i+1}} Q_{(i,i+1)}$ is zero. Thus in order to achieve simultaneous orthogonality with respect to $Q_{(i,i+1)}$ and $S_{N_{i+1}}Q_{(i,i+1)}$ we will use the following expression instead of (6.26):

$$\Psi_{[i+1,i]} q^{(i+1,i+1)} = v^{(i+1)} - Q_{(i,i+1)}Q^\top_{(i,i+1)} v^{(i+1)} - S_{N_{i+1}}Q_{(i,i+1)} \times \Big((S_{N_{i+1}}Q_{(i,i+1)})^\top S_{N_{i+1}}Q_{(i,i+1)}\Big)^{-1} (S_{N_{i+1}}Q_{(i,i+1)})^\top v^{(i+1)} \quad (6.27)$$

with $\Psi_{[i+1,i]}$ a normalisation factor such that $\|q^{(i+1,i+1)}\|_2 = 1$. By using this expression, the resulting Krylov subspace satisfies Proposition 6.10 up to machine precision, even in the presence of rounding errors.

Remark 6.2. Note that the left upper blocks of the matrices $S^0_{N_{i+1}}$, $S^{-k}_{N_{i+1}}$ and $S^k_{N_{i+1}}$ are equal to $S^0_{N_i}$, $S^{-k}_{N_i}$ and $S^k_{N_i}$, respectively. Furthermore, note that these matrices only depend on the delays and not on the system matrices. This observation implies for instance that in the single delay case ($m = 1$), where the delay can be rescaled to one by the substitution $\lambda \leftarrow \tau_1\lambda$, these matrices can be precomputed.

6.5 Numerical implementation for non-zero shift

In this subsection, it will be assumed that the shift σ is purely imaginary, i.e., $\sigma = \jmath\omega$. A similar result can be obtained when the shift σ is purely real, as will be explained in Remark 6.3.

Similar to the case $\sigma = 0$ we can derive a compact representation for the functions and operations in Algorithm 1 by choosing an appropriate structure for the initial function ϕ_1. More specifically, if

$$\phi(\theta) = P_N(\theta)e^{\jmath\omega\theta} + \overline{P_N(\theta)}e^{-\jmath\omega\theta} \tag{6.28}$$

with $P_N : [-\tau_m, \tau_m] \mapsto \mathbb{C}^{2n}$ an arbitrary complex vector-valued polynomial of degree N and $\overline{P_N(\theta)}$ the complex conjugate of $P_N(\theta)$, then the function $\mathcal{R}_\sigma^{-1}\phi$ is given by

$$\left(\mathcal{R}_\sigma^{-1}\phi\right)(\theta) = Q_{N+1}(\theta)e^{\jmath\omega\theta} + \overline{Q_{N+1}(\theta)}e^{-\jmath\omega\theta}, \tag{6.29}$$

in which $Q_{N+1}(\cdot)$ is a complex vector-valued polynomial of degree $N+1$. Using this representation, the extension step in Algorithm 1 can thus again be expressed in terms of operations on the vector-valued coefficients of these polynomials. This is formalized in the following theorem.

Theorem 6.3. If ϕ_i is given by

$$\phi_i(\theta) := \left(\sum_{l=0}^{N_i} q_l^{(i)}\, T_l\left(\frac{\theta}{\tau_K}\right)\right) e^{\jmath\omega\theta} + \left(\sum_{l=0}^{N_i} \overline{q_l^{(i)}}\, T_l\left(\frac{\theta}{\tau_K}\right)\right) e^{-\jmath\omega\theta} \tag{6.30}$$

then extension step can be preformed using basic linear algebra operations:

$$\varphi_{i+1}(\theta) = \left(\sum_{l=0}^{N_i+1} v_l^{(i+1)}\, T_l\left(\tfrac{\theta}{\tau_K}\right)\right) e^{\jmath\omega\theta} + \left(\sum_{l=0}^{N_i+1} \overline{v_l^{(i+1)}}\, T_l\left(\tfrac{\theta}{\tau_K}\right)\right) e^{-\jmath\omega\theta}, \tag{6.31}$$

in which the coefficient vectors $v_1^{(i+1)}, \ldots, v_{N_i+1}^{(i+1)}$ are given by

$$\begin{bmatrix} v_1^{(i+1)} & \ldots & v_{N_i+1}^{(i+1)} \end{bmatrix} \left(2\jmath\omega\tau_m \begin{bmatrix} \frac{1}{4} & & & & \\ & \frac{1}{6} & & & \\ \frac{-1}{4} & & \frac{1}{8} & & \\ & \ddots & & \ddots & \\ & & \frac{-1}{2N_i} & & \frac{1}{2(N_i+2)} \end{bmatrix} + \begin{bmatrix} 0 & & & \\ 1 & 0 & & \\ & \ddots & \ddots & \\ & & 1 & 0 \end{bmatrix} \right)$$

$$= \begin{bmatrix} q_0^{(i)} & \ldots & q_{N_i}^{(i)} \end{bmatrix} \tau_m^2 \begin{bmatrix} \frac{1}{4} & & & & \\ & \frac{1}{24} & & & \\ \frac{-1}{6} & & \frac{1}{48} & & \\ & \frac{-1}{16} & & \frac{1}{80} & \\ \frac{1}{24} & & \frac{-1}{30} & & \frac{1}{120} \\ & \ddots & & \ddots & & \ddots \\ & & \frac{1}{4(N_i-1)(N_i-2)} & & \frac{-1}{2(N_i-1)(N_i+1)} & & \frac{1}{4(N_i+1)(N_i+2)} \end{bmatrix} \tag{6.32}$$

and $v_0^{(i+1)}$ can be found by solving the following system

$$\jmath\omega\, M(\jmath\omega)\, v_0^{(i+1)} = (H_0 - \jmath\omega I_{2n}) \sum_{l=1}^{N_i+1} \left(\frac{\Re\left(v_l^{(i+1)}\right)}{\tau_m} T_l'(0) + \jmath\omega v_l^{(i+1)} T_l(0) \right) +$$

$$\sum_{k=1}^{m} \Big[H_k \sum_{l=1}^{N_i+1} \left(\frac{\Re\left(v_l^{(i+1)} e^{\jmath\omega\tau_k}\right)}{\tau_m} T_l'\left(\frac{\tau_k}{\tau_m}\right) + \jmath\omega v_l^{(i+1)} T_l\left(\frac{\tau_k}{\tau_m}\right) e^{\jmath\omega\tau_k} \right) +$$

$$H_{-k} \sum_{l=1}^{N_i+1} \left(\frac{\Re\left(v_l^{(i+1)} e^{-\jmath\omega\tau_k}\right)}{\tau_m} T_l'\left(\frac{-\tau_k}{\tau_m}\right) + \jmath\omega v_l^{(i+1)} T_l\left(\frac{-\tau_k}{\tau_m}\right) e^{-\jmath\omega\tau_k} \right) \Big] -$$

$$\sum_{l=0}^{N_i} \Re\left(q_l^{(i)}\right) T_l(0)$$

with $M(\cdot)$ the characteristic matrix as defined in (6.2).

Proof. For more details on deriving this result, see Appendix B.4. □

Remark 6.3. When the shift σ is purely real, similar results can be obtained. More specifically, if ϕ is given by

$$\phi(\theta) = P_N^+(\theta) e^{\sigma\theta} + P_N^-(\theta) e^{-\sigma\theta}$$

with $P_N^+(\cdot)$ and $P_N^-(\cdot)$ arbitrary real vector-valued polynomials of degree N, then $\mathcal{R}_\sigma^{-1}\phi$ is given by

$$\left(\mathcal{R}_\sigma^{-1}\phi\right)(\theta) = Q_{N+1}^+(\theta) e^{\sigma\theta} + Q_{N+1}^-(\theta) e^{-\sigma\theta}$$

with $Q_{N+1}^+(\cdot)$ and $Q_{N+1}^-(\cdot)$ real vector-valued polynomials of degree $N+1$.

From a theoretical point of view, the result obtained above is appealing: similarly to the case $\sigma = 0$ one can operate on the coefficients of polynomials of growing degree. Furthermore, due to the lower triangular structure of the matrix at the left side in (6.32), the main computational cost of the extension step consists of solving a system in $M(\jmath\omega)$ which is of dimension $2n$ and whose factorisation needs to be computed only once. However, there are three difficulties that render this approach unsuited in practice.

1. The condition number of the matrix at the left-hand side of (6.32) grows large as the number of iterations increases.
2. The range of the polynomial P_{N_i} tends to grow large, while the range of the overall function ϕ_i remains small, causing numerical issues when working in finite precision.

3. Evaluating inner product (6.22) is now less trivial.

4. When using the representation (6.28), the simultaneous orthogonalisation with respect to the inner product (6.22) and bilinear form $\mathbf{B}(\cdot, J\cdot)$ typically destroys the structure of ϕ_{i+1}.

The four difficulties mentioned above render the representation used in Theorem 6.3 unattractive in practice. Next, we therefore introduce a different approach to implement Algorithm 1 for $\sigma \neq 0$, based on a polynomial approximation of the functions in X_H. Similarly as in Chebfun [182], we approximate a function ψ by the unique polynomial of degree N_d, $\widehat{\psi}$, that interpolates ψ in the extreme points of the $N_d{}^{\text{th}}$ Chebyshev polynomial of the first kind rescaled to the interval $[-\tau_m, \tau_m]$, i.e.,

$$\widehat{\psi}(\theta) = \sum_{l=0}^{N_d} c_l T_l\Big(\tfrac{\theta}{\tau_m}\Big) \text{ such that } \widehat{\psi}(\theta_l) = \psi(\theta_l) \text{ for } l = 0, \ldots, N_d \tag{6.33}$$

with $\theta_l = \tau_m \cos\big(l\pi/N_d\big)$. The degree of the approximation, N_d, is chosen adaptively such that the approximation error is of order the machine precision. Such an interpolating polynomial can be computed efficiently using the `(i)fft`-transformation at a cost of $\mathcal{O}\big(2n\, N_d \log(N_d)\big)$ [2].

Previously, by invoking Theorems 6.2 and 6.3, the extension step could be computed efficiently due to the chosen structure of ϕ_1 (which was preserved in ϕ_i). For large n, the main computation cost consisted of solving a system involving a particular instance of (6.2). However, for arbitrary (non-structured) functions ϕ_i computing $\mathcal{R}_\sigma^{-1}\phi_i$ involves solving an ordinary differential equation subjected to conditions (6.15)-(6.16). A finite-dimensional approximate solution for this differential equation can be obtained using spectral discretisation. This would however involve solving a system of dimension $2nN_d$ with N_d a sufficiently large number of discretisation points. To avoid having to solve a system with such (large) dimensions, we will use the approach depicted in Figure 6.1, which is based on explicitly using the facotriazation $\mathcal{R}_\sigma^{-1} = (\mathcal{H}+\sigma\mathcal{I}_{X_H})^{-1}(\mathcal{H}-\sigma\mathcal{I}_{X_H})^{-1}$. First, we construct the polynomial $\chi_i(\cdot)$ of form (6.33) that approximates $\phi_i(\cdot)e^{-\sigma\cdot}$ up till machine precision, meaning that $\phi_i(\cdot) \approx \chi_i(\cdot)e^{\sigma\cdot}$. Next we can solve $(\mathcal{H} - \sigma\mathcal{I}_{X_H})^{-1}\chi_i(\cdot)e^{\sigma\cdot}$ analytically. More specifically, $(\mathcal{H} - \sigma\mathcal{I}_{X_H})^{-1}\chi_i(\cdot)e^{\sigma\cdot}$ is equal to $\xi_i(\cdot)e^{\sigma\cdot}$ with $\xi_i(\cdot)$ a vector-valued polynomial whose degree is equal to one plus the degree of $\chi_i(\cdot)$. Using the notation

$$\chi_i(\theta) = \sum_{l=0}^{N_1} a_l T_l\left(\tfrac{\theta}{\tau_m}\right) \text{ and } \xi_i(\theta) = \sum_{l=0}^{N_1+1} b_l T_l\left(\tfrac{\theta}{\tau_m}\right)$$

the coefficients of $\xi_i(\cdot)$ are given by

$$\begin{bmatrix} b_1 & \dots & b_{N_1+1} \end{bmatrix} = \begin{bmatrix} a_0 & \dots & a_{N_1} \end{bmatrix} \tau_m \begin{bmatrix} 1 & & & & \\ & \frac{1}{4} & & & \\ \frac{-1}{2} & & \frac{1}{6} & & \\ & \ddots & & \ddots & \\ & & \frac{-1}{2(N_1-1)} & & \frac{1}{2(N_1+1)} \end{bmatrix} \tag{6.34}$$

and

$$M(\sigma)\, b_0 = -\chi_i(0) + (H_0 - \sigma I_n) \sum_{l=1}^{N_1+1} b_l T_l(0) + \sum_{k=1}^{m} \left(H_k e^{\sigma\tau_k} \sum_{l=1}^{N_1+1} b_l T_l\left(\tfrac{\tau_k}{\tau_m}\right) + H_{-k} e^{-\sigma\tau_k} \sum_{l=1}^{N_1+1} b_l T_l\left(-\tfrac{\tau_k}{\tau_m}\right) \right) \tag{6.35}$$

with $M(\cdot)$ the matrix-valued function defined in (6.2). As before, the main computation cost is solving a system of dimension $2n$. (Notice that these expressions are similar to those in the extension step of the standard infinite Arnoldi method from [99].) Subsequently, we approximate $\xi_i(\cdot)e^{\sigma\cdot}$ by $\zeta_i(\cdot)e^{-\sigma\cdot}$ with $\zeta_i(\cdot)$ the interpolating polynomial of form (6.33) of $\xi_i(\cdot)e^{2\sigma\cdot}$. In step **(IV)** we compute $\Upsilon_i(\cdot)e^{-\sigma\cdot} = (\mathcal{H} + \sigma\mathcal{I}_{X_H})^{-1}\zeta_i(\cdot)e^{-\sigma\cdot}$ in which we can again derive an analytical expression for the coefficients of $\Upsilon_i(\cdot)$. Finally, $\widehat{\varphi}_{i+1}$ is obtained by computing the interpolating polynomial of form (6.33) of $\Upsilon_i(\cdot)e^{-\sigma\cdot}$. If the interpolating polynomials in steps **(I)**, **(III)** and **(V)** are computed up to machine precision, the resulting $\widehat{\varphi}_{i+1}$ is an accurate approximation for $\varphi_{i+1} = \mathcal{R}_\sigma^{-1}\phi_i$.

As the obtained function $\widehat{\varphi}_{i+1}$ is a polynomial expressed in the Chebyshev basis, also the orthogonalisation step can be implemented with finite-dimensional operations. More specifically, by using the representation of Figure 6.1 for $\phi_1, \dots, \phi_i$ and $\hat{\varphi}_{i+1}$, we can use an orthogonalisation procedure similar to that in (6.27) to ensure orthogonality with respect to both the inner product (6.22) and bilinear form $\mathbf{B}(\cdot, J\cdot)$: instead of padding the vectors to length $2n(N_{i+1}+1)$, the vectors now must be padded to length $2n\big(\max\{\max_{j=1,..,i}\{N_{\phi_j}\}, N_{\hat{\varphi}_{i+1}}\} + 1\big)$.

A disadvantage of the approach introduced above is that, in contrast to Theorems 6.2 and 6.3, the degree of the polynomial $\hat{\varphi}_{i+1}$ is not known beforehand and therefore might grow large. However, the example in Section 6.6.2 shows that if σ is sufficiently small, the degree of these functions only grows slowly. For large σ this is often no longer the case as the sought for eigenfunctions are either highly oscillator (large imaginary component) or fast growing exponentials (large real component). A polynomial representation inherently requires a high degree to accurately approximate such functions.

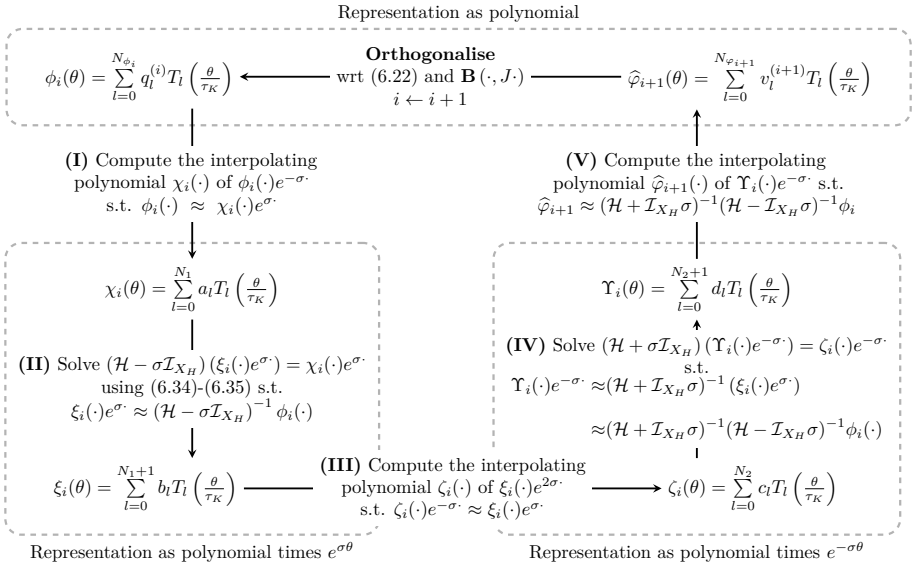

Figure 6.1: Structured representation of the used numerical implementation of Algorithm 1 for $\sigma \neq 0$.

6.6 Numerical illustration

In this section we consider two examples. The first example illustrates the advantage of the chosen shift-invert transformation and the explicit orthogonalisation with respect to $\mathbf{B}(\cdot, J\cdot)$ when computing purely imaginary eigenvalues of (6.1) in the presence of rounding errors. The second example shows the convergence behavior of the presented method for a large-scale example. Both experiments are carried out in MATLAB R2022a (version 9.12.0.1884302) on a Dell Latitude 7490 with a Intel(R) Core(TM) i7-8650U CPU @ 1.90GHz eight core processor with 16GB of RAM running Ubuntu 20.04.4 LTS. The code for these experiments is available from `https://twr.cs.kuleuven.be/research/software/delay-control/SPSIIA/index.html`.

6.6.1 Example 1

Consider the following characteristic matrix of form (6.2):

$$\lambda \begin{bmatrix} 1 & 0 \\ 0 & 1 \end{bmatrix} - \begin{bmatrix} 10 & 0.1 \\ c_0 & -10 \end{bmatrix} - \begin{bmatrix} a_1 & 0 \\ 0 & 0 \end{bmatrix} e^{-\lambda} - \begin{bmatrix} 0 & 0 \\ 0 & -a_1 \end{bmatrix} e^{\lambda} \tag{6.36}$$

with $a_1 = (3\pi^2/4)/(20+\pi)$ and $c_0 = -1000 - 10a_1^2 - 10a_1\pi - \frac{5\pi^2}{2}$. It can be verified that this NEP has purely imaginary eigenvalues at $\pm\jmath\pi$ and $\pm\frac{\jmath\pi}{2}$. Tables 6.1 and 6.2 compare three methods for computing these purely imaginary eigenvalues for $\sigma = 0$ and $\sigma = \jmath\frac{3\pi}{4}$, respectively. These three methods are:

1. applying the infinite Arnoldi method to $\mathcal{H}^{-1}$ and $(\mathcal{H} - \sigma\mathcal{I}_{X_H})^{-1}$, respectively, using a modification of the algorithm from [99] to deal with both positive and negative delays;
2. applying the infinite Arnoldi method to $\mathcal{R}_0^{-1}$ and $\mathcal{R}_\sigma^{-1}$ using the method presented in Section 6.4 and Section 6.5 (Figure 6.1), respectively, but without explicit orthogonalisation against $\mathbf{B}(\cdot, J\cdot)$ (i.e., using (6.26) instead of (6.27)); and
3. applying the infinite Arnoldi method to $\mathcal{R}_0^{-1}$ and $\mathcal{R}_\sigma^{-1}$ using the method presented in Section 6.4 and Section 6.5 (Figure 6.1), respectively, with explicit orthogonalisation against $\mathbf{B}(\cdot, J\cdot)$.

As initial function the constant function $\begin{bmatrix}0.6 & 0.8\end{bmatrix}^\top$ is used in all cases but one. When applying the infinite Arnoldi method to $(\mathcal{H} - \sigma\mathcal{I}_{X_H})^{-1}$, the function $\begin{bmatrix}0.6 & 0.8\end{bmatrix}^\top e^{\sigma\theta}$ is used instead, to be able to use the compact representation from [99] for the functions in the Krylov subspace.

For the first approach, we observe from Tables 6.1 and 6.2 that the obtained approximations have a significant non-zero real part, as this method does not explicitly take into account the symmetry of the spectrum with respect to the imaginary axis. For the second approach, we see that each purely imaginary eigenvalue appears twice. To understand this observations, recall that the eigenvalues $\pm\jmath\omega$ of $\mathcal{H}$ are mapped to the real eigenvalue $\mu = (-\omega^2 - \sigma^2)^{-1}$ of $\mathcal{R}_\sigma^{-1}$ with multiplicity 2 and that the eigenspace associated with μ is given by $\mathcal{L} = \operatorname{span}\{\varphi_+, \varphi_-\}$, with φ_+ and φ_- the eigenfunctions of $\mathcal{H}$ associated with $\jmath\omega$ and $-\jmath\omega$, respectively. Although in exact arithmetic only one linear independent component of $\mathcal{L}$ will be approximated in the Krylov subspace (a consequence of Theorem 6.1), this is typically no longer the case when working in finite precision as orthogonality with respect to $\mathbf{B}(\cdot, J\cdot)$ is typically lost due to rounding errors. As a consequence, the Krylov subspace will eventually also approximate a second linear independent component in the eigenspace $\mathcal{L}$, meaning the double eigenvalue μ of $\mathcal{R}_\sigma^{-1}$ will be approximated by a pair of Ritz values. One either gets two nearby real Ritz values or a pair of complex conjugate Ritz values. In the latter case, after re-transformation the obtained approximations for purely imaginary eigenvalues of $\mathcal{H}$ thus have a small real part. When, however, explicit orthogonalisation against $\mathbf{B}(\cdot, J\cdot)$ is preformed (approach 3), the Krylov subspace satisfies the condition in Proposition 6.10

up to machine precision. As to be expected, the approximations for the purely imaginary eigenvalues are now purely imaginary.

Finally, from Table 6.2, we observe that when using the shift-invert transformation $(\mathcal{H} - \sigma\mathcal{I}_{X_H})^{-1}$, the eigenvalues $\jmath\omega$ and $-\jmath\omega$ are approximated separately. In contrast, when using $\mathcal{R}_\sigma^{-1}$ this pair is really approximated as a pair.

Table 6.1: Obtained approximations after 21 iterations for the purely imaginary eigenvalues of (6.36) using approaches 1-3 for $\sigma = 0$ with the constant function $\begin{bmatrix}0.6 & 0.8\end{bmatrix}^\top$ as initial function.

Approach 1	Approach 2	Approach 3
$-2.5 \times 10^{-11} - \jmath 1.5707963268383$	$1.4 \times 10^{-12} - \jmath 1.5707963267947$	$\jmath 1.5707963267501$
$-2.5 \times 10^{-11} + \jmath 1.5707963268383$	$1.4 \times 10^{-12} + \jmath 1.5707963267947$	$-\jmath 1.5707963267501$
$-5.1 \times 10^{-9} - \jmath 3.1415926530069$	$-1.4 \times 10^{-12} - \jmath 1.5707963267947$	$\jmath 3.1415926538320$
$-5.1 \times 10^{-9} + \jmath 3.1415926530069$	$-1.4 \times 10^{-12} + \jmath 1.5707963267947$	$-\jmath 3.1415926538320$
	$-\jmath 3.1415926535917$	
	$\jmath 3.1415926535917$	
	$-\jmath 3.1415926532865$	
	$\jmath 3.1415926532865$	

Table 6.2: Obtained approximations after 21 iterations for the purely imaginary eigenvalues of (6.36) using approaches 1-3 for $\sigma = \jmath\frac{3\pi}{4}$. For approach 1 the initial function $\begin{bmatrix}0.6 & 0.8\end{bmatrix}^\top e^{\sigma\theta}$ is used, while for the other approaches the initial function $\begin{bmatrix}0.6 & 0.8\end{bmatrix}^\top$ is used.

Approach 1	Approach 2	Approach 3
$3.0 \times 10^{-13} + \jmath 1.5707963267928$	$8.3 \times 10^{-13} - \jmath 1.5707963267942$	$-\jmath 1.5707963266579$
$-3.2 \times 10^{-13} + \jmath 3.1415926535908$	$8.3 \times 10^{-13} + \jmath 1.5707963267942$	$\jmath 1.5707963266579$
$1.6 \times 10^{-6} - \jmath 1.5707080376626$	$-8.3 \times 10^{-13} - \jmath 1.5707963267942$	$-\jmath 3.1415926536191$
$-5.8 \times 10^{-4} - \jmath 3.1409926337637$	$-8.3 \times 10^{-12} + \jmath 1.5707963267942$	$\jmath 3.1415926536191$
	$-\jmath 3.1415926535916$	
	$\jmath 3.1415926535916$	
	$-\jmath 3.1415926535899$	
	$\jmath 3.1415926535899$	

6.6.2 Example 2

For the second example we consider the following dynamical system from [138], which describes a heated rod that is cooled using delayed feedback. The evolution of the temperature in the rod, v, is governed by the partial differential equation

$$\frac{\partial v(x,t)}{\partial t} = \frac{\partial^2 v(x,t)}{\partial x^2} + a_0(x)v(x,t) + a_1(x)v(\pi - x, t-1) \text{ for } x \in [0,\pi]$$

with $a_0(x) = -2\sin(x)$, $a_1(x) = 2\sin(x)$ and $v(0,t) = v(\pi,t) = 0$. Discretising this partial differential equation in the space coordinate x results in a system of delay differential equations of dimension n. To obtain a dynamical system of the form (6.5), we define a performance output matrix $C = \frac{1}{n}\begin{bmatrix}1 & \dots & 1\end{bmatrix}$ (which gives the average temperature of the rod) and a performance input matrix $B = C^\top$. Choosing $n = 1000$ and plotting the magnitude of the frequency response in function of ω, one observes that it is equal to 0.00018 for ω approximately equal to 2.009437, 3.790888, and 5.571120. It now follows from the discussion in Section 2.2.2 and the introduction of this chapter that for $\gamma = 0.00018$ the associated NEP of the form (6.6) must have purely imaginary eigenvalues around $\jmath 2.009437$, $\jmath 3.790888$, and $\jmath 5.571120$.

We first use the method presented in Section 6.4 to compute the eigenvalues near the shift $\sigma = 0$. Figure 6.2 shows the obtained approximations in the region $[-6,6] \times \jmath[-10,10]$ after 70 iterations and their convergence behavior. One observes a quick convergence to the eigenvalues close to the origin.

Next, we apply the method from Section 6.5, with implementation sketched in Figure 6.1, for $\sigma = \jmath 4.5$. Figure 6.3 shows the eigenvalues and the obtained approximations near this shift after 70 iterations. We have again fast convergence to the eigenvalues near the shift. Finally, recall that the degree of the polynomial $\hat{\varphi}_{i+1}$, defined in Figure 6.1, is not known beforehand. Figure 6.4 therefore shows the evolution of the degree of this polynomial with respect to the iteration number. We observe that the degree grows slowly with respect to the number of iterations.

6.7 Conclusion

In this chapter we presented an iterative method to approximate the eigenvalues of NEPs of form (6.1) closest to a given shift σ while preserving the symmetries of the spectrum. The presented work can thus be seen as a generalization of the results from [132, 131] to a class of NEPs.

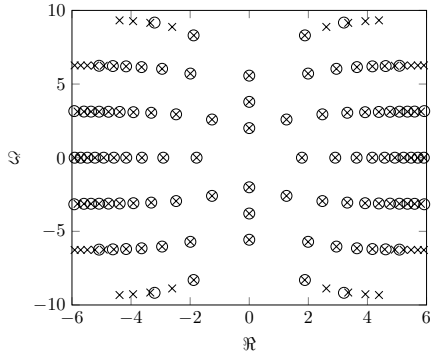

(a) Eigenvalues (crosses) and their approximations (circles) near $\sigma = 0$.

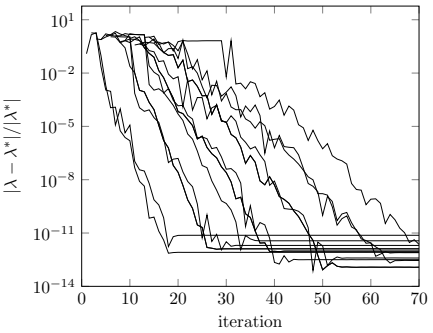

(b) Relative forward error

Figure 6.2: Approximated eigenvalues near the shift $\sigma = 0$ after 70 iterations and their convergence behavior for Example 2 obtained using the method from Section 6.4.

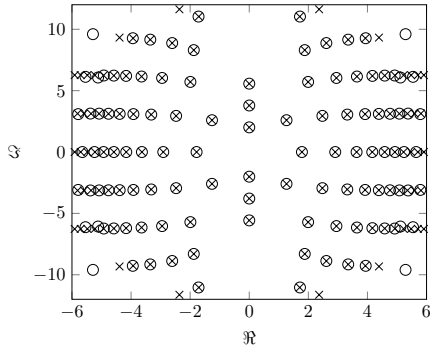

(a) Eigenvalues (crosses) and their approximations (circles) near $\sigma = \jmath 4.5$.

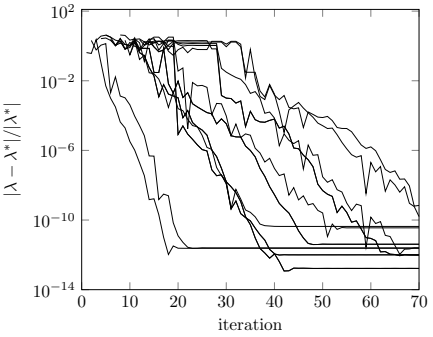

(b) Relative forward error

Figure 6.3: Approximated eigenvalues near the shift $\sigma = \jmath 4.5$ after 70 iterations and their convergence behavior for Example 2 obtained using the method from Section 6.5, as depicted in Figure 6.1.

To derive this method, the equivalence between the considered NEP and a linear but infinite-dimensional eigenvalue problem was used. Based on this equivalence, we introduced a shift-invert transformation that preserves the Hamiltonian structure of the spectrum. Next, the ideas behind the infinite Arnoldi method from [99], which operates on functions rather than on vectors, were applied

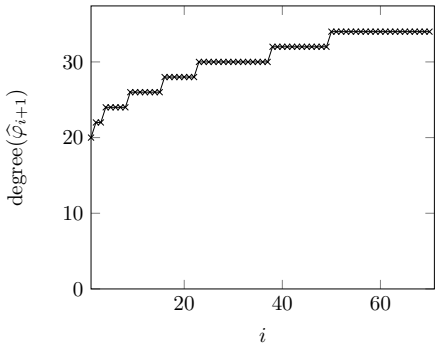

Figure 6.4: Evolution of the degree of $\widehat{\varphi}_{i+1}$, as defined in Figure 6.1, as function of the iteration number i.

to this transformed eigenvalue problem to construct a Krylov subspace. It was then shown that this subspace is orthogonal with respect to the bilinear functional $\mathbf{B}(\cdot, J\cdot)$. This result was subsequently used to demonstrate that the presented method generally finds simple purely imaginary approximations for purely imaginary eigenvalues. Although the method was initially defined on function spaces, Sections 6.4 and 6.5 showed how it can be implemented using finite-dimensional linear algebra operations. The performance of these numerical algorithms was finally verified using two numerical experiments in Section 6.6.

To conclude this chapter we give some directions for future research. Firstly, as mentioned in the introduction, the presented algorithm can be used as a building block in a level-set algorithm for computing the H_∞-norm of time-delay systems. Secondly, a more extensive study on the effect of the chosen initial function and the chosen inner product on the convergence behavior of the method is necessary. Thirdly, for large σ the representation in (6.28) has as advantage that it might require polynomials of a lower degree to approximate the eigenfunctions of nearby eigenvalues in comparison to purely polynomial approximations. The functions $e^{\jmath\omega\theta}$ and $e^{-\jmath\omega\theta}$ act in this case as carrier functions. However, as mentioned before, it is not yet clear how this representation can be used in practice because of problems with numerical stability.

CHAPTER

7 TDS-CONTROL: a software package for the analysis and controller-design of time-delay systems

ABSTRACT

This chapter briefly introduces TDS-CONTROL, a novel MATLAB package for the analysis and controller-design of linear time-invariant time-delay systems with discrete delays. This software package can deal with a broad class of time-delay systems, including neutral systems, systems with delays in the state, input, output or direct feed-through terms, and even delay descriptor systems. The employed controller-design algorithms are based on optimizing a certain objective function, such as the (strong) spectral abscissa or the (strong) H-infinity norm, with respect to the controller parameters. The class of considered controllers consists of static and dynamic output feedback controllers with a user-specified order. Furthermore, by allowing to fix certain entries in the controller matrices, it is also possible to design structured controllers such as decentralized, distributed, and PID controllers.

The content of this chapter is based on [17] and the TDS-CONTROL manual.

7.1 Introduction

The aim of the presented software package is to provide a unified, easy-to-use, and well-documented MATLAB toolbox for the analysis and controller-design of a broad range of linear time-invariant time-delay systems with discrete delays based on the framework described in [139]. More specifically, TDS-CONTROL can deal with

1. time-delay systems of **retarded** type,
2. time-delay systems of **neutral** type, and
3. time-delay systems described by **delay-differential algebraic equations**, also known as **delay descriptor systems**.

These systems are expected to be provided in state-space format for which delays can be present in the state, input, output, or direct feed-through terms. However, the package also offers functionality to create such a representation

based on a frequency domain model for the system such as its characteristic quasi-polynomial or its transfer function.

For the system classes listed above, `TDS-CONTROL` offers the following functionality.

1. **Stability analysis**
    - Computing the characteristic roots in a given right half-plane or rectangular region.
    - Computing the (strong) spectral abscissa.
2. **Stabilization**
    - Designing (strongly) stabilizing static and fixed-order dynamic output feedback controllers.
3. **Robust stability analysis and control**
    - Computing the (strong) H_∞-norm.
    - Designing controllers that (locally) minimize the closed-loop (strong) H_∞-norm.
    - Computing the pseudospectral abscissa with respect to structured uncertainties on both the system matrices and the delays for retarded delay differential equations.
    - Computing the distance to instability with respect to structured uncertainties on both the system matrices and the delays for retarded delay differential equations.

The design functions mentioned above are based on the direct optimization framework as discussed in Section 2.3.2. For example, to design a strongly stabilizing controller the strong spectral abscissa, as defined in Definition 2.5, is minimized. As a strictly negative strong spectral abscissa is a necessary and sufficient condition for strong exponential stability, the presented design method is not conservative and a stabilizing controller can be computed whenever it exists. Furthermore, the direct optimization framework allows to easily impose additional structure on the controller matrices in the form of a sparsity pattern, enabling the design of decentralized or distributed controllers. By exploiting the generality of the DDAE-based modeling framework, also PI(D) and delay-based controllers can be designed. The controller-design part of the presented software package can thus be seen as an extension of `HIFOO` [42, 80] or `hinfstruct` [8] to time-delay systems.

The remainder of this chapter will give an overview of the package's functionality by means of several examples, including the code that was used to generate Figures 2.1, 2.2, and 4.1. In Section 7.2 we discuss how to represent the system classes listed above in TDS-CONTROL and how to compute their rightmost characteristic roots. Section 7.3 illustrates how to design stabilizing feedback controllers by means of an example. In Section 7.4 we consider the computation of the (strong) H_∞-norm and the design of controllers that (locally) minimize the closed-loop (strong) H_∞-norm. Section 7.5 shows how to compute the pseudospectral abscissa of a retarded DDE with uncertainties on both the state matrices and the delays. Finally, Section 7.6 draws some concluding remarks.

7.2 Stability analysis

In this section, three examples will illustrate how to represent RDDEs, NDDEs, and DDAEs in the TDS-CONTROL package and how their characteristic roots and (strong) spectral abscissa can be computed.

7.2.1 Retarded delay differential equations

Example 7.1. Let us recall the RDDE (2.7):

$$\dot{x}(t) = -2\,x(t) + 2\,x(t-1) + x(t-1.5).$$

To represent this differential equation in MATLAB we use the following code:

```
A = {[-2],[2],[1]};
hA = [0 1 1.5];
rdde = tds_create(A,hA);
```

The function `tds_create(A,hA)` creates a `tds_ss`-object `rdde` that represents the RDDE. The first argument of this function (`A`) is a cell array containing the state matrices. The second argument (`hA`) is a one-dimensional array with the state delays.

Next, we compute the characteristic roots of this RDDE with real part larger than -4 using the function `tds_roots`. This function takes two mandatory input arguments, namely the `tds_ss`-object that we created before and a scalar that defines the desired right half-plane (in this case defined by $\Re(\lambda) \geq -4$).

```
cr = tds_roots(rdde,-4);
```

To capture all characteristic roots in the specified right half-plane, `tds_roots` implements the method from [201], which uses a two-step approach. First, it computes the eigenvalues of a spectral discretisation of the infinitesimal generator of the solution operator underlying the delay differential equation. For a sufficiently high discretization degree, these eigenvalues form a good approximation for the characteristic roots of the RDDE in the desired right half-plane. Subsequently, these approximations are improved using Newton's method. An appealing feature of the method in [201] is that it provides an empirical method to automatically determine the degree of the discretization for which all desired characteristic roots are sufficiently well approximated.

To plot the resulting characteristic roots we use the `tds_eigenplot` function.

```
tds_eigenplot(cr);
```

The result is shown in Figure 2.1.

To directly compute the spectral abscissa of (2.7), we can use the function `tds_sa`.

```
>> tds_sa(rdde,-4)

ans =

0.2486
```

◇

7.2.2 Neutral delay differential equations

Example 7.2. We consider the NDDE (2.11):

$$\dot{x}(t) = \frac{1}{4}x(t) - \frac{1}{3}x(t-1) + \frac{3}{4}\dot{x}(t-1) - \frac{1}{2}\dot{x}(t-2).$$

To create a corresponding `tds_ss`-object, we use the `tds_create_neutral` function

```
H = {[-3/4],[1/2]};
hH = [1 2];
A = {[1/4],[-1/3]};
hA = [0 1];
ndde = tds_create_neutral(H,hH,A,hA);
```

The `tds_create_neutral(H,hH,A,hA)` function takes as input arguments a cell array with the H matrices (`H`), a vector containing the corresponding

delays (`hH`), followed by a cell array with the A matrices (`A`) and an array the corresponding delays (`hA`). Note that the first term in (2.8), i.e., the term associated with $\dot{x}(t)$, should not be provided explicitly. This function returns a `tds_ss`-object of which we can again compute the characteristic roots. However, as for an NDDE a right half-plane may contain infinitely many characteristic roots, we now instead consider a rectangular region in the complex plane (in this case $[-0.9, 0.2] \times \jmath[-500, 500]$). Furthermore, we pass additional options to `tds_roots` to increase the maximal size of the discretized eigenvalue problem.

```
optns=tds_roots_options('max_size_evp', 2000);
region = [-0.9 0.2 -900 900];
[cr] = tds_roots(ndde,region,optns);
tds_eigenplot(cr);
```

Notice that the second input argument of `tds_roots` now is an array of length 4, instead of a scalar to indicate that we want to compute the roots in a rectangular region instead of a right half-plane. The result is shown in Figure 2.2a.
To examine the effect of a small delay perturbation (Figure 2.2b) we can replace the delay 2 by 2.05.

```
ndde2 = ndde; % Copy the original tds_ss object
ndde2.hH(2) = 2.05; % Change the delay
[cr2] = tds_roots(ndde2,region,optns);
tds_eigenplot(cr2);
```

Alternatively, we can directly compute the strong spectral abscissa (as defined in Definition 2.5):

```
>> tds_strong_sa(ndde)

ans =

0.1616
```

◇

7.2.3 Delay differential algebraic equations

Example 7.3. Finally, consider the following delay differential algebraic equation inspired by (4.25):

$$\begin{bmatrix} 1 & 0 & 0 \\ 0 & 0 & 0 \\ 0 & 0 & 0 \end{bmatrix} \dot{x}(t) = \begin{bmatrix} -10 & 4 & 0 \\ 0 & -1 & 0 \\ -8 & 4 & -1 \end{bmatrix} x(t) + \begin{bmatrix} 2 & 0 & 0 \\ 0 & 0 & 0 \\ 0 & 0 & 0 \end{bmatrix} x(t-1). \tag{7.1}$$

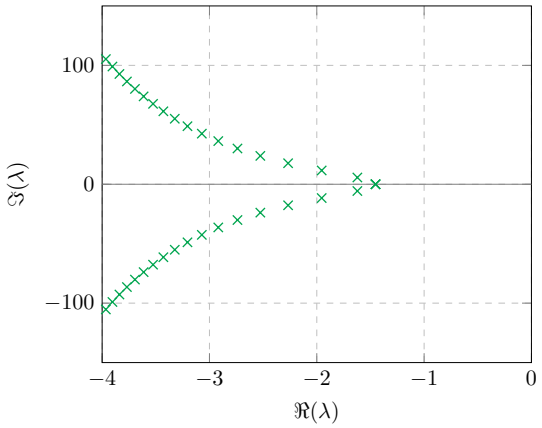

Figure 7.1: The characteristic roots of (7.1) with real part larger than -4.

We now use the function `tds_create_ddae` to create a representation for this differential equation.

```
E = [1 0 0;0 0 0;0 0 0];
A0 = [-10 4 0;0 -1 0;-8 4 -1];
A1 = [2 0 0;0 0 0;0 0 0];
ddae = tds_create_ddae(E,{A0,A1},[0 1]);
```

Next we use `tds_roots` to compute the characteristic roots with real part larger than -4.

```
cr = tds_roots(ddae,-4);
```

The result is shown in Figure 7.1. ◇

7.3 Stabilisation

To design stabilizing output feedback controllers of the form (2.26) or (2.27) one can use the functions `tds_stabopt_static` and `tds_stabopt_dynamic`, respectively. Furthermore, by imposing constraints on the system matrices, it is possible to design decentralized, overlapping or even PID controllers.

Example 7.4. To illustrate how to use these functions, we consider the networked system from Section 5.5 for $N = 3$. We will first design a centralized dynamic output feedback controller of the form (2.27) with $n_c = 6$. To this end, we start with defining the plant.

```
% System parameters
N = 3; M = 1; m = 0.05; g = 9.8; l = 1;
k = 1; tau_u = 0.1; tau_nc = 0.2;
% System matrices of the individual subsystems
A = [0 1 0 0;-2*k/M 0 -m*g/M 0;
0 0 0 1;2*k/(M*l) 0 g*(M+m)/(M*l) 0];
B = [0;1/M;0;-1/(M*l)];
Bn = [0;k/M;0;-k/(M*l)];
C = [1 0 0 0;0 0 1 0];
Cn = [2 0 0 0];
% Adjacency matrix of the network
P = diag(0.5*ones(1,N-1),-1)+diag(0.5*ones(1,N-1),1);

% System matrices of the overal system
AN = kron(eye(N),A)+kron(P,Bn*Cn);
BN = kron(eye(N),B);
CN = kron(eye(N),C);

% Create tds_ss object
plant = tds_create({AN},[0],{BN},[tau_u],{CN},[0]);
```

Notice that we now pass additional arguments to `tds_create` specifying the control input and output matrices and the corresponding delays. Next, we analyze the stability of the open-loop system (which is a delay-free system):

```
cr = tds_roots(plant,-4);
tds_eigenplot(cr)
tds_sa(plant,0)
```

We find that the spectral abscissa is equal to 3.204, meaning that the open-loop system is unstable. To design a stabilizing dynamic output feedback controller for this system we use the function `tds_stabopt_dynamic`.

```
nc = 6;
[K,CL] = tds_stabopt_dynamic(plant,nc);
```

This function takes two mandatory inputs arguments, namely the open-loop plant (`plant`) and the controller order (`nc`). To obtain a stabilizing controllor, the optimization approach described in Section 2.3.3 is used to minimize the (strong) spectral abscissa of the closed-loop system with respect to the entries of the controller matrices[1]. As the considered optimization problem is non-convex,

[1]The gradient sampling step is by default disabled, but can be enabled by specifying additional options.

the optimization procedure is by default restarted from 5 random initial points[2]. The first return argument is the resulting controller (in the form of a MATLAB `ss` object), while the second return argument contains a `tds_ss` representation for the corresponding closed-loop system. The obtained feedback matrices (rounded to two decimal place) are

$$A_c = \begin{bmatrix} -13.34 & 3.00 & 10.34 & 5.74 & -0.45 & -5.49 \\ -12.13 & -37.70 & 20.54 & -16.81 & -14.01 & -10.17 \\ -6.22 & -35.34 & -6.42 & -19.22 & 8.97 & -16.81 \\ 3.96 & -5.14 & 0.89 & -14.37 & 7.01 & -0.27 \\ -3.77 & 15.29 & 4.84 & 8.43 & -15.85 & -7.87 \\ -1.57 & -28.47 & 20.61 & -1.01 & 3.52 & -21.51 \end{bmatrix},$$

$$B_c = \begin{bmatrix} 4.31 & -28.63 & -2.92 & -15.89 & 1.31 & 0.82 \\ 8.47 & -43.22 & -10.60 & 10.39 & -1.71 & 36.26 \\ 3.47 & -22.34 & -3.93 & 22.86 & -10.46 & 24.90 \\ -1.51 & 22.78 & -4.99 & -16.81 & -3.44 & 55.16 \\ -2.87 & -22.01 & -4.75 & -29.99 & 3.78 & -23.18 \\ 8.03 & -62.43 & -1.93 & -17.90 & -6.18 & 36.88 \end{bmatrix},$$

$$C_c = \begin{bmatrix} 7.65 & 27.92 & -30.36 & -8.46 & 19.00 & 8.10 \\ -25.07 & -40.28 & 10.15 & -18.19 & -22.88 & 0.63 \\ -1.25 & -50.50 & 15.93 & -29.14 & -0.02 & -6.75 \end{bmatrix},$$

and

$$D_c = \begin{bmatrix} -6.50 & 95.48 & 0.90 & -13.16 & -9.58 & -5.57 \\ 7.56 & -25.49 & -8.71 & 85.38 & 1.76 & -22.71 \\ 10.40 & -4.45 & -7.49 & 21.87 & 0.97 & 122.09 \end{bmatrix}.$$

Computing the (strong) spectral abscissa of the resulting closed-loop system,

```
tds_strong_sa(CL,-4)
```

we find that it is equal to -2.008, meaning that the plant is stabilized.

Next, let us design a fully decentralized control architecture in which the local controllers are dynamic ouput feedback laws of order 2. (Note that in this case the local controllers do not need to be identical.) To this end, we need to specify a mask that indicates which entries of the controller matrices in (2.27) are allowed to be optimized and which should remain zero. This controller design problem can be implemented as follows:

[2]As a consequence, different runs of `tds_stabopt_dynamic` can result in a different controller. To get reproducible results, the best practice is to manually specify the initial values for the controller parameters using the `initial`-flag, which will be explained in more detail below.

```
nc = 2;
mask=ss(kron(eye(N),ones(nc)),kron(eye(N),ones(nc,2)),
    kron(eye(N),ones(1,nc)),kron(eye(N),ones(1,2)));
[Kdc,CL2]=tds_stabopt_dynamic(plant,N*nc,'mask',mask);
```

The `mask` object indicates that in this case only the block diagonal entries of the feedback matrices are optimization variables. The resulting feedback matrices are

$$A_c = \begin{bmatrix} -58.01 & 22.83 & 0.00 & 0.00 & 0.00 & 0.00 \\ 27.49 & -40.30 & 0.00 & 0.00 & 0.00 & 0.00 \\ 0.00 & 0.00 & -37.64 & 7.34 & 0.00 & 0.00 \\ 0.00 & 0.00 & 30.84 & -15.20 & 0.00 & 0.00 \\ 0.00 & 0.00 & 0.00 & 0.00 & -40.03 & -48.61 \\ 0.00 & 0.00 & 0.00 & 0.00 & -17.95 & -77.05 \end{bmatrix},$$

$$B_c = \begin{bmatrix} -10.56 & 104.30 & 0.00 & 0.00 & 0.00 & 0.00 \\ -60.32 & -225.36 & 0.00 & 0.00 & 0.00 & 0.00 \\ 0.00 & 0.00 & -38.18 & 98.41 & 0.00 & 0.00 \\ 0.00 & 0.00 & 2.75 & -129.38 & 0.00 & 0.00 \\ 0.00 & 0.00 & 0.00 & 0.00 & -30.59 & 7.21 \\ 0.00 & 0.00 & 0.00 & 0.00 & -42.33 & -104.32 \end{bmatrix},$$

$$C_c = \begin{bmatrix} -66.79 & 51.37 & 0.00 & 0.00 & 0.00 & 0.00 \\ 0.00 & 0.00 & -64.98 & 26.87 & 0.00 & 0.00 \\ 0.00 & 0.00 & 0.00 & 0.00 & -19.52 & 30.02 \end{bmatrix},$$

and

$$D_c = \begin{bmatrix} 47.61 & 293.60 & 0.00 & 0.00 & 0.00 & 0.00 \\ 0.00 & 0.00 & -16.44 & 283.79 & 0.00 & 0.00 \\ 0.00 & 0.00 & 0.00 & 0.00 & 15.43 & 127.89 \end{bmatrix}.$$

Notice that only the entries for which `mask` is equal to `1` are non-zero. Using `tds_strong_sa`, we find that the closed-loop system is again stable and now has a spectral abscissa of -1.542.

Finally, we design a centralized PID controller. To this end, we define the extended output

$$y_e(t) = \begin{bmatrix} y(t) \\ \dot{y}(t) \end{bmatrix} = \begin{bmatrix} I_N \otimes C_y \\ I_N \otimes C_y A_0 + P_N \otimes C_y B_{u_n} C_{y_n} \end{bmatrix} x(t) + \begin{bmatrix} 0 \\ I_N \otimes C_y B_u \end{bmatrix} u(t-\tau_u).$$

A PID controller can now be written in the form (2.27):

$$\begin{cases} \dot{x}_c(t) &= 0_{N\times N}\, x_c(t) + \begin{bmatrix} K_I & 0 \end{bmatrix} y_e(t), \\ u(t) &= x_c(t) + \begin{bmatrix} K_P & K_D \end{bmatrix} y_e(t). \end{cases}$$

To design this PID controller in TDS-CONTROL, we use both the optional 'mask' and 'basis' arguments. The former allows us to indicate which entries of the controller matrices are optimization variables, while the latter specifies the (fixed) value for the remaining entries.

```
% Create plant with extended output
plant2 = tds_create({AN},0,{BN},tau_u,{[CN;CN*AN]},0
        {[zeros(N*2,N);CN*BN]},[tau_u]);

% Indicate the optimization variables
mask2 = ss(zeros(N),[ones(N,2*N) zeros(N,2*N)],
        zeros(N),ones(N,4*N));
% Specify the fixed value for the other entries
basis2 = ss(zeros(N),zeros(N,4*N),eye(N),
        zeros(N,4*N));

% Design the controller
[KPID,CL3] = tds_stabopt_dynamic(plant2,N,'basis',
    basis2,'mask',mask2);

% Extract the PID feedback gains from the dynamic
    controller KPID
KP = KPID.D(:,1:6); KI = KPID.B(:,1:6); KD = KPID.D
    (:,7:12);
```

After extracting the PID feedback gains from the ss object KPID we find

$$K_P = \begin{bmatrix} 4.90 & 48.80 & -1.27 & -7.16 & -3.01 & -3.10 \\ 0.72 & 10.00 & 8.41 & 47.55 & -1.76 & -7.16 \\ 6.26 & 3.90 & 1.83 & 18.09 & 7.49 & 48.94 \end{bmatrix},$$

$$K_I = \begin{bmatrix} 7.66 & 5.08 & -8.65 & -1.36 & 4.73 & -1.53 \\ -2.44 & -0.85 & 5.14 & 3.02 & -2.37 & -1.27 \\ 0.52 & 1.80 & 1.11 & 1.46 & 1.12 & 2.92 \end{bmatrix},$$

and

$$K_D = \begin{bmatrix} 15.54 & 29.11 & -5.22 & -8.66 & 0.58 & 0.36 \\ -1.22 & -0.66 & 8.20 & 16.80 & -1.73 & -2.32 \\ 4.67 & 1.63 & 3.10 & 5.87 & 6.66 & 16.61 \end{bmatrix}.$$

The spectral abscissa of the corresponding closed-loop system is equal to -1.1243.

◇

7.4 The (strong) H-infinity norm and robust control

In this section, we will consider two examples to illustrate how to compute (= analysis) and minimize (= controller synthesis) the (strong) H_∞-norm of a time-delay system.

Example 7.5. Let us consider the system from (4.2):

$$\begin{cases} \dot{x}(t) = -2x(t) + x(t-1) - \ w(t) - 0.5w(t-2), \\ z(t) = -2x(t) + x(t-2) + 5w(t) + 1.5w(t-1) - 3w(t-2). \end{cases}$$

We start with creating a `tds_ss`-object for this system.

```
tau1 = 1; tau2 = 2;
sys = tds_create({-2,1},[0 tau1],'B2',{-1,-0.5},
        [0 tau2],'C2',{-2,1},[0 tau2],
        'D22',{5,1.5,-3},[0 tau1 tau2]);
```

We use the flags `'B2'`, `'C2'`, and `'D22'` to indicate that we specify the performance input, output and direct feed-through matrices and not the control input, output and direct feed-through matrices.

To plot the singular values of the corresponding frequency response we use the function `tds_sigma`.

```
omega = logspace(-1,3.5,10001);
T = tds_sigma(sys,omega);
semilogx(omega,T)
```

The result is shown in Figure 4.1a. Similarly, Figures 4.1b and 4.1c can be obtained by changing the delays.

To compute the strong H_∞-norm of this system (as defined in (4.3)), we use the function `tds_hinfnorm`.

```
>> >> tds_hinfnorm(sys)

ans =

9.5000
```

◇

Example 7.6. As a second example, we consider again the networked system from Section 5.5. Now we design a centralized dynamic output feedback controller that (locally) minimizes the (strong) H_∞-norm of the resulting closed-loop system using `tds_hiopt_dynamic`.

```
% Extend plant with performance inputs and outputs
Bw = [0 0;1/M -m/M;0 0;-1/(M*l) (M+m)/(M*l)];
Cz = [1 0 0 0;0 0 1 0];

BNw = kron(eye(N),Bw);
CNz = kron(eye(N),Cz);

plant.B2 = {BNw};
plant.hB2 = 0;
plant.C2 = {CNz};
plant.hC2 = 0;

options = tds_stabopt_options('nstart',1);
[Khinf,CL4] = tds_hiopt_dynamic(plant,6,'initial',K,
                'options',options);
```

First, we suplement the plant with the performance input and output terms. Next, we call `tds_hiopt_dynamic` with this new `tds_ss` object. This function has the same manditory input arguments as `tds_stabopt_dynamic`. In this case these manditory arguments are supplemented with two optional ones. Firstly, we use the argument `'initial'` to explicitly specify the initial values for the controller parameters. Here we use the entries of the stabilizing controller we designed before. Secondly, we use the `'options'` argument to indicate that the optimization procedure should only run once with the entries of the provided controller as initial value for the optimization parameters [3]. The resulting feedback matrices are

$$A_c = \begin{bmatrix} -13.34 & 3.00 & 10.34 & 5.74 & -0.45 & -5.49 \\ -12.13 & -37.70 & 20.55 & -16.81 & -14.01 & -10.17 \\ -6.22 & -35.34 & -6.42 & -19.22 & 8.97 & -16.81 \\ 3.96 & -5.14 & 0.89 & -14.37 & 7.01 & -0.27 \\ -3.77 & 15.29 & 4.84 & 8.43 & -15.85 & -7.87 \\ -1.57 & -28.48 & 20.61 & -1.01 & 3.52 & -21.51 \end{bmatrix},$$

[3] By default `tds_hiopt_dynamic` will generate additional initial parameters such that the total number of starting points equals five.

$$B_c = \begin{bmatrix} 4.31 & -28.63 & -2.92 & -15.89 & 1.31 & 0.82 \\ 8.47 & -43.21 & -10.60 & 10.39 & -1.71 & 36.26 \\ 3.47 & -22.34 & -3.93 & 22.86 & -10.46 & 24.90 \\ -1.52 & 22.78 & -4.98 & -16.81 & -3.44 & 55.16 \\ -2.87 & -22.01 & -4.75 & -29.99 & 3.78 & -23.18 \\ 8.03 & -62.43 & -1.93 & -17.90 & -6.18 & 36.88 \end{bmatrix},$$

$$C_c = \begin{bmatrix} 7.65 & 27.92 & -30.36 & -8.45 & 19.00 & 8.10 \\ -25.08 & -40.28 & 10.15 & -18.19 & -22.88 & 0.63 \\ -1.25 & -50.50 & 15.92 & -29.13 & -0.02 & -6.75 \end{bmatrix},$$

and

$$D_c = \begin{bmatrix} -6.49 & 95.48 & 0.89 & -13.16 & -9.58 & -5.57 \\ 7.55 & -25.49 & -8.71 & 85.38 & 1.76 & -22.71 \\ 10.41 & -4.45 & -7.50 & 21.87 & 0.97 & 122.09 \end{bmatrix}.$$

The corresponding closed-loop H_∞-norm is decreased from 38.10 to 34.77, at the cost of an increase in the spectral abscissa from -2.008 to -0.5197. ◇

7.5 Robust stability analysis

Recall from Section 2.2.1 that the pseudospectral abscissa, defined as the worst-case value of the spectral abscissa over all uncertainty values, allows to examine the robust stability of an uncertain differential equation. Here we will consider the pseudospectral abscissa for a class of uncertain retarded delay differential equations for which **structured uncertainties** can act **on both the system matrices and the delays**. More specifically, we consider L_M bounded matrix uncertainties that can **either be real or complex-valued** and whose **size is measured in either the Frobenius norm or the spectral norm**. For ease of notation, we denote the set of matrix uncertainties by $\delta = (\delta_1, \ldots, \delta_{L_M})$, in which $\delta_1, \ldots, \delta_{L_M}$ are real or complex-valued matrices whose dimensions are not necessarily the same. Note that **one uncertainty may affect multiple state matrices** (as the same uncertain parameter may appear at multiple locations, see Example 7.7) and **one state matrix may be affected by multiple uncertainties** (as one matrix may have multiple uncertain parameters). Similarly, we consider L_D bounded delay uncertainties and denote the set of delay uncertainties by $\delta\tau = (\delta\tau_1, \ldots, \delta\tau_{L_D})$, in which $\delta\tau_1, \ldots, \delta\tau_{L_D}$ are real-valued scalars.

Given these prerequisites, we consider the following uncertain retarded delay differential equation

$$\dot{x}(t) = \Big(A_0 + \tilde{A}_0(\delta)\Big)x(t) + \sum_{k=1}^{m_A} \Big(A_k + \tilde{A}_k(\delta)\Big)x\big(t - (\tau_k + \tilde{\tau}_k(\delta\tau))\big), \qquad (7.2)$$

in which $A_k \in \mathbb{R}^{n\times n}$ for $k = 0, \ldots, m_A$ are the nominal state matrices and τ_k for $k = 1, \ldots, m_A$ are the nominal delay values. The uncertain matrices $\tilde{A}_k(\delta)$ for $k = 0, \ldots, m_A$ are defined as

$$\tilde{A}_k(\delta) = \sum_{j=1}^{N_{A_k}} G_{k,j}\ \delta_{\mathtt{ind}_{A_k}[j]}\ H_{k,j}$$

with N_{A_k} the number of uncertain terms, $\mathtt{ind}_{A_k}[j]$ the jth element of the array $\mathtt{ind}_{A_k}$ of length N_{A_k} that indicates the index of the uncertainty in δ, and $G_{k,j}$ and $H_{k,j}$ real-valued shape matrices of appropriate dimension. This seemingly cumbersome notation is necessary to account for the fact that one uncertainty may affect multiple matrices and that one matrix may be affected by multiple uncertainties. Similarly, the delay uncertainties $\tilde{\tau}_k(\delta\tau)$ are defined as

$$\tilde{\tau}_k(\delta\tau) = \max\left\{-\tau_k, \sum_{j=1}^{N_{\tau_k}} w_{k,j}\,\delta\tau_{\mathtt{ind}_{\tau_k}[j]}\right\}$$

with N_{τ_k} the number of uncertain terms, $\mathtt{ind}_{\tau_k}[j]$ the jth element of the array $\mathtt{ind}_{\tau_k}$ that indicates the index of the uncertainty in $\delta\tau$, and $w_{k,j}$ a real-valued weighting coefficient. The corresponding ϵ-pseudospectrum is defined as

$$\Lambda^{\text{ps}}(\epsilon) := \bigcup_{\substack{\delta\in\mathcal{D}_\epsilon \\ \delta\tau\in\mathcal{D}\tau_\epsilon}} \left\{\lambda \in \mathbb{C} : \det\left(\lambda I_n - \left(A_0 + \tilde{A}_0(\delta)\right) + \sum_{k=1}^{m_A}\left(A_k + \tilde{A}_k(\delta)\right)\exp\left(-\lambda(\tau_k + \tilde{\tau}_k(\delta\tau))\right)\right) = 0\right\}$$

with $\mathcal{D}_\epsilon$ the set of admissible matrix uncertainties, i.e.,

$$\mathcal{D}_\epsilon = \left\{(\delta_1, \ldots, \delta_{L_M}) : \delta_l \in \mathbb{K}^{\varrho_l\times\varsigma_l} \text{ and } \|\delta_l\| \le \epsilon \text{ for } l = 1, \ldots, L_M\right\},$$

in which $\mathbb{K}$ can be replaced by either $\mathbb{R}$ or $\mathbb{C}$ (note that different uncertainties may belong to different sets). Similarly, for $\|\cdot\|$ both the spectral norm ($\|\cdot\|_2$) and the Frobenius norm ($\|\cdot\|_{\text{fro}}$) can be considered (again, different uncertainties can be measured in different norms). $\mathcal{D}\tau_\epsilon$ is the set of admissible delay uncertainties, i.e.,

$$\mathcal{D}\tau_\epsilon = \{(\delta\tau_1, \ldots, \delta\tau_{L_D}) : \delta_l \in \mathbb{R} \text{ and } |\delta_l| \le \epsilon \text{ for } l = 1, \ldots, L_D\}.$$

The corresponding ϵ-pseudospectral abscissa is defined as the smallest upper bound for the real part of the points in the ϵ-pseudospectrum

$$c^{\text{ps}}(\epsilon) := \sup\{\Re(\lambda) : \lambda \in \Lambda^{\text{ps}}(\epsilon)\}. \tag{7.3}$$

Example 7.7 (Inspired by [28])**.** Consider the following simple time-delay model for a turning process

$$\ddot{d}(t) + 2\xi\omega\,\dot{d}(t) + \omega^2\,d(t) = \frac{k}{m}\left(d(t-\tau) - d(t)\right)$$

with ω the natural angular frequency, ξ the damping ratio, m the modal mass, k the cutting force coefficient, and τ the time of one revolution of the work-piece. This model can be transformed into a standard first-order delay differential equation of retarded type by considering the state vector $x(t) = \begin{bmatrix} d(t) & \dot{d}(t) \end{bmatrix}^\top$

$$\dot{x}(t) = \begin{bmatrix} 0 & 1 \\ -\omega^2 - \frac{k}{m} & -2\xi\omega \end{bmatrix} x(t) + \begin{bmatrix} 0 & 0 \\ \frac{k}{m} & 0 \end{bmatrix} x(t-\tau). \tag{7.4}$$

Now we want to examine the robust stability of (7.4). Recall from Theorem 2.5 that the H_∞-norm provides a measure for the robust stability of an uncertain system. More specifically, the reciprocal of the H_∞-norm is equal to the distance to instability of the system with respect to a (structured) full-block complex-valued uncertainty acting on the matrix A_0. However, this might be a poor estimate for the "real" distance to instability of (7.4), as in practice the perturbations are real-valued and affect specific parameters in the model. In this example we will assume that the parameters k, ξ, and τ are uncertain. More specifically, we will assume that the parameter k lies in the interval $[k-\Delta_k, k+\Delta_k]$, ξ in $[\xi-\Delta_\xi, \xi+\Delta_\xi]$, and τ in $[\tau-\Delta_\tau, \tau+\Delta_\tau]$. By computing the pseudospectral abscissa with respect to these uncertainties we get a more realistic view of the robust stability of the system.

Below we compute the pseudospectral abscissa for the following parameter values: $k = 8\times10^6\,\mathrm{Nm}^{-1}$, $\omega = 775\,\mathrm{s}^{-1}$, $\tau = 0.012\,\mathrm{s}$, $\xi = 0.05$, $m = 50\,\mathrm{kg}$, $\Delta_k = 1\times10^6\,\mathrm{Nm}^{-1}$, $\Delta_\xi = 0.005$, and $\Delta_\tau = 0.001\,\mathrm{s}$. Let us start by representing the nominal system in `TDS-CONTROL`

```
k=8e6; omega=775; xi=0.05; tau=0.008; m=50;
A0=[0 1;-omega^2-k/m -2*xi*omega];A1=[0 0;k/m 0];
tds=tds_create({A0,A1},[0 tau]);
```

and computing its nominal spectral abscissa

```
tds_sa(tds,-30)
ans =
         -16.3646
```

We conclude that the system is exponentially stable. Next, we cast the uncertain system in the form (7.2):

$$\dot{x}(t) = \left(\begin{bmatrix} 0 & 1 \\ -\omega^2 - \frac{k}{m} & -2\xi\omega \end{bmatrix} + \begin{bmatrix} 0 \\ \frac{-1}{m} \end{bmatrix} \delta_1 \begin{bmatrix} \Delta_k & 0 \end{bmatrix} + \begin{bmatrix} 0 \\ -2\omega \end{bmatrix} \delta_2 \begin{bmatrix} 0 & \Delta_\xi \end{bmatrix} \right) x(t) + \left(\begin{bmatrix} 0 & 0 \\ \frac{k}{m} & 0 \end{bmatrix} + \begin{bmatrix} 0 \\ \frac{1}{m} \end{bmatrix} \delta_1 \begin{bmatrix} \Delta_k & 0 \end{bmatrix} \right) x\big(t - (\tau + \Delta_\tau \delta\tau_1)\big) \quad (7.5)$$

with $|\delta_1| \leq 1$, $|\delta_2| \leq 1$, and $|\delta\tau_1| \leq 1$. Note that the uncertainty δ_1 affects both state matrices, while A_0 is affected by both uncertainties. Next we will demonstrate how this uncertain RDDE can be represented in `TDS-CONTROL`. We start by creating a representation for the uncertainties δ_1 and δ_2 using the function `tds_create_delta`

```
delta=tds_create_delta({1,1},{1,1},{'r','r'},...
                       {'f','f'});
```

This function takes four cell arrays of length L_M (here equal to 2) as input. The first cell indicates the row dimension of the uncertainties, the second the column dimension, the third whether the uncertainty is real (`'r'`) or complex-valued (`'c'`), and the fourth whether its size should be measured using the spectral (`'s'`) or Frobenius norm (`'f'`).
Next, we create objects that represents the uncertain matrices $\tilde{A}_0(\delta)$ and $\tilde{A}_1(\delta)$ using the function `tds_uncertain_matrix`:

```
Delta_k=1e6; Delta_xi=0.005;
G01=[0;-1/m]; H01=[Delta_k 0];
G02=[0;-2*omega]; H02=[0 Delta_xi];
uA0=tds_uncertain_matrix({1,2},{G01,G02},{H01,H02});

G11=[0;1/m]; H11=[Delta_k 0];
uA1=tds_uncertain_matrix({1},{G11},{H11});
```

The function `tds_uncertain_matrix` takes three cell arrays as input argument: the first argument is the array $\texttt{ind}_{A_k}$, the second stores the left shape matrices, and the third stores the right shape matrices.
Subsequently we create the uncertain delay term $\tilde{\tau}_1(\delta\tau) = \Delta_\tau \delta\tau_1$:

```
Delta_tau=0.001;
uhA1=tds_uncertain_delay({1},{Delta_tau});
```

in which the function `tds_uncertain_delay` takes two cell arrays as input: the first is the array $\texttt{ind}_{\tau_k}$ and the second is a cell array with the weights. Finally

we use the method `add_uncertainty` to add these uncertainties to the nominal time delay system `tds`.

```
utds=tds.add_uncertainty(delta,1,{uA0,uA1},{[],uhA1});
```

In this case, the method `add_uncertainty` takes four input arguments: the set of matrix uncertainties δ, the number of delay uncertainties (in this case 1) and two cell arrays of length m_A, with respectively the uncertain matrices and delays[4]. The function returns an `utds_ss`-object that represents the uncertain delay differential equation of which we can compute the ϵ-pseudospectral abscissa using the function `tds_psa`.

```
>> epsilon=1;
>> tds_psa(utds,epsilon)

ans =

   20.7022
```

We thus conclude that the uncertain delay differential equation (7.5) is not stable for all admissible uncertainty values. Let us therefore compute the corresponding distance to instability.

```
tds_dins(utds,[0 1]);
```

We find that $r_{\text{ins}} = 0.4125$, meaning that the uncertain system is stable for all k in $(k - r_{\text{ins}}\Delta_k, k + r_{\text{ins}}\Delta_k)$, ξ in $(\xi - r_{\text{ins}}\Delta_\xi, \xi + r_{\text{ins}}\Delta_\xi)$, and τ in $(\tau - r_{\text{ins}}\Delta_\tau, \tau + r_{\text{ins}}\Delta_\tau)$. ◇

Remark 7.1. The computation of the pseudospectral abscissa is currently restricted to retarded time-delay systems. As mentioned in Chapter 2, the spectral abscissa of a particular retarded DDE corresponds to a finite number of rightmost characteristic roots. Consequently, also the pseudospectral abscissa typically corresponds to a finite number of points. To compute the pseudospectral abscissa we therefore solve the optimization problem in (7.3) using the gradient flow method (Section 4.7.2) by defining a path through the search space along which the real part of the rightmost eigenvalue monotonically increases. (For more details see, [27].) In contrast, recall from the stability analysis for neutral DDEs (Section 2.1.3) that for such differential equations the spectral abscissa might correspond to a vertical chain of characteristic roots and that the location of these chains might be sensitive to infinitesimal delay changes. Computing the pseudospectral abscissa of a NDDE is thus more complicated. For example, we need an additional step to find the smallest α

[4]If a term is not affected by the uncertainties, then one can just use an empty array instead of the uncertain matrix or delay.

for which the right half-plane $\{\lambda \in \mathbb{C} : \Re(\lambda) > \alpha\}$ only contains finitely many characteristic roots for all admissible uncertainty values (and arbitrarily small delay perturbations). For DDAEs the discussion is even more complex, see for example Section 4.4 in which we already restricted our attention to a specific uncertainty structure.

Remark 7.2. As the spectral abscissa is a nonconvex function of the entries of the state matrices and the delay values, the gradient flow method might end up in a locally rightmost point of the pseudospectrum. The `tds_psa` function will therefore re-run the gradient flow method from several initial points. Although we can only guarantee that the obtained value is an underestimate for the pseudospectral abscissa, for most test problems and ϵ sufficiently small, the global rightmost point of the pseudospectrum is found.

7.6 Conclusion

In this chapter we have illustrated the core functionality of the software package `TDS-CONTROL`, which allows to analyze and design feedback controllers for a broad range of LTI delay systems with discrete delays. The software and accompanying documentation are available from `https://gitlab.kuleuven.be/u0011378/tds-control`. The package is licensed under the GNU General Public License version 3. `TDS-CONTROL` integrates existing algorithms for stabilization [186], robust stability analysis [27], structured controller design [57] and H_∞-norm optimization [82].

Note that the approach for computing the pseudospectral abscissa is based on a similar approach as used in Chapter 4 to compute the robust strong H_∞-norm of an uncertain time-delay system, which exploited the equivalence between this quantity and the distance to instability of an uncertain delay differential algebraic equation.

CHAPTER

8 Conclusions

In this dissertation, we have analyzed and quantified the effect of certain model uncertainties on the behavior of dynamical systems with discrete delays, proposed robust controller design algorithms, developed a numerical algorithm that can be used for computing the H_∞-norm, an important quantity in robust control theory, of large-scale time-delay systems and developed a software package. More specifically, Chapter 3 considered the analysis and design of PID controllers with low-pass filtering of the derivative signal that are robust against sufficiently small modeling errors. In Chapter 4 we introduced the robust strong H_∞-norm, which quantifies the worst-case performance of an uncertain time-delay system while taking into account infinitesimal delay perturbations. Chapter 5 presented a scalable H_∞-controller design method for a class of networked systems. Subsequently, in Chapter 6 we developed a novel method to compute certain eigenvalues of large-scale Hamiltonian delay eigenvalue problems while preserving the symmetries of the spectrum. Finally, Chapter 7 introduced an integrated software package for the analysis and controller-design of time-delay systems with discrete delays. Below, we give a chapter-by-chapter overview of the main contributions of this thesis. Thereafter, we briefly discuss a few possible directions for future work.

8.1 Summary

Chapter 3 examined the closed-loop stability of the feedback interconnection of a dynamic system with state-delays and a PID controller. Motivated by a simple example (Example 3.1), we examined the effect of an arbitrarily small feedback delay (Section 3.3.1) and an arbitrarily accurate finite-difference approximation of the derivative signal (Section 3.3.2) on the exponential stability of the closed-loop system. We saw that under certain conditions on the derivative feedback gain (K_d) these perturbations may destroy exponential stability, even when made arbitrarily small. More specifically, these perturbations might introduce unstable characteristic roots that move to infinity without leaving the right half-plane as the size of the perturbation goes to zero. An intuitive way to resolve this fragility problem would therefore be to apply a low-pass filter to the derivative signal. However, as shown in Proposition 3.3, if $c(BK_dC) > 1$, this low-pass filter is itself destabilizing, even when the cut-off frequency is made arbitrarily large. Subsequently, we introduced a novel notion of well-posedness called *strong*

exponential stability in Section 3.4.2, which requires that there exists a $\hat{r} > 0$ such that the closed-loop system depicted in Figure 3.2 (in which the functions $R_1(\lambda; r_1)$, $R_2(\lambda; r_2)$, and $R_3(\lambda; r_3)$ satisfy Assumption 3.1) remains stable for all r_1, r_2, and r_3 in the half-open interval $[0, \hat{r})$. Proposition 3.4 showed that if the feedback interconnection of (3.1) and (3.2) is exponentially stable and if $c(BK_dC) < 1$, then the closed-loop system consisting of (3.1) and (3.12) (i.e., PID control with low-pass filtering of the derivative signal) is strongly exponentially stable. An example for which the regions in feedback parameter space corresponding to closed-loop exponential stability and strong exponential stability do not coincide was given in Section 3.4.3. Subsequently, Section 3.5 presented a novel numerical algorithm for the design of strongly stabilizing PID controllers with low-pass filtering of the derivative signal based on the direct optimization framework (Section 2.3.2). Finally, Section 3.6 presented extensions to systems with a relative degree larger than one, systems with an input delay, and systems with bounded uncertainties on the system matrices and the state delays.

Chapter 4 introduced the notion of the robust H_∞-norm for uncertain time-delay systems with real-valued uncertainties on the system matrices, which is a measure for robust performance. Special attention was paid to the potential sensitivity of the (robust) H_∞-norm of a time-delay system with multiple delays in the direct feed-through terms to infinitesimal perturbations on the delays. To resolve this potential fragility problem, we defined the robust *strong* H_∞-norm as the worst-case value of the strong H_∞-norm over all admissible uncertainty values. In contrast to the robust H_∞-norm, this quantity is a continuous function of both the system matrices and the delays. The main theoretical result of this section was Theorem 4.1 which provided a characterization of the robust (strong) H_∞-norm of an uncertain time-delay system in terms of the robust distance to instability of an uncertain delay differential algebraic equation. This characterization was subsequently illustrated using four examples, each focusing on a different destabilization mechanism, in Section 4.6. Finally, Section 4.7 introduced the first computational algorithm for exactly quantifying the robust strong H_∞-norm of an uncertain time-delay system.

Based on these results, **Chapter 5** presented a novel design method for the decentralized, robust control of a certain class of networked systems. More specifically, assuming that the dynamics of the individual subsystems and local controllers are identical and that the adjacency matrix describing the interconnection topology of the network satisfies Assumption 5.1, Theorem 5.1 states that the H_∞-norm of the overall closed-loop system corresponds to the maximal value of the H_∞-norm of a parameterized subsystem where the allowable parameter values correspond to the eigenvalues of the adjacency matrix of the network. By considering this parameter as a real-valued, scalar

uncertainty bounded to the interval $[a, b]$ (as defined in Assumption 5.1) the H_∞-norm of the overall network is upper bounded by the robust H_∞-norm of a single subsystem. This last quantity can be computed at a cost which does not depend on the number of subsystems. In contrast, the cost of computing the H_∞-norm for the complete networked system using the level-set method presented in [81], scales cubically with the number of subsystems. In Section 5.4 this result was used to derive a scalable H_∞-controller synthesis method consisting of minimizing this upper bound in the controller parameters instead of minimizing the actual H_∞-norm. Furthermore, if Assumption 5.1 holds for all N (= the number of subsystems) with the same interval $[a, b]$, then the aforementioned upper bound is valid for all N and the designed controller is in some sense robust against the number of subsystems. The resulting design procedure was illustrated using an example in Section 5.5.

In **Chapter 6**, we developed a structure-preserving infinite Arnoldi method to compute the eigenvalues of a large-scale Hamiltonian DEP closest to a given purely real or imaginary shift. On the one hand, the presented algorithm extends the existing methods for the standard eigenvalue problem [133], the generalized eigenvalue problem [131] and the polynomial eigenvalue problem [133] to the delay eigenvalue problem. On the other hand, it can be seen as a modification of the infinite Arnoldi method for general DEPs [99] to delay eigenvalue problems for which the spectrum admits Hamiltonian symmetry. The most important feature of the presented method is that the obtained approximations for simple, purely imaginary eigenvalues are typically simple, purely imaginary themselves, even in the presence of rounding errors. This feature makes the presented method appealing to be used as a component in a numerical method for computing the H_∞-norm of large-scale time-delay systems. After having derived the algorithm in terms of infinite-dimensional operators and function spaces in Section 6.3, Sections 6.4 and 6.5 described a numerical implementation in terms of finite-dimensional linear algebra operations for a zero and a non-zero shift, respectively. The practical applicability of these implementations was illustrated using two examples in Section 6.6.

Chapter 7 presented an integrated software package for the analysis and controller-design of linear-time invariant time-delay systems with discrete delays. Besides the code-base, an important aspect of the software package is the complementing manual that contains numerous examples, aimed at helping practitioners translate their own problems into the provided framework.

8.2 Future work

- In this thesis we have restricted our attention to the H_∞-norm. However, various design objectives in the robust control framework are formulated in terms of H_2-norm or mixed H_2-norm/H_∞-norm optimization problems [206]. For systems described by delay differential algebraic equations, it is however not trivial to verify whether the H_2-norm is finite as there might be "hidden" direct feed-through terms. Recently, a novel algorithm for checking the finite-ness of the H_2-norm has been presented in [72]. This result paves the way for developing novel algorithms for computing the H_2-norm of systems described by delay differential algebraic equations.

- The results in Chapter 6 can be generalized to Hamiltonian DEPs for which the leading identity matrix in (6.2) is replaced by a general (potentially singular) matrix N that satisfies $(JN)^\top = -JN$. This extension is necessary to enable the computation of the H_∞-norm of delay descriptor systems. However, if the matrix N is singular, the corresponding spectrum may contain vertical chains, similar as those encountered in Example 2.2 and Proposition 4.5, which furthermore may be sensitive to infinitesimal delay perturbations. In this case, a preliminary step is necessary to assure that these vertical chains are bounded away from the imaginary axis, even when sufficiently small delay perturbations are considered.

- This dissertation focused on systems with discrete delays. The presented results could be generalized to a broader class of functional differential equations, such as for example delay differential equations with distributed delays that arise in predictive control [139, Chapter 12] and biological systems [126].

- In this thesis, we have assumed that a (state-space) model for the considered systems (and the corresponding uncertainties) is given, likely obtained from first principles. Subsequently, a controller was designed based on this model and concepts from (robust) control theory such as minimizing the spectral abscissa or the H_∞-norm. However, a (recent) trend in the fields of system identification and control theory is the usage of tools from data analysis, statistics and machine learning, such as Koopman operator theory [129], reinforcement learning [177] and (deep) neural networks [102], to infer a model for the system or sometimes even directly a control law from data [39, 106]. It is an interesting question to see what strategy will prove dominant in the future, purely data-driven methods or methods based on first principles and (classical) control theory. Maybe the answer lies in an integration of both options [34, 113].

- Finally, although the proposed controller-design methods are capable of taking the effect of uncertainties into account, they assume that the model for the system (and the uncertainties) is known before hand (either via first principles or via a black-box data-driven approach) and remains unchanged over time. In contrast there is the recent development of adaptive, online control strategies, in which the controller improves its performance while in operation by evaluating the success of its actions and adapting its behavior accordingly [3, 7, 155]. It is an interesting question how one can guarantee that such control laws achieve stability and performance in practice.

APPENDIX

A Controlling the variable length pendulum: Analysis and design

Abstract

This chapter considers damping the swing of a pendulum by controlling its suspension length. We focus on the numerical solution of two open-loop optimal control problems. In the first problem we consider the velocity of the string length variation as the controlled input. The resulting solution suggests an instantaneous resetting of the string length at the swing angle equal to zero and at zero angular velocity, which is rather unrealistic from an application perspective. In the second optimization problem, we therefore consider a more realistic model which uses the force acting on the string as input, taking into account that the string can only exert a pull force. This leads to a more realistic (open-loop) control strategy. Subsequently, we briefly summarize the analysis of a bang-bang control law for the string length and the derivation of a Lyapunov-based feedback law for the force acting on the string obtained using a backstepping procedure. Finally, we experimentally compare this last feedback law with a time-delay based controller.

This chapter briefly summarizes results that were originally presented in [5], focusing on numerically solving two open-loop optimal control problems.

A.1 Introduction

In this chapter we study several control strategies to damp the swing of a pendulum by varying its suspension length. Even though the problem under consideration may seem purely theoretical, it has a high practical potential, particularly for cranes [1]. More specifically, consider the task of maneuvering a suspended payload from one position to another while taking into account trajectory constraints. An established technique for this problem is *input shaping*, in which the trajectory of the cable suspension point is shaped by a time-delay filter so that the payload sway is partly or fully pre-compensated [171, 170]. The presented research is motivated by the need to damp the residual oscillations of the payload at the final stage of the maneuver when the suspension point reaches the end-point position and remains fixed (as shown in the left-hand panel of Figure A.1). Such residual oscillations are very likely to appear even

when the previously mentioned method is applied, due to imperfections in the control system or external disturbances. Damping these residual oscillations by further maneuvering the suspension point may be inefficient or even impossible due to physical constraints. In this chapter we therefore study whether the Coriolis force acting on the payload can be utilized to damp the oscillation by changing the suspension length during the swing.

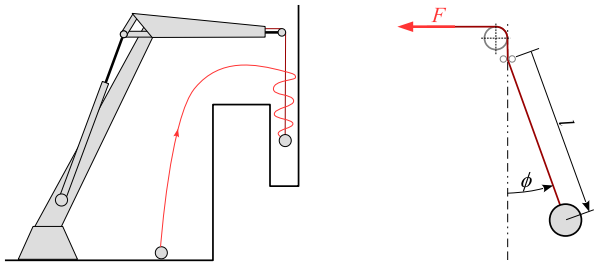

Figure A.1: Left: Problem motivation - damping the residual payload swing at the final stage of a crane maneuver using the Coriolis force acting on the payload; Right: Reformulation of the problem as controlling the variable length pendulum.

The use of the Coriolis force to damp the swing of a pendulum can be traced back to [176]. This work proposes a harmonic signal for the cable length that is synchronized with the swing motion using additional signal processing tools. In contrast, the closed-loop control law presented in [194] does not require any additional signal processing as synchronization is guaranteed by (delayed) feedback of the pendulum angle. The literature studying variable length pendulums is not limited to damping the swing. Let us for example mention the analysis of the periodic solutions induced by periodically varying the cable length [154, 204] and the analysis of the regimes of regular and chaotic motion when periodically varying the cable length [23].

The remainder of the chapter is organized as follows. Section A.2 presents the considered problem in more detail and introduces two state-space models that will be used throughout the chapter. Section A.3 considers two open-loop optimal control problems that are solved using a discretize-first approach. The next two sections briefly summarize the analysis of a bang-bang control law for the string length (Section A.4) and the derivation of a feedback law for the force acting on the string obtained using a backstepping procedure (Section A.5). The final section discusses an experimental comparison of this last feedback law with the time-delay based controller presented in [194].

A.2 Problem formulation

We start with deriving two different state-space models for the set-up depicted at the right-hand side of Figure A.1. In these models, the cable's mass and the friction corresponding to the lateral swing of the pendulum are neglected. The friction related to the contact of the cable at the pivot point is however taken into account and the corresponding friction coefficient is assumed to be known (denoted by κ). Further, let m stand for the mass of the load, g for the gravitational acceleration, $\phi(t)$ for the swing angle, and $l(t)$ for the cable length. Given these prerequisites, standard modeling gives the following system of nonlinear ordinary differential equations

$$\begin{cases} ml(t)\ddot{\phi}(t) + 2m\dot{l}(t)\dot{\phi}(t) + mg\sin\phi(t) = 0, & \text{(A.1a)} \\ m\ddot{l}(t) - ml(t)\dot{\phi}^2(t) - mg\cos\phi(t) + \kappa\dot{l}(t) + F(t) = 0. & \text{(A.1b)} \end{cases}$$

Furthermore, we assume that the swing angle ϕ is restricted to the open interval $(-\pi/2, \pi/2)$, as $|\phi| > \pi/2$ would cause (at least initially) free fall of the load rather than a pendulum-like motion. Finally, the string length l should obviously always be strictly positive. Below we will convert these ODEs to two different first-order state space models.

Firstly, using $x_1(t) := \phi(t)$, $x_2(t) := \dot{\phi}(t)$, $x_3(t) := l(t)$, and $u(t) := \dot{l}(t)$, we obtain

$$\begin{cases} \dot{x}_1(t) &= x_2(t), \\ \dot{x}_2(t) &= -\big(2x_2(t)u(t) + g\sin\big(x_1(t)\big)\big)/x_3(t), \\ \dot{x}_3(t) &= u(t). \end{cases} \qquad \text{(A.2)}$$

Note that in this model the velocity of the string length variation $\dot{l}$ is considered to be the controlled input, meaning that the dynamics in (A.1b) are ignored. Next, let us briefly analyze the linearization of this model around the equilibrium $x_{eq} = (0, 0, l_0)^\top$ (with l_0 some desired suspension length) and $u = 0$. Straightforward computations give that this linearization is equal to

$$\dot{\xi}(t) = \begin{bmatrix} 0 & 1 & 0 \\ -g/l_0 & 0 & 0 \\ 0 & 0 & 0 \end{bmatrix} \xi(t) + \begin{bmatrix} 0 \\ 0 \\ 1 \end{bmatrix} u(t) \text{ with } \xi(t) := x(t) - x_{eq}. \qquad \text{(A.3)}$$

Notice that this linearization is neither controllable, nor stabilizable, meaning that when using a smooth feedback law in the neighborhood of this equilibrium local exponential stability cannot be achieved.

Secondly, we consider the following four-dimensional state-space representation

$$\begin{cases} \dot{x}_1(t) &= x_2(t), \\ \dot{x}_2(t) &= -\left(2x_2(t)x_4(t) + g\sin\left(x_1(t)\right)\right)/x_3(t), \\ \dot{x}_3(t) &= x_4(t), \\ \dot{x}_4(t) &= \overline{u}(t) \end{cases} \tag{A.4}$$

with $x_1(t) := \phi(t)$, $x_2(t) := \dot{\phi}(t)$, $x_3(t) := l(t)$, $x_4(t) := \dot{l}(t)$, and

$$\overline{u}(t) := \ddot{l}(t) = l(t)\dot{\phi}(t)^2 + g\cos\left(\phi(t)\right) - (\kappa/m)\dot{l}(t) - F(t)/m. \tag{A.5}$$

Here, (A.5) is due to the previously ignored dynamics in (A.1b). Considering this four dimensional state-space model has several advantages. Firstly, it allows for a more realistic description of the string length variation as in reality the string can not push ($F(t)$ can not be negative). Secondly, it allows to explicitly take into account the friction of the cable at the pivot point. Finally note that when using this model a control law for $\overline{u}$ can easily be transformed into a law for the force F, which is the actual controlled input of the system.

A.3 Numerical optimization based open-loop control

To get an intuition for a good strategy to control the variable length pendulum, we will study two optimal control problems. Firstly, we will consider the following optimal control problem based on state-space model (A.2):

$$\begin{aligned} \underset{u}{\text{minimize}} \quad & \frac{1}{2}\int_0^T \left(x_1^2(t) + x_2^2(t)\right)\mathrm{d}t + \frac{\rho}{2}\left(x_1^2(T) + x_2^2(T)\right), \\ \text{subjected to} \quad & \text{(A.2)}, \\ & |x_3(t) - l_0| \leq \Delta l \text{ for all } t \in [0, T], \\ & x_1(0) = \pi/2,\ x_2(0) = 0,\ \text{and } x_3(0) = l_0 \end{aligned} \tag{A.6}$$

with the control horizon $T = 20$ s, $g = 9.81$ m/s^2, a nominal string length l_0 of 1 m, a maximal derivation from this nominal length of $\Delta l = 0.15$ m, and an arbitrary chosen weighting parameter $\rho = 40$. To compute an approximate solution for this continuous-time optimization problem, we employ a discretize-first approach. The states and control inputs are discretized by restricting to their values at equidistant time-points with time-step $h = 1/30$ s. The cost

function is discretized accordingly. A Runge-Kutta method of order four is used to approximate the system's dynamics in which the input signal is assumed to be zero-order hold. We now obtain a nonlinear optimization problem with the optimization variables being the discretized states and controls (we are using a so-called simultaneous approach), and the constraints being the discretized dynamics, the constraint on the maximal length variation and the initial state. We solve this optimization problem in MATLAB using the function `fmincon`. The derivatives of the nonlinear constraints are obtained using automatic differentiation, more specifically using ADiGator [198]. As initial value for the optimization variable, we used the discretized states and input corresponding to the undamped pendulum.

Figure A.2 plots the obtained solution in the time interval $[0,\ 10]$. We observe that the resulting trajectory for the string length approximates a bang-bang signal, quickly changing between its extreme values. As a consequence, the input signal ($u = \dot{l}$) is close to impulsive, resulting in an (almost) discontinuous trajectory for $x_2 = \dot{\phi}$. The control law achieves good damping for the pendulum's swing. However, the amplitude of the string length variation does not vanish over time, which is necessary to compensate for the non-controllability of the linearization (A.3) at the equilibrium to be reached.

By taking $\dot{l}$ as input, it is assumed that the string length can change arbitrarily fast. In the real-life setup however the string can only pull and the speed with which the string can extend is limited by the centrifugal and gravitational forces, or in other words $F(t)$ in (A.1b) can only be positive. To this end, we now will consider the following optimal control problem based on the four dimensional state-space model in (A.4):

$$
\begin{aligned}
\underset{u}{\text{minimize}} \quad & \frac{1}{2}\int_0^T \big(x_1^2(t) + x_2^2(t)\big)\,\mathrm{d}t + \frac{\rho}{2}\big(x_1^2(T) + x_2^2(T)\big), \\
\text{subjected to} \quad & \text{(A.4)}, \\
& F(t) = ml(t)\dot{\phi}(t)^2 + mg\cos\big(\phi(t)\big) - \kappa\dot{l}(t) - m\overline{u}(t) \geq 0, \\
& |x_3(t) - l_0| \leq \Delta l \text{ for all } t \in [0, T], \\
& x_1(0) = \pi/2,\ x_2(0) = 0, \text{ and } x_3(0) = l_0.
\end{aligned}
\tag{A.7}
$$

We use the same parameters as before and $\kappa = 0$. To solve this optimization problem we use a similar discretize-first approach as above. However, instead of using a Runge-Kutta discretization we use a forward Euler discretization, as the former results in a optimal control trajectory with spurious oscillations due the interplay between the used discretization scheme and the minimization

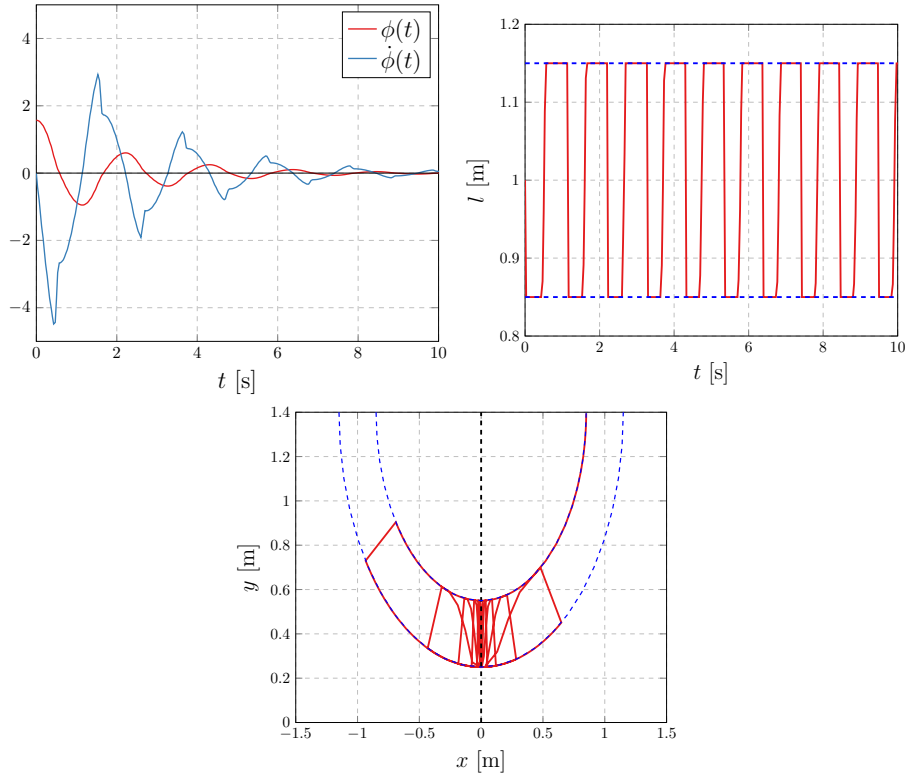

Figure A.2: Numerical solution to the optimal control problem (A.6). Top - left: the time evolution of the pendulum's angle (red) and its angular velocity (blue). Top - right: the time evolution of the string length. Bottom: the Carthesian trajectory of the mass.

procedure. To offset the lower order of this method we will reduce the step size to $h = 1/40$ s.

Figure A.3 shows the trajectories corresponding to the numerical solution of (A.7). Each cycle in these trajectories, which has half the period of the motion of the pendulum, can be understood as follow:

1. An impulsive force is applied to shorten the string;
2. The gravitational and centrifugal forces slow down the shortening. The initial impulsive force was chosen such that the shortening stops ($\dot{l} = 0$) at exactly $l_0 - \Delta l$;

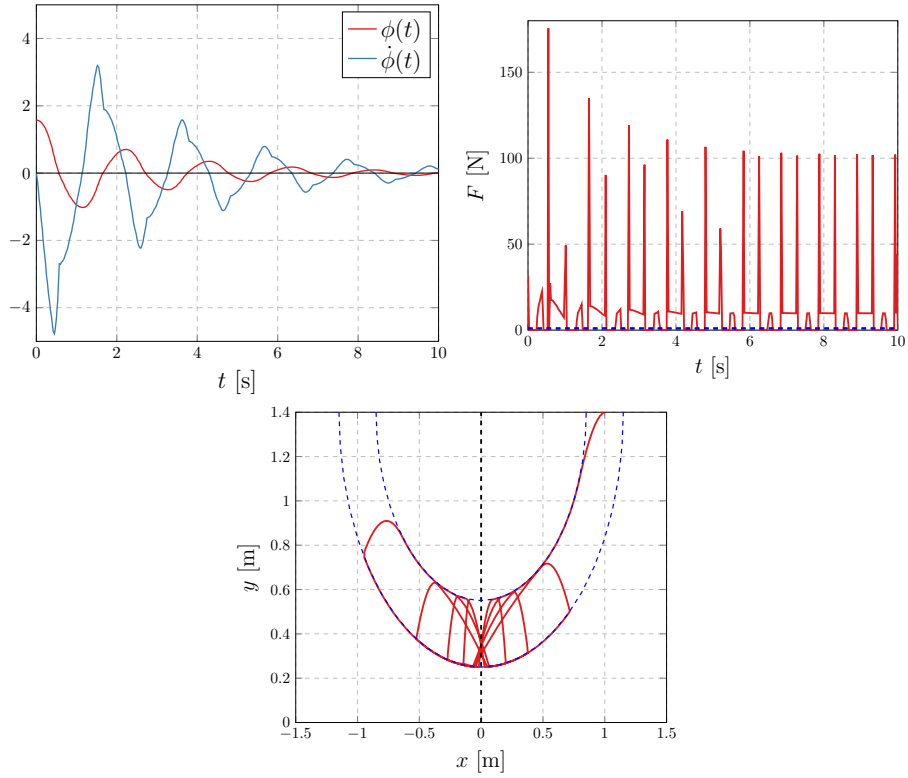

Figure A.3: Numerical solution to the optimal control problem (A.7). Top - left: the time evolution of the pendulum's angle (red) and its angular velocity (blue). Top - right: the time evolution of force F. Bottom: the Carthesian trajectory of the mass.

3. A pull force, increasing in size, is applied to counter gravitational and centrifugal forces and keep the string at its minimal length;

4. The pulling force is stopped. The string length increases due to the gravitational and centrifugal forces and reaches its maximal value around $\phi = 0$;

5. An impulsive force is applied to prevent the string length from exceeding its maximal value;

6. A force, decreasing in size, is applied to counter the gravitational and centrifugal forces and keep the string at its maximal length.

Compared to the result obtained with the idealized model in Figure A.2, the retraction at $\dot{\phi} = 0$ is no longer instantaneous, as the shortening of the string can not be stopped using a "push" force, but needs to be gradually slowed down by the gravitational and centrifugal forces.

It is clear that both control strategy cannot be applied in a open-loop fashion as they are very sensitive to perturbations. Firstly, the input sequence must be carefully synchronized with the motion of the pendulum. Secondly, when using the second law, the size of impulsive force in step 1 must be chosen carefully to precisely match the gravitational and centrifugal forces otherwise it will undershoot or overshoot the minimal length.

A.4 Analysis of a bang-bang control law

Inspired by the numerical solution for the optimal control problem (A.6), let us analyze the following bang-bang control law

$$l(t) = \begin{cases} l_0 - \Delta l & \text{when} \quad \phi(t)\dot{\phi}(t) < 0, \\ l_0 + \Delta l & \text{when} \quad \phi(t)\dot{\phi}(t) \geq 0. \end{cases} \tag{A.8}$$

This control law can be understood as follows, when the pendulum swings up, the string length is extended to its maximal value and when the pendulum swings down it is retracted to its minimal length. In other words, when the pendulum passes through $\phi = 0$ the string is extended to its maximal length, while it is retracted when the angular velocity becomes zero.

In terms of the state-space model (A.2), the closed-loop interconnection with the control law (A.8) can be described in terms of a hybrid system, which combines continuous and discrete dynamics. More specifically, at states for which $\phi \neq 0$ and $\dot{\phi} \neq 0$ the dynamics correspond to those of an undamped pendulum with a constant string length. However, if either $\phi = 0$ or $\dot{\phi} = 0$, then the load is instantaneously re-positioned causing discontinuous jumps in the trajectories of both $\dot{\phi}$ and l. Notice that these jumps also induce a switch in the dynamics as the string's length changes.

To understand the damping effect of this control law, let us examine the behavior of the pendulum during half a period of its swing. Assume we start from $\phi = 0$, $\dot{\phi} = \omega_0$ (with $\omega_0 > 0$ sufficiently small to avoid leaving the domain) and $l = l_0 + \Delta l$. The load will swing up till it reaches the maximal angle $\phi_{\max}$ with

$$mg(l_0 + \Delta l)\big(1 - \cos(\phi_{\max})\big) = \frac{m(l_0 + \Delta l)^2\omega_0^2}{2},$$

due to the conservation of energy. Subsequently, the string is shortened. Notice that this action does not change the angular velocity (which remains zero). Then, the pendulum swings back until it reaches the angle $\phi = 0$. The corresponding angular velocity ω_1 follows from

$$\frac{m(l_0 - \Delta l)^2 \omega_1^2}{2} = mg(l_0 - \Delta l)(1 - \cos(\phi_{\max})),$$

which is again due to the conservation of energy. During this motion, the angular velocity has thus increased with a factor

$$\frac{\omega_1}{\omega_0} = \left(\frac{l_0 + \Delta l}{l_0 - \Delta l}\right)^{\frac{1}{2}} > 1.$$

However, next the string is extended to its maximal length $l_0 + \Delta l$. As instantaneously re-positioning the mass does not change its angular momentum, the resulting angular velocity ω_2 follows from

$$m(l_0 + \Delta l)^2 \omega_2 = m(l_0 - \Delta l)^2 \omega_1 \text{ such that } \frac{\omega_2}{\omega_1} = \left(\frac{l_0 - \Delta l}{l_0 + \Delta l}\right)^2.$$

In combination with the result above, we conclude that each half-period the angular velocity is reduced with a factor

$$\frac{\omega_2}{\omega_0} = \left(\frac{l_0 - \Delta l}{l_0 + \Delta l}\right)^{\frac{3}{2}} < 1.$$

A.5 Backstepping procedure

Next, we examine a feedback controller for which stability is proven based on Lyapunov's second method. More specifically, starting from a stabilizing controller for the three-dimensional state-space model (A.2) a feedback law for the four-dimensional model (A.4), which takes the acceleration of the cable length variation as controlled input, is derived using a backstepping procedure [105, Section 14.3]. An advantage of deriving a control law for the suspension length's acceleration is that it is easy to implement, as it can directly be converted into a control law for the force F. In contrast, to realize a control law in terms of the suspension length or the velocity of its variation, a secondary controller is needed that outputs the required force F such that the length or velocity trajectory outputed by the primary control law is followed as close as possible. To achieve the expected performance in practice, a proper tuning of this additional controller is necessary. Furthermore, by considering (A.1b) the friction term $\kappa \dot{l}$ can explicitly be taken into account.

In [6] the following feedback law for (A.2) was derived using the control Lyapunov function framework:

$$u(x_1, x_2, x_3) = -K\left[g(1 - \cos x_1) - x_3 x_2^2 + c_1(x_3 - l_0)\right] \tag{A.9}$$

with $K > 0$ and $c_1 > 0$ free design parameters and the corresponding Lyapunov candidate function

$$V(x_1, x_2, x_3) = g x_3 (1 - \cos x_1) + \frac{x_3^2 x_2^2}{2} + c_1 \frac{(x_3 - l_0)^2}{2},$$

in which the penalty term $c_1 \frac{(x_3 - l_0)^2}{2}$ forces the control law to keep the suspension length close to its nominal length. Using LaSalle's invariance principle it can be shown that this control law asymptotically stabilizes the equilibrium $(0, 0, l_0)$.

The backstepping procedure now introduces the following extended Lyapunov candidate function for the four dimensional model (A.4):

$$\overline{V}(x_1, x_2, x_3, x_4) = V(x_1, x_2, x_3) + \frac{(x_4 - u(x_1, x_2, x_3))}{2},$$

in which the penalty term $\frac{(x_4 - u(x_1, x_2, x_3))}{2}$ forces $\dot{l}$ to closely follow the control input for the three dimensional model. The derivative of this function along a trajectory of (A.4) can be written as

$$\frac{\mathrm{d}}{\mathrm{d}t}\overline{V} = -\frac{u(x_1, x_2, x_3)^2}{K} - (x_4 - u(x_1, x_2, x_3)) \times \left[\frac{u(x_1, x_2, x_3)}{K} + \frac{\mathrm{d}}{\mathrm{d}t} u(x_1, x_2, x_3) - \overline{u}\right]$$

with $\frac{\mathrm{d}}{\mathrm{d}t} u(x_1, x_2, x_3)$ the time derivative of (A.9) along a trajectory of (A.4). Choosing

$$\bar{u}(x) = \frac{u(x_1, x_2, x_3)}{K} + \frac{\mathrm{d}}{\mathrm{d}t} u(x_1, x_2, x_3) - K_2 \left(x_4 - u(x_1, x_2, x_3)\right) \tag{A.10}$$

with $K_2 > 0$, results in

$$\frac{\mathrm{d}}{\mathrm{d}t}\overline{V} = -\frac{u(x_1, x_2, x_3)^2}{K} - K_2\big(x_4 - u(x_1, x_2, x_3)\big)^2 \leq 0.$$

Asymptotic stability now follows from a similar derivation as in the proof for the stability of the control law for the three dimensional model in [6].

Finally, note that (A.10) does not take into account that the string can not exert a pull force. When implementing this law, the controller should be supplemented with a saturation function that puts F to zero when it becomes negative.

A.6 Conclusion

In [5, Section 5], the control law (A.10) is compared experimentally with the following time-delay based feedback law from [194]

$$l(t) = l_0 - \left(\frac{4}{3}\xi l_0\right) \frac{\phi(t-\tau_2)^2 - e^{-\xi\pi}\phi(t-\tau_1-\tau_2)^2}{\phi(t-\tau_2)^2 + e^{-\xi\pi}\phi(t-\tau_1-\tau_2)^2} \tag{A.11}$$

with $\tau_1 = \frac{\pi}{2\Omega}$, $\tau_2 = \frac{\pi}{4\Omega}$, $\Omega = \sqrt{g/l}$ and ξ a tuning parameter that affects the damping rate of the pendulum's swing. It can be shown that this feedback law generates a sinusoidal-like signal for the string length whose period is equal to half the period of the pendulum's swing (and an amplitude that depends on ξ). In some sense, this control law can thus be seen as an approximation for the block wave in the bang-bang control law (A.8).

Figure A.4 shows the time-evolution of the swing angle and the string length for control laws (A.10) and (A.11). Initially both laws have equivalent damping performance. However, the pendulum's swing does not seem to vanish completely when using the Lyapunov-based controller. The slow damping for this control law is not surprising as it lacks local *exponential* stability. (The uncontrollability of the linearization (A.3) around the desired equilibrium point implies that exponential stability can not be achieved using a smooth feedback law.) In contrast, the damping efficiency of the time-delay based control law (A.11) can be attributed to the fact that it keeps the amplitude of the string length variation constant, even when the swing is already significantly suppressed. This gain in damping performance comes however with a considerable drawback: when the amplitude of the swing becomes small, noise will dominate the angle measurement and cause unpredictable jerky behavior. The time-delay based controller must therefore be switched off once the pendulum's swing is sufficiently damped. This is not the case for (A.10) which is entirely safe in this aspect, as the amplitude of the string length variation goes to zero when the amplitude of the swing becomes small.

Another advantage of the feedback law (A.10) over (A.11) is that it can be applied directly to a wide variety of crane set-ups as it only depends on some basic parameters such as the mass of the load and the required nominal length. On the contrary, feedback law (A.11) requires the tuning of an additional PD controller for the force F such that the string length dictated by (A.11) is closely followed.

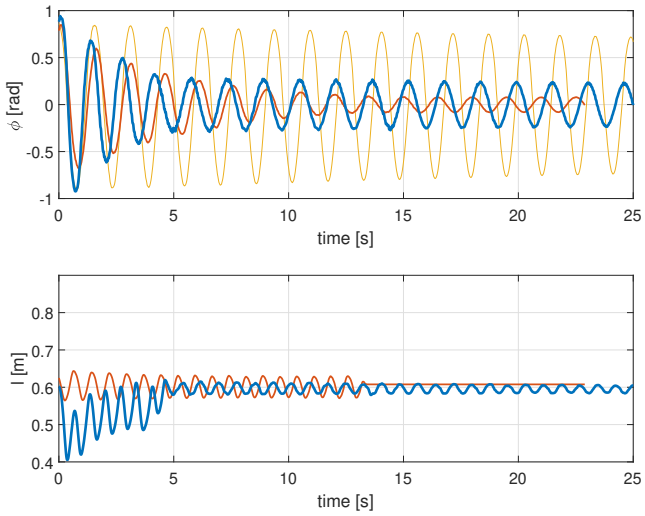

Figure A.4: The experimental time-evolution of the pendulum's angle (top) and the string length (bottom) for the backstepping based control law (A.10) (blue) and the time-delay based control law (A.11) (red). The time-evolution of the undamped swing angle for the nominal suspension length l_0 is superimposed (yellow).

APPENDIX

B Additional proofs for Chapter 6

B.1 Proof of Lemma 6.1

Here we restrict ourselves to the case $\sigma \neq 0$ as the proof for $\sigma = 0$ is similar. Using the definition of the bilinear form $\mathbf{B}(\cdot,\cdot)$ given in (6.14), and using (6.17) we find

$$\begin{aligned}
\mathbf{B}\left(\mathcal{R}_\sigma^{-1}\varphi, J\psi\right) = -\Bigg[& \psi(0)^\top J\Big(\mathrm{C}_\sigma[\varphi] + \mathrm{C}_{-\sigma}[\varphi]\Big) + \\
& \sum_{k=1}^{m} \Bigg(\int_0^{\tau_k} \psi(\theta)^\top J H_{-k} \Bigg[\Bigg(\mathrm{C}_\sigma[\varphi] + \int_0^{\theta-\tau_k} \tfrac{\varphi(\eta)}{2\sigma} e^{-\sigma\eta}\,\mathrm{d}\eta \Bigg) e^{\sigma(\theta-\tau_k)} + \\
& \qquad \Bigg(\mathrm{C}_{-\sigma}[\varphi] - \int_0^{\theta-\tau_k} \tfrac{\varphi(\eta)}{2\sigma} e^{\sigma\eta}\,\mathrm{d}\eta \Bigg) e^{-\sigma(\theta-\tau_k)} \Bigg]\,\mathrm{d}\theta \\
& - \int_0^{\tau_k} \psi(\theta-\tau_k)^\top J H_k \Bigg[\Bigg(\mathrm{C}_\sigma[\varphi] + \int_0^{\theta} \tfrac{\varphi(\eta)}{2\sigma} e^{-\sigma\eta}\,\mathrm{d}\eta \Bigg) e^{\sigma\theta} + \\
& \qquad \Bigg(\mathrm{C}_{-\sigma}[\varphi] - \int_0^{\theta} \tfrac{\varphi(\eta)}{2\sigma} e^{\sigma\eta}\,\mathrm{d}\eta \Bigg) e^{-\sigma\theta} \Bigg]\,\mathrm{d}\theta \Bigg) \Bigg].
\end{aligned}$$

Firstly, observe that

$$\begin{aligned}
& \int_0^{\tau_k} \psi(\theta)^\top J H_{-k} \int_0^{\theta-\tau_k} \tfrac{\varphi(\eta)}{2\sigma} e^{-\sigma\eta}\,\mathrm{d}\eta\; e^{\sigma(\theta-\tau_k)}\,\mathrm{d}\theta \\
& \qquad = \int_0^{-\tau_k} \int_0^{\tau_k+\eta} \psi(\theta)^\top e^{\sigma(\theta-\tau_k)}\,\mathrm{d}\theta\; J H_{-k} \tfrac{\varphi(\eta)}{2\sigma} e^{-\sigma\eta}\,\mathrm{d}\eta \\
& \qquad = \int_{\tau_k}^{0} \int_0^{\hat\eta} \psi(\theta)^\top e^{\sigma(\theta-\tau_k)}\,\mathrm{d}\theta\; J H_{-k} \tfrac{\varphi(\hat\eta-\tau_k)}{2\sigma} e^{-\sigma(\hat\eta-\tau_k)}\,\mathrm{d}\hat\eta \\
& \qquad = -\int_0^{\tau_k} \int_0^{\hat\eta} \tfrac{\psi(\theta)}{2\sigma}^\top e^{\sigma\theta}\,\mathrm{d}\theta\; e^{-\sigma\hat\eta} J H_{-k} \varphi(\hat\eta-\tau_k)\,\mathrm{d}\hat\eta,
\end{aligned}$$

in which we first interchanged the integrating variables, then made the change of variable $\hat{\eta} = \tau_k + \eta$ and finally interchanged the integration boundaries and reordered the terms. Using the same procedure we find:

$$-\int_0^{\tau_k} \psi(\theta)^\top J H_{-k} \int_0^{\theta-\tau_k} \tfrac{\varphi(\eta)}{2\sigma} e^{\sigma\eta}\,\mathrm{d}\eta\; e^{-\sigma(\theta-\tau_k)}\,\mathrm{d}\theta =$$

$$\int_0^{\tau_k}\int_0^{\hat{\eta}} \tfrac{\psi(\theta)}{2\sigma}^\top e^{-\sigma\theta}\,\mathrm{d}\theta e^{\sigma\hat{\eta}} J H_{-k}\varphi(\hat{\eta}-\tau_k)\,\mathrm{d}\hat{\eta}.$$

In a similar fashion we obtain:

$$-\int_0^{\tau_k} \psi(\theta-\tau_k)^\top J H_k \int_0^{\theta} \tfrac{\varphi(\eta)}{2\sigma} e^{-\sigma\eta}\,\mathrm{d}\eta e^{\sigma\theta}\,\mathrm{d}\theta =$$

$$\int_0^{\tau_k}\int_0^{\eta-\tau_k} \tfrac{\psi(\hat{\theta})}{2\sigma}^\top e^{\sigma\hat{\theta}}\,\mathrm{d}\hat{\theta} e^{-\sigma(\eta-\tau_k)} J H_k \varphi(\eta)\,\mathrm{d}\eta$$

and

$$\int_0^{\tau_k} \psi(\theta-\tau_k)^\top J H_k \int_0^{\theta} \tfrac{\varphi(\eta)}{2\sigma} e^{\sigma\eta}\,\mathrm{d}\eta e^{-\sigma\theta}\,\mathrm{d}\theta =$$

$$-\int_0^{\tau_k}\int_0^{\eta-\tau_k} \tfrac{\psi(\hat{\theta})}{2\sigma}^\top e^{-\sigma\hat{\theta}}\,\mathrm{d}\hat{\theta} e^{\sigma(\eta-\tau_k)} J H_k \varphi(\eta)\,\mathrm{d}\eta,$$

in which we used the change of variables $\hat{\theta} = \theta - \tau_k$. Next, by grouping the terms with $\mathrm{C}_\sigma[\varphi]$ and using $J^\top = -J$, $JH_{-k} = (JH_k)^\top$ and $J\big(2\sigma M(\sigma)\big)^{-1} = -\big(2\sigma M(-\sigma)\big)^{-T} J$ we find

$$\left(\psi(0)^\top J + \sum_{k=1}^m \left[\int_0^{\tau_k} \psi(\theta)^\top J H_{-k} e^{\sigma(\theta-\tau_k)}\,\mathrm{d}\theta - \int_0^{\tau_k} \psi(\theta-\tau_k)^\top J H_k e^{\sigma\theta}\,\mathrm{d}\theta\right]\right) C_\sigma[\varphi]$$

$$= \left(\psi(0)^\top - \sum_{k=1}^m \left[\int_0^{\tau_k} \psi(\theta)^\top H_k^\top e^{\sigma(\theta-\tau_k)}\,\mathrm{d}\theta - \int_0^{\tau_k} \psi(\theta-\tau_k)^\top H_{-k}^\top e^{\sigma\theta}\,\mathrm{d}\theta\right]\right) J\mathrm{C}_\sigma[\varphi]$$

$$= \mathrm{C}_{-\sigma}[\psi]^\top J \left(\varphi(0) - \sum_{k=1}^m \Big[- H_{-k} \int_0^{\tau_k} \varphi(\eta-\tau_k) e^{-\sigma\eta}\,\mathrm{d}\eta + H_k \int_0^{\tau_k} \varphi(\eta) e^{-\sigma(\eta-\tau_k)}\,\mathrm{d}\eta\Big]\right).$$

Similarly for the terms with $C_{-\sigma}[\varphi]$ we find

$$\left(\psi(0)^\top J + \sum_{k=1}^{m}\left[\int_0^{\tau_k}\psi(\theta)^\top J H_{-k} e^{-\sigma(\theta-\tau_k)}\,\mathrm{d}\theta - \int_0^{\tau_k}\varphi(\theta-\tau_k)^\top J H_k e^{-\sigma\theta}\,\mathrm{d}\theta\right]\right)\mathrm{C}_{-\sigma}[\varphi]$$

$$= C_\sigma[\psi]^\top J\left(\varphi(0) + \sum_{k=1}^{m}\left[H_{-k}\int_0^{\tau_k}\varphi(\eta-\tau_k)e^{\sigma\eta}\,\mathrm{d}\eta - H_k\int_0^{\tau_k}\varphi(\eta)e^{\sigma(\eta-\tau_k)}\,\mathrm{d}\eta\right]\right).$$

Combining all these relations, we obtain the desired result.

B.2 Proof that $\mathbf{B}(\cdot, J\cdot)$ is anti-symmetric

Lemma B.1. The bilinear form $\mathbf{B}(\cdot, J\cdot)$ is anti-symmetric, this means that the equality $\mathbf{B}(\varphi, J\psi) = -\mathbf{B}(\psi, J\varphi)$ holds.

Proof.

$$\begin{aligned}
\mathbf{B}(\varphi, J\psi) &= -\Big[\psi(0)^\top J\varphi(0) + \\
&\qquad \sum_{k=1}^{m}\Big(\int_0^{\tau_k}\psi(\theta)^\top J H_{-k}\varphi(\theta-\tau_k)\,\mathrm{d}\theta - \int_0^{\tau_k}\psi(\theta-\tau_k)^\top J H_k\varphi(\theta)\,\mathrm{d}\theta\Big)\Big] \\
&= -\Big[\varphi(0)^\top J^\top\psi(0) + \\
&\qquad \sum_{k=1}^{m}\Big(\int_0^{\tau_k}\varphi(\theta-\tau_k)^\top (JH_{-k})^\top\psi(\theta)\,\mathrm{d}\theta - \int_0^{\tau_k}\varphi(\theta)^\top (JH_k)^\top\psi(\theta-\tau_k)\,\mathrm{d}\theta\Big)\Big] \\
&= \Big[\varphi(0)^\top J\psi(0) + \\
&\qquad \sum_{k=1}^{m}\Big(\int_0^{\tau_k}\varphi(\theta)^\top J H_{-k}\psi(\theta-\tau_k)\,\mathrm{d}\theta - \int_0^{\tau_k}\varphi(\theta-\tau_k)^\top J H_k\psi(\theta)\,\mathrm{d}\theta\Big)\Big] \\
&= -\mathbf{B}(\psi, J\varphi)
\end{aligned}$$

□

B.3 Derivation of the extension step for $\sigma = 0$

Let $\phi_i(\theta)$ and $\varphi_{i+1}(\theta)$ be as defined in Theorem 6.2, then the equality $\mathcal{R}_0\varphi_{i+1} = \phi_i$ becomes

$$\Big(\mathcal{R}_0\varphi_{i+1}(\theta) = \Big) \sum_{l=2}^{N_i+2} \frac{v_l^{(i+1)}}{(\tau_m)^2} T_l''\left(\frac{\theta}{\tau_m}\right) = \sum_{l=0}^{N_i} q_l^{(i)} T_l\left(\frac{\theta}{\tau_m}\right) \Big(= \phi_i(\theta)\Big).$$

Expression (6.23) now follows by noting that

$$\begin{aligned} T_0(t) &= T_2''(t)/4, \\ T_1(t) &= T_3''(t)/24, \\ T_2(t) &= T_4''(t)/48 - T_2''(t)/6, \text{ and} \\ T_l(t) &= \frac{T_{l+2}''(t)}{4(l+1)(l+2)} - \frac{T_l''(t)}{2(l+1)(l-1)} + \frac{T_{l-2}''(t)}{4(l-1)(l-2)} \text{ for } l \geq 3. \end{aligned} \tag{B.1}$$

The expressions for $v_1^{(i+1)}$ follows directly from (6.16) and using this result $v_0^{(i+1)}$ can be computed from (6.15).

B.4 Derivation of the extension step for $\sigma = \jmath\omega$

Let ϕ_i and φ_{i+1} be as defined in (6.30) and (6.31), then the equality $\mathcal{R}_\sigma\varphi_{i+1} = \phi_i$ becomes

$$\begin{aligned} &\left[\frac{2\jmath\omega}{\tau_m} \sum_{l=1}^{N_i+1} v_l^{(i+1)} T_l'\left(\tfrac{\theta}{\tau_m}\right) + \sum_{l=2}^{N_i+1} \frac{v_l^{(i+1)}}{\tau_m^2} T_l''\left(\tfrac{\theta}{\tau_m}\right)\right] e^{\jmath\omega\theta} + \\ &\qquad \left[-\frac{2\jmath\omega}{\tau_m} \sum_{l=1}^{N_i+1} \overline{v_l^{(i+1)}} T_l'\left(\tfrac{\theta}{\tau_m}\right) + \sum_{l=2}^{N_i+1} \frac{\overline{v_l^{(i+1)}}}{\tau_m^2} T_l''\left(\tfrac{\theta}{\tau_m}\right)\right] e^{-\jmath\omega\theta} \\ &\qquad\qquad = \sum_{l=0}^{N_i} q_l^{(i)} T_l\left(\tfrac{\theta}{\tau_m}\right) e^{\jmath\omega\theta} + \sum_{l=0}^{N_i} \overline{q_l^{(i)}} T_l\left(\tfrac{\theta}{\tau_m}\right) e^{-\jmath\omega\theta}. \end{aligned}$$

Matching the terms associated with $e^{\jmath\omega\theta}$ and $e^{-\jmath\omega\theta}$, gives the equality

$$\frac{2\jmath\omega}{\tau_m} \sum_{l=1}^{N_i+1} v_l^{(i+1)} T_l'\left(\tfrac{\theta}{\tau_m}\right) + \sum_{l=2}^{N_i+1} \frac{v_l^{(i+1)}}{\tau_m^2} T_l''\left(\tfrac{\theta}{\tau_m}\right) = q_l^{(i)} T_l\left(\tfrac{\theta}{\tau_m}\right).$$

Using (B.1) in combination with

$$T_1'(t) = T_2''(t)/4 \text{ and}$$

$$T_l'(t) = \frac{T_{l+1}''(t)}{2(l+1)} - \frac{T_{l-1}''(t)}{2(l-1)} \text{ for } l \geq 2$$

results in (6.32). The expression for $v_0^{(i+1)}$ follows again from (6.15) and (6.16).

Bibliography

[1] Abdel-Rahman, E. M., Nayfeh, A. H., and Masoud, Z. N. Dynamics and Control of Cranes: A Review. *Journal of Vibration and Control*, 9(7):863–908, 2003 (Cited on page 173).

[2] Ahmed, N. and Fisher, P. Study of algorithmic properties of Chebyshev coefficients. *International Journal of Computer Mathematics*, 2(1–4):307–317, 1968 (Cited on page 140).

[3] Alamir, M. Learning against uncertainty in control engineering. *Annual Reviews in Control*, 53:19–29, 2022 (Cited on page 171).

[4] Aliyev, N., Benner, P., Mengi, E., Schwerdtner, P., and Voigt, M. Large-scale computation of $\mathcal{L}_\infty$-norms by a greedy subspace method. *SIAM Journal on Matrix Analysis and Applications*, 38(4):1496–1516, 2017 (Cited on pages 4, 27).

[5] Anderle, M., Appeltans, P., Čelikovský, S., Michiels, W., and Vyhlídal, T. Controlling the variable length pendulum: Analysis and Lyapunov based design methods. *Journal of the Franklin Institute*, 359(3):1382–1406, 2022 (Cited on pages 6, 173, 183, 213).

[6] Anderle, M., Michiels, W., Čelikovský, S., and Vyhlídal, T. Damping a pendulum's swing by string length adjustment - design and comparison of various control methods. In *Proceedings of the 2019 American Control Conference (ACC)*, 4399–4405, 2019 (Cited on page 182).

[7] Annaswamy, A. M. and Fradkov, A. L. A historical perspective of adaptive control and learning. *Annual Reviews in Control*, 52:18–41, 2021 (Cited on page 171).

[8] Apkarian, P. and Noll, D. Nonsmooth H_∞ synthesis. *IEEE Transactions on Automatic Control*, 51(1):71–86, 2006. **Note:** the `HINFSTRUCT` software package is available from `http://pierre.apkarian.free.fr/Software.html`. (Cited on pages 34, 38, 150).

[9] Apkarian, P. and Noll, D. `hinfstruct` - H_∞-tuning of fixed structure controllers. MathWorks®. URL: `%5Curl%7Bhttps://www.mathworks.com/help/robust/ref/lti.hinfstruct.html%7D` (Cited on page 38).

[10] Apkarian, P., Noll, D., and Falcoz, A. How we saved the Rosetta mission, ONERA, Department of System Dynamics, Toulouse (France), 2014 (Cited on page 34).

[11] Appeltans, P. and Michiels, W. Computing the robust H-infinity norm of time-delay LTI systems with real-valued and structured uncertainties. *IFAC-PapersOnLine*, 52(18):127–132, 2019 (Cited on pages 5, 65, 213).

[12] Appeltans, P. and Michiels, W. A pseudo-spectrum based characterization of the robust strong H-infinity norm of time-delay systems with real-valued and structured uncertainties. *IMA Journal of Mathematical Control and Information*, 38(1):267–296, 2020 (Cited on pages 5, 65, 213).

[13] Appeltans, P. and Michiels, W. A structure preserving shift-invert infinite Arnoldi algorithm for a class of delay eigenvalue problems with Hamiltonian symmetry. *SIAM Journal On Matrix Analysis And Applications*, 2022. (Accepted for publication) (Cited on pages 6, 117, 213).

[14] Appeltans, P. and Michiels, W. *A scalable controller synthesis method for the robust control of networked systems.* In *Controlling Delayed Dynamics: Advances in Theory, Methods and Applications.* Breda, D., editor. Springer, Cham (Switzerland), 2023, 289–310 (Cited on pages 6, 105, 213).

[15] Appeltans, P., Niculescu, S.-I., and Michiels, W. Analysis and Design of Output Feedback PD Controllers for Time-Delay Systems. In *Proceedings of the 2021 European Control Conference (ECC)*, 447–452, 2021 (Cited on pages 5, 39, 214).

[16] Appeltans, P., Niculescu, S.-I., and Michiels, W. Analysis and design of strongly stabilizing PID controllers for time-delay systems. *SIAM Journal on Control and Optimization*, 60(1):124–146, 2022 (Cited on pages 5, 39, 56, 57, 62, 213).

[17] Appeltans, P., Silm, H., and Michiels, W. TDS-CONTROL: a MATLAB package for the analysis and controller-design of time-delay systems. *IFAC-PapersOnLine*, 55(16):272–277, 2022 (Cited on pages 6, 149, 214).

[18] Arzelier, D., Deaconu, G., Gumussoy, S., and Henrion, D. H2 for HIFOO. In Presented at the International Conference on Control and Optimization With Industrial Applications (August 22-24, 2011, Ankara, Turkey) (Cited on page 38).

[19] Åström, K. J. and Hägglund, T. *Advanced PID control.* ISA - The Instrumentation, Systems, and Automation Society, Research Triangle Park (NC), 2006 (Cited on pages 3, 33, 34).

[20] Bakule, L. Decentralized control: An overview. *Annual Reviews in Control*, 32(1):87–98, 2008 (Cited on page 105).

[21] Bellman, R. E. and Cooke, K. L. *Differential-Difference Equations.* Academic Press, New York (NY), 1963 (Cited on pages 7–9).

[22] Beltrami, E. J. *Mathematics for dynamic modeling.* Academic press, Boston (MA), 2nd edition, 1998 (Cited on page 1).

[23] Belyakov, A. O., Seyranian, A. P., and Luongo, A. Dynamics of the pendulum with periodically varying length. *Physica D: Nonlinear Phenomena*, 238(16):1589–1597, 2009 (Cited on page 174).

[24] Benner, P., Kressner, D., and Mehrmann, V. Skew-Hamiltonian and Hamiltonian Eigenvalue Problems: Theory, Algorithms and Applications. In *Proceedings of the Fourth Conference on Applied Mathematics and Scientific Computing*, 3–39, 2005 (Cited on page 119).

[25] Benner, P. and Mitchell, T. Extended and improved criss-cross algorithms for computing the spectral value set abscissa and radius. *SIAM Journal on Matrix Analysis and Applications*, 40(4):1325–1352, 2019 (Cited on page 22).

[26] Benner, P. and Voigt, M. A structured pseudospectral method for $\mathcal{H}_\infty$-norm computation of large-scale descriptor systems. *Mathematics of Control, Signals, and Systems*, 26(2):303–338, 2014 (Cited on pages 4, 30, 71, 101).

[27] Borgioli, F. *Spectrum-based methods and algorithms for the Robustness Stability Analysis of Delay Systems*. PhD thesis, KU Leuven, Leuven (Belgium), 2020 (Cited on pages 165, 166).

[28] Borgioli, F. and Michiels, W. A novel method to compute the structured distance to instability for combined uncertainties on delays and system matrices. *IEEE Transactions on Automatic Control*, 65(4):1747–1754, 2019 (Cited on pages 3, 23, 63, 66, 98, 99, 101, 102, 163).

[29] Borgioli, F., Michiels, W., Lu, D., and Vandereycken, B. A globally convergent method to compute the real stability radius for time-delay systems. *Systems & Control Letters*, 127:44–51, 2019 (Cited on page 23).

[30] Boyd, S. and Balakrishnan, V. A regularity result for the singular values of a transfer matrix and a quadratically convergent algorithm for computing its L_∞-norm. *Systems & Control Letters*, 15(1):1–7, 1990 (Cited on page 29).

[31] Boyd, S., Balakrishnan, V., and Kabamba, P. A bisection method for computing the H_∞ norm of a transfer matrix and related problems. *Mathematics of Control, Signals and Systems*, 2(3):207–219, 1989 (Cited on pages 28, 29).

[32] Boyd, S. and Desoer, C. A. Subharmonic functions and performance bounds on linear time-invariant feedback systems. *IMA Journal of Mathematical control and Information*, 2(2):153–170, 1985 (Cited on page 83).

[33] Boyd, S., El Ghaoui, L., Feron, E., and Balakrishnan, V. *Linear matrix inequalities in system and control theory*. SIAM, Philadelphia (PA), 1994 (Cited on pages 9, 35).

[34] Bradley, W., Kim, J., Kilwein, Z., Blakely, L., Eydenberg, M., Jalvin, J., Laird, C., and Boukouvala, F. Perspectives on the integration between first-principles and data-driven modeling. *Computers & Chemical Engineering*, 166:107898, 2022 (Cited on page 170).

[35] Brayton, R. K. Nonlinear oscillations in a distributed network. *Quarterly of Applied Mathematics*, 24(4):289–301, 1967 (Cited on page 9).

[36] Breda, D., Maset, S., and Vermiglio, R. *TRACE-DDE: a tool for robust analysis and characteristic equations for delay differential equations*. In *Topics in Time Delay Systems: Analysis, Algorithms and Control*. Loiseau, J. J., Michiels, W., Niculescu, S.-I., and Sipahi, R., editors. Springer Berlin, Heidelberg (Germany), 2009, 145–155. **Note:** the TRACE-DDE software package is available from `http://cdlab.uniud.it/software#TRACE-DDE` (Cited on page 14).

[37] Breda, D., Maset, S., and Vermiglio, R. *Stability of linear delay differential equations: A numerical approach with MATLAB*. Springer, New York (NY), 2014 (Cited on page 9).

[38] Bruinsma, N. and Steinbuch, M. A fast algorithm to compute the H_∞-norm of a transfer function matrix. *Systems & Control Letters*, 14(4):287–293, 1990 (Cited on page 29).

[39] Brunton, S. L. and Kutz, J. N. *Data-Driven Science and Engineering: Machine Learning, Dynamical Systems, and Control*. Cambridge University Press, Cambridge (United Kingdom), 2nd edition, 2022 (Cited on page 170).

[40] Bueler, E. Error bounds for approximate eigenvalues of periodic-coefficient linear delay differential equations. *SIAM Journal on Numerical Analysis*, 45(6):2510–2536, 2007 (Cited on page 13).

[41] Bunse-Gerstner, A., Byers, R., Mehrmann, V., and Nichols, N. K. Feedback design for regularizing descriptor systems. *Linear Algebra and Its Applications*, 299(1-3):119–151, 1999 (Cited on page 73).

[42] Burke, J. V., Henrion, D., Lewis, A. S., and Overton, M. L. HIFOO – a MATLAB package for fixed-order controller design and H_∞ optimization. *IFAC Proceedings Volumes*, 39(9):339–344, 2006. **Note:** the HIFOO software package is available from `https://cs.nyu.edu/~overton/software/hifoo/`. (Cited on pages 34, 38, 150).

[43] Burke, J. V., Lewis, A. S., and Overton, M. L. Robust stability and a criss-cross algorithm for pseudospectra. *IMA Journal of Numerical Analysis*, 23(3):359–375, 2003 (Cited on page 21).

[44] Burke, J. V., Curtis, F. E., Lewis, A. S., Overton, M. L., and Simões, L. E. A. *Gradient sampling methods for nonsmooth optimization.* In *Numerical Nonsmooth Optimization: State of the Art Algorithms.* Bagirov, A. M., Gaudioso, M., Karmitsa, N., Mäkelä, M. M., and Taheri, S., editors. Springer, Cham (Switzerland), 2020, 201–225 (Cited on page 38).

[45] Burke, J. V., Lewis, A. S., and Overton, M. L. A robust gradient sampling algorithm for nonsmooth, nonconvex optimization. *SIAM Journal on Optimization*, 15(3):751–779, 2005 (Cited on page 38).

[46] Butcher, E. A., Ma, H., Bueler, E., Averina, V., and Szabo, Z. Stability of linear time-periodic delay-differential equations via Chebyshev polynomials. *International Journal for Numerical Methods in Engineering*, 59(7):895–922, 2004. **Note:** the corresponding software is available from `https://bueler.github.io/ddes/DDEcharts.htm` (Cited on page 13).

[47] Byers, R. A bisection method for measuring the distance of a stable matrix to the unstable matrices. *SIAM Journal on Scientific and Statistical Computing*, 9(5):875–881, 1988 (Cited on page 21).

[48] Byers, R., He, C., and Mehrmann, V. Where is the nearest non-regular pencil? *Linear algebra and its applications*, 285(1-3):81–105, 1998 (Cited on page 21).

[49] Campbell, S. L. Singular linear systems of differential equations with delays. *Applicable Analysis*, 11(2):129–136, 1980 (Cited on page 72).

[50] Campbell, S. L. Nonregular 2D descriptor delay systems. *IMA Journal of Mathematical Control and Information*, 12(1):57–67, 1995 (Cited on page 72).

[51] Chen, Y.-H. New type of controller: the proportional integral minus delay controller. *International Journal of Systems Science*, 18(11):2033–2041, 1987 (Cited on page 39).

[52] Datko, R. and You, Y. Some second-order vibrating systems cannot tolerate small time delays in their damping. *Journal of Optimization Theory and Applications*, 70(3):521–537, 1991 (Cited on page 41).

[53] Datko, R. F. *Time-delayed perturbations and robust stability.* In *Differential Equations, Dynamical Systems, and Control Science.* Elworthy, K., Everitt, W., and Lee, E., editors. Marcel Dekker, New York (NY), 1994, 457–468 (Cited on page 9).

[54] de Souza, C. E. and Li, X. Delay-dependent robust H_∞ control of uncertain linear state-delayed systems. *Automatica*, 35(7):1313–1321, 1999 (Cited on pages 3, 65).

[55] Delves, L. M. and Lyness, J. N. A numerical method for locating the zeros of analytic functions. *Mathematics of Computation*, 21:543–560, 100, 1967 (Cited on page 14).

[56] Dileep, D., Borgioli, F., Hetel, L., Richard, J. P., and Michiels, W. A scalable design method for stabilising decentralised controllers for networks of delay-coupled systems. *IFAC-PapersOnLine*, 51(33):68–73, 2018 (Cited on pages 3, 5, 106, 113).

[57] Dileep, D., Van Parys, R., Pipeleers, G., Hetel, L., Richard, J.-P., and Michiels, W. Design of robust decentralised controllers for MIMO plants with delays through network structure exploitation. *International Journal of Control*, 93(10):2275–2289, 2020 (Cited on pages 4, 106, 110, 166).

[58] Doyle, J. Analysis of feedback systems with structured uncertainties. *IEE Proceedings D (Control Theory and Applications)*, 129(6):242–250, 1982 (Cited on page 21).

[59] Eising, R. The distance between a system and the set of uncontrollable systems. In *Proceedings of the Mathematical Theory of Networks and Systems (MTNS-83) International Symposium*, 303–314, 1984 (Cited on page 21).

[60] El'sgol'ts, L. E. and Norkin, S. B. *Introduction to the theory and application of differential equations with deviating arguments*. Nauka, Moscow (Russia), 1971. Translated by Casti, J. L., volume 105 of *Mathematics in science and engineering*. Academic Press, New York (NY), 1973 (Cited on page 8).

[61] Engelborghs, K., Luzyanina, T., and Roose, D. Numerical bifurcation analysis of delay differential equations using DDE-BIFTOOL. *ACM Transactions on Mathematical Software*, 28(1):1–21, 2002 (Cited on page 13).

[62] Erneux, T. *Applied delay differential equations*. Springer, New York (NY), 2009 (Cited on page 9).

[63] Fišer, J., Zítek, P., and Vyhlídal, T. Neutral PID control loop investigated in terms of similarity theory. *IFAC-PapersOnLine*, 51(14):212–217, 2018 (Cited on page 40).

[64] Franklin, G. F., Powell, J. D., and Emami-Naeini, A. *Feedback control of dynamic systems*. Prentice Hall, Upper Saddle River (NJ), 4th edition, 2002 (Cited on page 1).

[65] Freitag, M. A., Spence, A., and Dooren, P. V. Calculating the H_∞-norm using the implicit determinant method. *SIAM Journal on Matrix Analysis and Applications*, 35(2):619–635, 2014 (Cited on page 27).

[66] Fridman, E. Stability of linear descriptor systems with delay: A Lyapunov-based approach. *Journal of Mathematical Analysis and Applications*, 273(1):24–44, 2002 (Cited on pages 72, 73).

[67] Fridman, E. *Introduction to time-delay systems: Analysis and control*. Birkhäuser, Cham (Switzerland), 2014 (Cited on pages 8, 9, 35).

[68] Gahinet, P. and Apkarian, P. A linear matrix inequality approach to H_∞ control. *International Journal of Robust and Nonlinear Control*, 4(4):421–448, 1994 (Cited on page 35).

[69] Gantmacher, F. R. *Theory of Matrices*. Translated by Hirsch, K. Chelsea Publishing Company, New York (NY), 1959 (Cited on page 72).

[70] Georgiou, T. T. and Smith, M. C. w-Stability of feedback systems. *Systems & Control Letters*, 13(4):271–277, 1989 (Cited on pages 40, 47).

[71] Gomez, M. A., Egorov, A. V., and Mondié, S. Lyapunov matrix based necessary and sufficient stability condition by finite number of mathematical operations for retarded type systems. *Automatica*, 108:108475, 2019 (Cited on page 9).

[72] Gomez, M. A., Jungers, R. M., and Michiels, W. On the m-dimensional Cayley–Hamilton theorem and its application to an algebraic decision problem inferred from the H2 norm analysis of delay systems. *Automatica*, 113:108761, 2020 (Cited on page 170).

[73] Gu, K., Kharitonov, V. L., and Chen, J. *Stability of Time-Delay Systems*. Birkhäuser, Boston (MA), 2003 (Cited on pages 8, 9).

[74] Guglielmi, N. On the Method by Rostami for Computing the Real Stability Radius of Large and Sparse Matrices. *SIAM Journal on Scientific Computing*, 38(3):A1662–A1681, 2016 (Cited on page 23).

[75] Guglielmi, N., Gürbüzbalaban, M., Mitchell, T., and Overton, M. L. Approximating the real structured stability radius with Frobenius-norm bounded perturbations. *SIAM Journal on Matrix Analysis and Applications*, 38(4):1323–1353, 2017 (Cited on page 23).

[76] Guglielmi, N., Gürbüzbalaban, M., and Overton, M. L. Fast approximation of the H_∞ norm via optimization over spectral value sets. *SIAM Journal on Matrix Analysis and Applications*, 34(2):709–737, 2013 (Cited on pages 4, 30).

[77] Guglielmi, N. and Lubich, C. Differential equations for roaming pseudospectra: paths to extremal points and boundary tracking. *SIAM Journal on Numerical Analysis*, 49(3):1194–1209, 2011 (Cited on pages 22, 30, 31, 99, 101, 102).

[78] Guglielmi, N. and Lubich, C. Low-Rank Dynamics for Computing Extremal Points of Real Pseudospectra. *SIAM Journal on Matrix Analysis and Applications*, 34(1):40–66, 2013 (Cited on pages 23, 99).

[79] Guglielmi, N. and Overton, M. L. Fast Algorithms for the Approximation of the Pseudospectral Abscissa and Pseudospectral Radius of a Matrix. *SIAM Journal on Matrix Analysis and Applications*, 32(4):1166–1192, 2011 (Cited on page 22).

[80] Gumussoy, S., Henrion, D., Millstone, M., and Overton, M. L. Multiobjective robust control with HIFOO 2.0. IFAC Proceedings Volumes, 42(6):144–149, 2009 (Cited on pages 38, 150).

[81] Gumussoy, S. and Michiels, W. A predictor-corrector type algorithm for the pseudospectral abscissa computation of time-delay systems. *Automatica*, 46(4):657–664, 2010 (Cited on pages 22, 169).

[82] Gumussoy, S. and Michiels, W. Fixed-order H-infinity control for interconnected systems using delay differential algebraic equations. *SIAM Journal on Control and Optimization*, 49(5):2212–2238, 2011 (Cited on pages 4, 29, 66, 67, 69, 70, 106, 115, 118, 166).

[83] Gündeş, A. N., Özbay, H., and Özgüler, A. B. PID controller synthesis for a class of unstable MIMO plants with I/O delays. *Automatica*, 43(1):135–142, 2007 (Cited on page 40).

[84] Güttel, S. and Tisseur, F. The nonlinear eigenvalue problem. *Acta Numerica*, 26:1–94, 2017 (Cited on pages 14, 119).

[85] Güttel, S., Van Beeumen, R., Meerbergen, K., and Michiels, W. NLEIGS: a class of fully rational Krylov methods for nonlinear eigenvalue problems. *SIAM Journal on Scientific Computing*, 36(6):A2842–A2864, 2014 (Cited on pages 14, 120).

[86] Hale, J. K. *Effects of delays on dynamics*. In *Topological Methods in Differential Equations and Inclusions*. Granas, A., Frigon, M., and Sabidussi, G., editors. Springer, Dordrecht (The Netherlands), 1995, 191–237 (Cited on page 41).

[87] Hale, J. K. *Theory of functional differential equations*, volume 3 of *Applied mathematical sciences*. Springer, New York (NY), 2nd edition, 1977 (Cited on pages 8, 126).

[88] Hale, J. K. *History of delay equations*. In *Delay Differential Equations and Applications*. Arino, O., Hbid, M. L., and Ait Dads, E., editors. Springer, Dordrecht (The Netherlands), 2006, 1–28 (Cited on page 8).

[89] Hale, J. K. and Verduyn Lunel, S. M. *Introduction to Functional Differential Equations*, volume 99 of *Applied Mathematical Sciences*. Springer, New York (NY), 1993 (Cited on pages 8, 9).

[90] Hale, J. K. and Verduyn Lunel, S. M. Strong stabilization of neutral functional differential equations. *IMA Journal of Mathematical Control and Information*, 19(1 and 2):5–23, 2002 (Cited on pages 15, 41).

[91] Hilhorst, G., Pipeleers, G., Michiels, W., and Swevers, J. Sufficient LMI conditions for reduced-order multi-objective H2/H∞ control of LTI systems. *European Journal of Control*, 23:17–25, 2015 (Cited on page 35).

[92] Hinrichsen, D. and Pritchard, A. J. Destabilization by output feedback. *Differential and Integral Equations*, 5(2):357–386, 1992 (Cited on page 21).

[93] Hinrichsen, D. and Pritchard, A. J. *Mathematical Systems Theory I: Modelling, State Space Analysis, Stability and Robustness*, volume 48 of *Texts in Applied Mathematics*. Springer-Verlag, Berlin (Germany), 2005 (Cited on pages 18, 20, 22).

[94] Huba, M. and Vrančič, D. Comparing filtered PI, PID and PIDD2 control for the FOTD plants. *IFAC-PapersOnLine*, 51(4):954–959, 2018 (Cited on page 59).

[95] Insperger, T. and Stépán, G. Stability of the milling process. *Periodica Polytechnica Mechanical Engineering*, 44(1):47–57, 2000 (Cited on page 9).

[96] Insperger, T. and Stépán, G. Semi-discretization method for delayed systems. *International Journal for numerical methods in engineering*, 55(5):503–518, 2002 (Cited on page 13).

[97] Insperger, T. and Stépán, G. *Semi-Discretization for Time-Delay Systems: Stability and Engineering Applications*, volume 178 of *Applied Mathematical Sciences*. Springer, New York (NY), 2011 (Cited on page 13).

[98] Jarlebring, E., Bennedich, M., Mele, G., Ringh, E., and Upadhyaya, P. NEP-PACK: a Julia package for nonlinear eigenproblems. *arXiv*, 2018. **Note**: the NEP-PACK software package is available from `https://github.com/nep-pack` (Cited on pages 14, 119).

[99] Jarlebring, E., Meerbergen, K., and Michiels, W. A Krylov Method for the Delay Eigenvalue Problem. *SIAM Journal on Scientific Computing*, 32(6):3278–3300, 2010 (Cited on pages 14, 119, 132, 133, 136, 141, 143, 146, 169).

[100] Jarlebring, E., Michiels, W., and Meerbergen, K. A linear eigenvalue algorithm for the nonlinear eigenvalue problem. *Numerische Mathematik*, 122(1):169–195, 2012 (Cited on page 119).

[101] Ji, X., Su, H., and Chu, J. An LMI approach to robust H-infinity control for uncertain singular time-delay systems. *Journal of Control Theory and Applications*, 4(4):361–366, 2006 (Cited on pages 3, 65).

[102] Ji, X. A. and Orosz, G. Learning time delay systems with neural ordinary differential equations. *IFAC-PapersOnLine*, 55(36):79–84, 2022 (Cited on page 170).

[103] Jirinec, T. *Stabilization and control of unmanned quadcopter*. Master's thesis, Czech Technical University, Prague (Czech Republic), 2011 (Cited on page 57).

[104] Karow, M. *Geometry of spectral value sets*. PhD thesis, Universitat Bremen, Bremen (Germany), 2003 (Cited on page 21).

[105] Khalil, H. K. *Nonlinear Systems*. Prentice Hall, Upper Saddle River (NJ), 3th edition edition, 2002 (Cited on page 181).

[106] Khargonekar, P. P. and Dahleh, M. A. Advancing systems and control research in the era of ML and AI. *Annual Reviews in Control*, 45:1–4, 2018 (Cited on page 170).

[107] Kokame, H., Kobayashi, H., and Mori, T. Robust H_∞ performance for linear delay-differential systems with time-varying uncertainties. *IEEE Transactions on Automatic Control*, 43(2):223–226, 1998 (Cited on pages 3, 65).

[108] Kolmanovskii, V. and Myshkis, A. *Applied theory of functional differential equations*, volume 85 of *Mathematics and its Applications*. Kluwer, Dordrecht (The Netherlands), 1992 (Cited on page 8).

[109] Krasovskii, N. N. *Stability of motion: Applications of Lyapunov's Second Method to Differential Systems and Equations with Delay*. Fizmatlít, Moscow (Russia), 1959. Translated by Brenner, J. L. Stanford University Press, Stanford (CA), 1963 (Cited on pages 8, 9).

[110] Kravanja, P. and Van Barel, M. *Computing the Zeros of Analytic Functions*, volume 1727 of *Lecture Notes in Mathematics*. Springer Berlin, Heidelberg (Germany), 2000 (Cited on page 14).

[111] Kressner, D. A block Newton method for nonlinear eigenvalue problems. *Numerische Mathematik*, 114(2):355–372, 2009 (Cited on page 14).

[112] Kressner, D. and Vandereycken, B. Subspace methods for computing the pseudospectral abscissa and the stability radius. *SIAM Journal on Matrix Analysis and Applications*, 35(1):292–313, 2014 (Cited on page 22).

[113] Lam, R. R., Horesh, L., Avron, H., and Willcox, K. E. Should You Derive, Or Let the Data Drive? An Optimization Framework for Hybrid First-Principles Data-Driven Modeling. *arXiv*, 2017 (Cited on page 170).

[114] Lamnabhi-Lagarrigue, F., Annaswamy, A., Engell, S., Isaksson, A., Khargonekar, P., Murray, R. M., Nijmeijer, H., Samad, T., Tilbury, D., and Van den Hof, P. Systems & Control for the future of humanity, research agenda: Current and future roles, impact and grand challenges. *Annual Reviews in Control*, 43:1–64, 2017 (Cited on page 2).

[115] Lehoucq, R. B., Sorensen, D. C., and Yang, C. *ARPACK users' guide: solution of large-scale eigenvalue problems with implicitly restarted Arnoldi methods*. SIAM, 1998 (Cited on page 31).

[116] Lewis, A. S. and Overton, M. L. Nonsmooth optimization via quasi-Newton methods. *Mathematical Programming*, 141(1):135–163, 2013 (Cited on page 38).

[117] Li, X.-G., Niculescu, S.-I., Chen, J.-X., and Chai, T. Characterizing PID controllers for linear time-delay systems: a parameter-space approach. *IEEE Transactions on Automatic Control*, 66(10):4499–4513, 2020 (Cited on page 40).

[118] Li, X. and de Souza, C. E. Robust stabilization and H_∞ control of uncertain linear time-delay systems. *IFAC Proceedings Volumes*, 29(1):3508–3513, 1996 (Cited on pages 3, 65).

[119] Logemann, H. Destabilizing effects of small time delays on feedback-controlled descriptor systems. *Linear Algebra and its Applications*, 272(1):131–153, 1998 (Cited on page 41).

[120] Logemann, H., Rebarber, R., and Weiss, G. Conditions for robustness and nonrobustness of the stability of feedback systems with respect to small delays in the feedback loop. *SIAM Journal on Control and Optimization*, 34(2):572–600, 1996 (Cited on page 41).

[121] Logemann, H. and Townley, S. The effect of small delays in the feedback loop on the stability of neutral systems. *Systems & Control Letters*, 27(5):267–274, 1996 (Cited on page 41).

[122] London, W. P. and Yorke, J. A. Recurrent outbreaks of measles, chickenpox and mumps: I. Seasonal variation in contact rates. *American Journal of Epidemiology*, 98(6):453–468, 1973 (Cited on page 9).

[123] Lu, D. and Vandereycken, B. Criss-cross type algorithms for computing the real pseudospectral abscissa. *SIAM Journal on Matrix Analysis and Applications*, 38(3):891–923, 2017 (Cited on page 22).

[124] Lyapunov, A. M. *The general problem of the stability of motion*. Kharkov Mathematical Society, 1892. Translated by Davaux, É. and Fuller, A. Taylor & Francis, London, 1992 (Cited on page 9).

[125] Ma, D., Chen, J., Liu, A., Chen, J., and Niculescu, S.-I. Explicit bounds for guaranteed stabilization by PID control of second-order unstable delay systems. *Automatica*, 100:407–411, 2019 (Cited on page 40).

[126] MacDonald, N. *Biological Delay Systems: Linear Stability Theory*. Cambridge University Press, Cambridge (United Kingdom), 1989 (Cited on pages 8, 170).

[127] Mahmoud, M. S. Robust H_∞ control of linear neutral systems. *Automatica*, 36(5):757–764, 2000 (Cited on pages 3, 65).

[128] Massioni, P. and Verhaegen, M. Distributed control for identical dynamically coupled systems: A decomposition approach. *IEEE Transactions on Automatic Control*, 54(1):124–135, 2009 (Cited on pages 106, 110).

[129] Mauroy, A., Susuki, Y., and Mezić, I. *Koopman operator in systems and control*. Lecture Notes in Control and Information Sciences. Springer, Cham (Switzerland), 2020 (Cited on page 170).

[130] Mehrmann, V. L. *The autonomous linear quadratic control problem : theory and numerical solution*. Springer, Berlin (Germany), 1991 (Cited on page 119).

[131] Mehrmann, V., Schröder, C., and Simoncini, V. An implicitly-restarted Krylov subspace method for real symmetric/skew-symmetric eigenproblems. *Linear Algebra and Its Applications*, 436(10):4070–4087, 2012 (Cited on pages 4, 119, 123, 124, 145, 169).

[132] Mehrmann, V. and Watkins, D. Structure-Preserving Methods for Computing Eigenpairs of Large Sparse Skew-Hamiltonian/Hamiltonian Pencils. *SIAM Journal on Scientific Computing*, 22(6):1905–1925, 2001 (Cited on pages 4, 119–124, 128, 145).

[133] Mehrmann, V. and Watkins, D. Polynomial eigenvalue problems with Hamiltonian structure. *Electronic Transactions on Numerical Analysis*, 13:106–118, 2002 (Cited on pages 119, 120, 169).

[134] Michiels, W. Spectrum-based stability analysis and stabilisation of systems described by delay differential algebraic equations. *IET Control Theory & Applications*, 5(16):1829–1842, 2011 (Cited on pages 61, 73, 74).

[135] Michiels, W., Engelborghs, K., Roose, D., and Dochain, D. Sensitivity to infinitesimal delays in neutral equations. *SIAM Journal on Control and Optimization*, 40(4):1134–1158, 2002 (Cited on page 41).

[136] Michiels, W. and Guglielmi, N. An iterative method for computing the pseudospectral abscissa for a class of nonlinear eigenvalue problems. *SIAM Journal on Scientific Computing*, 34(4):A2366–A2393, 2012 (Cited on page 22).

[137] Michiels, W. and Gumussoy, S. Characterization and computation of $\mathcal{H}_\infty$ norms for time-delay systems. *SIAM Journal on Matrix Analysis and Applications*, 31(4):2093–2115, 2010 (Cited on pages 29, 118, 121, 125, 126).

[138] Michiels, W., Jarlebring, E., and Meerbergen, K. Krylov-Based Model Order Reduction of Time-delay Systems. *SIAM Journal on Matrix Analysis and Applications*, 32(4):1399–1421, 2011 (Cited on page 145).

[139] Michiels, W. and Niculescu, S.-I. *Stability, Control, and Computation for Time-Delay Systems. An eigenvalue based approach.* Society for Industrial and Applied Mathematics (SIAM), Philadelphia (PA), 2nd edition edition, 2014 (Cited on pages 2, 8, 9, 12, 43, 45, 149, 170).

[140] Michiels, W., Vyhlídal, T., Huijberts, H., and Nijmeijer, H. Stabilizability and Stability Robustness of State Derivative Feedback Controllers. *SIAM Journal on Control and Optimization*, 47(6):3100–3117, 2009 (Cited on pages 40, 41, 46, 47, 52).

[141] Michiels, W. and Zhou, B. On the strong relative degree of time-delay systems with noncommensurate delays. *SIAM Journal on Control and Optimization*, 60(6):3384–3408, 2022 (Cited on page 60).

[142] Morărescu, I., Méndez-Barrios, C., Niculescu, S., and Gu, K. Stability crossing boundaries and fragility characterization of PID controllers for SISO systems with I/O delays. In *Proceedings of the 2011 American Control Conference*, 4988–4993, 2011 (Cited on page 40).

[143] Morgül, Ö. On the stabilization and stability robustness against small delays of some damped wave equations. *IEEE Transactions on Automatic Control*, 40(9):1626–1630, 1995 (Cited on page 41).

[144] Morris, K. and Rebarber, R. Feedback invariance of SISO infinite-dimensional systems. *Mathematics of Control, Signals, and Systems*, 19(4):313–335, 2007 (Cited on page 58).

[145] Myškis, A. D. General theory of differential equations with retarded arguments. *Uspekhi Matematicheskikh Nauk*, 4(5):99–141, 1949. English translation: American Mathematical Society, 1951 (Cited on page 8).

[146] Niculescu, S.-I. *Delay effects on stability: a robust control approach*, volume 269 of *Lecture Notes in Control and Information Sciences*. Springer, London (United Kingdom), 2001 (Cited on page 9).

[147] Novella-Rodríguez, D. F., del Muro Cuéllar, B., Márquez-Rubio, J. F., Hernández-Pérez, M. Á., and Velasco-Villa, M. PD–PID controller for delayed systems with two unstable poles: a frequency domain approach. *International Journal of Control*, 92(5):1196–1208, 2019 (Cited on page 40).

[148] O'dwyer, A. *Handbook of PI and PID Controller Tuning Rules*. Imperial College Press, London (United Kingdom), 2003 (Cited on pages 3, 33, 34).

[149] Olgac, N. and Holm-Hansen, B. A novel active vibration absorption technique: delayed resonator. *Journal of Sound and Vibration*, 176(1):93–104, 1994 (Cited on page 9).

[150] Overton, M. HANSO: hybrid algorithm for non-smooth optimization. URL: %5Curl%7Bhttps://cs.nyu.edu/~overton/software/hanso/%7D (Cited on page 38).

[151] Özbay, H. and Gündeş, A. Resilient PI and PD controllers for a class of unstable MIMO plants with I/O delays. *IFAC Proceedings Volumes*, 39(10):258–263, 2006. 6th IFAC Workshop on Time Delay Systems (Cited on page 40).

[152] Özer, S. M. and İftar, A. Eigenvalue optimisation-based centralised and decentralised stabilisation of time-delay systems. *International Journal of Control*:1–22, 2021 (Cited on page 34).

[153] Packard, A. and Doyle, J. C. The complex structured singular value. *Automatica*, 29(1):71–109, 1993 (Cited on pages 21, 80).

[154] Pinsky, M. and Zevin, A. Oscillations of a pendulum with a periodically varying length and a model of swing. *International Journal of Non-Linear Mechanics*, 34(1):105–109, 1999 (Cited on page 174).

[155] Poveda, J. I., Benosman, M., and Teel, A. R. Hybrid online learning control in networked multiagent systems: a survey. *International Journal of Adaptive Control and Signal Processing*, 33(2):228–261, 2019 (Cited on page 171).

[156] Press, W. H., Teukolsky, S. A., Vetterling, W. T., and Flannery, B. P. *Numerical recipes in Fortran 77 : the art of scientific computing*, volume 1 of *Fortran Numerical Recipes*. Cambridge University press, Cambridge (United Kingdom), 2nd edition, 1992 (Cited on pages 32, 98).

[157] Puntanen, S. and Styan, G. P. H. *Historical Introduction: Issai Schur and the Early Development of the Schur Complement*. In *The Schur complement and its applications*. Zhang, F., editor. Volume 4. Numerical Methods and Algorithms. Springer, New York (NY), 2005. Chapter 0 (Cited on pages 81, 84).

[158] Qiu, L., Bernhardsson, B., Rantzer, A., Davison, E. J., Young, P. M., and Doyle, J. C. A formula for computation of the real stability radius. *Automatica*, 31(6):879–890, 1995 (Cited on page 22).

[159] Ramírez, A., Mondié, S., Garrido, R., and Sipahi, R. Design of Proportional-Integral-Retarded (PIR) Controllers for Second-Order LTI Systems. *IEEE Transactions on Automatic Control*, 61(6):1688–1693, 2016 (Cited on page 39).

[160] Razumikhin, B. On the stability of systems with delay. *Prikladnaya Matematika i Mekhanika*, 20:500–512, 1956 (Cited on page 9).

[161] Saad, Y. *Iterative Methods for Sparse Linear Systems*. Society for Industrial and Applied Mathematics (SIAM), Philadelphia (PA), 2nd edition, 2003 (Cited on pages 22, 31, 119).

[162] Safonov, M. G., Goh, K.-C., and Ly, J. H. Q. Control system synthesis via bilinear matrix inequalities. In *Proceedings of the 1994 American Control Conference*, 45–49, Baltimore (MD), 1994 (Cited on page 35).

[163] Scherer, C. and Weiland, S. *Linear matrix inequalities in control*. Lecture Notes, Dutch Institute for Systems and Control (DISC). Delft (The Netherlands), 2004 (Cited on page 35).

[164] Schur, I. Uber potenzreihen, die im innern des einheitskreises beschränkt sind. *Journal für die reine und angewandte Mathematik*, 1917(147):205–232, 1917 (Cited on page 81).

[165] Schwerdtner, P., Mengi, E., and Voigt, M. Certifying global optimality for the L_∞-norm computation of large-scale descriptor systems. *IFAC-PapersOnLine*, 53(2):4279–4284, 2020 (Cited on page 4).

[166] Shanmugathasan, N. and Johnston, R. D. Exploitation of time delays for improved process control. *International Journal of Control*, 48(3):1137–1152, 1988 (Cited on page 9).

[167] Sharpe, F. and Lotka, A. J. Contribution to the analysis of malaria epidemiology. IV. Incubation lag. *American Journal of Hygiene*, 3(Supplementary material):96–112, 1923. (reprint: in *The Golden Age of Theoretical Ecology: 1923–1940*. Volume 22, Lecture Notes in Biomathematics, 348–368. Springer, Berlin (Germany), 1978) (Cited on page 8).

[168] Šiljak, D. D. *Decentralized Control of Complex Systems*, volume 184 of *Mathematics in Science and Engineering*. Academic Press, Boston (MA), 1991 (Cited on page 105).

[169] Silva, G. J., Datta, A., and Bhattacharyya, S. P. *PID controllers for time-delay systems*. Birkhuser, Boston (MA), 2005 (Cited on pages 3, 40).

[170] Singh, T. and Vyhlídal, T. Recent results in reference prefiltering for precision motion control. *IFAC-PapersOnLine*, 53(2):12, 2020 (Cited on page 173).

[171] Singhose, W. Command shaping for flexible systems: A review of the first 50 years. *International Journal of Precision Engineering and Manufacturing*, 10(4):153–168, 2009 (Cited on page 173).

[172] Sipahi, R., Arslan, G., and Niculescu, S.-I. Some remarks on control strategies for continuous gradient play dynamics. In *Proceedings of the 45th IEEE Conference on Decision and Control*, 1966–1971, 2006 (Cited on page 41).

[173] Siqueira, D., Moreira, F. J. O., and Paglione, P. Design of robust static output feedback flight control law using structured singular value optimization. *IFAC Proceedings Volumes*, 45(25):94–99, 2012 (Cited on page 34).

[174] Sreedhar, J., Dooren, P. V., and Tits, A. L. *A fast algorithm to compute the real structured stability radius.* In *Stability theory: Hurwitz Centenary Conference*. Jeltsch, R. and Mansour, M., editors. Birkhäuser, Basel (Switserland), 1996, 219–230 (Cited on page 22).

[175] Stépán, G. *Retarded dynamical systems: stability and characteristic functions*, volume 210 of *Pitman research notes in mathematics Series*. Longman Scientific & Technical, Harlow (England), 1989 (Cited on page 9).

[176] Stilling, D. S. and Szyszkowski, W. Controlling angular oscillations through mass reconfiguration: a variable length pendulum case. *International Journal of Non-Linear Mechanics*, 37(1):89–99, 2002 (Cited on page 174).

[177] Tipaldi, M., Iervolino, R., and Massenio, P. R. Reinforcement learning in spacecraft control applications: advances, prospects, and challenges. *Annual Reviews in Control*, 54:1–23, 2022 (Cited on page 170).

[178] Titchmarsh, E. C. *The theory of functions*. Oxford University Press, Oxford (United Kingdom), 1939, 116–117 (Cited on page 49).

[179] Toker, O. and Özbay, H. On the NP-hardness of solving bilinear matrix inequalities and simultaneous stabilization with static output feedback. In *Proceedings of 1995 American Control Conference*, 2525–2526, Seattle (WA), 1995 (Cited on page 35).

[180] Tran Dinh, Q., Gumussoy, S., Michiels, W., and Diehl, M. Combining convex-concave decompositions and linearization approaches for solving BMIs, with application to static output feedback. *IEEE Transactions on Automatic Control*, 57(6):1377–1390, 2012 (Cited on page 35).

[181] Trefethen, L. N. and Embree, M. *Spectra and Pseudospectra: The Behavior of Nonnormal Matrices and Operators*. eng. Princeton University Press, Princeton (NJ), 2005 (Cited on page 21).

[182] Trefethen, L. N. *Approximation Theory and Approximation Practice*. Society for Industrial and Applied Mathematics (SIAM), Philadelphia (PA), 2013 (Cited on pages 132, 140).

[183] Trofino, A. Sufficient LMI conditions for the design of static and reduced order controllers. In *Proceedings of the 48th IEEE Conference on Decision and Control (CDC)*, 6668–6673, 2009 (Cited on page 35).

[184] Van Loan, C. F. A symplectic method for approximating all the eigenvalues of a Hamiltonian matrix. *Linear Algebra and its Applications*, 61:233–251, 1984 (Cited on page 119).

[185] Van Loan, C. F. How near is a stable matrix to an unstable matrix. In *Linear algebra and its role in systems theory (Proceedings of the AMS-IMS-SIAM Summer Research Conference, July 29-August 4,1984,Brunswick, Main)*, 465–478, Providence (RI). American Mathematical Society, 1985 (Cited on page 21).

[186] Vanbiervliet, J., Verheyden, K., Michiels, W., and Vandewalle, S. A nonsmooth optimisation approach for the stabilisation of time-delay systems. *ESAIM: Control, Optimisation and Calculus of Variations*, 14(3):478–493, 2008 (Cited on pages 4, 34, 37, 166).

[187] Varah, J. M. *The computation of bounds for the invariant subspaces of a general matrix operator*. PhD thesis, Stanford University. Department of Mathematics, 1967 (Cited on page 21).

[188] Verhees, D., Van Beeumen, R., Meerbergen, K., Guglielmi, N., and Michiels, W. Fast algorithms for computing the distance to instability of nonlinear eigenvalue problems, with application to time-delay systems. *International Journal of Dynamics and Control*, 2(2):133–142, 2014 (Cited on page 22).

[189] Verriest, E. I. and Michiels, W. Inverse Routh table construction and stability of delay equations. *Systems & Control Letters*, 55(9):711–718, 2006 (Cited on page 15).

[190] Vidyasagar, M. *Control System Synthesis: A Factorization Approach*. MIT Press, Cambridge (MA), 1985 (Cited on page 50).

[191] Volterra, V. Sur la théorie mathématique des phénomenes héréditaires. *Journal de mathématiques pures et appliquées*, 7:249–298, 1928 (Cited on page 8).

[192] Volterra, V. *Leçons sur la théorie mathématique de la lutte pour la vie*. Brelot, M., editor. Gauthier-Villars, Paris (France), 1931, 141–196. Chapter 4: Sur les actions Héréditaries comparées en biologie et en mecanique (Cited on page 8).

[193] Voss, H. *Nonlinear Eigenvalue Problems*. In *Handbook of Linear Algebra*. Hogben, L., editor. 2nd edition. Chapman and Hall/CRC, Boca Raton (FL), 2nd edition, 2014, 115:1–115:24 (Cited on page 119).

[194] Vyhlídal, T., Anderle, M., Bušek, J., and Niculescu, S.-I. Time-delay algorithms for damping oscillations of suspended payload by adjusting the cable length. *IEEE/ASME Transactions on Mechatronics*, 22(5):2319–2329, 2017 (Cited on pages 174, 183).

[195] Vyhlídal, T., Olgac, N., and Kučera, V. Delayed resonator with acceleration feedback – complete stability analysis by spectral methods and vibration absorber design. *Journal of Sound and Vibration*, 333(25):6781–6795, 2014 (Cited on page 9).

[196] Vyhlídal, T. and Zítek, P. Mapping based algorithm for large-scale computation of quasi-polynomial zeros. *IEEE Transactions on Automatic Control*, 54(1):171–177, 2009 (Cited on page 13).

[197] Vyhlídal, T. and Zítek, P. *QPmR-quasi-polynomial root-finder: algorithm update and examples*. In *Delay systems: From Theory to Numerics and Applications*. Vyhlídal, T., Lafay, J.-F., and Sipahi, R., editors. Springer, Cham (Switzerland), 2014, 299–312 (Cited on page 13).

[198] Weinstein, M. J. and Rao, A. V. Algorithm 984: ADiGator, a toolbox for the algorithmic differentiation of mathematical functions in MATLAB using source transformation via operator overloading. *ACM Transactions on Mathematical Software (TOMS)*, 44(2):21, 2017 (Cited on page 177).

[199] Wilkinson, J. H. *Rounding Errors in Algebraic Processes*. Prentice Hall, Englewood Cliffs (NJ), 1963 (Cited on page 21).

[200] Wright, E. M. A functional equation in the heuristic theory of primes. *The Mathematical Gazette*, 45(351):15–16, 1961 (Cited on page 9).

[201] Wu, Z. and Michiels, W. Reliably computing all characteristic roots of delay differential equations in a given right half plane using a spectral method. *Journal of Computational and Applied Mathematics*, 236(9):2499–2514, 2012 (Cited on pages 14, 152).

[202] Xie, L. and de Souza, C. E. Robust H_∞ control for linear systems with norm-bounded time-varying uncertainty. *IEEE Transactions on Automatic Control*, 37(8):1188–1191, 1992 (Cited on page 65).

[203] Zames, G. Feedback and optimal sensitivity: model reference transformations, multiplicative seminorms, and approximate inverses. *IEEE Transactions on Automatic Control*, 26(2):301–320, 1981 (Cited on page 40).

[204] Zevin, A. and Filonenko, L. Qualitative study of oscillations of a pendulum with periodically varying length and a mathematical model of swing. *Journal of Applied Mathematics and Mechanics*, 71(6):892–904, 2007 (Cited on page 174).

[205] Zhao, C. and Guo, L. Control of Nonlinear Uncertain Systems by Extended PID. *IEEE Transactions on Automatic Control*, 2020 (Cited on page 59).

[206] Zhou, K., Doyle, J. C., and Glover, K. *Robust and Optimal Control*. Prentice Hall, Upper Saddle River (NJ), 1996 (Cited on pages 18, 170).

[207] Zhou, K. and Doyle, J. C. *Essentials of robust control*. Prentice Hall, Upper Saddle River (NJ), 1998 (Cited on pages 1, 18, 25).

[208] Zítek, P. and Fišer, J. A universal map of three-dominant-pole assignment for PID controller tuning. *International Journal of Control*, 93(9):2267–2274, 2020 (Cited on page 40).

[209] Zítek, P., Fišer, J., and Vyhlídal, T. Dynamic similarity approach to control system design: delayed PID control loop. *International Journal of Control*, 92(2):329–338, 2019 (Cited on page 40).

Curriculum Vitae

Personal information

Name:	Pieter Appeltans
Date of birth:	July 16th, 1995
Place of birth:	Genk (Belgium)
E-mail:	appeltanspieter@gmail.com

Education

Sep 2018 –	Doctoral Programme in Engineering Science at KU Leuven, Belgium
Sep 2016 – Jun 2018	Master in de ingenieurswetenschappen: wiskundige ingenieurstechnieken at KU Leuven, Belgium (*English:* Master of Science in Mathematical Engineering)
Sep 2013 – Jun 2016	Bachelor in de ingenieurswetenschappen at KU Leuven, Belgium (*English:* Bachelor in the Engineering Sciences)

Experience

2022	Developing `C++`-code for solving algebraic Riccati equations on behalf of Siemens
2021 – 2022	President KU Leuven SIAM Student Chapter
2018 – 2022	Teaching assistant "Numerieke Wiskunde" and "Technisch Wetenschappelijke Software/ Scientific Sofware"
2018	Student job at Trendminer, Hasselt, Belgium
2017 – 2018	Teaching assistant "Elktromagnetische golven"

Awards

Best Student Award (2014) by the faculty of Engineering Sciences.
Award for the ten first year students with the highest grades in the bachelor Engineering Sciences and Engineering Sciences: architecture.

The Young Researcher Award (2019) at the 15th IFAC Workshop on Time Delay Systems.

9 - 11 September 2019, Sinaia, Romania

List of publications

Articles in internationally peer reviewed scientific journals

- Appeltans, P. and Michiels, W. A pseudo-spectrum based characterization of the robust strong H-infinity norm of time-delay systems with real-valued and structured uncertainties. *IMA Journal of Mathematical Control and Information*, 38(1):267–296, 2020
- Appeltans, P., Niculescu, S.-I., and Michiels, W. Analysis and design of strongly stabilizing PID controllers for time-delay systems. *SIAM Journal on Control and Optimization*, 60(1):124–146, 2022
- Anderle, M., Appeltans, P., Čelikovský, S., Michiels, W., and Vyhlídal, T. Controlling the variable length pendulum: Analysis and Lyapunov based design methods. *Journal of the Franklin Institute*, 359(3):1382–1406, 2022
- Appeltans, P. and Michiels, W. A structure preserving shift-invert infinite Arnoldi algorithm for a class of delay eigenvalue problems with Hamiltonian symmetry. *SIAM Journal On Matrix Analysis And Applications*, 2022. (Accepted for publication)

Book chapters

- Appeltans, P. and Michiels, W. *A scalable controller synthesis method for the robust control of networked systems.* In *Controlling Delayed Dynamics: Advances in Theory, Methods and Applications.* Breda, D., editor. Springer, Cham (Switzerland), 2023, 289–310

Articles in international conference proceedings

- Appeltans, P., Zegers, J., and Van hamme, H. Practical Applicability of Deep Neural Networks for Overlapping Speaker Separation. In *Proceedings of the Annual Conference of the International Speech Communication Association (INTERSPEECH)*, 1353–1357, 2019
- Appeltans, P. and Michiels, W. Computing the robust H-infinity norm of time-delay LTI systems with real-valued and structured uncertainties. *IFAC-PapersOnLine*, 52(18):127–132, 2019 (Presented at the 15th IFAC Workshop on Time Delay Systems, Sinaia, Romania, 9 Sep 2019 - 11 Sep 2019)

- Appeltans, P., Niculescu, S.-I., and Michiels, W. Analysis and Design of Output Feedback PD Controllers for Time-Delay Systems. In *Proceedings of the 2021 European Control Conference (ECC)*, 447–452, 2021 (Presented at the European Control Conference 2021, online, 29 Jun 2021 - 2 Jul 2021)
- Appeltans, P., Silm, H., and Michiels, W. TDS-CONTROL: a MATLAB package for the analysis and controller-design of time-delay systems. *IFAC-PapersOnLine*, 55(16):272–277, 2022 (Presented at the 18th IFAC Workshop on Control Applications of Optimization, Paris, France, 18 Jul 2022 - 22 Jul 2022)

Abstracts in international conference proceedings

- Appeltans, P. and Michiels, W. Computing and Optimizing the Robust Strong H-Infinity Norm of Uncertain Time-Delay Systems. (Presented at the IFAC World Congress 2020, online, 11 Jul 2020 - 17 Jul 2020)
- Appeltans, P., Silm, H., and Michiels, W. `TDS_STABIL`: a MATLAB tool for fixed-order stabilization problems for time-delay systems. (Presented at the 16th IFAC Workshop on Time Delay Systems, hybrid conference, Guangzhou, China, 29 Sep 2021 - 01 Oct 2021)
- Appeltans, P., Silm, H., and Michiels, W. `TDS-CONTROL`: a MATLAB package for the analysis and controller-design of time-delay systems. (Presented at the 17th IFAC Workshop on Time Delay Systems, Montreal, Canada, 27 Sep 2022 - 30 Sep 2022)
- Appeltans, P. and Michiels, W. A structure preserving shift-invert infinite Arnoldi algorithm for a class of delay eigenvalue problems with Hamiltonian symmetry. (Presented at the 17th IFAC Workshop on Time Delay Systems, Montreal, Canada, 27 Sep 2022 - 30 Sep 2022)



FACULTY OF ENGINEERING SCIENCE
DEPARTMENT OF COMPUTER SCIENCE
NUMERICAL ANALYSIS AND APPLIED MATHEMATICS (NUMA)
Celestijnenlaan 200A box 2402
B-3001 Leuven